

Photodegradable Hydrogels for tissue gluing



UNIVERSITÄT
DES
SAARLANDES

Maria Villiou

Dissertation

zur Erlangung des Grades der Doktorin

“Doctor rerum naturalium (Dr. rer. nat.)”

der Naturwissenschaften der Naturwissenschaftlich-Technischen Fakultät

der Universität des Saarlandes

Saarbrücken, September 2020



Members of Examination Board – Committee

Dean: **Prof. Dr. Christian Motz**

1st examiner: **Prof. Dr. Aranzazu del Campo**

2nd examiner: **Prof. Dr. Marleen Kamperman**

Chair of the board: **Prof. Dr. Markus Gallei**

Member of the non-professorial academic staff: **Dr. Lola Gonzalez-Garcia**

Date of the examination: **Wednesday 08 of September 2021**

Photodegradable Hydrogels for tissue gluing

Maria Villiou

geb. in Serres, Greece

Dissertation

INM – Leibniz Institute for New Materials, Saarbrücken, Germany

Saarbrücken, September 2020

I hereby declare that I wrote the dissertation submitted without any unauthorized external assistance and used only sources acknowledged in the work. All textual passages which are appropriated verbatim or paraphrased from published and unpublished texts as well as all information obtained from oral sources are duly indicated and listed in accordance with bibliographical rules. In carrying out this research, I complied with the rules of standard scientific practice as formulated in the statutes of Saarland University in Saarbrücken to insure standard scientific practice.

Maria Villiou

Dedicated to my lovely Parents

Nikolaos Villios & Despoina Ilanidou-Villiou

And in the memory of my amazing Grandparents

Georgios Ilanidis & Vasiliki Korda-Ilanidou

Michael Villios & Maria Lazoudi-Villiou

Acknowledgements

Acknowledgements

The research presented in this doctoral thesis has been performed at the INM-Leibniz-Institute for New Materials (Saarbrücken) and was funded by the European Union within the Marie Skłodowska-Curie Innovative Training School (BioSmartTrainee, Project No. 642861).

Foremost, I would like to express my sincere gratitude to my supervisor Prof. Dr. Aránzazu del Campo Bécares (Arancha) who provided me an opportunity to join her team. Without her precious support, personal advices, ongoing interest in the progress of this work, creation of an outstanding and creative working atmosphere; it would not be possible to conduct this research. Her insight and knowledge into the subject matter steered me through this research. I further very much appreciate the possibility of active participation in numerous local and global scientific meetings, discussions, and conferences.

Besides my supervisor, I would like to thank my advisor and mentor Dr. Julieta Paez for the continuous support of my PhD study and research, for her patience, motivation, enthusiasm, and immense knowledge. Her guidance helped me in all the time of research and writing of this thesis. Furthermore, I would like to thank Dr. Małgorzata K. Włodarczyk-Bieguna (Gosia) who gave me the opportunity to work with her on fascinating projects and she was always there to support me in my professional and personal life!

Also, I would like to thank my examiner Prof. M.M.G. (Marleen) Kamperman and the rest of the thesis committee for their encouragement and insightful comments.

Especially, I would like to express my thanks to PD Dr. habil. Alla Synytska and Sandra Martinka for the passionate scientific BioSmartTrainee program, as well as for numerous social events creating a great and inspiring climate. I thank my ESR fellow mates for the amazing time that we spend all together, professional and personal support: Vaishali Chopra, Justine Tavera, Aurélie Féat, Mehdi Vahdati, Francisco J. Cedano, Ki Woong (Victor) Kang, Ugo G. Sidoli, Marco Dompe and Dimitris Mintis.

I thank from my heart my dearest friends that I met at INM. Thank you for being there always with me! Thanks for adding truckloads of joy and happiness in my life, every day; Qiyang Jiang, Desna Joseph, Dr. Essak Khan, Rebecca Ludwig, Stefan Brück, Juraj Držic, my “sis” Prof. Arzu Çolak, my “brother” Dr. Ioannis Kanelidis (ευχαριστώ για όλα, που είσαι πάντα δίπλα μου στα εύκολα και στα δύσκολα!), Dr. Jun Feng and Dr. Jingnan Zhang. I would like to thank Dr.

Acknowledgements

Shrikrishnan Sankaran, Dr. Rosna V. Nair, Dr. Samuel Pearson, Dr. Mitchell Han and Prof. Dr. Yijun Zheng, for helpful and stimulating discussions and for all the fun we have had in the last four years. In particular, I am grateful to Dieter Anschütz, Dr. Claudia Fink-Straube, Ha Rimbach-Nguyen and Dr. Klaus Hollemeyer for mass spectrometry measurements; Dr. Markus Koch for help with ESEM measurements; Dr. Emmanuel Terriac, Dr. Thomas Ruckelshausen and Dr. Karin Kiefer for help with microscopy; Dr. Jennifer Yvonne Kasper, my friends Rocío Valbuena Mendoza and Dr. Aleeza Farrukh for their help with the cells and with the biolab. Also, I thank all of my colleagues for their friendships.

I thank Mrs. Martina Bonnard, Mr. Bernd Rus, Ms. Sabine Müller and Ms. Miriam Badziong for always helping me in tackling social issues at INM and outside.

I want to thank from my heart some Professors and researchers who always believing in me and professionally support and guided me: Prof. Stavros Taraviras, Prof. George Malliaras, Prof. Vassilis Karanassios, Prof. Giannis Poulios, Prof. Vasiliki Sarli, Prof Nicholas K. Moschonas, Prof. Zarkadis Ioannis, Prof. Alexandros L. Zografos, Dr. Petros Gkizis and Dr. Diego Andrada.

Outside from my working environment, I would like to thank my good friends that there were always there for me, in my ups and downs. Thank for being crazy and amazing friends! Being friends with you makes me want to celebrate every day as a Friendship day; Anna Kalas, Athanasia Akritidou, Ourania (Rania) Georgiou, Paraskevi (Evi) Tserou, Chrisavgi Zarnakoupi, Margarita-Aggeliki Pappa, Panagiotis Chatzgiovanakis, Christos Balouksis, Tom Dearden, Dr. Ionas Spyridon Haberis, Dr. Gabirel Eduardo Sanoja Lopez, Dr. Dimitris Razis, Dr. George Galaris, blessed Vasilis Chronopoulos, Hedwiga Pasc (Heidi), Isabella Chronopoulou, Veronika (Vera) Bountakidou, Effie Tesliou, Euaggelia Patlitziana, Xhino Pinari, Juna Maçi, Romeo Doksanı, George Panagiotopoulos, Elpiniki (Elpi) Panagiotopoulou, Panagiotis Paradeisopoulos, Nikolaos Retzos, Kleio Demou, Meletis Rizos, Alina Bulku, Erald Shuli, Fatjona Skenderi, Murat Özel, Christos Diamantakis, Akis Glouftios, Apostolis Ketesisidis, Thomas Papazoglou, Vyron Papathanasiou, Nestoras Nikas and Tasos Theocharidis. All of you supported me with different ways (psychological, spiritual, partying, job applications, examinations etc.). I personally thank each of you!

Especially, I would like to thank from my heart Ergi Pinari (zouzounaki), who made my last 2 stressful years of my PhD, more beautiful and easier for me. You are always there to

Acknowledgements

support me, to hug me and to motivate me. Your love, positive energy and smile fulfill me in my difficulties and in my daily life! Te dua!

Of course, last but most important, I would like to thank all of my family members (my blessed grandma Vasiliki Korda-Ilanidou) and especially my parents: Nikolaos Villios and Despoina Villiou-Ilanidou, for their love, support, motivation and encouragement! Without you, I would not have succeeded until this point. I love you with all of my heart and my mind! I want you always to be healthy, strong, happy and proud of me. I am lucky to have you both and thanks God for giving me you! You are the best! Thank you for being you, thank you that you are always there for me, thank you for your love! I never thank you enough for guiding me in the right direction! From the bottom of my heart till the universe I love you! Σας αγαπώ με όλη μου την ψυχή! Να είστε πάντοτε καλά, υγιέστατοι και χαρούμενοι! Σας ευχαριστώ για όλα!

Acknowledgements

Abstract

Abstract

Hydrogel biomaterials for wound care dressing and tissue gluing need to adhere to tissue and on-demand disappear. Advanced tissue adhesives also envision the encapsulation of therapeutic drugs or cells to promote the healing process. The design of hydrogels with all these functionalities is challenging. In this PhD, hydrogels that fulfil several of the previous properties for wound dressing at reasonable chemical complexity is presented. These hydrogels can be formed in situ and encapsulate cells, they can adhere to tissue and detach after use by light exposure at cytocompatible doses.

The developed photodegradable hydrogels are based on 4-star PEG end-catechol precursors for crosslinking, and intercalate photocleavable o-nitrobenzyl groups in their structure. These gels can form at mild oxidative conditions and encapsulate cells or microparticles. UV-vis light exposure ($\lambda = 365$ or 405 nm) photocleavables the nitrobenzyl moiety and promotes degradation. This can occur at cytocompatible doses, and enables on-demand detachment from tissue and release of the encapsulated materials or cells. These biomaterials are interesting for the development of advanced tissue adhesives and cell therapies, by expanding the range of functionality of existing choices.

Abstrakt

Abstrakt

Hydrogel-Biomaterialien für die Wundversorgung und das Verkleben von Gewebe müssen am Gewebe haften und bei Bedarf verschwinden indem sie sich von der Haut lösen oder sich im Körper zersetzen. Fortschrittliche Gewebeklebstoffe sehen auch die Einkapselung von therapeutischen Arzneimitteln oder Zellen vor, um den Heilungsprozess zu fördern. Es ist eine Herausforderung, solche Hydrogele mit minimaler struktureller Komplexität zu gestalten und herzustellen. In dieser Doktorarbeit wird die Entwicklung von Hydrogelen mit angemessener chemischer Komplexität vorgestellt, die mehrere der üblichen Eigenschaften für einen Wundverband besitzen. Diese Hydrogele können *in situ* gebildet werden, Zellen einkapseln, an Gewebe haften und anschließend durch Belichtung mit einer zytokompatiblen Lichtdosis mit hoher räumlich-zeitlicher Kontrolle gelöst werden.

Die entwickelten photodegradierbaren Hydrogele basieren auf 4-Stern-PEG, das in dieser Arbeit chemisch mit endständigen Catecholgruppen und photospaltbaren o-Nitrobenzylgruppen modifiziert wurde. Die Vernetzung erfolgt über die Catecholgruppen unter oxidativen Bedingungen in HEPES-Puffer mit 9-18 mM Natriumperiodat als Oxidationsmittel. Diese Bedingungen sind mild genug, um lebende Zellen oder Mikropartikeln in das Material einzubetten. Bei Belichtung mit UV (λ 365 nm) oder sichtbarem Licht (λ 405 nm) in zytokompatiblen Lichtdosen fördert die photospaltbare Nitrobenzyleinheit den Hydrogelabbau, was die on-demand Freisetzung von Zellen und das Ablösen vom Gewebe ermöglicht. Diese Biomaterialien sind interessant für die Entwicklung fortschrittlicher Gewebeklebstoffe und Zelltherapien, und erweitern den Funktionsumfang gegenüber bisherigen Auswahlmöglichkeiten.

Abbreviations

Abbreviations

δ (Chemical shift)

λ_{max} (Wavelength of the absorbance maximum)

ACN (Acetonitrile)

DCC (N,N'-Dicyclohexylcarbodiimide)

DCM (Dichloromethane)

DIPEA (*N,N*-Diisopropylethylamine)

Dop (Dopamine Hydrochloride)

DMAP (4-Dimethylaminopyridine)

DMF (Dimethylformamide)

eq (Molecular Equivalent)

ESI-MS⁺ (Electrospray Ionisation Mass Spectrometry)

Fmoc (9-fluorenylmethoxycarbonyl protecting group)

h (Hour)

HBTU (*N,N,N',N'*-Tetramethyl-*O*-(1*H*-benzotriazol-1-yl)uronium hexafluorophosphate)

HEPES (4-(2-hydroxyethyl)-1-piperazineethanesulfonic acid))

HOEt (1-Hydroxybenzotriazole Hydrate)

HPLC (High performance liquid chromatography)

Hz (Hertz)

J (Coupling constant in Hz (NMR))

M (Month)

M (Molarity (mol/l))

M (Starting Material (ESI-MS+))

MW Molecular weight

MeOH (Methanol)

min (Minute)

MgSO₄ (Magnesium Sulfate)

Ms-Cl (Methanesulfonyl Chloride)

Na₂CO₃ (Sodium Carbonate)

NaNO₂ (Sodium nitrite)

Abbreviations

NDop (Nitrodopamine)
NH₂ (Amino group)
NHS (N-hydroxysuccinimide)
NMM (*N*-methylmorpholine)
NNPE (Nitronorepinephrine)
OH (Hydroxyl)
OMe (Methoxy)
o-NB (o-nitrobenzyl group)
o-NBe (o-nitrobenzyl ester group)
o-NBt (o-nitrobenzyl triazole group)
o-NP (o-nitrophenyl ethyl group)
PEG (Polyethylene glycol)
PEG-Dop (PEG-Dopamine)
PEG-NDop (PEG-Nitrodopamine)
PEG-NNPE (PEG-Nitronorepinephrine)
PEG-SCM or PEG-NHS or PEG-OSu (4arm PEG Succinimidyl Carboxymethyl Ester)
r.t. (Room temperature)
s (Second)
UV8 (Ultraviolet)
UV/VIS (Linear optical absorption spectroscopy in the ultraviolet and visible spectral region)
VIS Visible spectral range
w (Week)
wt% Weight percentage
X Leaving group
¹H-NMR (Proton NMR spectroscopy)

All other abbreviations, as physical and chemical units, have their usual meaning if not stated otherwise.

Copyrights

9/3/2020

Rightslink® by Copyright Clearance Center



RightsLink®

Home

Help

Email Support

Maria Villiou ▾



Photodegradable Macromers and Hydrogels for Live Cell Encapsulation and Release

Author: Donald R. Griffin, Andrea M. Kasko

Publication: Journal of the American Chemical Society

Publisher: American Chemical Society

Date: Aug 1, 2012

Copyright © 2012, American Chemical Society

PERMISSION/LICENSE IS GRANTED FOR YOUR ORDER AT NO CHARGE

This type of permission/license, instead of the standard Terms & Conditions, is sent to you because no fee is being charged for your order. Please note the following:

- Permission is granted for your request in both print and electronic formats, and translations.
- If figures and/or tables were requested, they may be adapted or used in part.
- Please print this page for your records and send a copy of it to your publisher/graduate school.
- Appropriate credit for the requested material should be given as follows: "Reprinted (adapted) with permission from (COMPLETE REFERENCE CITATION). Copyright (YEAR) American Chemical Society." Insert appropriate information in place of the capitalized words.
- One-time permission is granted only for the use specified in your request. No additional uses are granted (such as derivative works or other editions). For any other uses, please submit a new request.

If credit is given to another source for the material you requested, permission must be obtained from that source.

BACK

CLOSE WINDOW

© 2020 Copyright - All Rights Reserved | Copyright Clearance Center, Inc. | Privacy statement | Terms and Conditions
Comments? We would like to hear from you. E-mail us at customercare@copyright.com

Copyrights

9/3/2020

Rightslink® by Copyright Clearance Center



RightsLink®



Maria Villiou ▾

The Mechanism of the Self-Initiated Thermal Polymerization of Styrene. Theoretical Solution of a Classic Problem



Author: Kelli S. Khuong, Walter H. Jones, William A. Pryor, et al

Publication: Journal of the American Chemical Society

Publisher: American Chemical Society

Date: Feb 1, 2005

Copyright © 2005, American Chemical Society

PERMISSION/LICENSE IS GRANTED FOR YOUR ORDER AT NO CHARGE

This type of permission/license, instead of the standard Terms & Conditions, is sent to you because no fee is being charged for your order. Please note the following:

- Permission is granted for your request in both print and electronic formats, and translations.
- If figures and/or tables were requested, they may be adapted or used in part.
- Please print this page for your records and send a copy of it to your publisher/graduate school.
- Appropriate credit for the requested material should be given as follows: "Reprinted (adapted) with permission from (COMPLETE REFERENCE CITATION). Copyright (YEAR) American Chemical Society." Insert appropriate information in place of the capitalized words.
- One-time permission is granted only for the use specified in your request. No additional uses are granted (such as derivative works or other editions). For any other uses, please submit a new request.

If credit is given to another source for the material you requested, permission must be obtained from that source.

BACK

CLOSE WINDOW

© 2020 Copyright - All Rights Reserved | Copyright Clearance Center, Inc. | Privacy statement | Terms and Conditions
Comments? We would like to hear from you. E-mail us at customercare@copyright.com

Copyrights

9/3/2020

Rightslink® by Copyright Clearance Center



RightsLink®



Maria Villiou ▾

Design and Characterization of a Synthetically Accessible, Photodegradable Hydrogel for User-Directed Formation of Neural Networks



Author: Daniel D. McKinnon, Tobin E. Brown, Kyle A. Kyburz, et al

Publication: Biomacromolecules

Publisher: American Chemical Society

Date: Jul 1, 2014

Copyright © 2014, American Chemical Society

PERMISSION/LICENSE IS GRANTED FOR YOUR ORDER AT NO CHARGE

This type of permission/license, instead of the standard Terms & Conditions, is sent to you because no fee is being charged for your order. Please note the following:

- Permission is granted for your request in both print and electronic formats, and translations.
 - If figures and/or tables were requested, they may be adapted or used in part.
 - Please print this page for your records and send a copy of it to your publisher/graduate school.
 - Appropriate credit for the requested material should be given as follows: "Reprinted (adapted) with permission from (COMPLETE REFERENCE CITATION). Copyright (YEAR) American Chemical Society." Insert appropriate information in place of the capitalized words.
 - One-time permission is granted only for the use specified in your request. No additional uses are granted (such as derivative works or other editions). For any other uses, please submit a new request.
- If credit is given to another source for the material you requested, permission must be obtained from that source.

BACK

CLOSE WINDOW

© 2020 Copyright - All Rights Reserved | Copyright Clearance Center, Inc. | Privacy statement | Terms and Conditions
Comments? We would like to hear from you. E-mail us at customercare@copyright.com

Copyrights

9/3/2020

Rightslink® by Copyright Clearance Center



Copyright
Clearance
Center

RightsLink®

Home

?

✉

Email Support

👤

Maria Villiou ▾

Photodegradable Hydrogels for Cell Encapsulation and Tissue Adhesion



Author: Maria Villiou, Julieta I. Paez, Aránzazu del Campo

Publication: Applied Materials

Publisher: American Chemical Society

Date: Aug 1, 2020

Copyright © 2020, American Chemical Society

PERMISSION/LICENSE IS GRANTED FOR YOUR ORDER AT NO CHARGE

This type of permission/license, instead of the standard Terms & Conditions, is sent to you because no fee is being charged for your order. Please note the following:

- Permission is granted for your request in both print and electronic formats, and translations.
- If figures and/or tables were requested, they may be adapted or used in part.
- Please print this page for your records and send a copy of it to your publisher/graduate school.
- Appropriate credit for the requested material should be given as follows: "Reprinted (adapted) with permission from (COMPLETE REFERENCE CITATION). Copyright (YEAR) American Chemical Society." Insert appropriate information in place of the capitalized words.
- One-time permission is granted only for the use specified in your request. No additional uses are granted (such as derivative works or other editions). For any other uses, please submit a new request.

BACK

CLOSE WINDOW

© 2020 Copyright - All Rights Reserved | Copyright Clearance Center, Inc. | Privacy statement | Terms and Conditions
Comments? We would like to hear from you. E-mail us at customercare@copyright.com

Copyrights

Dear Maria Villiou,

We hereby grant permission for the requested use expected that due credit is given to the original source.

Any third party material is expressly excluded from this permission. If any of the material you wish to use appears within our work with credit to another source, authorization from that source must be obtained.

Credit must include the following components:

- Journals: Author(s) Name(s); Title of the Article; Name of the Journal; Publication year; Volume; Page(s); Copyright Wiley-VCH GmbH. Reproduced with permission.

This permission does not include the right to grant others permission to photocopy or otherwise reproduce this material except for accessible versions made by non-profit organizations serving the blind, visually impaired and other persons with print disabilities (VIPs).

Kind regards

Bettina Loycke
Senior Rights Manager
Rights & Licenses

Wiley-VCH GmbH
Boschstraße 12
69469 Weinheim
Germany

www.wiley-vch.de

T +(49) 6201 606-280
F +(49) 6201 606-332
rightsDE@wiley.com

Copyrights

This Agreement between Ms. Maria Villiou ("You") and The American Association for the Advancement of Science ("The American Association for the Advancement of Science") consists of your license details and the terms and conditions provided by The American Association for the Advancement of Science and Copyright Clearance Center.

License Number 4901370300934

License date Sep 03, 2020

Licensed Content Publisher The American Association for the Advancement of Science

Licensed Content Publication Science

Licensed Content Title Photodegradable Hydrogels for Dynamic Tuning of Physical and Chemical Properties

Licensed Content Author April M. Kloxin,Andrea M. Kasko,Chelsea N. Salinas,Kristi S. Anseth

Licensed Content Date Apr 3, 2009

Licensed Content Volume 324

Licensed Content Issue 5923

Volume number 324

Copyrights

Issue number 5923

Type of Use Thesis / Dissertation

FOR A THESIS OR DISSERTATION

If you are using figure(s)/table(s), permission is granted for use in print and electronic versions of your dissertation or thesis. A full text article may be used in print versions only of a dissertation or thesis.

Permission covers the distribution of your dissertation or thesis on demand by ProQuest / UMI, provided the AAAS material covered by this permission remains in situ.

If you are an Original Author on the AAAS article being reproduced, please refer to your License to Publish for rules on reproducing your paper in a dissertation or thesis.

Copyrights

This Agreement between Ms. Maria Villiou ("You") and Springer Nature ("Springer Nature") consists of your license details and the terms and conditions provided by Springer Nature and Copyright Clearance Center.

License Number 4901380339369

License date Sep 03, 2020

Licensed Content Publisher Springer Nature

Licensed Content Publication Nature Chemistry

Licensed Content Title Cytocompatible click-based hydrogels with dynamically tunable properties through orthogonal photoconjugation and photocleavage reactions

Licensed Content Author Cole A. DeForest et al

Licensed Content Date Oct 23, 2011

Type of Use Thesis/Dissertation

Requestor type academic/university or research institute

Format print and electronic

Portion figures/tables/illustrations

Number of 3

INDEX

Motivation	1
Chapter 1. Background and literature review	4
1.1 Tissue adhesives.....	4
1.2 Mussel-inspired catechol-based biomedical adhesives.....	6
1.3 Degradable biomedical adhesives.....	9
1.4 Photodegradable hydrogels for cell encapsulation.....	13
1.5 Poly(ethylene glycol) based hydrogels for cell encapsulation and biomedical applications.....	17
1.6 References.....	19
Chapter 2. Synthesis and photochemical characterization of photodegradable PEG-catechol precursors.....	28
2.1 Abstract	28
2.2 Introduction.....	28
2.3 Molecular design of photodegradable PEG-catechol precursors.....	32
2.4 Results and Discussion	34
2.4.1 Synthesis of macromers.....	34
2.4.2 Synthesis of control macromers.....	46
2.4.3 Synthesis of small molecule analogues.....	47
2.4.4 Characterization of photolytic properties of model molecules and macromers... ...	48
2.4.5 Photolysis studies of model compounds.....	48
2.4.6 Photolysis studies of PEG-catechol macromers	55
2.4.7 Hydrolytic stability of the macromers.....	59
2.5 Conclusions.....	61
2.6 References.....	61
Chapter 3. Preparation & Characterization of Photodegradable Adhesive PEG-catechol hydrogels.....	65
3.1 Abstract	65

INDEX

3.2 Introduction.....	65
3.3 Results and Discussion	68
3.3.1 Characterization of crosslinking kinetics.....	68
3.3.2 Characterization of hydrogel's photodegradation by rheology.....	73
3.3.3 Quantification of photodegradation by gravimetry.....	83
3.3.4 Photopatterning of PEG-catechol gels.....	86
3.3.5 Adhesion of PEG-NBt-c hydrogels to tissue and light-mediated debonding.....	94
3.4 Conclusions.....	97
3.5 References.....	98
 Chapter 4. Photodegradable PEG-catechol hydrogels for cell encapsulation	105
4.1 Abstract	105
4.2 Introduction.....	105
4.3 Results and Discussion	108
4.3.1 Cytocompatibility study of PEG-catechol hydrogels.....	108
4.3.2 Analysis of toxicity of photolysis products.....	112
4.3.3 Cell encapsulation in PEG-NBt-c gels and light-triggered cell release.....	113
4.3.4 3D cell encapsulation with PEG-NBt-c gels and in situ photodegradation	117
4.4 Conclusions.....	123
4.5 References.....	124
 Conclusions & Outlook.....	128
 Appendix (Instrumentation & Experimental Section)...	131
 List of Scientific Contributions...	202
Curriculum Vitae (CV)	207

Motivation

Over 500 million major surgical procedures and 21 million cosmetic plastic surgeries are performed annually worldwide. Most surgical procedures require the use of a wound closure material. The ideal wound closure procedure should be easy to apply, painless, cost-effective and easily removable or degradable at a rate that depends on the particular healing process. In this context, tissue glues offer clear advantages vs. stitching or stapling methods. However, reliable gluing in the presence of complex body fluids is complicated. Moreover, commercial available tissue glues do not allow degradation on demand.

The ability of mussels to firmly stick to varied surfaces, even in turbulent seawater, has inspired considerable research in tissue glues in recent years. Mussel foot adhesive proteins are rich in the non-common amino acid 3,4-dihydroxyphenylalanine (DOPA), whose catechol unit can interact covalently and non-covalently with almost any kind of substrate under physiological conditions, including living tissues. The versatility of DOPA chemistry has inspired medical adhesive designs in the last two decades, and numerous demonstrations of catechol-derived hydrogels have been tested for tissue gluing in a variety of biomedical scenarios.

In this context, this PhD project aimed to develop mussel-inspired adhesive hydrogels with the possibility of degradation on-demand. For this purpose, catechol derived hydrogels were further equipped with photocleavable units. This allowed degradation (depolymerization) of the adhesive hydrogel upon light exposure. Particular attention was paid to the design of photocleavable units that could be cleaved at cell-compatible doses, in order to minimize the risk of photodamage of living cells. The good cytocompatibility of catechol chemistry and the low phototoxicity during degradation of the hydrogel opened the possibility to use this gels also for cell encapsulation, expanding the functionality of these materials for advanced medical applications.

The thesis is organized as follows:

Chapter 1 summarizes the state-of-the-art literature on tissue adhesives. It focusses on mussel-inspired catechol-based biomedical adhesives and degradable biomedical adhesives; it describes the design rules for photodegradable hydrogels for cell encapsulation, and especially for poly(ethylene glycol) based hydrogels for cell encapsulation and biomedical applications.

Motivation

Chapter 2 describes the design and synthesis of several photodegradable PEG-catechol precursors containing nitrobenzyl triazole or nitrobenzyl ester unit for photodegradation. The physicochemical and photochemical properties of the obtained photodegradable macromers is compared.

Chapter 3 describes the synthesis and properties of photodegradable adhesive PEG-catechol hydrogels. The crosslinking kinetics, mechanical properties and photodegradation kinetics were studied by rheology. The spatiotemporally controlled release of micro-particles and the debonding from tissue by light-induced degradation is demonstrated.

Chapter 4 presents cytocompatibility studies of the photodegradable hydrogels during gel formation and photodegradation.

Finally, a **conclusions section** summarizes the most important results from the presented work and provides a brief outlook on future directions.

The Appendix includes information about the materials and instrumentation, the experimental section with details on the synthesis of hydrogel precursors (NMR, HPLC, FT-IR, ESI-MS) and their photolysis studies (UV-Vis); additional rheological, microscopy and biological studies of hydrogels; and supplementary figures.



1.1 Tissue adhesives

Wound management is an important part of a daily medical practice. Established wound closure methods such as sutures or staples present several limitations. They require penetration of the healthy tissue, causing further tissue damage and pain, mechanical stress concentration and additional potential infection sites.^{1, 2} As alternative approach, a variety of bioadhesive polymers have been developed as tissue glues for wound closure. As fluids, they can be applied on irregularly shaped cavities and seal injured tissue. Tissue adhesion in this case is mediated by the application of a (pre)-polymer liquid solution, which then solidifies via *in situ* polymerization or cross-linking reaction.¹ Tissue glues present the following advantages vs. suturing or stapling: easier and faster application, as well as more flexibility to adapt to the particular medical scenario. The market share for medical glues was ~\$ 9.3 billion in 2018 and was estimated to grow at an annual growth rate of 8.0% from 2019 to 2025.³ Tissue adhesives are used in different biomedical areas (Figure 1.1) such as dentistry, cardiovascular orthopedics, traumatology, otorhinolaryngology and for plastic and maxillofacial surgical applications.⁴

Hydrogels are soft hydrophilic networks which can uptake and retain large amounts of fluids, mimicking the natural scaffold of living tissues. These properties make them good candidates for tissue adhesives and sealants⁵⁻⁸, for wound dressings and for scaffolds for 3D cell encapsulation.^{1, 4}

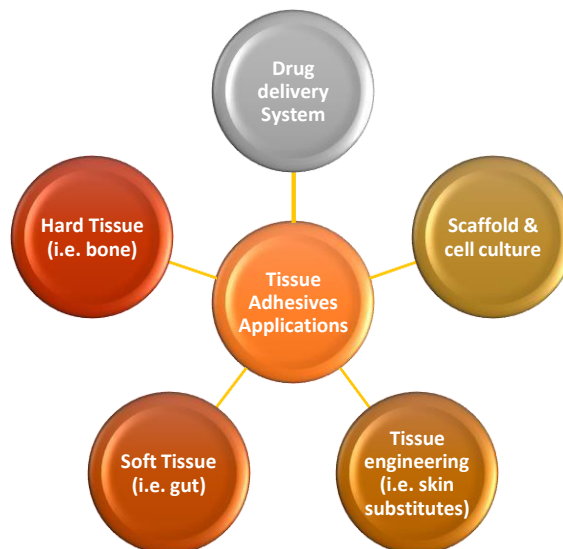


Figure 1.1 Tissue adhesive biomedical applications.⁴

Specifically, for tissue adhesion, sealant or wound dressing applications, hydrogels need to adhere to tissue, and then easily be removed (i.e. replacement of a wound dressing) or gradually decomposed (i.e. for controlled drug release or during tissue regeneration).^{9, 10} In addition, the following properties are necessary for a good tissue glue: strong adhesion to the target tissue in the presence of body fluids, biocompatibility, degradability, fast polymerization, adaptability to the mechanical properties of the tissue, and low cost.¹¹

Commercially available tissue glues (Table 1.1) rely on electrostatic interactions between tissue and charged polymers, for example alginate (e.g. Algisite®, Smith & Nephew) or polyacrylate (UrgoClean®, Urgo). Tissue adhesives based on natural polymers such as fibrin glue (e.g. Tisseel® and Artiss®, Baxter; Evarrest®, Ethicon), albumin (BioGlue®, CryoLife), gelatin (FloSeal®, Baxter) or chitosan (Celox®, MedTrade), also exist. Other systems use covalent interactions between isocyanates (TissuGlu®, B. Braun), cyanoacrylate (Dermabond®, Ethicon; Leukosan®, BSN Medical; Histoacryl®, B. Braun), N-hydroxysuccinimide (NHS) esters (CoSeal®, Baxter; DuraSeal®, Integra LifeSciences), or aldehydes (BioGlue®, Cryolife), among others, with biomolecules that are present in natural tissue (see Table 1.1). Cyanoacrylate glues are also widely employed for external tissue repair.^{11, 12}

Academically, mussel-inspired catechol chemistry has been widely explored for tissue adhesion,^{11, 13, 14} sealing,^{15, 16} as hemostatic agents¹⁷ or wound dressings.^{18, 19} This chemistry has been recently transferred to promote adhesion of commercially hemostatic pads (InnoSEAL®, InnoTherapy). The catechol group has many different reaction possibilities and partners in a natural environment²⁰ (see Figure 1.2) and provides a generic solution for a wide range of biomedical application scenarios.^{4, 21}

Table 1.1 Examples of commercial biomedical adhesives used for soft tissue repair

Application	Polymer backbone and <i>in situ</i> crosslinking	Commercial name	Citation

Topical skin adhesives	cyanoacrylate adhesive (The acryl groups in the resin rapidly polymerize in the presence of water)	Dermabond® (Ethicon)	12
		Histoacryl® (B. Braun)	
		Leukosan® (BSN Medica)	
	polyacrylate adhesive (free radical or anionic polymerization techniques)	Leukomed® (BSN Medica)	22
		Covermed® (BSN Medica)	23
		UrgoSterile® (URGO)	24
Sealants	Albumin and glutaraldehyde	BioGlue (Cryolife Inc)	25, 26
		PREVELEAK® (Baxter)	
		ProGel® (NeoMend)	
	Fibrin sealant (With calcium, thrombin facilitates the activated factor XIII to polymerize the fibrin)	Tisseel (Baxter Inc.)	27
		Evicel (Ethicon Inc., Bridgewater, NJ)	
		Crosseal (OMRIX Biopharmaceuticals Ltd. Israel)	
		Hemaseel (Heamacure Corp., Canada)	
Tissue adhesive for internal organs	lysine-derived urethane polymer (curing in the presence of moisture)	TissuGlu (B. Braun)	28

1.2 Mussel-inspired catechol-based biomedical adhesives

Over the last years, 3,4-dihydroxyphenylalanine (DOPA) chemistry has inspired new concepts for the design of adhesives for medical applications.²⁹ In nature, mussels secrete adhesive proteins that are used to achieve underwater attachment to surfaces. These proteins have a high content (5-30%) of DOPA amino acid. The catechol side group of DOPA is capable of strong interfacial binding and cohesion by different reversible interactions and irreversible reactions with itself and with organic and inorganic substrates (Figure 1.2).³⁰

Catechols form strong and reversible complexes with metal ions (Fe^{3+} , Ca^{2+} , Cu^{2+} , Ti^{3+} , Ti^{4+} , Mn^{2+} , Mn^{3+} , Zn^{2+}) with different stoichiometry (i.e., mono-, bis-, and tris-complexes) depending of the pH; Figure 1.2(1).^{30, 31} At low pH, mono complexes are created. When the pH increases, stable bis and tris complexes are formed. Coordination protects the catechol from becoming oxidized under basic conditions.

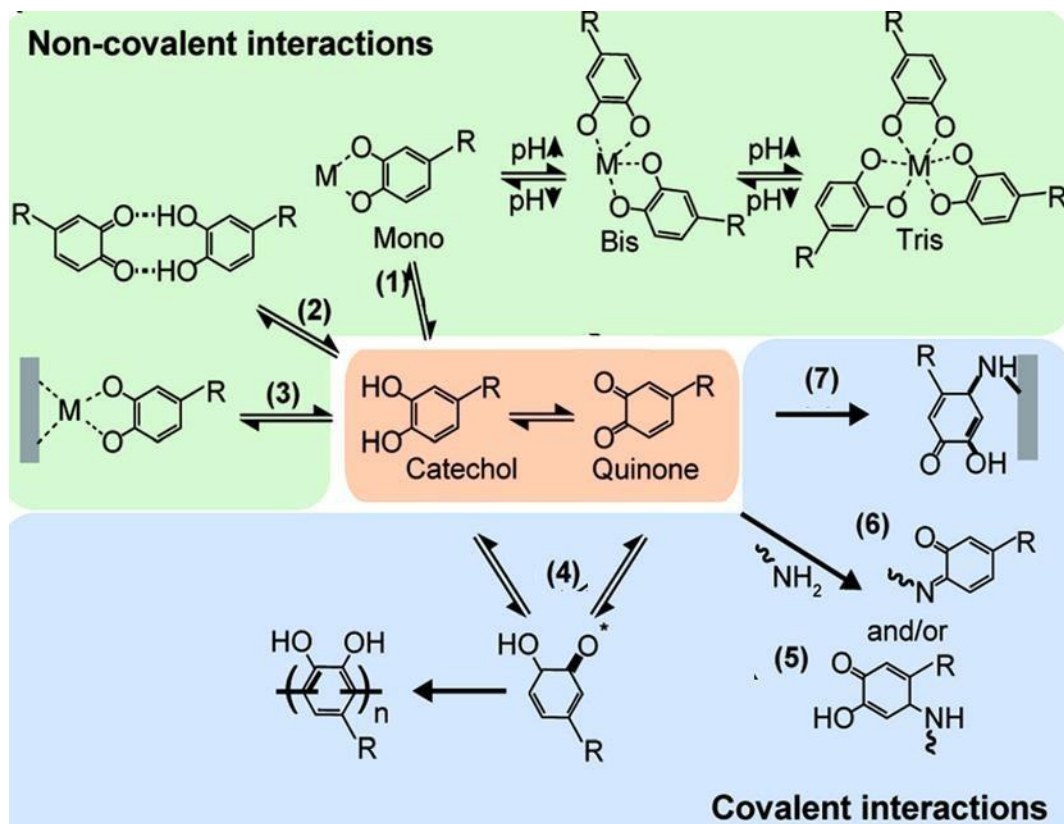


Figure 1.2 Overview of catechol chemistry. Center: the catechol to quinone redox equilibrium is affected by pH and oxidative environment. 1) Catechol chelates metal ions to form complexes with different stoichiometry depending on the solution pH .2) Example of catechols and quinones ability to participate in hydrogen bonding. 3) Adhesion to inorganic substrates via coordination bonds with metal oxide surfaces. 4) Self-coupling through semiquinone radical. 5) Michael-type addition with amine (or thiol) group. 6) Schiff base reaction with amine group. 7) Adhesion to organic surface (here shown for an amine-functionalized surface). Modified after permission from Wiley Online Library.³⁰

In the presence of oxidizing reagents (i.e. NaIO₄, H₂O₂, enzyme etc.), the catechol group is oxidized to the quinone form.³² Quinones have the ability to form covalent interactions. They are very reactive electrophiles and can react with nucleophiles located at organic substrates (such as amines and thiols), and form strong irreversible covalent bonds (Figure 1.2(4-7)). This reactivity of catechols has been exploited for hydrogel crosslinking and adhesion to tissue and therefore used as effective bioinspired medical adhesives and sealants.³³ Quinones can also self-react to form covalent bonds and cross-linked polyDOPA networks (Figure 1.2(4)).³⁰ This chemistry has been extensively used to form hydrogels that crosslink *in situ*. The reaction of the catechol groups is dependent on pH and oxidant concentration. Under mild acidic conditions (pH=5.7-6.7), the catechol crosslinks slower in contrast to neutral or basic pH (pH=7.4-8) where the crosslinking is faster.^{34, 35} At low pH, the crosslinking of the catechol is slow because of the increased stability of temporary oxidation intermediates (i.e., quinone), which decreases the rate of subsequent crosslinking reactions.^{34, 35} Metal complexation has also been exploited for *in situ* hydrogel formation.^{36, 37} Star poly(ethylene glycol) (PEG) with terminal catechol groups have been widely used as hydrogel precursors for fast curing, injectable tissue adhesives or sealants.^{15, 38} Such biomaterials have demonstrated good cytocompatibility, similar or higher adhesive properties in comparison to commercial fibrin glue,^{39, 40} and have successfully sealed traumatized human fetal membrane.^{15, 41}

Messersmith and his team demonstrated the *in vivo* performance of mussel-inspired PEG-catechol adhesives in mice, including biocompatibility and integrity of the adhesive-tissue interface.²⁰ Mixtures of an oxidant (sodium periodate) and non-degradable four-arm PEG-catechol solutions were applied on adipose tissue, where they formed adherent hydrogels *in situ*. Histological evaluation after implantation showed minimal inflammatory cell infiltrate and little evidence of fibrotic capsule formation. The adhesive hydrogel did not degrade within 4 months and the surrounding adipose tissue was healthy and well vascularized. Chen et al., developed a mussel-inspired tissue-adhesive hydrogel consisting of poly(-glutamic acid) and DOPA (PGA-DA). They showed that it could be used as tissue adhesive and hemostatic sealant (liver puncture in animal models) in a wet environment. This cytocompatible PGA-DA hydrogel demonstrated 12-fold stronger wet tissue adhesion strength and better hemostasis (41.2% less bleeding) than clinically used fibrin glue.⁴²

Mussel-inspired hydrogels have also been used as materials for 2D cell culture⁴³ and 3D cell encapsulation.^{43, 44} Pioneering work by Messersmith and coworkers²⁰ reported the use of mussel-inspired hydrogels to facilitate minimally invasive cell therapies for amelioration of type I diabetes in mice. A PEG-catechol hydrogel was used to affix transplanted islet cells to the surface of epididymal fat pad and liver tissues. The transplanted construct remained tissue-adhered for over 4 months; cells remained functional and secreted insulin. Islet re-vascularization was not impaired and minimal inflammatory response was observed. Cho *et al*⁴⁵ demonstrated that cell-laden catechol-hyaluronic acid hydrogels administered *in vivo* by a simple ‘painting’ procedure adhered to liver and heart tissues, facilitated the direct engraftment of cell-encapsulating hydrogels onto these organs’ surface and supported cell viability and function. Stable and tight gel’s adhesion onto those tissues enabled to localize the therapeutic construct up to 2-4 weeks after transplantation in defected and diseased animal models while avoiding injection or invasive procedures. Oomen *et al*⁴⁶ also profited from the tissue adhesion properties of catechol-hyaluronic acid gels for suture-free and compartmentalized implantation of stem cells to the surface of eye for cornea regeneration and demonstrated this concept in *ex vivo* porcine models. Although these examples initially showed the potential of mussel-inspired gels for cell therapies, in some of these cases the migration of the transplanted cells and ultimately their integration with the host tissue was not optimal.^{45, 46} One crucial material property that could be modulated to improve this aspect is the kinetics of the degradation of the hydrogel.⁴⁷

1.3 Degradable biomedical Adhesives

Tissue adhesives need to either be removed or degrade in a time scale which depends on the particular application.⁴⁸ Approaches for removal of the hydrogel glue are typically based on physically crosslinked hydrogels that can be dissolved by temperature⁴⁹ or pH⁵⁰ changes, or chemically by addition of soluble molecules that compete with the network chains for crosslinking.⁵¹ Alternatively, hydrolytically⁵², enzymatically⁵³ or light⁵⁴⁻⁵⁶ cleavable units are introduced in the polymeric network and allow gradual dissolution of the network (see Table 1.2 for more information about degradable bioadhesives). For example, Paoletti and co-workers, developed a hydrolytically degradable tissue adhesive based on dopamine-grafted, polysaccharide (alginate and hyaluronic acid), presenting high adhesion *in vitro* and *in vivo* on pig

intestine tissue that degraded during 11 days of incubation in Hank's Balanced Salt Solution (HBSS).⁵⁷ Also, Brubaker *et al.*, developed the enzymatically degradable Ala-Ala dipeptide to a DOPA end-functionalized 4-arm PEG macromonomer (cAAPPEG). This system showed a slow neutrophil elastase-mediated degradation *in vivo* (\approx 16 weeks) with minimal inflammatory response.⁵⁷ Hemostatic fibrin glues such as Tisseel (Baxter Inc.), E vicel (Ethicon Inc. (Johnson & Johnson Co)), Vitagel (Orthovita Inc.), Cryoseal system (ThermoGenesis Corp.) or Beriplast® P (AventisBehring) degrade by plasmin-mediated fibrinolysis within 10 to 14 days in a fibrinolytic environment.⁴⁸

Examples of tissue adhesive hydrogels that can be removed by light exposure are rare. Chitosan and NHS-terminated polyethylene glycol (PEG) hydrogels containing nitrobenzyl groups have been designed as *in situ* crosslinking and photodegradable hydrogels that can adhere to skin tissue and be used for wound dressing. The storage modulus of the hydrogels ranged 500-3500 Pa depending of the concentration of the photocleavable cross-linker and the adhesive strength was between 2350-7000 Pa (being comparable with the commercial fibrin glue Greenplast® \approx 5000 Pa). Depending on the crosslinking density the depolymerisation of the material needed 100-400 min (at 10 mW cm⁻², this corresponds to an irradiation dose = 60-240 mJ cm⁻²).⁵⁸ Also, a photoswitchable hydrogel has been commercialized as skin adhesive (Lumina™), presenting strong fixation to skin and easy removal. It is made out of a switchable polyurethane adhesive, which can easily be removed by illumination either with a special torch ($\lambda= 365$ nm) or by sun light.⁵⁹

Reported systems for tissue adhesion up to now combine two key properties, either tissue adhesion and photodegradability,⁵⁸ tissue adhesion and cell encapsulation ability²⁰, or cell encapsulation ability and photodegradability.⁶⁰ Combination of tissue adhesion, cell encapsulation ability and photorelease possibilities in a single material has not been realized yet. Such a system would expand the use of such hydrogels for advanced medical applications.

Table 1.2 Overview of reported degradable bioadhesives

Hydrogel chemical design		Degradation mode and time scale	Commercial name (if available)	Application	Citation
Polymer backbone	Crosslinking system				
Fibrin monomers (fibrinogen)	With calcium, thrombin facilitates the activated factor XIII to polymerize the fibrin	Fibrinolysis (10-14 d)	Tisseel (Baxter Inc.)	Hemostatic sealant used for gastrointestinal anastomosis, perforated peptic ulcer, hepatic and splenic lacerations, laparoscopic hernia repair or common bile duct exploration, pancreatic resection, treatment of anal fistulas, vascular surgery, intra-abdominal adhesions, other miscellaneous applications	48, 61, 62
			Evicel (Ethicon Inc.)		
			Vitagel (Orthovita Inc.)		
			Cryoseal system (ThermoGenesis Corp.)		
			Beriplast® P (AventisBehring)		
PEG-catechol + citric acid	DOPA oxidation by sodium (meta) periodate	Hydrolysis (1-25 d depending on the crosslinking density)	n.c.a.	Hemostasis, wound closure	63, 64
Poly(glycerol-co-sebacate acrylate)	Cured by UV light	Enzymatic or Hydrolytic (8 d)	n.c.a.	Sealing wounds	48, 64

Aldehyde sodium alginate: amino gelatine	via Schiff base reaction	Enzymatic (\approx 5 d)	n.c.a.	Soft tissue adhesive	⁶⁵
Aldehyde dextran: chitosan	Schiff's base formation between amine and aldehyde	Enzymatic by dextranase (73 d)	n.c.a.	Drug delivery, hemostat, tissue adhesive	⁶⁶
Aldehyde dextran: ϵ -poly(L-lysine)	Schiff's base formation	Hydrolysis (8 d)	LYDEX® (BMG)	Hemostat, sealant, adhesion-prevention, wound care dressings with endoscope, drug delivery	^{67, 68}
Photoreactive gelatin: PEG-diacrylate	UV Photocurable	Enzymatic Hydrolysis with collagenase (30 d)	n.c.a.	Hemostasis, anastomosis, endoscopic surgery	⁶⁹
Aldehyde-dextran: PEG-amine	Schiff's base formation	Hydrolytic (7-15 d)	n.c.a.	Sealants, wound dressings, ophthalmic procedures, cataract surgery, vitreoretinal surgery, corneal transplantation, oculoplastics	^{70, 71}
Tannic acid: PEG (TAPE)	intra- and inter-molecular	Hydrolytic (3-21 d)	n.c.a.	Hemostatic adhesive, drug depot, adhesive patch	⁷²

	hydrogen bonding				
Gelatin modified with catechol	Catechol-Fe ion complexation , Genipin for stabilization	Enzymatic Hydrolysis (14-28 d)	n.c.a.	Internal tissue adhesion, sealing, and hemostasis	⁷³
PEG-incorporated with Ala-Ala dipeptide	DOPA oxidation by periodate	Enzymatic (112 d)	n.c.a.	soft-tissue adhesion (gut, vasculature), adhesion in chronically inflamed environments (hernia)	⁷⁴

n.c.a. not commercially available

1.4 Photodegradable hydrogels for cell encapsulation

Photodegradable hydrogels allow light-regulated control of the properties of the network and derived cell responses.⁷⁵ Most examples of photodegradable hydrogels include photocleavable or photolabile compounds in the network structure. When these compounds are incorporated into the polymer backbones or as crosslinkers, light exposure can cause irreversible degradation of the material.^{76, 77} Such groups are stable in the dark, but can be cleaved upon illumination with UV- or visible light.⁷⁵ For application in a biomedical context, the photocleavable group should have high photolytic efficiency, hydrolytic and enzymatic stability, water solubility and no cytotoxicity.^{78,79} In combination with degradable polymers for biomedical scenarios, the coumarinyl and o-nitrobenzyl photoremoveable protecting groups have been mostly used (Figure 1.4).

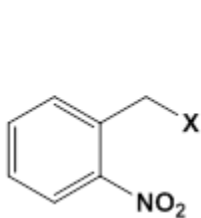
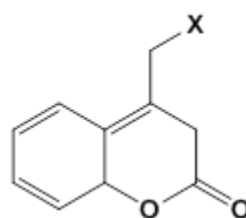
A. o-Nitrobenzyl**B. Coumarinyl**

Figure 1.4 Commonly used photocleavable groups for development of photodegradable biomaterials; (A) o-Nitrobenzyl and (B) Coumarinyl group. X represents leaving groups. Many structural variations exist for each photocleavable group, depending on its substituents.

The photolysis mechanism of ortho-nitrobenzyl (o-NB) derivatives was first reported for the release of adenosine triphosphate (ATP) using a 2-nitrobenzyl ester.⁸⁰ The photochemical reaction starts by a radical formation at the nitro moiety upon light excitation (Figure 1.5). After rearrangement of the molecule, cyclization reaction occurs between the hydroxyl group of the nitro group and the benzylic carbon. The molecule rearranges again with bond cleavage between nitrogen and oxygen in the ring and oxygen and benzylic carbon to form a ketone or carbamic acid. With rearrangement of carbamic acid, carbon dioxide is released and an amine is formed.^{80, 81}

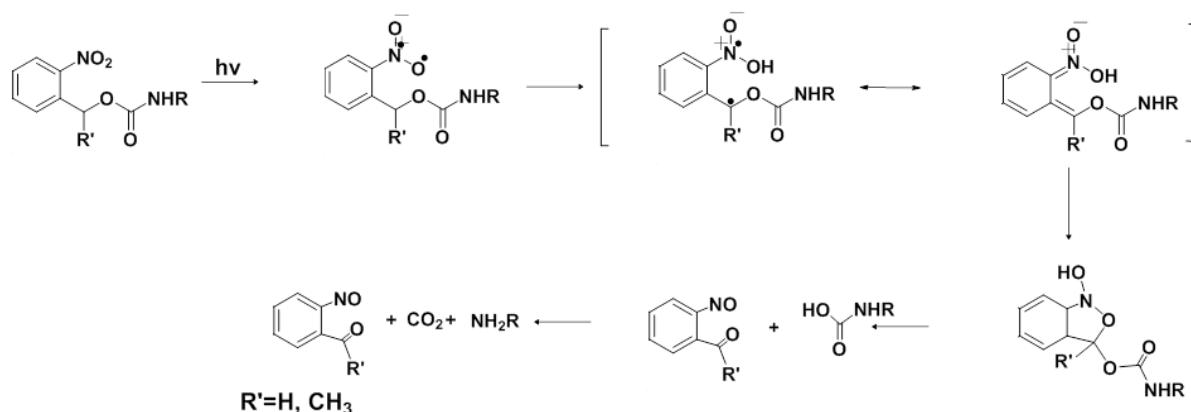


Figure 1.5 Photodegradation mechanism for the o-nitrobenzyl group. Formation of the aci-nitro intermediates and stereoisomers. Final formation of the hemiacetal by ring-opening, and release of the leaving group.⁸²

The rate and quantum yield of the photolysis reaction depend on the leaving group. Also, the photo-absorptive properties and photolysis rates of the o-NB group can be precisely changed by small modifications to the structure such as adding different substitution groups on the aromatic ring of the o-NB (Figure 1.6). The benzylic position can be either primary ($R_1 = -H$) or secondary ($R_1 = -CH_3$).⁸³ Increasing the number of aryl esters (positions X, R_1 , R_2 and R_3) also decreases the quantum yield of the o-NB group at 365 nm.⁶⁰ Insertion of electron donating groups at meta position in o-nitrobenzyl ring (e.g. $-OMe$) leads to increased stability and red shift in cleavage wavelength (λ_{max} shifts from 345 nm to 365 nm) (Figure 1.6).⁸² Various photoreversible groups, substituted at the end site of a wide range of biomolecules, are used for development of photoactive biomaterials.

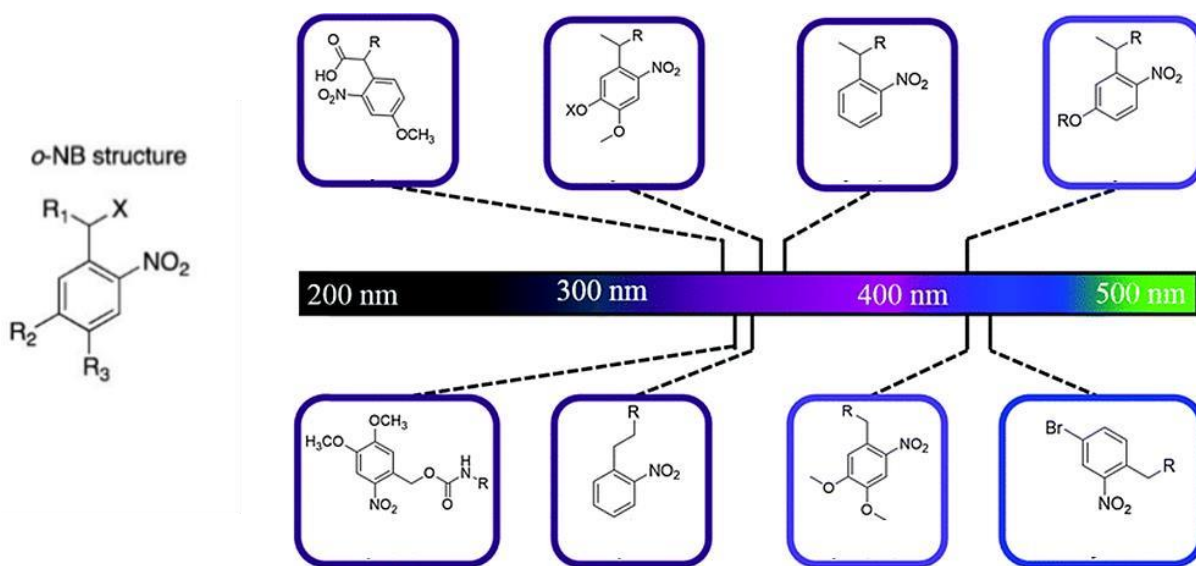


Figure 1.6 Variety of o-Nitrobenzyl derivatives, with different substitution groups tested for their influence in wavelength-selective systems. Structure of o-NB group with common substitutions at R_1 , R_2 and R_3 positions. Images modified with permission from American Chemical Society⁶⁰ and Royal Society of Chemistry.⁸²

The o-NB chemistry has been applied to the design of photodegradable gels for 3D cell culture. Anseth et al.⁸⁴ presented photodegradable hydrogels using an acrylated o-nitrobenzyl ether moiety attached to PEG backbone (PEG-diPDA). These hydrogels degraded

spatiotemporally upon UV-Vis (365 - 405 nm) or two-photon IR light (740 nm) exposure at cytocompatible doses. Hydrogel's photodegradation promoted spreading of encapsulated human mesenchymal stem cells (hMSC) as compared to non-irradiated control hydrogels.⁸⁴ In a different report,⁶⁰ o-nitrobenzyl groups with different cleavable kinetics were incorporated into PEG polymer backbone (Figure 1.7). Red fluorescent protein (RFP)-expressed and green fluorescent protein (GFP)-hMSCs were encapsulated into the hydrogels which were selectively photodegraded in order to release one specific stem cell population.

These initial photodegradable hydrogel systems have evolved to incorporate the capability of multi-function and actuation. Some representative examples are their use as shape-changing, actuating materials for the formation of tubular structures for tissue engineering applications^{60, 77, 84, 85} and the high-throughput culture and release of bacterial cell chips.⁸⁶ Other than their use as matrices for dynamic cell culture and release, the scope of biomedical applications of photodegradable gels is currently moving towards its development as light-based removable wound dressing materials⁵⁸ and their incorporation as dynamic actuators in implantable medical devices, for example in bariatric balloons and esophageal stents.⁸⁷ These exciting applications are transforming our capability to precisely control the activity and performance of biomedical devices *in vivo*. In this line, the possibility to integrate new functions into photodegradable gels is expected to boost the development of novel biomaterials for personalized and less invasive therapies.

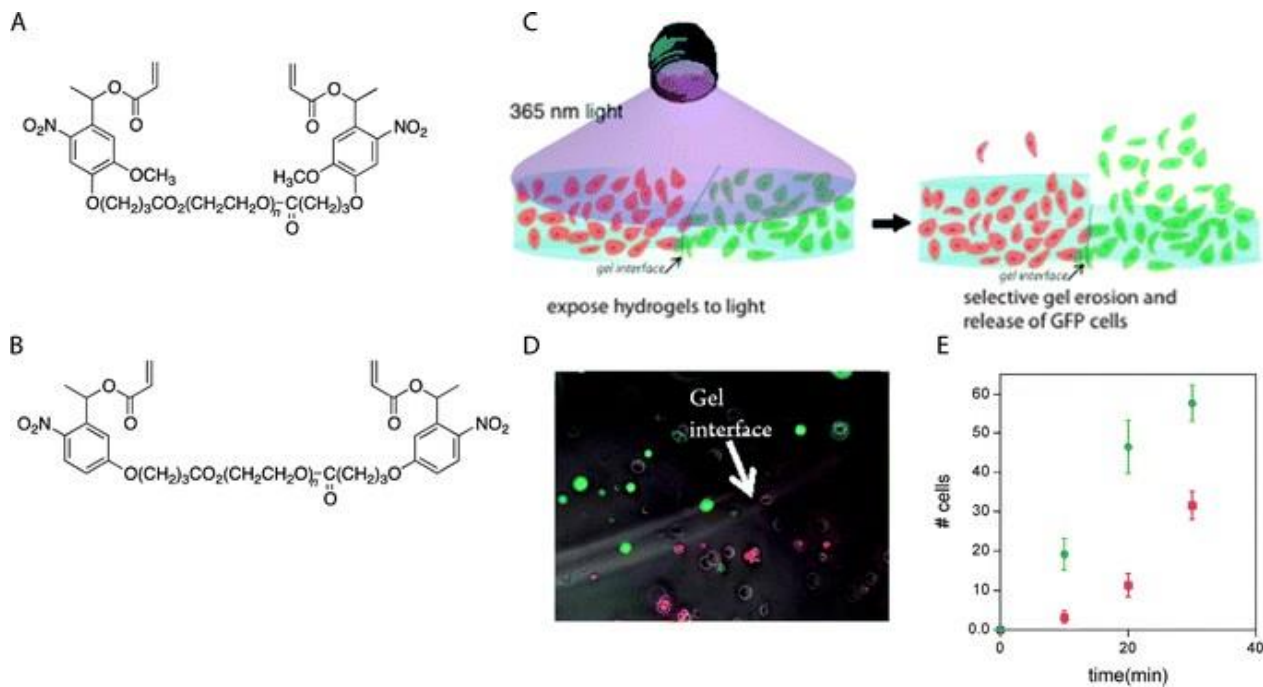


Figure 1.7 Selective photodegradation and cell release using different cleavable linkers. (A), (B) o-Nitrobenzyl linkers; (C) RFP-hMSCs and GFP-MSCs were encapsulated into the hydrogels made with the 2 different o-nitrobenzyl linkers. The 2 hydrogels were in direct contact with each other. (D) The interface between the 2 hydrogels; (E) hydrogels were exposed to light (10 mW cm^{-2} at 365 nm , 30 min , 18 J cm^{-2}). Cell release of one cell population over another occurred ($R_{\text{GFP}}/R_{\text{RFP}} \sim 2.4$) which was consistent with the degradation rate constants of (A) and (B) ($k_{\text{app A}}/k_{\text{app B}} \sim 2.5$). (RFP = red fluorescent protein, GFP = green fluorescent protein) Image reproduced with permission from American Chemical Society. Copyright (2012).⁶⁰

1.5 Poly(ethylene glycol) based hydrogels for cell encapsulation and biomedical applications

Hydrogels are ideal materials for cell culture by being hydrated and having mechanics and crosslinked architecture similar to soft tissues.^{88, 89} The source and composition of the polymer can be natural, such as collagen, gelatin, chitosan to alginates, or synthetic, such as polyethylene glycol (PEG), poly(2-hydroxyethylmethacrylate) (PHEMA), polyacrylamide (PAM), poly(vinyl alcohol) (PVA), or mixtures of them. For cell encapsulation and implantation, the cyto- and biocompatibility is a critical parameter for hydrogels' design.⁹⁰ Numerous natural polymers (i.e. alginate, collagen and fibrin) and a few synthetic (i.e. PEG, PLGA, and PLA) have demonstrated

suitable compatibility and have been approved for specific clinical applications by the Food and Drug Administration (FDA). Hydrogel synthesis should avoid cytotoxic monomers, initiator or crosslinkers. In addition, the by-products of the gelation reaction and those resulting from hydrogel degradation should not be toxic.⁹⁰

Polyethylene glycol (PEG) is a synthetic, nontoxic polymer approved by FDA for usage in different pharmaceutical formulations, food, and cosmetics.⁹¹ It is obtained from ethylene oxide and contains the repeating unit—(O—CH₂—CH₂)—.⁹² PEG is available in a range of molecular weights (Mw <100,000). Star-shaped, multi-arm PEGs (4-,6-,8-arm) are extensively used as precursor molecules for hydrogels for biomedical applications (drug delivery, 3D cell encapsulation or tissue engineering) due to their biocompatibility and low immune response *in vivo*.⁹²⁻⁹⁴ 4-arm PEG is commercially offered in a range of molar masses (Mw = 2.5 KDa, 5 KDa, 10 KDa, 20 KDa or 40 KDa) with different end functional groups depending of the chemical design and final application.⁸⁵

In order to obtain PEG hydrogels, the terminal group of PEG chains should carry reactive groups for crosslinking, such as maleimides, acrylates, vinyl sulfones, thiols, azide, alkynes or catechols (Figure 1.10).⁸⁵ Depending on the crosslinking functionality, PEG hydrogels can be formed via free-radical UV polymerization of PEG diacrylates; Michael-addition reaction between thiol and maleimide or vinyl-sulfone groups;⁹³ strain promoted azide-cyclooctyne cycloaddition⁹⁵, or oxidant-induced reaction of catechol groups^{17, 96-98}

PEG	$\text{R}-\text{O}-\left(\text{CH}_2-\text{CH}_2\right)_n-\text{R}$
R:	Acrylate, methacrylate
	Allyl ether
	Maleimide
	Vinyl sulfone
	NHS ester
	Vinyl ether

Figure 1.10 Some of the end groups of different commercial PEG macromers.⁸⁵

(Copyright to every image belongs to the original source, linked as reference in each text around the image.)

1.6 References

1. Vernengo, A. J., Adhesive materials for biomedical applications. *Adhesives-Applications and Properties* 2016, 6, 111-133.
2. Lauto, A.; Mawad, D.; Foster, L. J. R., Adhesive biomaterials for tissue reconstruction. *Journal of Chemical Technology & Biotechnology: International Research in Process, Environmental & Clean Technology* 2008, 83 (4), 464-472.
3. <https://www.grandviewresearch.com/industry-analysis/medical-adhesives-market>
4. Rahimnejad, M.; Zhong, W., Mussel-inspired hydrogel tissue adhesives for wound closure. *RSC advances* 2017, 7 (75), 47380-47396.
5. Patenaude, M.; Smeets, N. M. B.; Hoare, T., Designing Injectable, Covalently Cross-Linked Hydrogels for Biomedical Applications. *Macromol. Rapid Commun.* 2014, 35 (6), 598-617.
6. Ding, X.; Wang, Y., Weak bond-based injectable and stimuli responsive hydrogels for biomedical applications. *J. Mater. Chem. B* 2017, 5 (5), 887-906.
7. Caló, E.; Khutoryanskiy, V. V., Biomedical applications of hydrogels: A review of patents and commercial products. *Eur. Polym. J.* 2015, 65, 252-267.
8. Paez, J. I.; Farrukh, A.; Valbuena-Mendoza, R.; Włodarczyk-Biegun, M. K.; del Campo, A., Thiol-Methylsulfone-Based Hydrogels for 3D Cell Encapsulation. *ACS Appl. Mater. Interfaces* 2020, 12 (7), 8062-8072.
9. Ghobril, C.; Grinstaff, M. W., The chemistry and engineering of polymeric hydrogel adhesives for wound closure: a tutorial. *Chemical Society Reviews* 2015, 44 (7), 1820-1835.
10. Bouten, P. J. M.; Zonjee, M.; Bender, J.; Yauw, S. T. K.; van Goor, H.; van Hest, J. C. M.; Hoogenboom, R., The chemistry of tissue adhesive materials. *Progress in Polymer Science* 2014, 39 (7), 1375-1405.
11. Feng, J.; Ton, X.-A.; Zhao, S.; Paez, J. I.; Del Campo, A., Mechanically reinforced catechol-containing hydrogels with improved tissue gluing performance. *Biomimetics* 2017, 2 (4), 23.

12. Bochyńska, A.; Hannink, G.; Grijpma, D.; Buma, P., Tissue adhesives for meniscus tear repair: an overview of current advances and prospects for future clinical solutions. *Journal of Materials Science: Materials in Medicine* 2016, 27 (5), 85.
13. Liu, Y.; Meng, H.; Konst, S.; Sarmiento, R.; Rajachar, R.; Lee, B. P., Injectable dopamine-modified poly (ethylene glycol) nanocomposite hydrogel with enhanced adhesive property and bioactivity. *ACS applied materials & interfaces* 2014, 6 (19), 16982-16992.
14. Kowalik, L.; Chen, J. K., Illuminating developmental biology through photochemistry. *Nat. Chem. Biol.* 2017, 13 (6), 587-598.
15. Bilic, G.; Brubaker, C.; Messersmith, P. B.; Mallik, A. S.; Quinn, T. M.; Haller, C.; Done, E.; Gucciardo, L.; Zeisberger, S. M.; Zimmermann, R., Injectable candidate sealants for fetal membrane repair: bonding and toxicity in vitro. *American journal of obstetrics and gynecology* 2010, 202 (1), 85. e1-85. e9.
16. Kastrup, C. J.; Nahrendorf, M.; Figueiredo, J. L.; Lee, H.; Kambhampati, S.; Lee, T.; Cho, S.-W.; Gorbatov, R.; Iwamoto, Y.; Dang, T. T.; Dutta, P.; Yeon, J. H.; Cheng, H.; Pritchard, C. D.; Vegas, A. J.; Siegel, C. D.; MacDougall, S.; Okonkwo, M.; Thai, A.; Stone, J. R.; Coury, A. J.; Weissleder, R.; Langer, R.; Anderson, D. G., Painting blood vessels and atherosclerotic plaques with an adhesive drug depot. *Proceedings of the National Academy of Sciences* 2012, 109 (52), 21444-21449.
17. Ryu, J. H.; Lee, Y.; Kong, W. H.; Kim, T. G.; Park, T. G.; Lee, H., Catechol-functionalized chitosan/pluronic hydrogels for tissue adhesives and hemostatic materials. *Biomacromolecules* 2011, 12 (7), 2653-2659.
18. Puertas-Bartolomé, M.; Vázquez-Lasa, B.; San Román, J., Bioactive and Bioadhesive Catechol Conjugated Polymers for Tissue Regeneration. *Polymers* 2018, 10 (7), 768.
19. Chen, T.; Chen, Y.; Rehman, H. U.; Chen, Z.; Yang, Z.; Wang, M.; Li, H.; Liu, H., Ultratough, Self-Healing, and Tissue-Adhesive Hydrogel for Wound Dressing. *ACS Applied Materials & Interfaces* 2018, 10 (39), 33523-33531.
20. Brubaker, C. E.; Kissler, H.; Wang, L.-J.; Kaufman, D. B.; Messersmith, P. B., Biological performance of mussel-inspired adhesive in extrahepatic islet transplantation. *Biomaterials* 2010, 31 (3), 420-427.

21. Pandey, N.; Soto-Garcia, L. F.; Liao, J.; Philippe, Z.; Nguyen, K. T.; Hong, Y., Mussel-inspired bioadhesives in healthcare: design parameters, current trends, and future perspectives. *Biomaterials Science* 2020, 8 (5), 1240-1255.
22. <https://www.bsnmedical.com/products/wound-care-vascular/category-product-search/acute-wound-care/dressings/leukomedr.html>
23. <https://www.bsnmedical.com/products/wound-care-vascular/category-product-search/acute-wound-care/dressings/covermedr.html>
24. <http://www.urgomedical.com/products/urgostерile/>
25. <https://advancedsurgery.baxter.com/products/preveleak>
26. Pandey, N.; Soto-Garcia, L. F.; Liao, J.; Zimmern, P.; Nguyen, K. T.; Hong, Y., Mussel-inspired bioadhesives in healthcare: design parameters, current trends, and future perspectives. *Biomaterials Science* 2020, 8 (5), 1240-1255.
27. Annabi, N.; Yue, K.; Tamayol, A.; Khademhosseini, A., Elastic sealants for surgical applications. *European journal of pharmaceutics and biopharmaceutics* 2015, 95, 27-39.
28. <https://www.bbraun-asiapacific.com/en/products/b0/tissuglu.html>
29. Liu, Y., Design Of Robust Hydrogel Based On Mussel-Inspired Chemistry. 2017.
30. Krogsgaard, M.; Nue, V.; Birkedal, H., Mussel-inspired materials: self-healing through coordination chemistry. *Chemistry—A European Journal* 2016, 22 (3), 844-857.
31. Martin, S. T.; Kesselman, J. M.; Park, D. S.; Lewis, N. S.; Hoffmann, M. R., Surface structures of 4-chlorocatechol adsorbed on titanium dioxide. *Environmental science & technology* 1996, 30 (8), 2535-2542.
32. Yamamoto, H., Oxidation of synthetic precursors of adhesive proteins from mytilid bivalves using tyrosinase. *J. Mar. Biotechnol.* 1995, 2, 95-100.
33. Jvernengo, A., Adhesive materials for biomedical applications. *Adhesives: Applications and Properties* 2016, 99.
34. Cencer, M.; Liu, Y.; Winter, A.; Murley, M.; Meng, H.; Lee, B. P., Effect of pH on the rate of curing and bioadhesive properties of dopamine functionalized poly (ethylene glycol) hydrogels. *Biomacromolecules* 2014, 15 (8), 2861-2869.
35. Li, J.; Christensen, B. M., Effect of pH on the oxidation pathway of dopamine and dopa. *Journal of Electroanalytical chemistry* 1994, 375 (1-2), 219-231.

36. Burke, S. A.; Ritter-Jones, M.; Lee, B. P.; Messersmith, P. B., Thermal gelation and tissue adhesion of biomimetic hydrogels. *Biomedical materials* 2007, 2 (4), 203.
37. Lee, B. P.; Messersmith, P. B.; Israelachvili, J. N.; Waite, J. H., Mussel-inspired adhesives and coatings. *Annual review of materials research* 2011, 41, 99-132.
38. Lee, B. P.; Dalsin, J. L.; Messersmith, P. B., Synthesis and gelation of DOPA-modified poly(ethylene glycol) hydrogels. *Biomacromolecules* 2002, 3 (5), 1038-1047.
39. Harris, J. M.; Dust, J. M.; McGill, R. A.; Harris, P. A.; Edgell, M. J.; Sedaghat-Herati, R. M.; Karr, L. J.; Donnelly, D. L., New polyethylene glycols for biomedical applications. ACS Publications: 1991.
40. Catron, N. D.; Lee, H.; Messersmith, P. B., Enhancement of poly(ethylene glycol) mucoadsorption by biomimetic end group functionalization. *Biointerphases* 2006, 1 (4), 134-141.
41. Haller, C.; Buerzle, W.; Kivelio, A.; Perrini, M.; Brubaker, C.; Gubeli, R.; Mallik, A.; Weber, W.; Messersmith, P.; Mazza, E., Mussel-mimetic tissue adhesive for fetal membrane repair: An ex vivo evaluation. *Acta biomaterialia* 2012, 8 (12), 4365-4370.
42. Chen, W.; Wang, R.; Xu, T.; Ma, X.; Yao, Z.; Chi, B.; Xu, H., A mussel-inspired poly(γ -glutamic acid) tissue adhesive with high wet strength for wound closure. *Journal of Materials Chemistry B* 2017, 5 (28), 5668-5678.
43. Hong, S.; Yang, K.; Kang, B.; Lee, C.; Song, I. T.; Byun, E.; Park, K. I.; Cho, S.-W.; Lee, H., Hyaluronic Acid Catechol: A Biopolymer Exhibiting a pH-Dependent Adhesive or Cohesive Property for Human Neural Stem Cell Engineering. *Advanced Functional Materials* 2013, 23 (14), 1774-1780.
44. Lee, C.; Shin, J.; Lee, J. S.; Byun, E.; Ryu, J. H.; Um, S. H.; Kim, D.-I.; Lee, H.; Cho, S.-W., Bioinspired, Calcium-Free Alginate Hydrogels with Tunable Physical and Mechanical Properties and Improved Biocompatibility. *Biomacromolecules* 2013, 14 (6), 2004-2013.
45. Shin, J.; Lee, J. S.; Lee, C.; Park, H.-J.; Yang, K.; Jin, Y.; Ryu, J. H.; Hong, K. S.; Moon, S.-H.; Chung, H.-M.; Yang, H. S.; Um, S. H.; Oh, J.-W.; Kim, D.-I.; Lee, H.; Cho, S.-W., Tissue Adhesive Catechol-Modified Hyaluronic Acid Hydrogel for Effective, Minimally Invasive Cell Therapy. *Advanced Functional Materials* 2015, 25 (25), 3814-3824.

46. Koivusalo, L.; Kauppila, M.; Samanta, S.; Parihar, V. S.; Ilmarinen, T.; Miettinen, S.; Oommen, O. P.; Skottman, H., Tissue adhesive hyaluronic acid hydrogels for sutureless stem cell delivery and regeneration of corneal epithelium and stroma. *Biomaterials* **2019**, *225*, 119516.
47. Madl, C. M.; Heilshorn, S. C.; Blau, H. M., Bioengineering strategies to accelerate stem cell therapeutics. *Nature* **2018**, *557* (7705), 335-342.
48. Mehdizadeh, M.; Yang, J., Design strategies and applications of tissue bioadhesives. *Macromolecular bioscience* **2013**, *13* (3), 271-288.
49. Ignacio, C.; Barcellos, L.; Ferreira, M. D.; Moura, S. A. L.; Soares, I. A.; Oréfice, R. L., In vivo tests of a novel wound dressing based on biomaterials with tissue adhesion controlled through external stimuli. *Journal of Materials Science: Materials in Medicine* **2011**, *22* (5), 1357-1364.
50. Chen, F.; Zhu, Y., Chitosan enclosed mesoporous silica nanoparticles as drug nano-carriers: Sensitive response to the narrow pH range. *Microporous and Mesoporous Materials* **2012**, *150*, 83-89.
51. Konieczynska, M. D.; Villa-Camacho, J. C.; Ghobril, C.; Perez-Viloria, M.; Tevis, K. M.; Blessing, W. A.; Nazarian, A.; Rodriguez, E. K.; Grinstaff, M. W., On-Demand Dissolution of a Dendritic Hydrogel-based Dressing for Second-Degree Burn Wounds through Thiol–Thioester Exchange Reaction. *Angewandte Chemie International Edition* **2016**, *55* (34), 9984-9987.
52. Xu, Q.; Guo, L.; A, S.; Gao, Y.; Zhou, D.; Greiser, U.; Creagh-Flynn, J.; Zhang, H.; Dong, Y.; Cutlar, L.; Wang, F.; Liu, W.; Wang, W.; Wang, W., Injectable hyperbranched poly(β -amino ester) hydrogels with on-demand degradation profiles to match wound healing processes. *Chemical Science* **2018**, *9* (8), 2179-2187.
53. Sadat Ebrahimi, M. M.; Schönherr, H., Enzyme-Sensing Chitosan Hydrogels. *Langmuir* **2014**, *30* (26), 7842-7850.
54. Wang, L.; Neumann, M.; Fu, T.; Li, W.; Cheng, X.; Su, B.-L., Porous and responsive hydrogels for cell therapy. *Current Opinion in Colloid & Interface Science* **2018**, *38*, 135-157.
55. Ruskowitz, E. R.; Deforest, C. A., Photoresponsive biomaterials for targeted drug delivery and 4D cell culture. *Nature Reviews Materials* **2018**, *3*.

56. Truong, V. X.; Tsang, K. M.; Simon, G. P.; Boyd, R. L.; Evans, R. A.; Thissen, H.; Forsythe, J. S., Photodegradable Gelatin-Based Hydrogels Prepared by Bioorthogonal Click Chemistry for Cell Encapsulation and Release. *Biomacromolecules* 2015, 16 (7), 2246-2253.
57. Bhagat, V.; Becker, M. L., Degradable adhesives for surgery and tissue engineering. *Biomacromolecules* 2017, 18 (10), 3009-3039.
58. Wu, H.; Qin, Z.; Yu, X.; Li, J.; Lv, H.; Yang, X., On-demand removable hydrogels based on photolabile cross-linkings as wound dressing materials. *Journal of Materials Chemistry B* 2019, 7 (37), 5669-5676.
59. Website: <https://www.lumina.se>; accessed on April 2020
60. Griffin, D. R.; Kasko, A. M., Photodegradable macromers and hydrogels for live cell encapsulation and release. *Journal of the American chemical society* 2012, 134 (31), 13103-13107.
61. <https://www.beriplast.de/>
62. Lee, M.-G. M.; Jones, D., Applications of fibrin sealant in surgery. *Surgical innovation* 2005, 12 (3), 203-213.
63. Mehdizadeh, M.; Weng, H.; Gyawali, D.; Tang, L.; Yang, J., Injectable citrate-based mussel-inspired tissue bioadhesives with high wet strength for sutureless wound closure. *Biomaterials* 2012, 33 (32), 7972-7983.
64. Mahdavi, A.; Ferreira, L.; Sundback, C.; Nichol, J. W.; Chan, E. P.; Carter, D. J.; Bettinger, C. J.; Patanavanich, S.; Chignozha, L.; Ben-Joseph, E., A biodegradable and biocompatible gecko-inspired tissue adhesive. *Proceedings of the National Academy of Sciences* 2008, 105 (7), 2307-2312.
65. Yuan, L.; Wu, Y.; Fang, J.; Wei, X.; Gu, Q.; El-Hamshary, H.; Al-Deyab, S. S.; Morsi, Y.; Mo, X., Modified alginate and gelatin cross-linked hydrogels for soft tissue adhesive. *Artificial cells, nanomedicine, and biotechnology* 2017, 45 (1), 76-83.
66. Balakrishnan, B.; Soman, D.; Payanam, U.; Laurent, A.; Labarre, D.; Jayakrishnan, A., A novel injectable tissue adhesive based on oxidized dextran and chitosan. *Acta biomaterialia* 2017, 53, 343-354.
67. http://www.bmg-inc.com/en/prod_and_res/research/lydex.html
68. Matsumura, K.; Nakajima, N.; Sugai, H.; Hyon, S.-H., Self-degradation of tissue adhesive based on oxidized dextran and poly-L-lysine. *Carbohydrate polymers* 2014, 113, 32-38.

69. Nakayama, Y.; Matsuda, T., Photocurable surgical tissue adhesive glues composed of photoreactive gelatin and poly (ethylene glycol) diacrylate. *Journal of biomedical materials research* 1999, 48 (4), 511-521.
70. Artzi, N.; Shazly, T.; Crespo, C.; Ramos, A. B.; Chenault, H. K.; Edelman, E. R., Characterization of star adhesive sealants based on PEG/dextran hydrogels. *Macromolecular bioscience* 2009, 9 (8), 754-765.
71. Chenault, H. K.; Bhatia, S. K.; DiMaio Jr, W. G.; Vincent, G. L.; Camacho, W.; Behrens, A., Sealing and healing of clear corneal incisions with an improved dextran aldehyde-PEG amine tissue adhesive. *Current eye research* 2011, 36 (11), 997-1004.
72. Kim, K.; Lee, H.; Hong, S., TAPE: a biodegradable hemostatic glue inspired by a ubiquitous compound in plants for surgical application. *JoVE (Journal of Visualized Experiments)* 2016, (112), e53930.
73. Fan, C.; Fu, J.; Zhu, W.; Wang, D.-A., A mussel-inspired double-crosslinked tissue adhesive intended for internal medical use. *Acta biomaterialia* 2016, 33, 51-63.
74. Brubaker, C. E.; Messersmith, P. B., Enzymatically degradable mussel-inspired adhesive hydrogel. *Biomacromolecules* 2011, 12 (12), 4326-4334.
75. Brieke, C.; Rohrbach, F.; Gottschalk, A.; Mayer, G.; Heckel, A., Light-controlled tools. *Angewandte Chemie International Edition* 2012, 51 (34), 8446-8476.
76. Tibbitt, M. W.; Rodell, C. B.; Burdick, J. A.; Anseth, K. S., Progress in material design for biomedical applications. *Proceedings of the National Academy of Sciences* 2015, 112 (47), 14444-14451.
77. Kasko, A. M.; Wong, D. Y., Two-photon lithography in the future of cell-based therapeutics and regenerative medicine: a review of techniques for hydrogel patterning and controlled release. *Future medicinal chemistry* 2010, 2 (11), 1669-1680.
78. Petersen, S.; Alonso, J. M.; Specht, A.; Duodu, P.; Goeldner, M.; del Campo, A., Phototriggering of cell adhesion by caged cyclic RGD peptides. *Angewandte Chemie International Edition* 2008, 47 (17), 3192-3195.
79. Klán, P.; Šolomek, T. s.; Bochet, C. G.; Blanc, A. I.; Givens, R.; Rubina, M.; Popik, V.; Kostikov, A.; Wirz, J., Photoremovable protecting groups in chemistry and biology: reaction mechanisms and efficacy. *Chemical reviews* 2013, 113 (1), 119-191.

80. Gaplovsky, M.; Il'ichev, Y. V.; Kamdzhilov, Y.; Kombarova, S. V.; Mac, M.; Schwörer, M. A.; Wirz, J., Photochemical reaction mechanisms of 2-nitrobenzyl compounds: 2-nitrobenzyl alcohols form 2-nitroso hydrates by dual proton transfer. *Photochemical & Photobiological Sciences* 2005, 4 (1), 33-42.
81. Šolomek, T.; Mercier, S.; Bally, T.; Bochet, C. G., Photolysis of ortho-nitrobenzylic derivatives: the importance of the leaving group. *Photochemical & Photobiological Sciences* 2012, 11 (3), 548-555.
82. Klán, P.; Solomek, T.; Bochet, C. G.; Blanc, A. I.; Givens, R.; Rubina, M.; Popik, V.; Kostikov, A.; Wirz, J., Photoremovable protecting groups in chemistry and biology: reaction mechanisms and efficacy. *Chemical reviews* 2012, 113 (1), 119-191.
83. Zhao, H.; Sterner, E. S.; Coughlin, E. B.; Theato, P., o-Nitrobenzyl alcohol derivatives: opportunities in polymer and materials science. *Macromolecules* 2012, 45 (4), 1723-1736.
84. Kloxin, A. M.; Kasko, A. M.; Salinas, C. N.; Anseth, K. S., Photodegradable hydrogels for dynamic tuning of physical and chemical properties. *Science* 2009, 324 (5923), 59-63.
85. Kasko, A., Degradable poly (ethylene glycol) hydrogels for 2D and 3D cell culture. *Aldrich Materials Science* 2013, 67-75.
86. van der Vlies, A. J.; Barua, N.; Nieves-Otero, P. A.; Platt, T. G.; Hansen, R. R., On Demand Release and Retrieval of Bacteria from Microwell Arrays Using Photodegradable Hydrogel Membranes. *ACS Applied Bio Materials* 2018, 2 (1), 266-276.
87. Raman, R.; Hua, T.; Gwynne, D.; Collins, J.; Tamang, S.; Zhou, J.; Esfandiary, T.; Soares, V.; Pajovic, S.; Hayward, A.; Langer, R.; Traverso, G., Light-degradable hydrogels as dynamic triggers for gastrointestinal applications. *Science Advances* 2020, 6 (3), eaay0065.
88. Caliari, S. R.; Burdick, J. A., A practical guide to hydrogels for cell culture. *Nature methods* 2016, 13 (5), 405.
89. Tibbitt, M. W.; Anseth, K. S., Hydrogels as extracellular matrix mimics for 3D cell culture. *Biotechnology and bioengineering* 2009, 103 (4), 655-663.
90. Kharkar, P. M.; Kiick, K. L.; Kloxin, A. M., Designing degradable hydrogels for orthogonal control of cell microenvironments. *Chemical Society Reviews* 2013, 42 (17), 7335-7372.
91. <https://www.sigmadralich.com/materials-science/material-science-products.html?TablePage=20204110>

92. Hutana, D.; Frishberg, M. D.; Guo, L.; Darie, C. C., Recent applications of polyethylene glycols (PEGs) and PEG derivatives. *Mod. Chem. Appl.* 2014, 2 (2), 1-6.
93. Phelps, E. A.; Enemchukwu, N. O.; Fiore, V. F.; Sy, J. C.; Murthy, N.; Sulcek, T. A.; Barker, T. H.; García, A. J., Maleimide cross-linked bioactive peg hydrogel exhibits improved reaction kinetics and cross-linking for cell encapsulation and in situ delivery. *Advanced materials* 2012, 24 (1), 64-70.
94. Marchant, R.; Anderson, J.; Dillingham, E., In vivo biocompatibility studies. VII. Inflammatory response to polyethylene and to a cytotoxic polyvinylchloride. *Journal of biomedical materials research* 1986, 20 (1), 37-50.
95. DeForest, C. A.; Sims, E. A.; Anseth, K. S., Peptide-functionalized click hydrogels with independently tunable mechanics and chemical functionality for 3D cell culture. *Chemistry of materials* 2010, 22 (16), 4783-4790.
96. Kim, K.; Ryu, J. H.; Lee, D. Y.; Lee, H., Bio-inspired catechol conjugation converts water-insoluble chitosan into a highly water-soluble, adhesive chitosan derivative for hydrogels and LbL assembly. *Biomaterials science* 2013, 1 (7), 783-790.
97. Neto, A. I.; Cibrão, A. C.; Correia, C. R.; Carvalho, R. R.; Luz, G. M.; Ferrer, G. G.; Botelho, G.; Picart, C.; Alves, N. M.; Mano, J. F., Nanostructured Polymeric Coatings Based on Chitosan and Dopamine-Modified Hyaluronic Acid for Biomedical Applications. *Small* 2014, 10 (12), 2459-2469.
98. Quan, W.-Y.; Hu, Z.; Liu, H.-Z.; Ouyang, Q.-Q.; Zhang, D.-Y.; Li, S.-D.; Li, P.-W.; Yang, Z.-M., Mussel-inspired catechol-functionalized hydrogels and their medical applications. *Molecules* 2019, 24 (14), 2586.

Chapter 2: Synthesis and physicochemical characterization of photodegradable and tissue-adhesive PEG-catechol precursors

2.1 Abstract

In this chapter the molecular design and synthesis of photodegradable and tissue-adhesive macromers is reported. The chemical structure is based on star-polyethylene glycol (PEG) macromers terminated with catechol groups for crosslinking and bonding. A photocleavable nitrobenzyl triazole or nitrobenzyl ester unit for photodegradation is intercalated in the polymer backbone. The synthesis pathway and the structural characterization of the polymers as well as the analysis of the photochemical and hydrolytic stability properties are described.

2.2 Introduction

The ability of mussels¹ to firmly stick to wet rocks is based on the high content of the amino acid L-3,4-dihydroxyphenylalanine (DOPA) in their mussel foot adhesive proteins. DOPA contains a catechol side chain that can form metal complexes with inorganic oxides, and also be oxidized in seawater to form reactive quinone intermediates that covalently interact with nucleophiles (i.e., $-NH_2$, $-SH$) in the protein structure to form an insoluble protein material (see Figure 1.2, Chapter 1).^{1,2}

The versatility of catechol to take part in several chemical reaction pathways has inspired the chemical design of hydrogel materials to attach to tissues and to encapsulate living cells. Several examples of catechol containing polymers have been reported for envisioned application as medical tissue adhesives, sealants, hemostatic agents, and materials for 2D and 3D cell culture.³

⁶ Pioneering work by Messersmith and coworkers⁷ first reported the use of mussel-inspired hydrogels as carrier material for islet cell transplantation. A hydrogel based on polyethylene glycol (PEG) functionalized with catechols was used for this purpose. The transplanted construct remained adhered to liver tissue for over 4 months, and the embedded islet cells remained functional and secreted insulin.

Nitro-substituted catechol derivatives are also naturally occurring molecules. For example 6-nitrodopamine (NDop) and 5-nitronorepinephrine (NNPE) (Figure 2.1) take part in nitric oxide

(NO) metabolism and in the neural system.⁸ The presence of the electron-withdrawing nitro group at the 6-position changes the electronic properties of the catechol ring: the pKa of the catechol hydroxyl groups decreases ($pKOH_1 \approx 6.5$ and $pKOH_2 \approx 10$ for nitrocatechols vs $pKOH_1 \approx 9.2$ and $pKOH_2 \approx 13$ for unsubstituted catechols)⁹ and the acidity and hydrogen bond donor character increases, as well as their stability against oxidation.¹⁰ In addition, the presence of the nitro group in NDop and NNPE makes these molecules photoactive. In fact, o-nitrophenylethyl (o-NP) and o-nitrobenzyl (o-NB) moieties are the most widely applied photoremoveable groups in biomaterials development^{10, 11}.

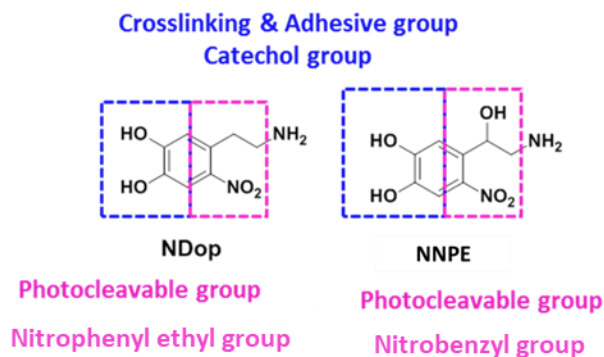


Figure 2.1 Chemical structure of **NDop** and **NNPE**. The catechol group, which shows crosslinking and adhesive properties, is highlighted in blue; while the photocleavable nitro-containing group is highlighted in pink.

The photolysis mechanism of o-NP derivatives is represented in Figure 2.2. It starts with the formation of an aci-nitro intermediate by intramolecular H-transfer from the exocyclic α -position to the nitro group. Then, a protolytic dissociation of the aci-nitro derivative follows with the release of the leaving functional group (in the Figure, an amide is shown).¹⁰ The α -substituent prevents the side reactions between the photoproduct (o-nitrostyrene) and amine to form an imine.

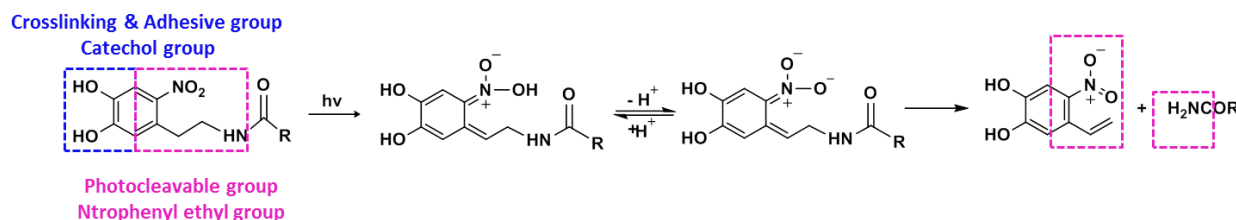


Figure 2.2 Mechanism of the photofragmentation of o-nitrophenylethyl (o-NP) derivatives, in this case exemplified by the photolysis of nitro-dopamine (NDop) moiety.

Del Campo's group reported a photodegradable mussel-inspired hydrogel system based on the nitro-dopamine (NDop) group as photodegradable and adhesive unit.¹⁰ For this purpose, a star-PEG was end-functionalized with terminal NDop (PEG-NDop, Figure 2.3). The nitro-catechol groups allowed crosslinking under mild oxidative conditions and generation of a chemically crosslinked hydrogel. Light exposure to UV irradiation at $\lambda = 360$ nm (Figure 2.3) allowed depolymerization of the hydrogel by photolysis of the o-NP linker (see Fig. 2.2).¹⁰ However, the required irradiation dose for the photodegradation of PEG-NDop polymer was very high (84.7 J cm⁻²) due to the low photolytic efficiency inherent to the nitro-dopamine chromophore (a o-NP chromophore where the amide is a poor leaving group) .^{10, 12} This feature makes this system incompatible with living cells and not applicable to an *in vivo* scenario. An alternative molecular design based on nitro-norepinephrine will be presented in this chapter. This novel design involves an o-NB group which confers better photodegradability to the hydrogel and was selected due to its favorable absorbance properties and photo-kinetics,¹³ as well as demonstrated non-toxicity of photolysis products *in vitro* and *in vivo*.¹⁴ Under light illumination ($\lambda = 365\text{-}405$ nm), the o-NB moiety is cleaved to generate a nitroso-benzyl derivative and therefore enables photomodulated depolymerization of the hydrogel.

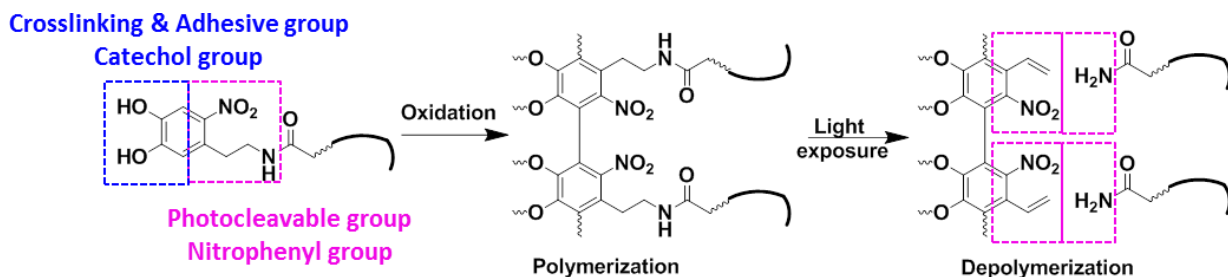


Figure 2.3 Polymerization and depolymerization of PEG-NDop polymer, $\lambda = 360$ nm. Modified after permission from Wiley Online Library¹⁰

Light-degradable hydrogels based on o-nitrophenyl chemistry have been developed by other groups as well. Anseth and her team¹⁵ reported acrylated terminated PEG-based hydrogels modified with nitrobenzyl ester (NBe) derivatives that cleave upon UV-light exposure at 365 nm

(Fig. 2.4 a).⁴⁻⁶ The NBe group has high photosensitivity due to the good leaving character of the ester group. However it lacks long-term hydrolytic stability: under physiological conditions, the ester group hydrolyzes⁵. This feature makes derived hydrogels not suitable for long term cell culture. In contrast to NBe, the nitrobenzyl triazole linkage, NBt, is expected to present higher hydrolytic stability. Qvortrupa and Nielsen presented the first photolabile NBt linker (see photolysis mechanism in Fig. 2.4b).¹⁶ The triazole group has been employed as hydrolytically stable mimic for amide in acidic and basic conditions used in solid-phase synthesis of oligonucleotides and peptides.

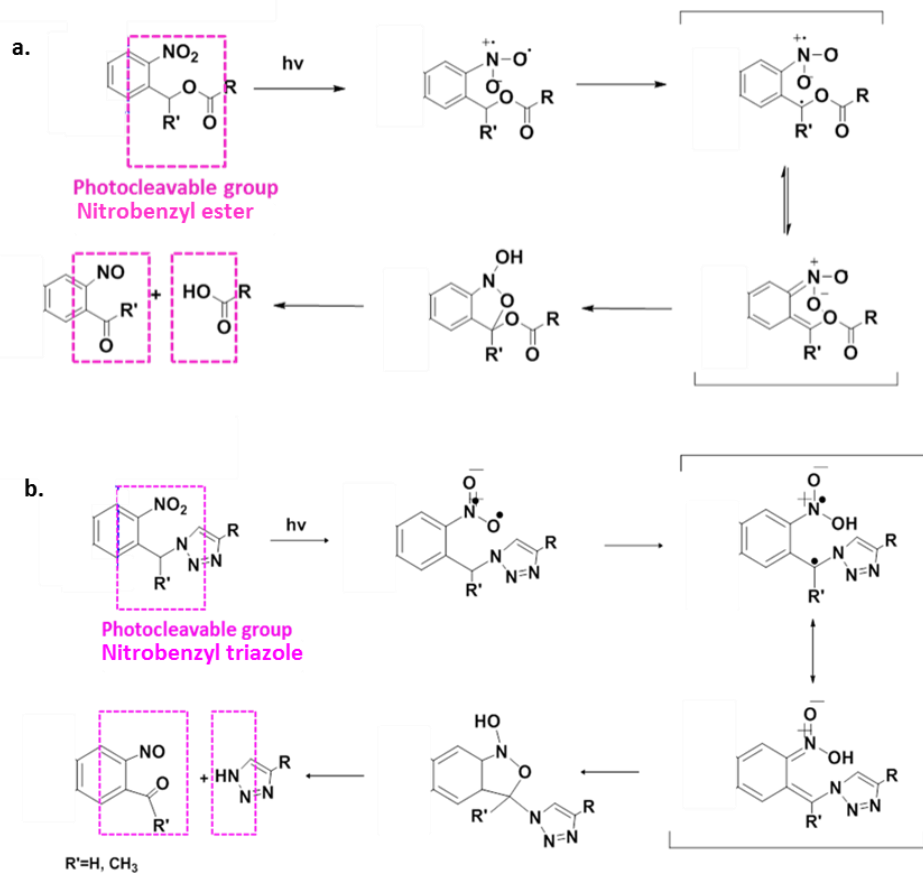


Figure 2.4 a) Photolysis of a NBe moiety, $\lambda = 365$ nm.¹⁷ Upon light exposure, the photochemical mechanism starts with radical formation at nitro moiety, following by cyclization reaction between the hydroxyl moiety of nitro group and benzylic carbon. The molecule rearranges with cleavage of bond between nitrogen and oxygen in the ring and oxygen and benzylic carbon to form ketone or aldehyde and carbamic acid.¹⁸ b) Photolysis of a NBt moiety, as reported by Qvortrupa and Nielsen.¹⁶

Exposure doses between 5 and 36 J cm⁻² ($\lambda = 365$ nm, Irradiance = 5 – 20 mW cm⁻² and time exposure time 2 – 30 min) have been demonstrated to be cytocompatible while being enough to degrade NB based hydrogels.⁴⁻⁶ These gels were formed starting from 10 - 20 kDa star-PEGs at 5 wt% concentration, and presented a mechanical strength signed by a shear modulus, G', of 1.5 - 5 kPa.⁴⁻⁶ This composition range will guide the design of photodegradable hydrogels in this chapter. The targeted hydrogel precursors will contain photolabile groups based on the o-nitrobenzyl moiety (o-NB, Figure 2.5), which has a higher photosensitivity than the o-nitrobenzylethyl group in NDop. The physicochemical and photolytic properties of the precursors and derived hydrogels will be evaluated and compared to previous reported photodegradable PEG derivatives. The new designs target long-term hydrolytic stability for cell culture and a photolytic efficiency that is good enough to allow hydrogel degradation under cytocompatible exposure conditions.

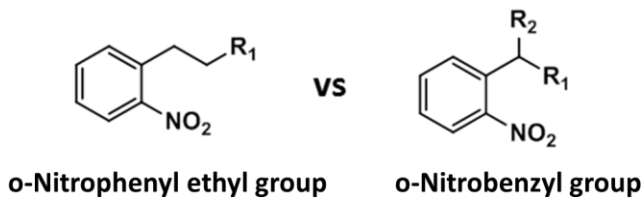


Figure 2.5 Photodegradable chromophores; o-Nitrophenyl ethyl vs o-Nitrobenzyl group.

2.3 Molecular design of photodegradable PEG-catechol precursors

Two different molecular designs were explored to introduce crosslinkable, tissue-adhesive and photodegradable units to PEG backbones (Figure 2.6). In the first approach, adhesion and photolysis functionalities were included within the terminal group of the PEG-macromer (Figure 2.6A). For this purpose 6-nitronorepinephrine (NNPE) was selected since it contains crosslinkable and photodegradable moieties in a single unit. Previous work from our group (results not shown) demonstrated a significantly higher photoefficiency of the nitro-norepinephrine (NNPE) group in relation to the nitro-dopamine (NDop) chromophore. In particular, **PEG-NNPE** (Irradiation dose = 11.8 J cm⁻²), showed 10 fold¹⁹ better photolytic efficiency ($\lambda = 420$ nm, Irradiance: = 4.7 mW cm⁻²) compared to **PEG-NDop** (Irradiation dose = 135.5 J cm⁻²). These results indicate that nitrobenzyl

group contained in **PEG-NNPE** has good photolytic efficiency, which is the first requirement towards reasonable cytocompatibility for use in live cell culture and imaging.^{20, 21} The NNPE was linked to a dibenzocyclooctyne (DBCO) terminated PEG via a triazole unit (Figure 2.3A). By introducing a triazole group at the benzylic site, an electronic effect is expected that would increase the photoefficiency of the system in comparison to o-nitrophenyl ethyl group.¹⁷ The terminal catechol group allows crosslinking and tissue adhesion.

In an alternative design, the light-cleavable and tissue-adhesive functionalities were decoupled from each other: a nitrobenzyl photocleavable group was intercalated between the PEG chain and terminal catechol units (Figure 2.6B). The nitrobenzyl group was linked to the PEG by a triazole (Figure 2.6Bi) or by an ester group (Figure 2.76Bii). The substitution at benzylic carbon tunes the photochemical properties of nitro-derivatives. For example, the introduction of substituent (e.g. methyl group) at benzylic carbon increases the quantum yield and also influences hydrolytic stability and solubility of the molecule.¹⁷ This is the first report where the photoefficiency of the triazole unit is compared to an ester substitution. Moreover, under physiological conditions, the triazole linker is expected to be more hydrolytically stable than the ester group.¹⁵

In both designs, 4-arm poly(ethylenglycol) (PEG) were used as the cytocompatible polymeric precursor²² of molar mass= 10 and 20 kDa, since previous work demonstrated that such size range is relevant for 3D cell encapsulation applications.²³ The photodegradable hydrogel precursors were modified with adhesive and crosslinkable catechol end-groups, since they are able to interact covalently and non-covalently with a variety of materials,² including the surface of living cells²⁴ and tissues.^{7, 25}

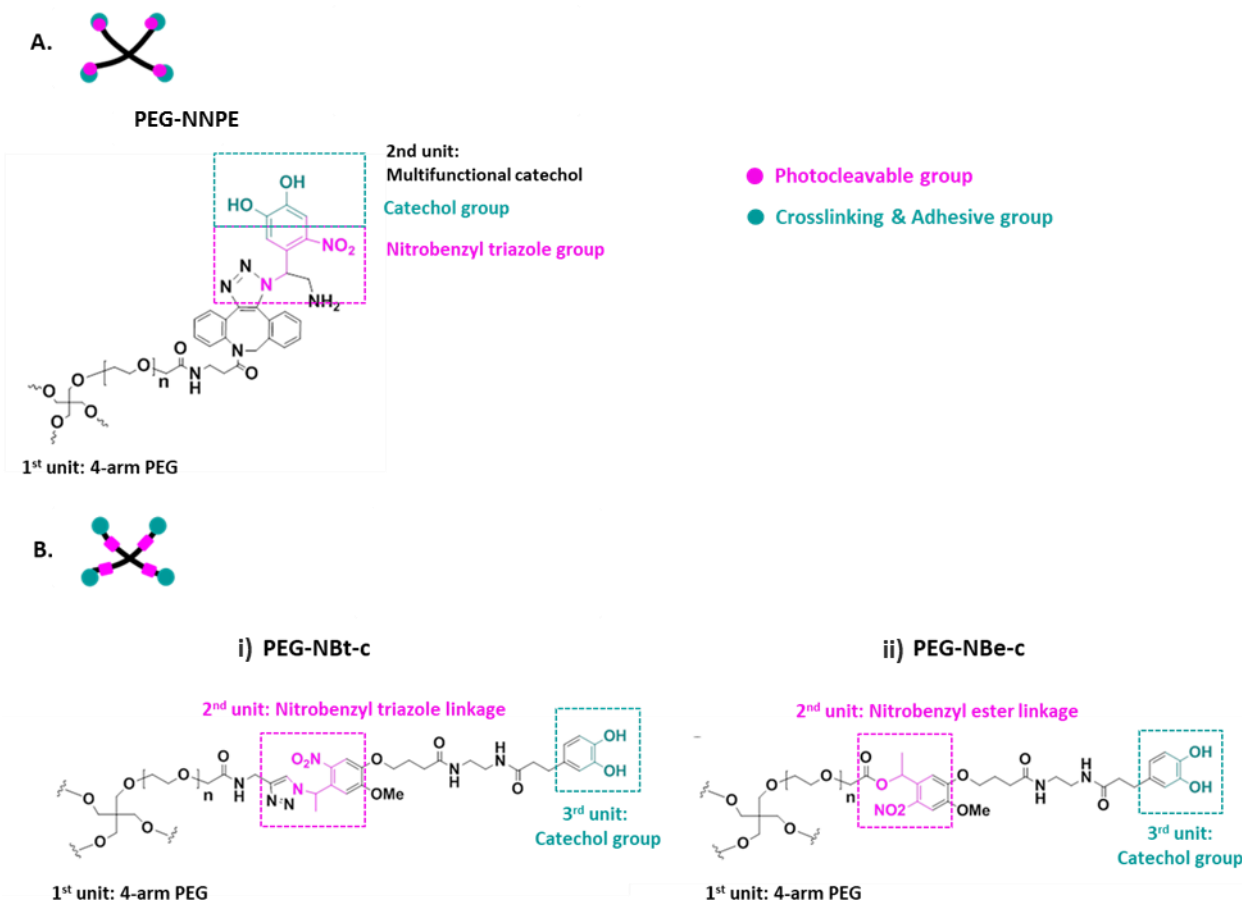


Figure 2.6 Chemical structures of the new synthesized photodegradable PEG-catechol precursors:
A) PEG-NNPE; B) PEG-Nbt-c (i) and PEG-NBe-c (ii).

2.4 Results and Discussion

2.4.1 Synthesis of macromers

The synthesis and isolation of catechol-containing compounds needs to take into account the high susceptibility of the catechol ring to oxidation, and the reactivity of the oxidized products towards nucleophiles. Several synthetic strategies were tested for preparation of the multifunctional macromers, including varying the coupling order among the different blocks, using protected catechols and free catechols, and using different connectivity between PEG and the photocleavable linker (ester and triazole linkages).

PEG-NNPE

In the first synthetic approach, linking 6-nitronorepinephrine to $-COOH$ terminated starPEG was attempted. For this purpose norepinephrine was first nitrated by electrophilic aromatic substitution using $NaNO_2$ (Figure 2.7i). 6-nitronorepinephrine (**1**) was obtained in good yield (85 %). In order to avoid interference of the free amine in the following steps, (**1**) was protected with a fluorenylmethyloxycarbonyl (Fmoc) to obtain (**2**). First attempts to link (**2**) to a 4-arm PEG-COOH polymer through chemoselective acylation of the secondary $-OH$ group proved unsuccessful (Figure 2.8). A mixture of acylation products of the secondary $-OH$ and the aromatic $-OH$ were obtained, presumably due to the comparable reactivity of those functional groups.²⁶ An alternative route was taken by first protecting the catechol hydroxyls (**3**), and then acylating the secondary $-OH$ with PEG-COOH. Acylation was possible (**4**), but the ester linkage cleaved off in the following deprotection conditions: either amine deprotection reaction (20 % piperidine in DMF); or catechol deprotection reaction (25% TFA, H_2O) shown in the Figure 2.7.

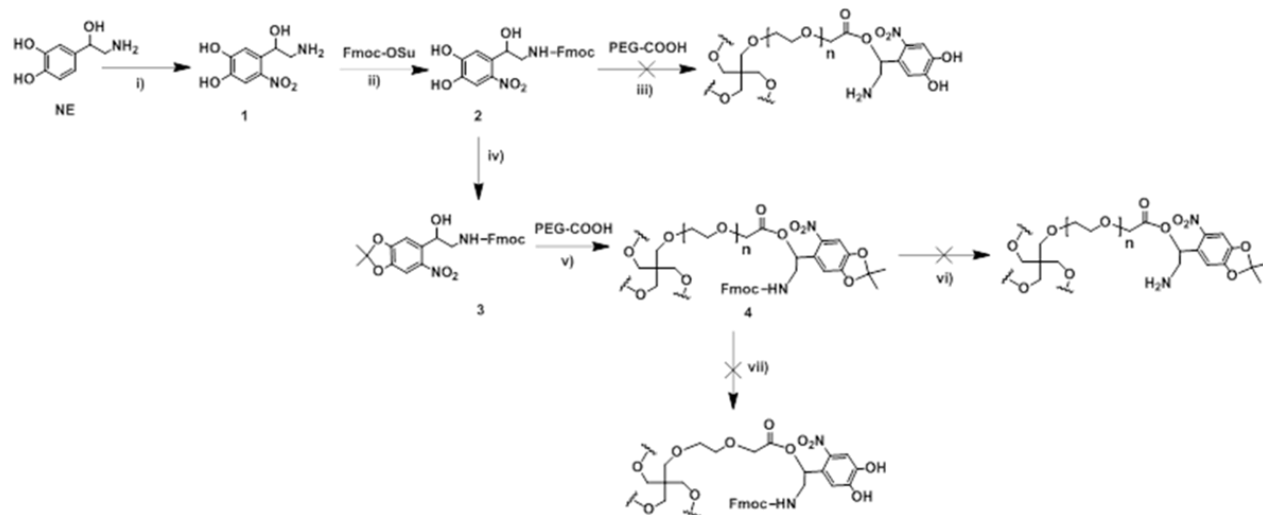


Figure 2.7 First synthetic pathways to obtain PEG-NNPE macromer. Reagents and conditions: i) $NaNO_2$ / water 20% H_2SO_4 , 0 °C, 1 h, yield= ??; ii) 10% Na_2CO_3 :dioxane, 24 h, yield=40%; iii) DCC,DCM,DMAP, room temperature, overnight; iv) DMP, PTSA, toluene, reflux, overnight, yield=80%; v) DCC, DCM, DMAP, room temperature, overnight, yield=75%; vi) 20 % piperidine, DMF, N_2 , room temperature, overnight; vii) 25% TFA, H_2O , 3 h, room temperature.

An alternative approach to avoid the need of catechol protection was pursued (Figure 2.8) by derivatization of (**1**) with an azide group, and reaction with dibenzylcyclooctyne (DBCO) functionalized PEG by a catalyst-free click reaction. The $-N_3$ group is orthogonal to many other

functionalities and provides the possibility for chemo-selective conjugation to the strained alkyne in DBCO (Figure 2.8). In order to avoid interference of the free amine in the following steps, the amine was protected with Fmoc group, and then the secondary –OH of (**2**) was converted into an azide group by bimolecular nucleophilic substitution in two steps, followed by HPLC, FT-IR, ¹H-NMR and mass analysis. The –OH was first derivatized to a -Cl group by reaction with thionyl chloride to yield (**3**). The -Cl substitution was identified by a strong band in the FT-IR spectrum at $\nu = 800 \text{ cm}^{-1}$ (stretching vibration of Cl-C bond) (Section 2.2, Appendix) and by the appearance of a new peak in HPLC chromatography at retention time 28 min (Section 2.2, Appendix). The -Cl group was converted to an azide group (**4**) by reaction with sodium azide. The reaction was confirmed by FT-IR (appearance of a new signal at $\nu = 2105 \text{ cm}^{-1}$ indicating the stretching vibration of azide group) and mass analysis with peaks at 462.2 ([M+H]⁺, 479.2 [M+NH₄]⁺). (Section 2.2, Appendix). In addition, a new peak at retention time 26 min was observed by HPLC chromatography (Section 2.2, Appendix). Fmoc deprotection in 20 % piperidine afforded (**5**) and was confirmed by the disappearance of the Fmoc protons (chemical shift: 7-8 ppm) in ¹H-NMR (Figure 2.9). HPLC chromatography showed a new peak at retention time 3-4 min, and mass analysis gave the expected peak at 278.0 [M+K]⁺. The reaction conditions for each step were optimized (optimizing the concentration of the reagents, temperature and reaction time) to obtain yields between 40 and 70%.

In parallel, commercial PEG functionalized with N-hydroxysuccinimide (NHS) ester (**PEG-NHS**) was reacted with DBCO-amine to synthesize the macromer **PEG-DBCO**. The ¹H-NMR spectrum showed the protons corresponding to the DBCO-end group at 7-8 ppm. These signals were compared to the signals corresponding to the PEG core at 3.4-3.7 ppm, and therefore the functionalization degree was quantified as >82% (Section 2.2, Appendix). Then, (**5**) was covalently linked to **PEG- DBCO** by strain-promoted azide-cyclooctyne cycloaddition to obtain **PEG-NNPE** macromer. The end-group functionalization degree was determined by comparing the area of the aromatic protons of (**5**) at 7.49 and 7.66 ppm and the catechol signal at 8.95 ppm in the ¹H-NMR spectrum(Figure 2.10). A >84% substitution degree was obtained. PEG-NNPE was soluble in water and PBSat final concentration 10 wt%.

PEG-NNPE was obtained at low scale (< 30 mg). Attempts to upscaling were unsuccessful because the intermediates (**3**) and (**5**) were unstable. Disappearance of the catechol protons

during storage at -20°C was observed by $^1\text{H-NMR}$ within 20 days, presumably due to oxidation. Moreover, the precursor PEG-DBCO also showed poor stability (< 2-3 weeks) and had to be prepared fresh. These features make this synthetic route and the derived compound not suitable from an application point of view. Therefore, alternative molecular designs were planned to obtain stable macromers at higher scale.

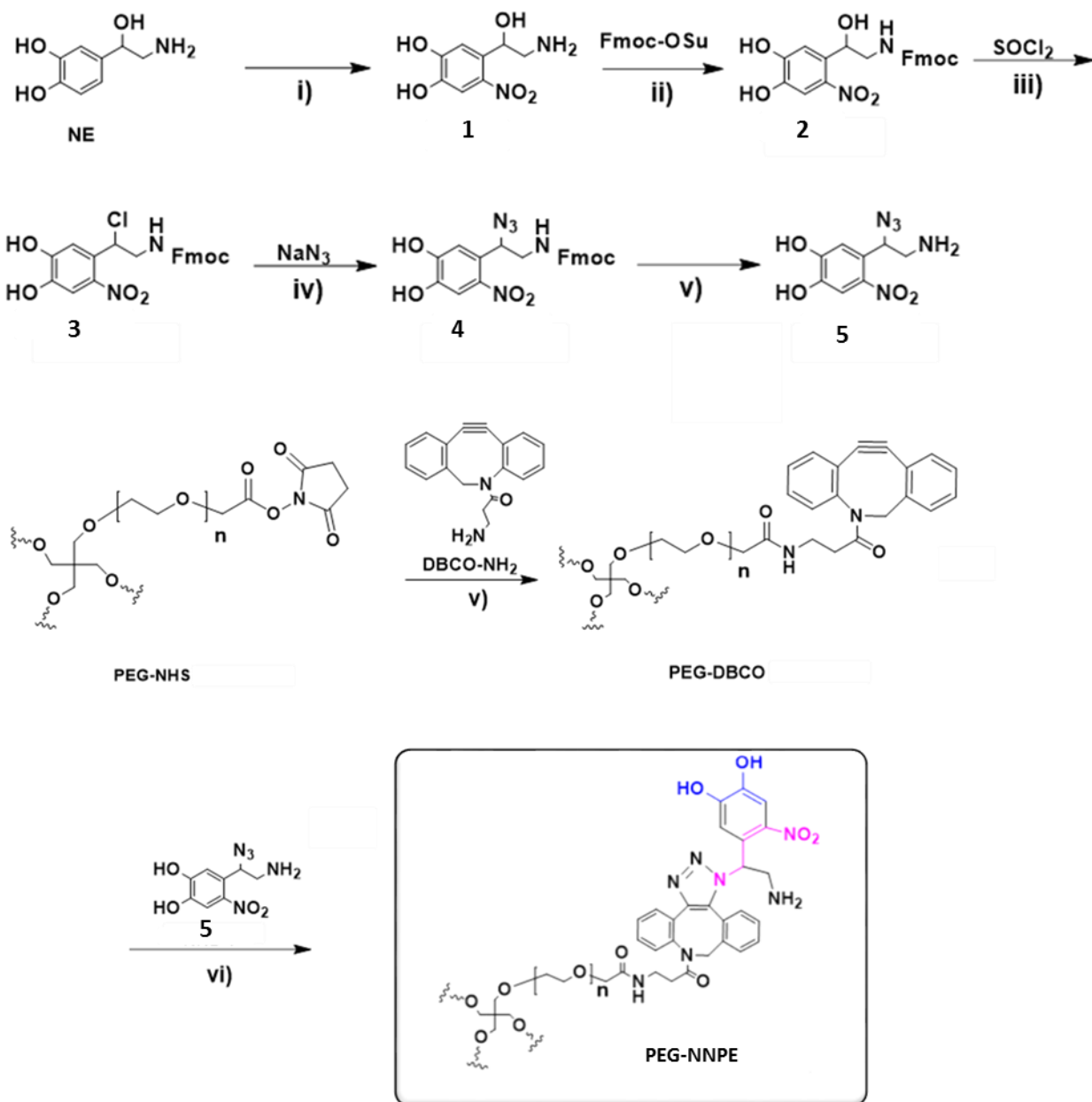


Figure 2.8 Second synthesis route of PEG-NNPE. Reagents and conditions: i) NaNO_2 / water 20% H_2SO_4 , 0 °C, 1 h; ii) 10% Na_2CO_3 :dioxane, 24 h, yield=40%; iii) DCM, DMF, room temperature, 3 h;

iv) DMF, 60 °C, overnight, yield=70%; v) 20% piperidine, DMF, room temperature, 10 min; v) NMM, DMF, N₂, room temperature, overnight, yield=87%; vi) 4NMP:H₂O, room temperature, overnight, yield=85%.

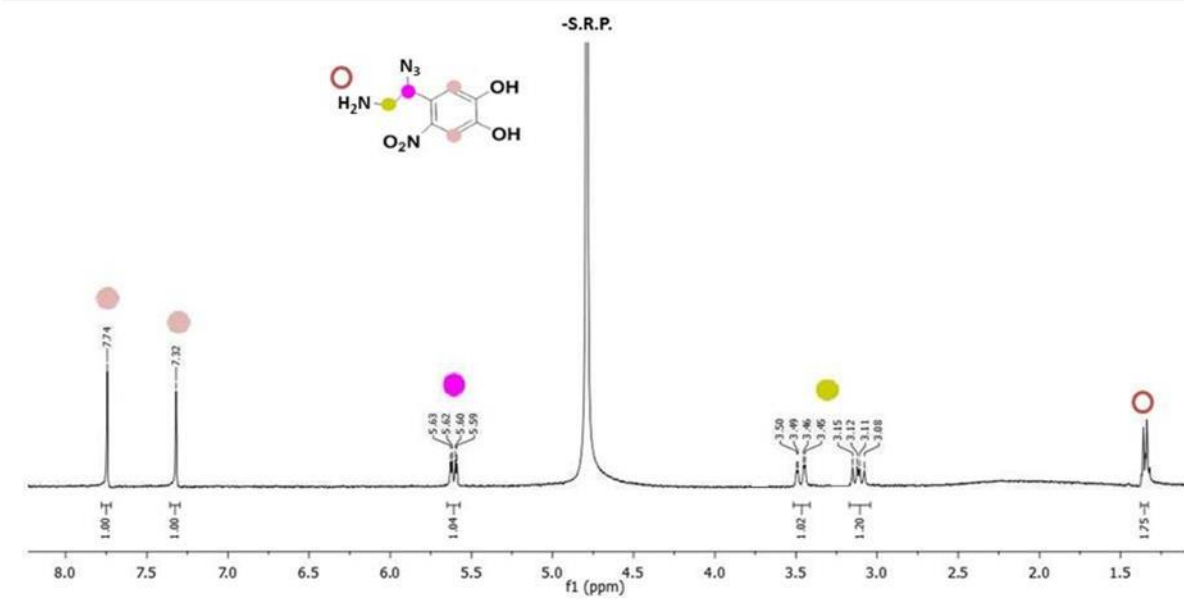
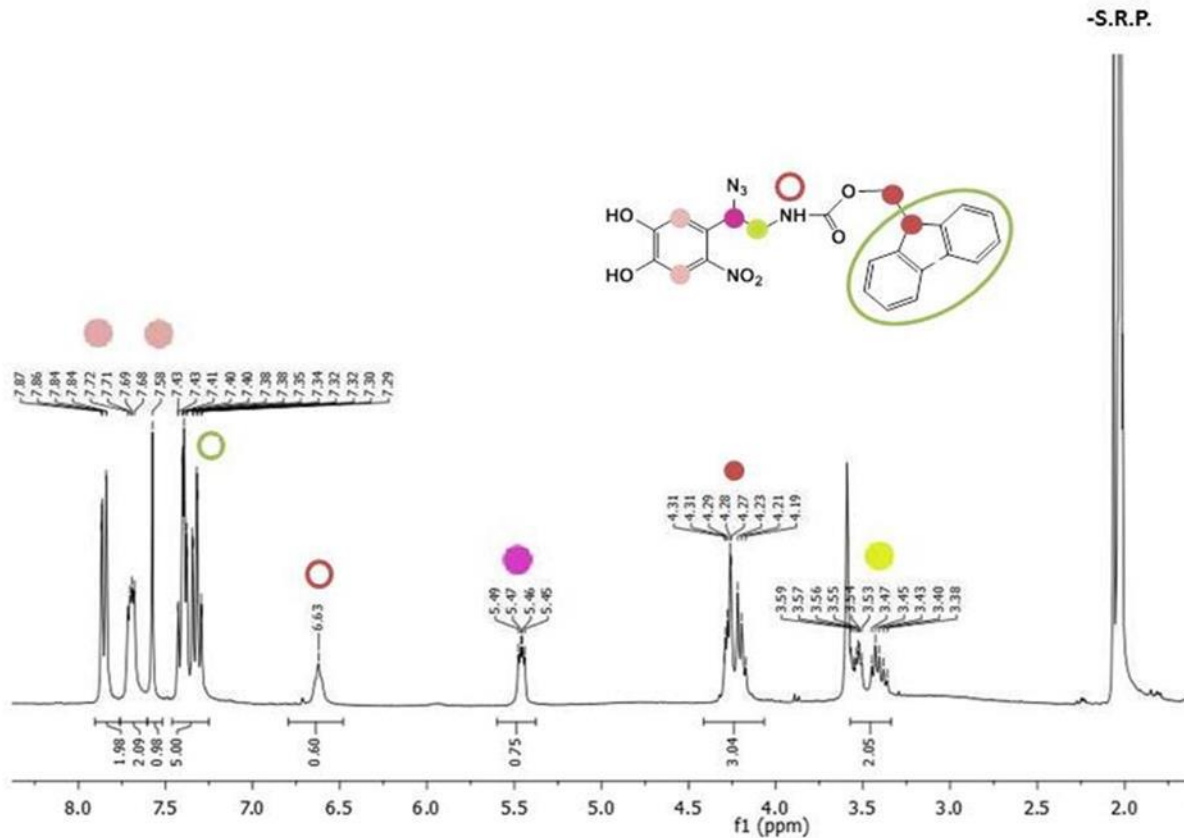


Figure 2.9 ^1H spectrum of NNPE derivatives (**4, 5**)

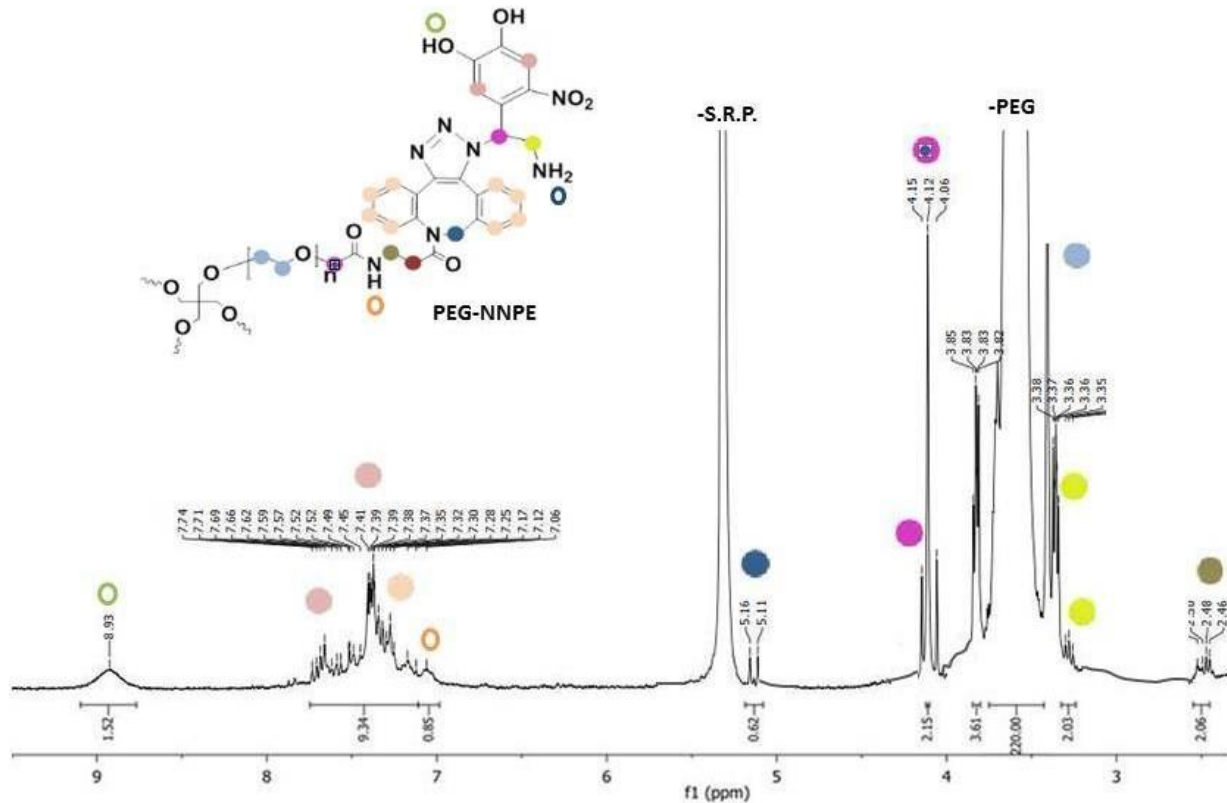


Figure 2.10 ^1H spectrum of PEG-NNPE

Synthesis of PEG-NBt-c and PEG-NBe-c

An alternative molecular design was conceived, in which the photocleavable and catechol groups would be added sequentially to the macromer. This way should allow incorporation of the reactive catechol group at the final step of the synthesis route and improve the scalability of the synthesis. Figure 2.3B shows the final molecular structures, **PEG-NBt-c** and **PEG-NBe-c**. NB stands for nitrobenzyl group; “t” or “e” stand for triazole or ester linkage, and refer to the chemical connectivity between the nitrobenzyl group and the PEG backbone; “c” stands for the terminal catechol group.

PEG-NBt-c

The carboxylic acid of the commercial chromophore 4-[4-(1-Hydroxyethyl)-2-methoxy-5-nitrophenoxy]butyric acid (**NB**) was reacted to the amine group of N-Boc-ethylendiamine to obtain **NB-1**. Amide formation was favored vs. the ester formation (the latter is the undesired coupling of –COOH to the –OH groups) by the choice of reaction conditions: room temperature, reaction time 6 h, use of an highly polar organic solvent as DMF and coupling agents mixture (HBTU, HOBT and DIPEA). The amide formation was identified by the new signal of the proton of the amide group at 6.08 ppm, also the Boc signal from N-Boc-ethylendiamine showed a characteristic signal at 1.38 ppm (**NB-1**, Figure 2.12). The –OH of **NB-1** was converted into –N₃ group by two nucleophilic substitution steps: mesylation (**NB-2**) followed by azidation with NaN₃ to form an azide group (**NB-3**, Figure 2.11). The final product was identified by ¹H-NMR (Section 2.3, Appendix) where the amide signal was shifted from 6.08 ppm to 5.11 ppm; by FT-IR spectroscopy ($\nu = 2112\text{ cm}^{-1}$ indicating the stretching vibration of azide group, Section 2.3, Appendix) and by mass spectrometry ($[\text{M}+\text{H}]^+ = 467.2$). The reaction conditions for each step were optimized to obtain yields between 40 and 80%.

To avoid the use of PEG-DBCO (for stability reasons mentioned above), a copper-catalyzed azide-alkyne cycloaddition was devised to anchor **NB-3** to PEG-alkyne.¹⁶ **PEG-alkyne** was synthesized by reacting **PEG-NHS** with propargyl amine. The introduction of the alkyne group was corroborated by the appearance of a ¹H signal from the alkyne proton ($t: 2.24\text{-}2.23\text{ ppm}$) in the ¹H-NMR spectrum. The substitution degree was calculated from alkyne (Section 2.3, Appendix) was > 90%. **NB-3** was conjugated to PEG-alkyne following a reported protocol for solid-phase peptide synthesis of 4-substituted NH-1,2,3-triazoles¹⁶. After the reaction, the crude product was centrifuged and the supernatant solution was purified by dialysis against acetone and 20 wt% EDTA in water to remove inorganic reactants. The reaction was confirmed by the appearance of Boc-protons ($s: 1.40\text{ ppm}$) in ¹H-NMR spectra (Figure 2.13). Then, acidic cleavage of the Boc protecting group from **PEG-NBt-Boc** macromer to obtain the free amine (**PEG-NBt-amine**) was performed. The reaction was confirmed by the absence of the Boc group ($s: 1.40\text{ ppm}$). Finally, the amine group was coupled to hydrocaffeic acid. The success of the reaction was confirmed the presence of new characteristic signals, the aromatic protons of the hydrocaffeic acid (6.52-6.68 ppm) and the new amine bond (7.32 ppm) (Figure 2.14). The substitution degree was calculated

by end-group determination and amounted >85% (Figure 2.14). The final macromer, **PEG-NBt-c**, was obtained at 250 mg scale.

The intermediates and final macromers were stable for more than 10 months during storage at -20°C protected from light. This is advantageous in comparison to **PEG-NNPE**. **PEG-NBt-c** macromers were soluble in water, PBS, HEPES buffer and cell culture medium up to a tested final concentration of 20 wt%.

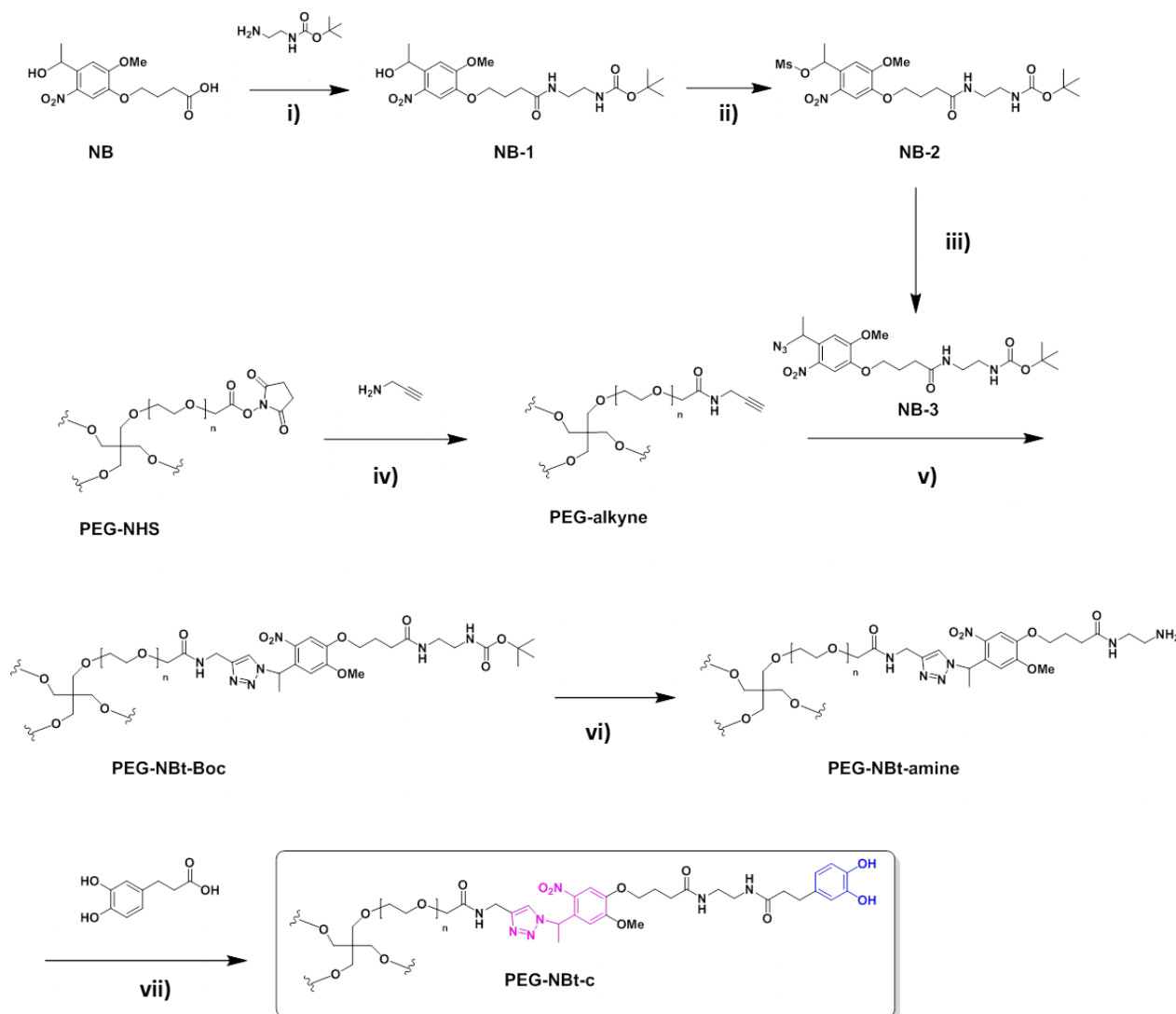


Figure 2.11 Synthesis of the PEG-NBt-c. Reagents and conditions: i) HBTU, HOBT, DIPEA, dry DMF, room temperature, 6 h, yield= 62%; ii) MsCl, TEA, dry DCM, room temperature, 3h, iii) NaN₃, dry DMF, 60°C, overnight, yield= 47%; iv) NMM, dry DMF, N₂, room temperature, overnight, yield=

96%; v) Cul, sodium ascorbate, 2,6-lutidine, NMP:water (4:1), room temperature, overnight, yield=89%; vi) TFA:water (95:5), room temperature, 1 h, yield= 72%.; vii) HBTU, HOBT, DIPEA, N₂, dry DMF, room temperature, overnight, yield= 61%.

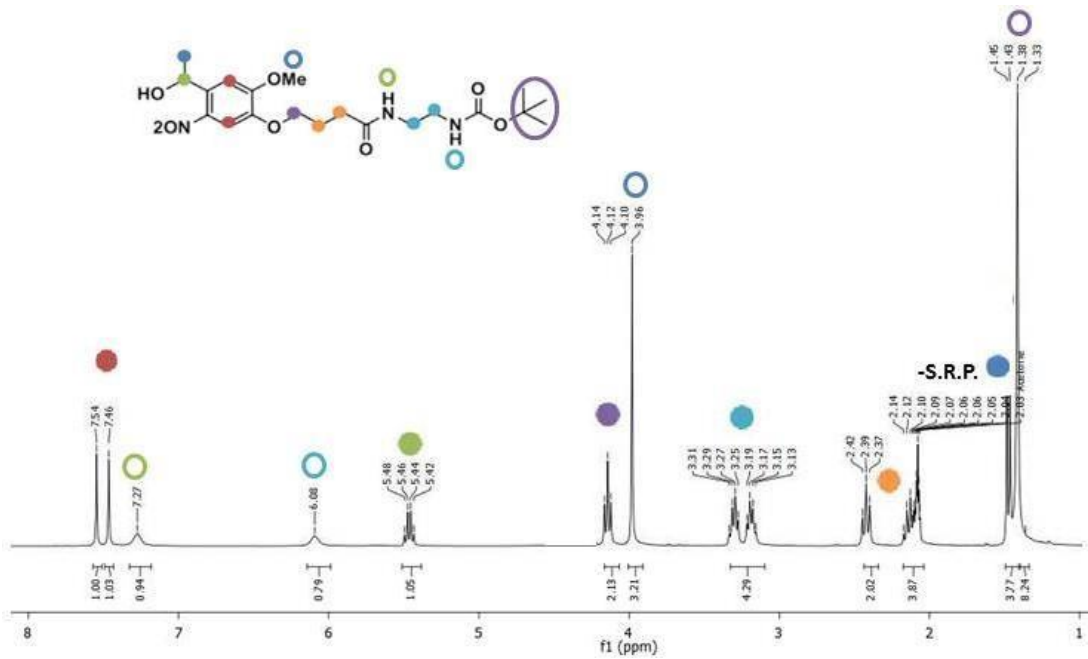


Figure 2.12 ^1H spectrum of NB-1 derivative

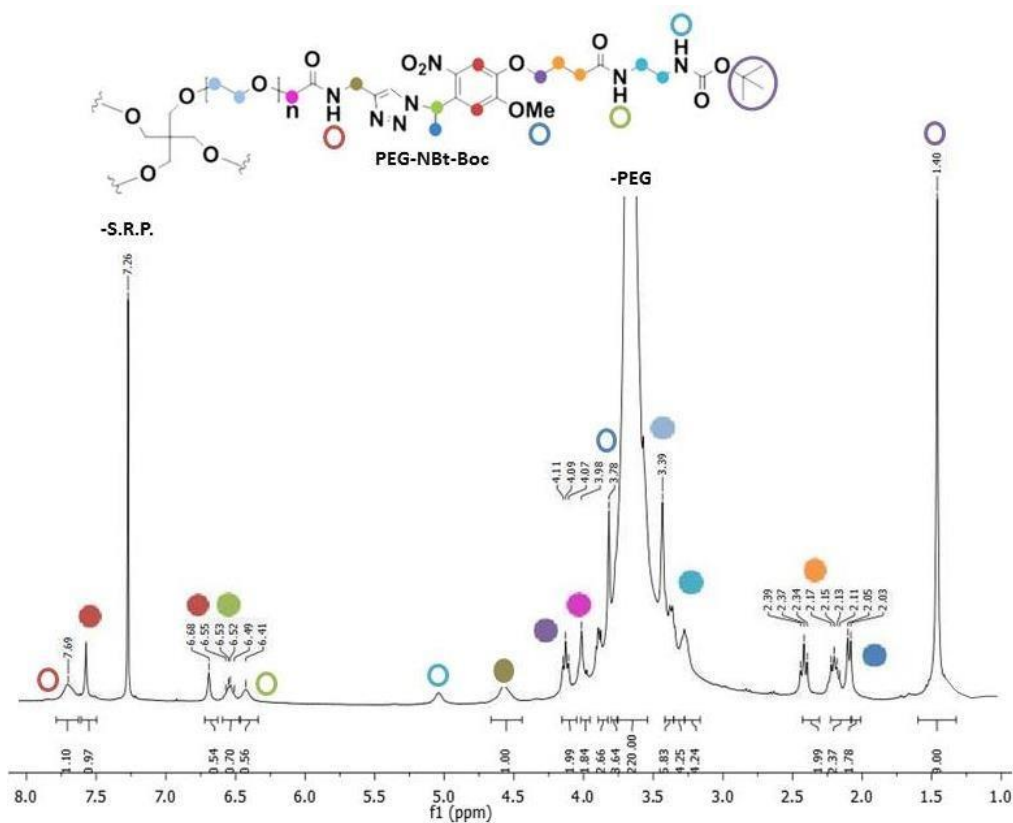


Figure 2.13 ^1H spectrum (CDCl_3 , 300 MHz) of 4-arm, 10 kDa, **PEG-NBt-Boc**

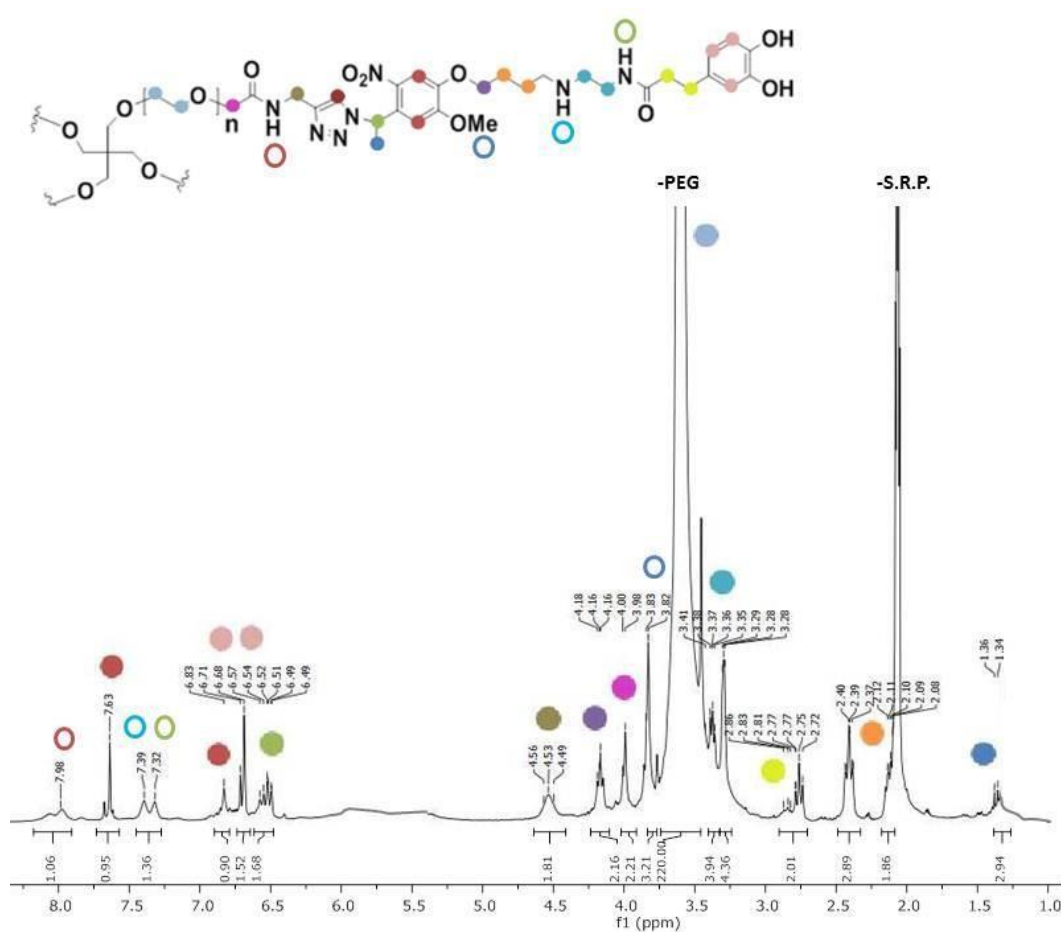


Figure 2.14 ¹H spectrum of 4-arm,10 kDa, **PEG-NBt-c**

Synthesis of PEG-NBe-c

PEG-COOH was esterified with **NB-1**. The reaction was confirmed by the presence of the Boc group (s: 1.39 ppm), the aromatic protons of the **NB-1** (d: 7.60-7.55 ppm and s: 7.47 ppm, isomeric product) and the new ester bond formed between the carboxylic acid and the alcohol which was detected from the shift of the proton of the tertiary carbon to which the alcohol was linked (from m: 5.48-5.42 to m: 1.65-1.45 ppm) in the ¹H-NMR spectra. The substitution degree was calculated by end-group determination >80%. Then, the acidic cleavage of the Boc protecting group was performed and the reaction was confirmed by the loss of the signal from the Boc group (s: 1.39 ppm). The free amine was coupled to hydrocaffeic acid to obtain **PEG-NBe-c** (Figure 2.15) at 71 mg scale. The reaction was confirmed by the presence of aromatic protons of the hydrocaffeic acid (8.37-8.18 ppm) and the protons of the new amine bond (bs: 7.83 ppm) (Figure 2.16). End-

group analysis by $^1\text{H-NMR}$ confirmed a substitution degree of >85%, by comparing the signals of ethyl groups of hydrocaffeic acid at (m: 2.24-2.09 and m: 2.27-2.25 ppm) to PEG backbone. The macromer was soluble in water at low concentration (2 wt%), but it was not soluble in PBS, HEPES buffer or cell culture medium at 1wt% concentration.

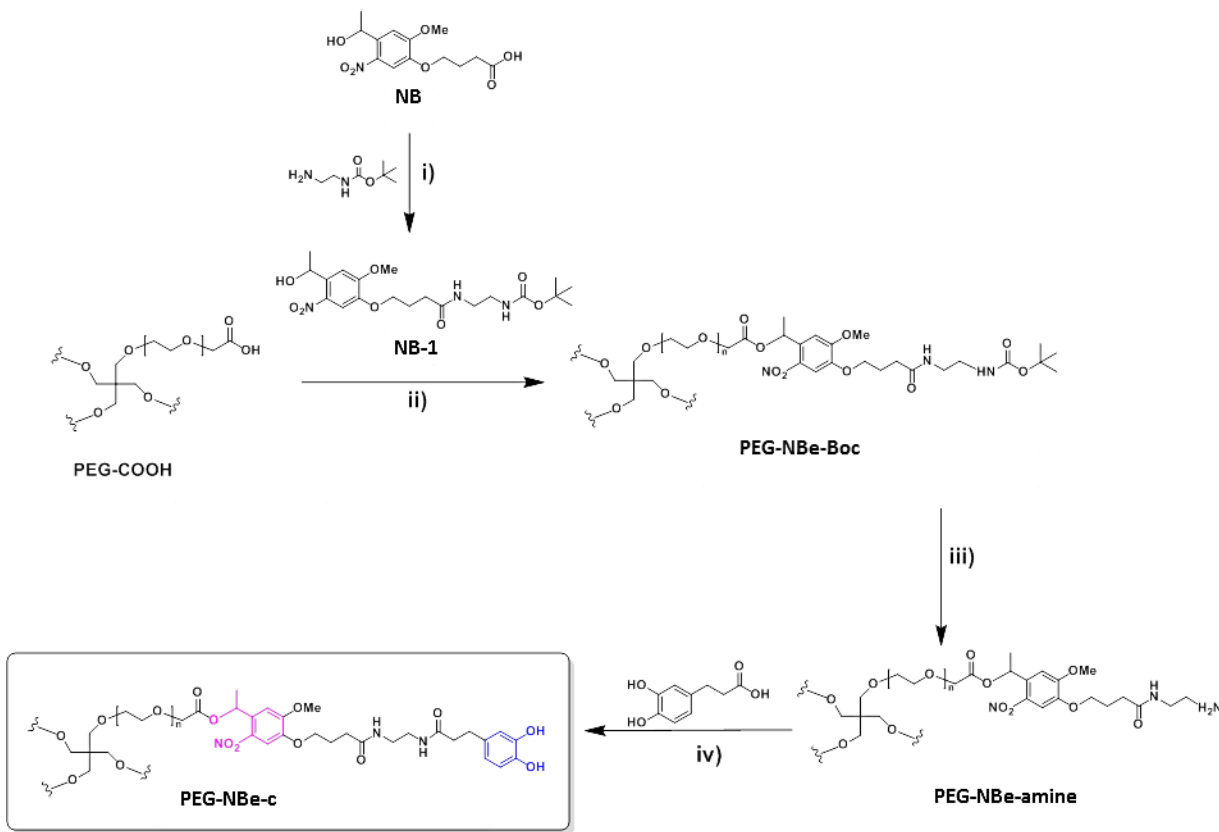


Figure 2.15 Synthesis of the **PEG-NBe-c** macromer. Reagents and conditions: i) HBTU/HOBT, DIPEA, dry DMF, room temperature, 6 h, yield=89%; ii) DCC, DMAP, DCM, N₂, room temperature, overnight, yield=75%; iii) TFA:water (95:5), room temperature, 1-2 h; iv) HBTU, HOBT, DIPEA, N₂, dry DMF, room temperature, overnight, yield=71%.

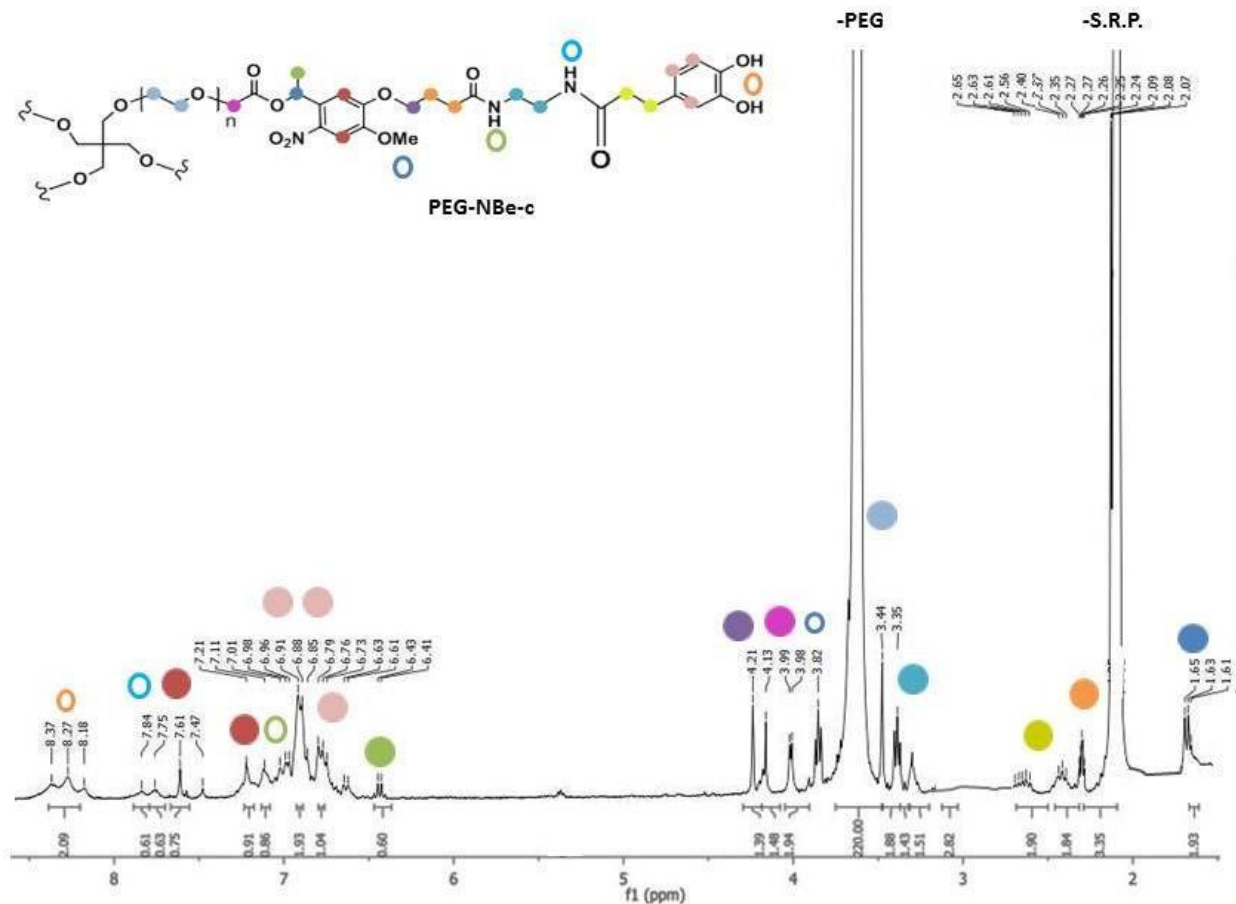


Figure 2.16 1H spectrum (C3D6O-d6, 300 MHz) of 4-arm, 10 kDa, isomeric mixture of PEG-NBe-c

2.4.2 Synthesis of control macromers

The macromers **PEG-Dop** and **PEG-NDop** (Figure 2.17) were also synthesized as controls.⁴⁻

⁶ The **PEG-Dop** macromer presents the catechol group as single functionality and will be used as crosslinkable, tissue adhesive and non-photodegradable control. This macromer was synthesized following reported protocols.²⁷ **PEG-NDop** presents the terminal nitro-catechol group and therefore is crosslinkable, tissue adhesive and photodegradable however with poor photolytic efficiency. This macromer was synthetized according to a previous reports.¹⁰

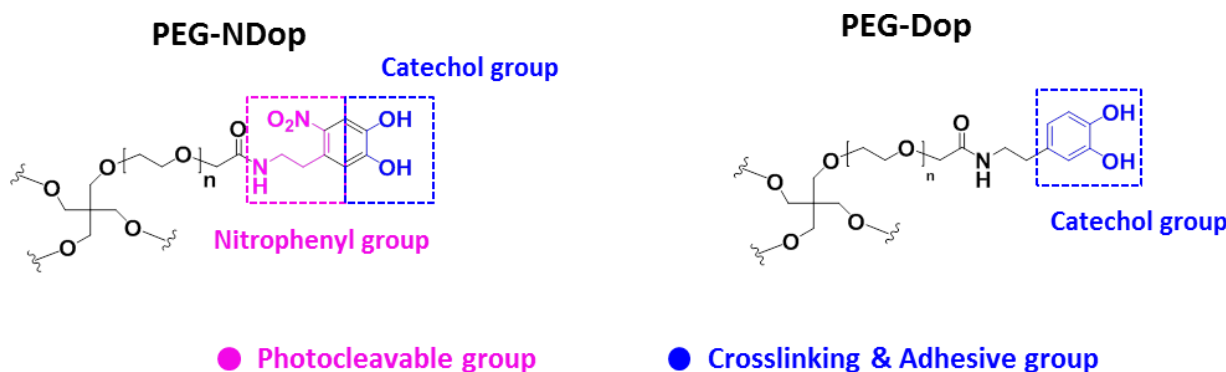
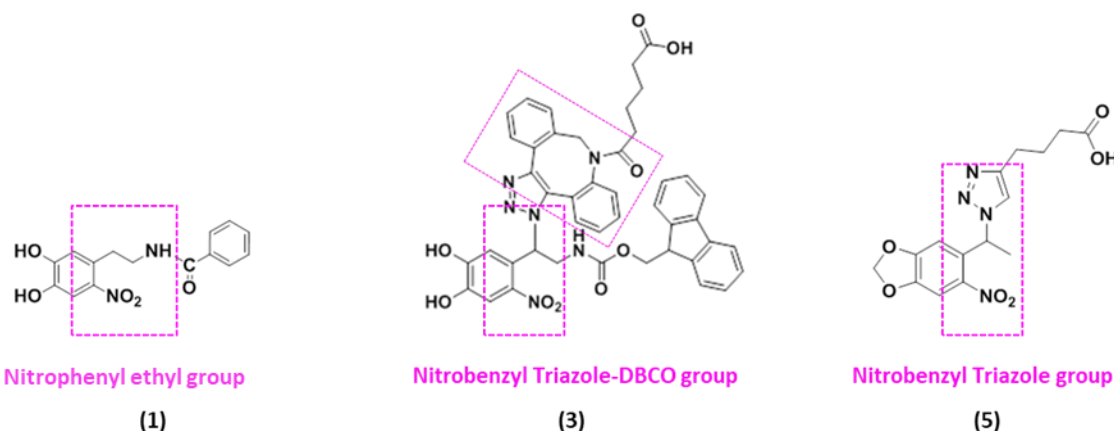


Figure 2.17 Control hydrogels: **PEG-NDop** and **PEG-Dop** (non-photodegradable).

2.4.3 Synthesis of small molecule analogues

Four small molecule analogues (**1**, **3**, **5** and **7**, Figure 2.18) with similar photosensitive groups to the macromers were synthesized to perform photolysis experiments. The model molecule **1** presents a nitrophenyl ethyl photocleavable system and a nitro-catechol group. This compound, already synthesized by the group from nitrodopamine and benzoic acid, is analogue to the **PEG-NDop** macromer. Compound **3** presents a nitrobenzyl DBCO-triazole group and a free nitro-catechol, as in **PEG-NNPE**. This small molecule was synthesized by coupling the azide group of intermediate (**4**) (Figure 2.8) to DBCO-COOH by strain-promoted azide-alkyne cycloaddition. Compound **5** has a nitrobenzyl triazole as a photodegradable moiety as in **PEG-NBt-c**. It was synthesized by copper-free azide-alkyne cycloaddition¹⁶. Compound **7** models the nitrobenzyl ester of **PEG-NBe-c** and was obtained by esterification of the –OH group of **NB-1** with octanoid acid. Further details on the synthesis of the model molecules are provided in section 2.7, Appendix.



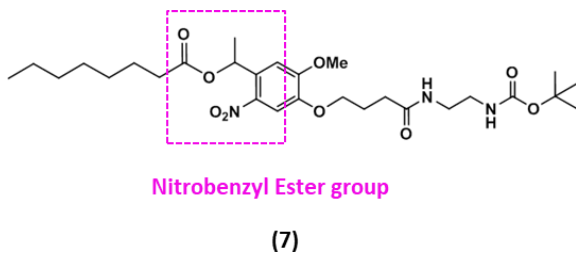


Figure 2.18 Small molecule analogues synthetized as mimics of **PEG-NDop** macromer **(1)**, **PEG-NNPE** macromer **(3)**, **PEG-NBt-c** macromer **(5)** and **PEG-NBe-c** macromer **(7)**.

2.4.4 Characterization of photolytic properties of model molecules and macromers

The photolysis of the model molecules **1**, **3**, **5** and **7** and the PEG-catechol macromers **PEG-NDop**, **PEG-NNPE**, **PEG-NBt-c** and **PEG-NBe-c** was analyzed. 1 mM solutions of the model molecules in acetonitrile, and 1 μM solutions of the PEG-catechol macromers in water were used for this purpose. The solutions were placed in a quartz cuvette and irradiated at $\lambda = 365 \text{ nm}$ (Irradiance= 1.2 mW cm^{-2}) for increasing exposure times. At selected time points UV-Vis spectra of the irradiated solutions were measured. HPLC and mass spectrometry (ESI-MS) analysis of the irradiated solutions of model compounds were also recorded. In ESI-MS, the evolution of the m/z peaks corresponding to the model molecule and to the expected photolysis products was analyzed. In analytic HPLC, the decay in the absorbance peak of the model molecules was followed.

2.4.5 Photolysis studies of model compounds

Model compound 1

The solution of **1** was irradiated for 180 min (Irradiation dose = 13.1 J cm^{-2}), until the UV-vis spectrum did not show further changes (Figure 2.19A). UV-Vis showed a photolysis reaction with a decrease of the absorbance at 350 nm and increase at 280 nm, 320 nm and above 400 nm indicating the new products. ESI-MS analysis of an irradiated aliquot (160 min) showed the presence of the expected o-nitro-styrene ($m/z = 182.0$ for $\text{M}+\text{H}$) and benzamide ($m/z = 122.0$ for $\text{M}+\text{H}$) photolysis products (Figure 2.2), as well as unreacted compound **1** ($m/z = 303.0$ for $\text{M}+\text{H}$),

along with and several other m/z peaks corresponding to byproducts formed during the prolonged irradiation. In the RP-HPLC analysis, the starting molecule was still observed after 160 min of irradiation, along with several other peaks. The long irradiation time reflects that this system has poor photolytic efficiency. The reason for the multiple peaks of byproducts may be the poor stability of the produced styrene, which can self-polymerize under exposure conditions by self-initiated radical polymerization. Figure 2.20 shows some self-polymerization reactions proposed in the literature for styrene. Mayo suggested that two styrenes form a Diels-Alder styrene dimer (AH), which then transfers a hydrogen to a third monomer (molecular assisted homolysis) to form monoradicals (M·). (AH) can also generate an inactive trimer A-Styrene (A-sty). Flory show that two styrene monomers (M) form a 1,4-diradical (M₂··), which either ring-closes to form 1,2-diphenylcyclobutane (DCB) or reacts with a third styrene monomer to produce two mono- or diradicals (M·, M₂··) via hydrogen transfer or abstraction (Figure 2.20).²⁸

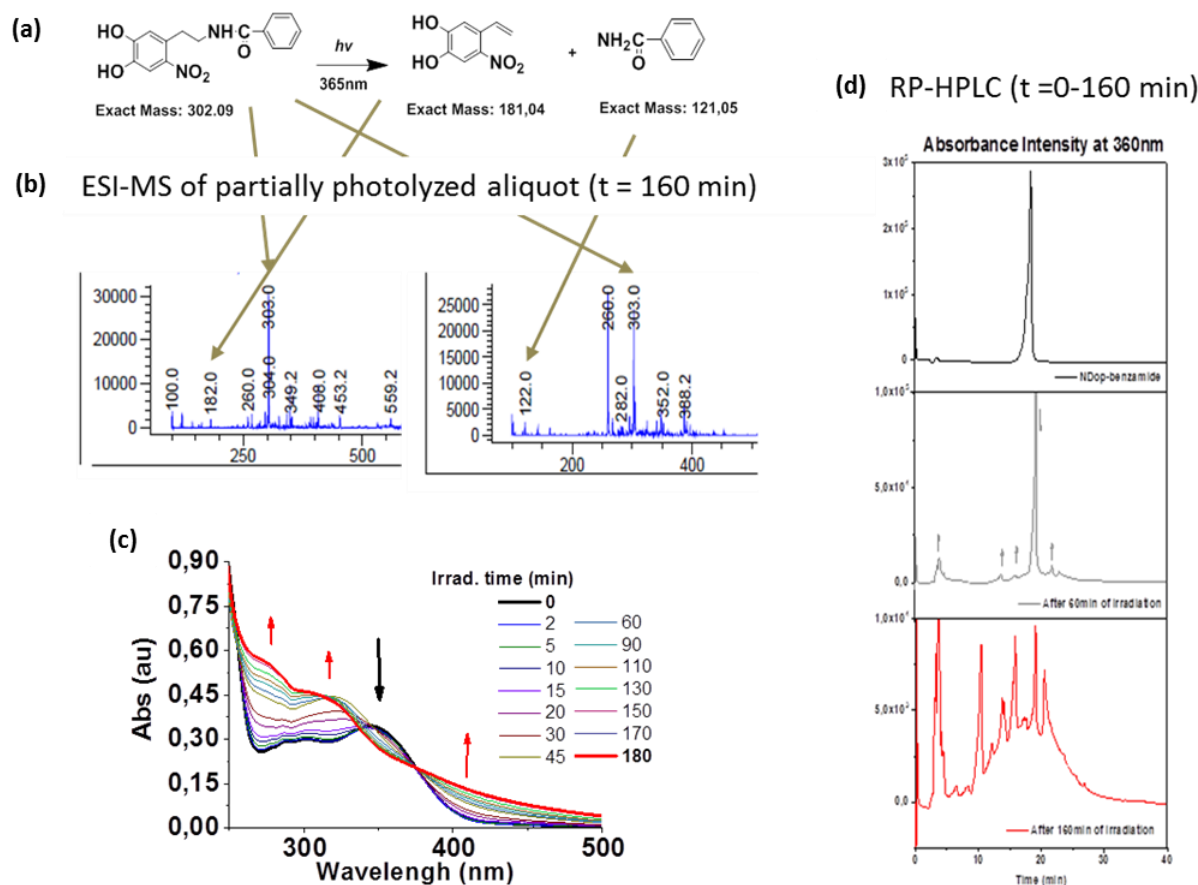


Figure 2.19 Photolysis of compound **1**. Photocleavage reaction of the o-nitro phenyl ethyl moiety of compound **1** (a). 1 μ M solution of analogue **1** in acetonitrile at increasing exposure times (0–180 min) (c). ESI-MS analysis of partially photolyzed solution ($t = 160$ min) (b). The RP-HPLC analysis shows the total time of the consumption of starting material, λ detection = 360 nm at 160 min. Irradiation conditions: $\lambda = 365$ nm, 1.2 mW cm $^{-2}$ (d).

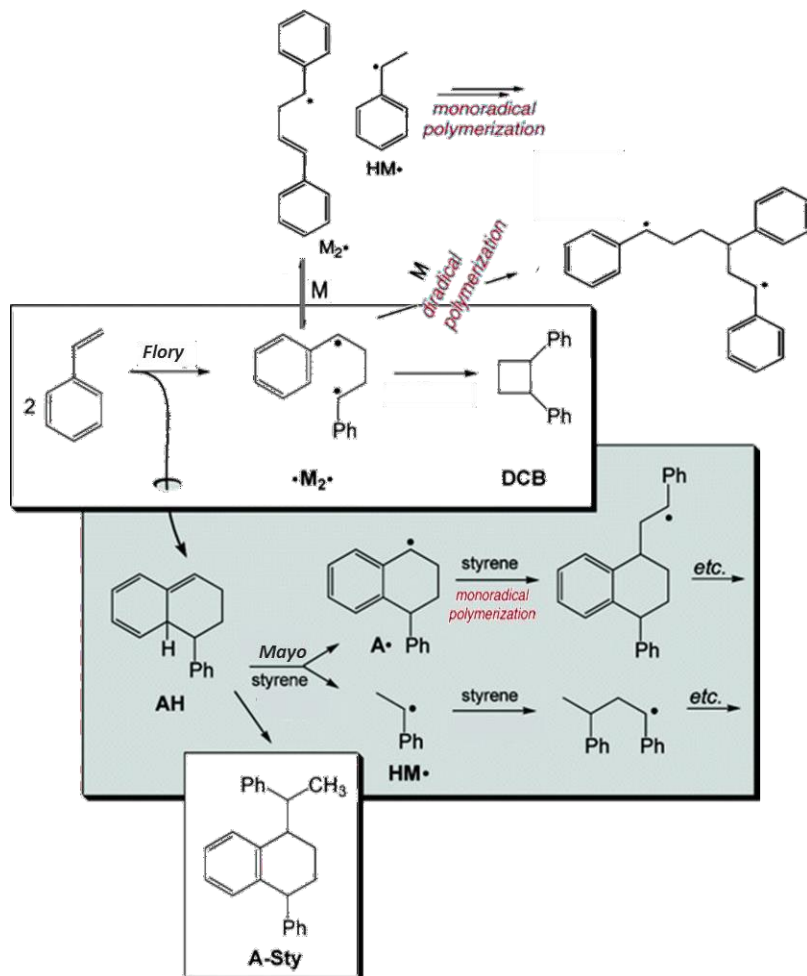


Figure 2.20 Self-initiated radical polymerization of styrene by Mayo and Flory. Modified after permission from Polymer Journal.²⁸

Model compound 3

In this case, UV-Vis studies indicated the occurrence of an efficient and clean photolysis reaction (completed in 40 min, irradiation dose = 2.88 J cm^{-2}), while mass spectrometry studies confirmed the identity of the photolysis products (Figure 2.21(b)). Upon irradiation, UV-Vis absorbance decreased at 350 nm and increased at 320, 385 and 475 nm. The clear isosbestic points of the UV spectra ($\lambda = 340$ and 360 nm) at increasing exposure dose suggest that no secondary reactions occur. In this photofragmentation reaction, of o-nitrobenzyl triazole (o-NB) derivatives, a stable DBCO-triazole ($\lambda_{\text{max}} = 320 \text{ nm}$, $m/z = 377.2$ for $M+\text{H}$) and a nitroso-ketone ($\lambda_{\text{max}} = 385 \text{ nm}$, $m/z = 436.2$ for $M+\text{NH}_4$) are expected to be the photolysis products (see proposed photolysis mechanism in Figure 2.4b). This was confirmed by ESI-MS at 30 min.^{15, 16} 95% consumption of starting material was confirmed by RP-HPLC, after 45 min of irradiation.

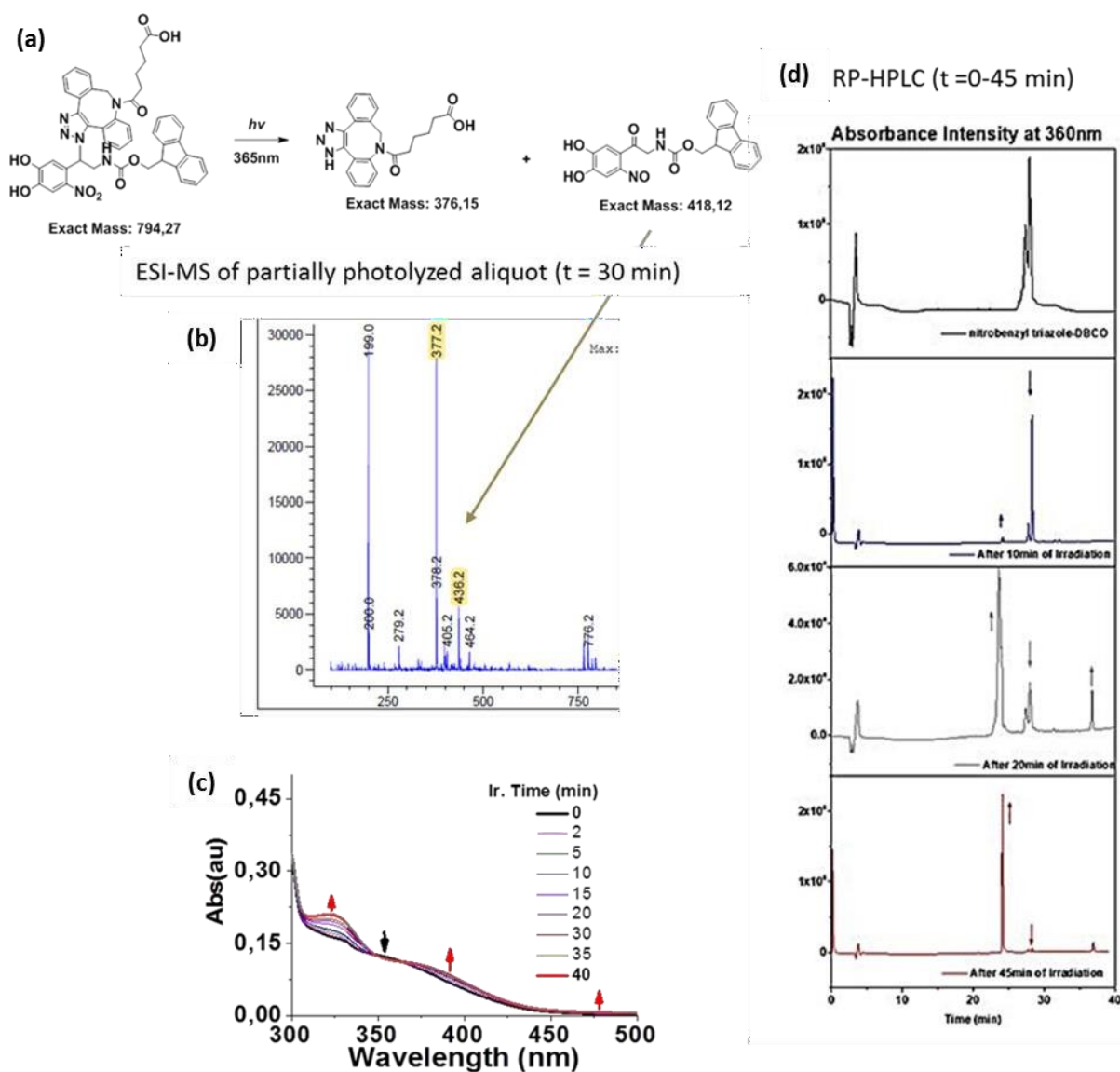


Figure 2.21 Photolysis 1 μM solution of **3** in acetonitrile at exposure time between 0 and 40 min (a, c). (b) ESI-MS analysis of partially photolyzed solution ($t = 30$ min). (d) The RP-HPLC analysis shows the total time of the consumption of starting material, λ detection = 360 nm at 45 min. Irradiation conditions: $\lambda = 365$ nm, 1.2 mW cm^{-2} .

Model compound 5

The photolysis of model compound **5** was carried out (Figure 2.22). The UV-Vis spectra indicated the occurrence of an efficient and clean photolysis reaction (completed in 30 min, irradiation dose = 2.16 J cm^{-2}). A decrease in absorbance at 350 nm and an increase at 315 and 400 nm was observed. The clear isosbestic points of the UV spectra ($\lambda = 330$ and 360 nm) at increasing exposure dose suggest that no secondary reactions occur. The release of photolysis products was confirmed by ESI-MS: the nitrosobenzyl ketone ($m/z = 194.0$ for $M+\text{H}$) and the triazole ($m/z = 156.0$ for $M+\text{H}$), in agreement with previously reported data,¹⁶ as well as the signal for the original molecule were detected ($m/z = 349.2$ for $M+\text{H}$).

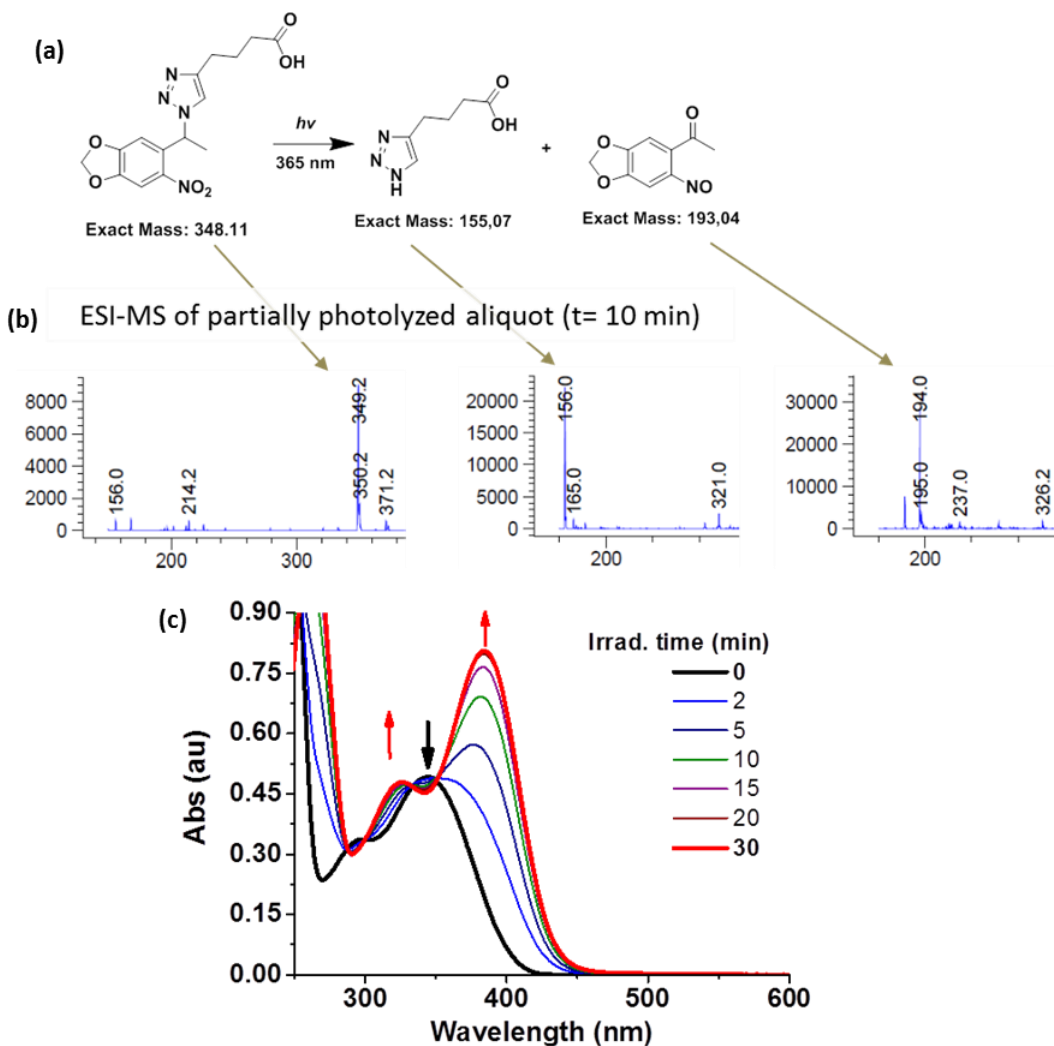


Figure 2.22 Photolysis study of compound 5. (a) Photocleavage reaction. (b) UV-Vis spectra of 1 μM solution of 5 in acetonitrile at increasing exposure times (0-30 min). (c) ESI-MS analysis of partially photolyzed solution ($t = 10$ min). Irradiation conditions: $\lambda = 365$ nm, 1.2 mW cm^{-2} .

Model compound 7

According to the UV-Vis spectra, the photolysis of compound 7 was completed after 45 min exposure (irradiation dose = 3.24 J cm^{-2} , Figure 2.23(b)) in a clean process, according to the profiles of the UV spectra and the occurrence of two isosbestic points. UV-Vis absorbance decreased at 300 nm and increased at 280, 325 and 375 nm. In this photocleavage reaction a nitroso-ketone ($\lambda_{\text{max}} = 375$ nm, $m/z = 462.4$ for M+K) and octanoic acid are expected to be the photolysis products (see proposed photolysis mechanism in Figure 2.4a).¹⁵ These products were

confirmed by ESI-MS at 40 min. 90% consumption of starting material is confirmed by RP-HPLC, after 45 min of irradiation.

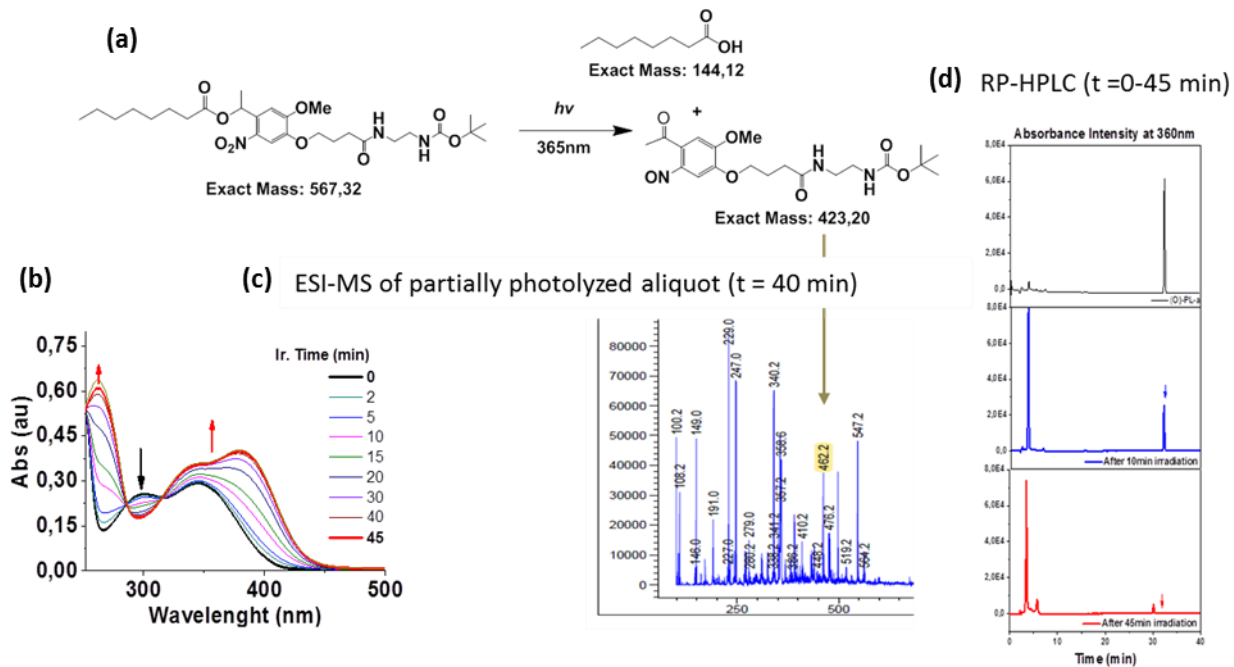


Figure 2.23 Photolysis studies in solution, followed by UV-Vis spectroscopy (b). Photocleavage reaction of the o-nitro phenyl ethyl moiety of compound **7** (a). 1 μ M solution of analogue **7** in acetonitrile at increasing exposure times (0-45 min). ESI-MS analysis of partially photolyzed solution ($t = 40$ min) (c). The RP-HPLC analysis shows the total time of the consumption of starting material, λ detection = 360 nm at 45 min. Irradiation conditions: $\lambda = 365$ nm, 1.2 mW cm^{-2} (d).

Comparison of photolysis of model compounds

The photolysis efficiency of **1,3,5** and **7** at the same exposure conditions (1 mM solutions in acetonitrile; Irradiation conditions: $\lambda = 365$ nm, 1.2 mW cm^{-2}) was compared (Figure 2.24). According to the changes in the UV spectra, full photocleavage of **5** occurred 1.4, 1.6 and 6 times more efficiently than **3**, **7** and **1** respectively. These results demonstrate the superior performance of o-nitrobenzyl triazol as photocleavable protecting group than the previously reported o-nitrobenzyl ester¹⁵ and the o-nitrophenyl ethyl system.¹⁰

Figure 2.26 compares the photolytic conversion of the different chromophores used in this work. The NBt showed similar photolytic efficiency than NBe, and these could be cleaved more efficiently than the nitrophenyl ethyl analogue under same experimental conditions. After 60 min of irradiation (dose = 4.3 J cm^{-2}), photolysis conversion was 99% for nitrobenzyl triazole, 95% for nitrobenzyl ester and 51% for nitrophenyl ethyl. These photolysis studies complement previous result by Nielsen et al.¹⁶ and, together with the observed clean spectra during photolysis, confirm the better performance of nitrobenzyl triazole moiety as photocleavable linker vs. to nitrobenzyl esters for the preparation of photodegradable hydrogels. These results validate the molecular design presented in section 2.3, above.

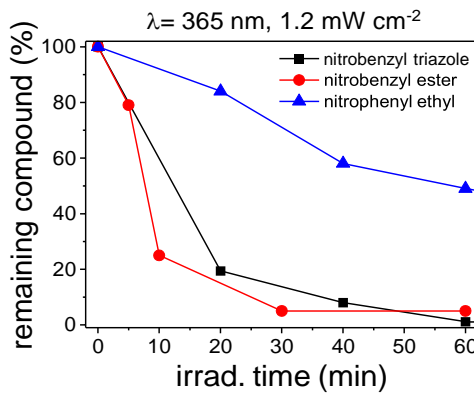


Figure 2.24 Comparison of photolysis conversion as function of exposure time for the different model compounds quantified by analytical HPLC.

2.4.6 Photolysis studies of PEG-catechol macromers

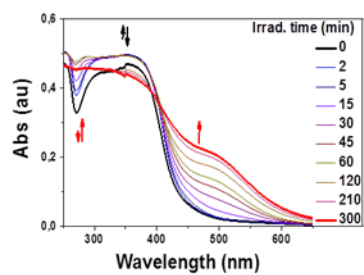
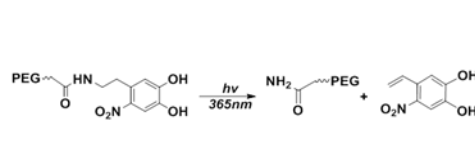
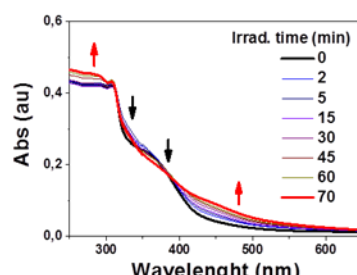
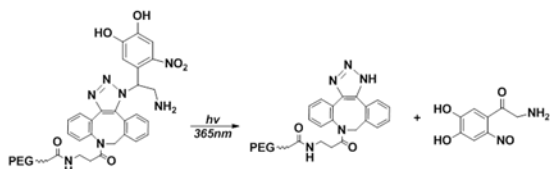
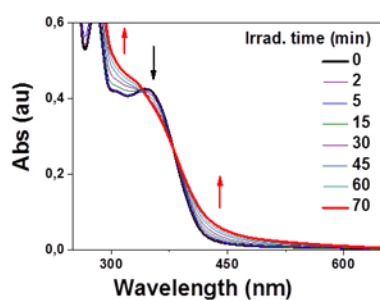
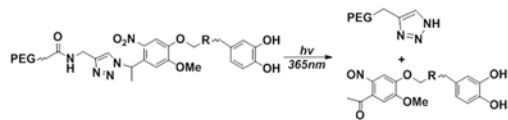
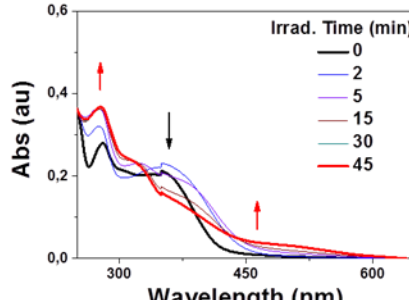
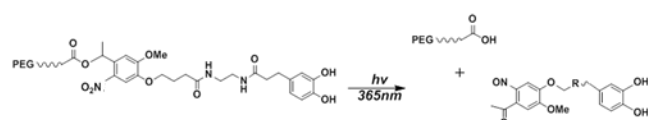
A. PEG-NDop**B. PEG-NNPE****C. PEG-NBt-c****D. PEG-NBe-c**

Figure 2.25 Photolysis of PEG-catechol macromers ($\lambda = 365$ nm, 1.2 mW cm^{-2}): A) **PEG-NDop**, B) **PEG-NNPE**, C) **PEG-NBt-c** and D) **PEG-NBe-c**. The photocleave reaction scheme and the UV-Vis spectra of $1 \mu\text{M}$ solutions of the PEG-catechol macromers in water after irradiation at increasing times are shown for each case.

PEG-NDop

The photolysis of a $1 \mu\text{M}$ **PEG-NDop** solution in water (365 nm, 1.2 mW cm^{-2}) for increasing time was followed by UV-Vis spectroscopy (Figure 2.25A). The characteristic spectral changes during photolysis of nitrophenyl ethyl derivatives¹⁶ were observed: a decay of absorbance at $\lambda_{\text{max}} = 350$ nm and the increase in absorbance at wavelengths 280 and 490 nm. This is in agreement with the profile expected for the consumption of the nitrophenyl ethyl group¹⁴ and

the formation of PEG-benzamide and nitro-styrene as expected photolysis products. The spectrum did not change further around 300 min of exposure, irradiation dose = 21.6 J cm^{-2}). No clear isosbestic points in the UV spectra at increasing exposure dose where observed. This would indicate that secondary reactions take place, in agreement with the high reactivity of styrenes explained above.

In comparison to the model compound **1**, upon long irradiation time ~ 180 min, absorbance presented similar decrease at 345 nm and increase at 280, 310 and 420 nm. These results are in agreement with the **PEG-NDop** macromer system, indicating similar photolysis mechanism and the presence of the expected photolysis products.

PEG-NNPE

The photo-degradability of **PEG-NNPE** macromer was studied. The spectral change was analyzed by UV-Vis spectroscopy (Figure 2.25B). The evolution of the UV-Vis spectra showed a decrease of absorbance at 325 nm and 365 nm (due to consumption of the nitrobenzyl group), and increase of the absorbance at 450 nm (explained by the appearance of the nitrosobenzyl ketone as photolysis product). This is a characteristic photolytic profile of a nitrobenzyl chromophore.²⁹ The absorbance at 275 nm increased as well, probably due to the release of the triazole group as photolysis product. The photolysis reaction was completed in 70 min (irradiation dose = 5.04 J cm^{-2}).

In comparison to the model compound **3**, upon 45 min irradiation, the isomeric mixture is almost consumed. Absorbance presented the same clear isosbestic points of the UV spectra ($\lambda = 340$ and 360 nm) with the **PEG-NNPE** macromer and also similar UV-vis profile, decreasing at 350 nm and increasing at 320 nm and above 385 nm.

PEG-NBt-c

Upon irradiation, **PEG-NBt-c** displayed the characteristic spectral changes during photolysis of nitrobenzyl derivatives²⁹ (Figure 2.25C): a decay of absorbance at λ_{max} (365 nm) due to the consumption of the nitrobenzyl group, and the increase in absorbance at wavelengths >400 nm associated to the formation of nitroso-benzyl ketone photolysis product. This is a characteristic photolytic profile of a nitrobenzyl chromophore.²⁹ The clear isosbestic points of the

UV spectra ($\lambda = 340$ and 380 nm) at increasing exposure dose suggest that no secondary reactions occur. The photolysis reaction was completed in 70 min (irradiation dose = 5.04 J cm^{-2}).

In relation to the UV-vis profile of the molecule **5**, both systems showed a very clean photolysis mechanism. During 30 min of photolysis reaction of **5**, absorbance decreased at 345 nm and increased at 320 and 385 nm, equally to the **PEG-NBt-c** macromer.

PEG-NBe-c

PEG-NBe-c macromer solution was light exposed (Figure 2.25D). The evolution of the UV-Vis spectra showed a decrease of absorbance at 365 nm (due to consumption of the nitrobenzyl group) and the increase at 450 nm (appearance of the nitrosobenzyl ketone as photolysis product). The absorbance at 275 nm increased as well, probably due to the release of the triazole group. This is a characteristic photolytic profile of a nitrobenzyl chromophore.²⁹ The photolysis reaction was completed in 45 min (irradiation dose = 3.24 J cm^{-2}).

In comparison to the model compound **7**, absorbance decreased at 300 nm and increase at 280 , 325 and 375 nm. These results are in agreement with the **PEG-NBe-c** macromer system, where the photolysis reaction were completed in the same time (45 min) indicating the same photocleavage trend.

Comparison of photolysis efficiency of the different polymers

PEG-NBt-c was photolysed 1.1 times more efficiently than **PEG-NNPE** and 4 times more than **PEG-NDop** in water. **PEG-NBe-c** was photolysed 1.4 times more efficiently than **PEG-NBt-c** and 1.6 times more efficiently than **PEG-NNPE**. These results demonstrate that **PEG-NBt-c** and **PEG-NNPE** synthesized in this work are better photocleavable candidates than the previously reported **PEG-NDop** system, but not as efficient as the reported **PEG-NBe-c**. The photolysis efficiency of o-nitrophenyl ethyl photocleavable derivatives depends on different molecular aspects.^{21,22} Another relevant factor is the nature of the linkage between the protected group and the chromophore which affects the leaving group character. Amide linkages, as in **PEG-NDop**, are poor leaving groups. In contrast, the NBe group has higher photosensitivity due to the better leaving character of the ester group⁵. Additionally, triazole linkage is providing similar photolytic efficiency to the NBe analogue.

These results demonstrate that the **PEG-NBt-c** and **PEG-NNPE** macromers are much more efficient towards photocleavage than the previously reported **PEG-NDop**; however they have a lower photocleavage efficiency than **PEG-NBe-c**. This is in contrast to small analogues photolysis studies, where the Nbt linkage showed slightly better photolytic efficiency than Nbe.

2.4.7 Hydrolytic stability of the macromers

The stability of **PEG-NBt-c** and **PEG-NBe-c** macromers in water solutions was analyzed by MALDI-TOF and HPLC. Boc-derivatives were used to avoid interference of the catechol unit, which could oxidize and self-react in the experimental conditions used. 1 mM solutions in 50 mM HEPES buffer (pH 7.5.) of 10-kDa **PEG-NBt-Boc** and **PEG-NBe-Boc** were used for the analysis. The solutions were prepared in an amber vial and maintained in the dark at room temperature for 8 days. Fresh solutions ($t= 0$ day) showed a strong peak centered at $m/z \sim 11$ kDa, consistent with intact macromers. Samples at $t = 8$ days showed peaks at lower molar masses ($m/z < 10$ kDa), meaning that **PEG-NBt-c** and **PEG-NBe-c** were partially hydrolyzed. The intensity of the peaks with $m/z < 10$ kDa was higher in **PEG-NBe-Boc** (Figure 2.26A,B) indicating a lower hydrolytic stability of ester vs. triazole linkage. These results were complemented with HPLC analysis. A lower remaining concentration of **PEG-NBe-Boc** (88%), and consequent higher amount of byproducts at day 8, was found in comparison to the triazole derivative (97% intact after 8 days).

UV-Vis studies in combination with ESI-MS analysis were also attempted to detect the small fragments of the hydrolysis. The spectra (not shown) displayed many peaks that could not be directly correlated to the mass of the expected products.

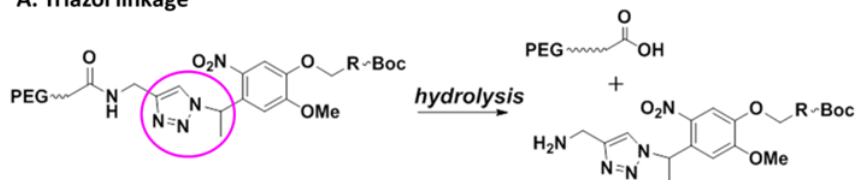
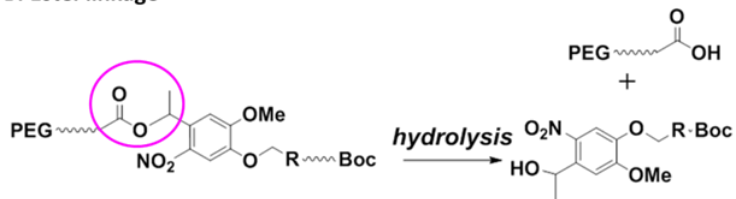
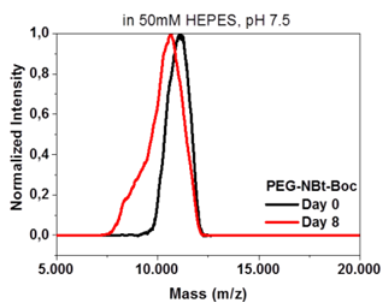
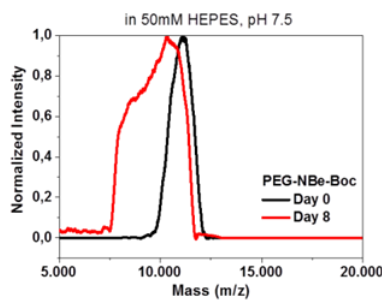
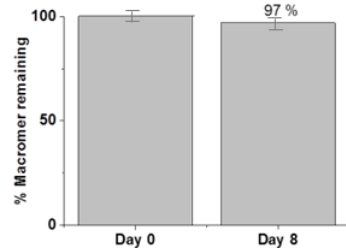
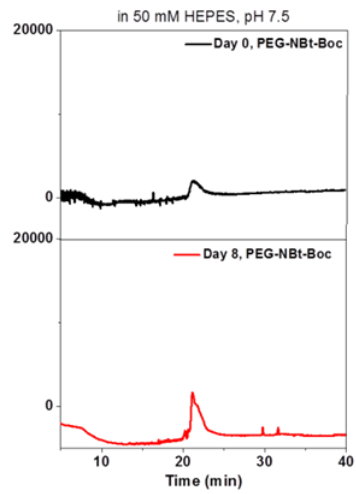
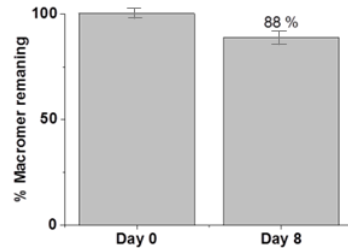
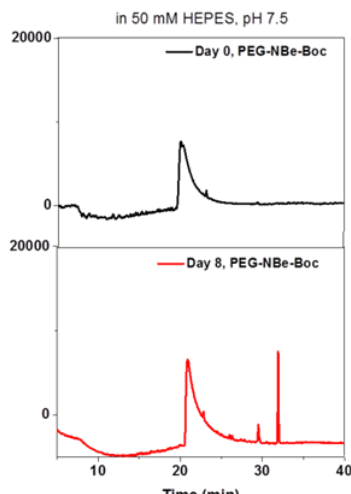
A. Triazol linkage**B. Ester linkage****A. MALDI-TOF****B. MALDI-TOF****A. HPLC****B. HPLC**

Figure 2.26 Comparative studies of hydrolytic stability of A) **PEG-NBt-Boc** vs. B) **PEG-NBe-Boc** by MALDI-TOF and HPLC analyses. Conditions: 1 mM solution in 50 mM HEPES buffer, pH 7.5; incubated in the dark at room temperature for 0 and 8 days. The pink circles display the different connectivity, triazole vs ester group. Detection channel for HPLC studies $\lambda = 280$ nm. Statistical analysis was conducted by ANOVA followed by post-hoc Tukey test.

2.5 Conclusions

Three hydrogel precursors comprising a star-PEG polymer backbone, an adhesive and crosslinkable unit, and a photodegradable moiety were successfully synthesized. Hydrogel precursors with high substitution degree (> 85%) were obtained. The synthesis of the precursors differed in the following aspects: synthetic effort (4 to 7 steps), stability during storage (days to months), scale of synthesis (30 to 250 mg), macromer's solubility, macromer's hydrolytic stability in aqueous media, and macromer's photolytic properties.

The **PEG-NNPE** macromer presented good solubility in aqueous solvents and showed 2.5 times higher photoefficiency than the photodegradable control, **PEG-NDop**. However, the synthetic sequence to **PEG-NNPE** precursor required 7 steps, involved labile intermediates and the final precursor could only be obtained in low scale (< 30 mg).

PEG-NBt-c macromer presented good solubility in aqueous solutions and required 7 synthesis steps, but could be obtained successfully at 250 mg scale. The triazole linkage showed higher hydrolytic stability, and similar photolytic efficiency to the nitrobenzyl ester derivative (**PEG-NBe-c**). The exposure doses required for photodegradation of **PEG-NBt-c** precursor were within cytocompatible ranges.

The **PEG-NBe-c** macromer was synthesized in 4 steps at 71 mg scale. Despite having good photolytic properties, this macromer presented limited solubility in aqueous solvents and lower hydrolytic stability than **PEG-NBt-c**.

In the next chapters, the preparation and characterization of photodegradable hydrogels fabricated from **PEG-NNPE** and **PEG-NBt-c** will be presented and compared to **PEG-NBe** used elsewhere.⁴⁻⁶

2.6 References

1. Waite, J. H., Adhesion a la moule. *Integrative and comparative biology* 2002, 42 (6), 1172-1180.
2. Krogsgaard, M.; Nue, V.; Birkedal, H., Mussel-inspired materials: self-healing through coordination chemistry. *Chemistry—A European Journal* 2016, 22 (3), 844-857.
3. Ryu, J. H.; Lee, Y.; Kong, W. H.; Kim, T. G.; Park, T. G.; Lee, H., Catechol-functionalized chitosan/pluronic hydrogels for tissue adhesives and hemostatic materials. *Biomacromolecules* 2011, 12 (7), 2653-2659.
4. Huynh, C. T.; Nguyen, M. K.; Tonga, G. Y.; Longé, L.; Rotello, V. M.; Alsberg, E., Photocleavable Hydrogels for Light-Triggered siRNA Release. *Adv. Healthcare Mater.* 2016, 5 (3), 305-310.
5. Ruskowitz, E. R.; DeForest, C. A., Photoresponsive biomaterials for targeted drug delivery and 4D cell culture. *Nature Reviews Materials* 2018, 3 (2), 17087.
6. LeValley, P. J.; Neelarapu, R.; Sutherland, B. P.; Dasgupta, S.; Kloxin, C. J.; Kloxin, A. M., Photolabile Linkers: Exploiting Labile Bond Chemistry to Control Mode and Rate of Hydrogel Degradation and Protein Release. *J. Am. Chem. Soc.* 2020, 142 (10), 4671-4679.
7. Brubaker, C. E.; Kissler, H.; Wang, L.-J.; Kaufman, D. B.; Messersmith, P. B., Biological performance of mussel-inspired adhesive in extrahepatic islet transplantation. *Biomaterials* 2010, 31 (3), 420-427.
8. Huotari, M.; Passlin, M.; Nordberg, H.-L.; Forsberg, M.; Kotisaari, S.; Tuomisto, L.; Shintani, F.; Tanaka, K.; Reenilä, I.; Laitinen, K., Effect of intracerebral 6-nitronoradrenaline, an endogenous catechol-O-methyltransferase (COMT) inhibitor, on striatal dopamine metabolism in anaesthetised rats. *Journal of neuroscience methods* 2001, 109 (1), 47-52.
9. Cui, J.; Iturri, J.; Paez, J.; Shafiq, Z.; Serrano, C.; d'Ischia, M.; del Campo, A., Dopamine-Based Coatings and Hydrogels: Toward Substitution-Related Structure–Property Relationships. *Macromolecular Chemistry and Physics* 2014, 215 (24), 2403-2413.
10. Shafiq, Z.; Cui, J.; Pastor-Pérez, L.; San Miguel, V.; Gropeanu, R. A.; Serrano, C.; del Campo, A., Bioinspired underwater bonding and debonding on demand. *Angewandte Chemie International Edition* 2012, 51 (18), 4332-4335.
11. Greco, C. T. Controlled nucleic acid delivery using photo-responsive polymeric formulations. University of Delaware, 2017.

12. Corrie, J. E.; Kaplan, J. H.; Forbush, B.; Ogden, D. C.; Trentham, D. R., Photolysis quantum yield measurements in the near-UV; a critical analysis of 1-(2-nitrophenyl) ethyl photochemistry. *Photochemical & Photobiological Sciences* 2016, 15 (5), 604-608.
13. Ruskowitz, E. R.; Deforest, C. A., Photoresponsive biomaterials for targeted drug delivery and 4D cell culture. *Nature Reviews Materials* 2018, 3.
14. Raman, R.; Hua, T.; Gwynne, D.; Collins, J.; Tamang, S.; Zhou, J.; Esfandiary, T.; Soares, V.; Pajovic, S.; Hayward, A.; Langer, R.; Traverso, G., Light-degradable hydrogels as dynamic triggers for gastrointestinal applications. *Science Advances* 2020, 6 (3), eaay0065.
15. Kloxin, A. M.; Kasko, A. M.; Salinas, C. N.; Anseth, K. S., Photodegradable hydrogels for dynamic tuning of physical and chemical properties. *Science* 2009, 324 (5923), 59-63.
16. Qvortrup, K.; Nielsen, T. E., A photolabile linker for the solid-phase synthesis of 4-substituted N H-1, 2, 3-triazoles. *Chemical Communications* 2011, 47 (11), 3278-3280.
17. Klán, P.; Šolomek, T.; Bochet, C. G.; Blanc, A. I.; Givens, R.; Rubina, M.; Popik, V.; Kostikov, A.; Wirz, J., Photoremovable protecting groups in chemistry and biology: reaction mechanisms and efficacy. *Chemical reviews* 2012, 113 (1), 119-191.
18. Šolomek, T.; Mercier, S.; Bally, T.; Bochet, C. G., Photolysis of ortho-nitrobenzyllic derivatives: the importance of the leaving group. *Photochemical & Photobiological Sciences* 2012, 11 (3), 548-555.
19. Ustahüseyin, Oya (2018): Tuning mechanical properties of hydrogels. Johannes Gutenberg-Universität Mainz. Thesis. urn:nbn:de:hebis:77-diss-1000018899
20. Zhao, Y.; Zheng, Q.; Dakin, K.; Xu, K.; Martinez, M. L.; Li, W.-H., New caged coumarin fluorophores with extraordinary uncaging cross sections suitable for biological imaging applications. *Journal of the American Chemical Society* 2004, 126 (14), 4653-4663.
21. Álvarez, M.; Best, A.; Pradhan-Kadam, S.; Koynov, K.; Jonas, U.; Kreiter, M., Single-Photon and Two-Photon Induced Photocleavage for Monolayers of an Alkyltriethoxysilane with a Photoprotected Carboxylic Ester. *Advanced Materials* 2008, 20 (23), 4563-4567.
22. Caliari, S. R.; Burdick, J. A., A practical guide to hydrogels for cell culture. *Nature Methods* 2016, 13 (5), 405-414.
23. Phelps, E. A.; Enemchukwu, N. O.; Fiore, V. F.; Sy, J. C.; Murthy, N.; Sulcek, T. A.; Barker, T. H.; García, A. J., Maleimide cross-linked bioactive PEG hydrogel exhibits improved reaction

- kinetics and cross-linking for cell encapsulation and in situ delivery. *Advanced Materials* 2012, 24 (1), 64-70.
24. Yang, S. H.; Kang, S. M.; Lee, K.-B.; Chung, T. D.; Lee, H.; Choi, I. S., Mussel-Inspired Encapsulation and Functionalization of Individual Yeast Cells. *Journal of the American Chemical Society* 2011, 133 (9), 2795-2797.
25. Feng, J.; Ton, X.-A.; Zhao, S.; Paez, J. I.; del Campo, A., Mechanically Reinforced Catechol-Containing Hydrogels with Improved Tissue Gluing Performance. *Biomimetics* 2017, 2 (4), 23.
26. Nahmany, M.; Melman, A., Studies on the synthesis of DNA-damaging part of leinamycin: regioselectivity in Ti (O*i*Pr) 4 mediated opening of hydroxy epoxides with carboxylic acids. *Tetrahedron* 2005, 61 (31), 7481-7488.
27. Paez, J. I.; Ustahüseyin, O.; Serrano, C.; Ton, X.-A.; Shafiq, Z.; Auernhammer, G. K.; d'Ischia, M.; del Campo, A., Gauging and Tuning Cross-Linking Kinetics of Catechol-PEG Adhesives via Catecholamine Functionalization. *Biomacromolecules* 2015, 16 (12), 3811-3818.
28. Takahashi, T.; Ikejiri, Y.; Himori, S.; Gotoh, H., Polymerization inhibition mechanism of 1, 4-naphthoquinone by experimentation and DFT calculations. *Polymer Journal* 2019, 51 (9), 929-934.
29. Hansen, M. J.; Velema, W. A.; Lerch, M. M.; Szymanski, W.; Feringa, B. L., Wavelength-selective cleavage of photoprotecting groups: strategies and applications in dynamic systems. *Chemical Society Reviews* 2015, 44 (11), 3358-3377.

Chapter 3: Preparation & Characterization of Photodegradable Adhesive PEG-catechol hydrogels

3.1 Abstract

In this chapter, the synthesis and the characterization of the properties of hydrogels derived from macromers described in Chapter 2 are presented. Hydrogels are formed under mild oxidative conditions by self-condensation of the catechol end-groups. Light-irradiation allows cleavage of the intercalated nitrobenzyl group and mediates depolymerization. The rheological properties of these hydrogels (crosslinking kinetics mechanical strength and photodegradation kinetics) are analyzed. Finally, the on-demand release of embedded particles and debonding from tissue mediated by light is demonstrated.

3.2 Introduction

Hydrogels are soft matrices widely used as biomaterials, due to their excellent biocompatibility, diversity of functionality, tunable biochemical and physical properties. The role played by the material is linked to the therapeutic action mode in tissue engineering,¹⁻⁴ medical adhesives^{5, 6} or drug delivery.⁷ The properties of the hydrogel such as mechanics, microstructure or degradation can be specifically programmed depending on the particular application. Designing mechanically stable hydrogels with exceptional spatiotemporally degradable properties remains a challenge. Direct manipulation of hydrogel degradation can be highly advantageous for biomedical applications. In the last years, a few approaches to obtain dynamic hydrogels with the ability to change properties on demand have been reported. Photodegradation is one way that such control could be accomplished.

Light is an useful stimulus to fine regulate the system's properties, since it can be spatiotemporally controlled and administered in variable wavelength and intensity,⁸ and it provides possibilities for uncomplicated integration into medical devices for *in vitro* and *in vivo* applications. PEG hydrogels were the first reported examples of photodegradable hydrogels.⁹⁻¹¹ Anseth *et al.* introduced an o-nitrobenzyl ether photocleavable group into a PEG macromer in order to soften the hydrogel after light exposure (Fig. 3.1.A-C).¹² Kloxin *et al.* used a similar

strategy, incorporating o-nitrobenzyl groups with PEG diacrylate to create the first 3D photolabile hydrogel network, demonstrating spatiotemporal control and precise patterning with a two-photon laser scanning microscope (Fig. 3.1.D-F).¹¹

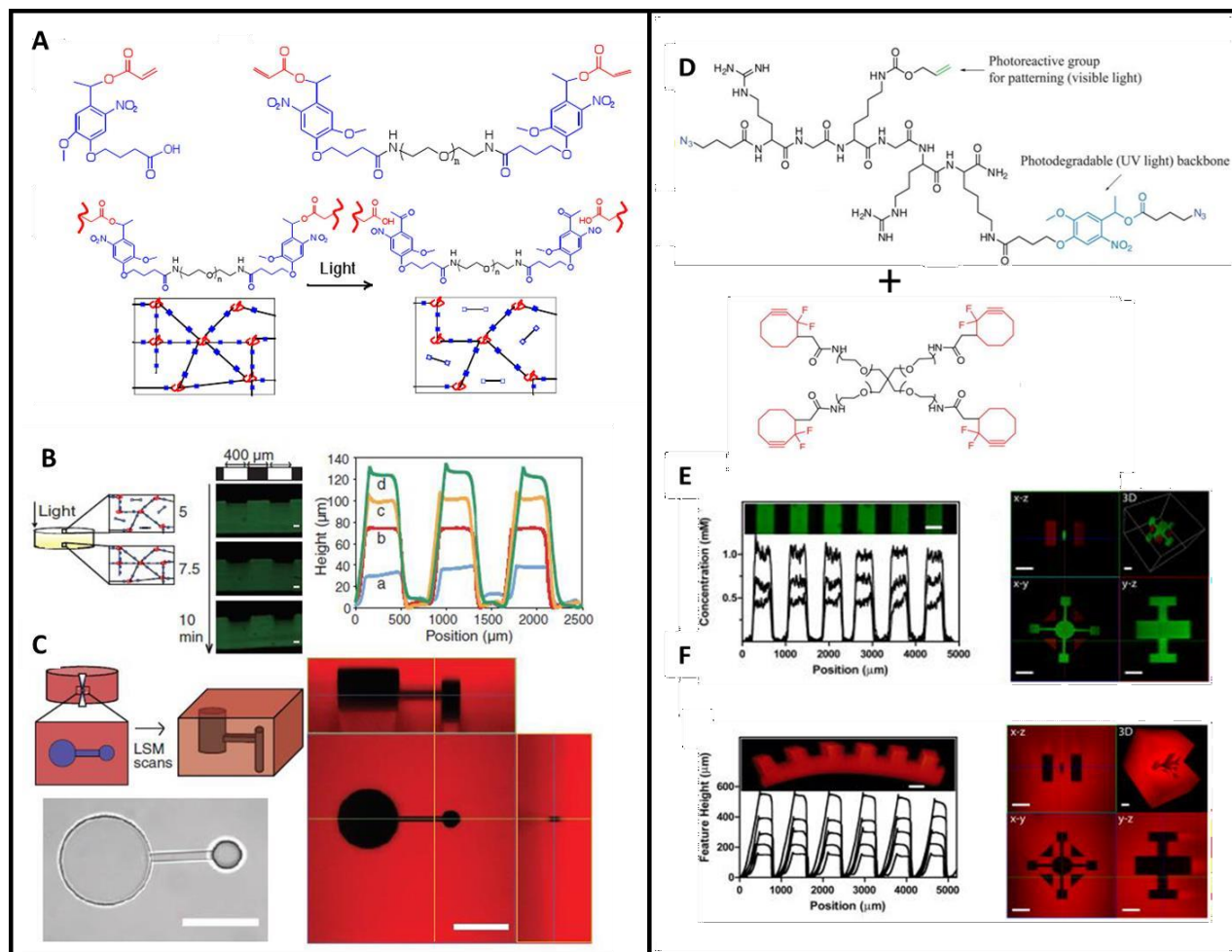


Figure 3.1 Light modulated patterning of 3D hydrogels. (A) Fabrication of a photodegradable hydrogel and photodegradation for tuning gel properties. (B-C) Two and three-dimensional patterning of photodegradable hydrogels. Thick gels demonstrate surface erosion upon irradiation (B). Interconnected three-dimensional channels were fabricated within a photodegradable gel (C).⁴ (D) Click-functionalized macromolecular precursors (PEG-tetraDIFO3 and bis(azide)-functionalized polypeptides), light triggered degradation of PEG hydrogel containing o-nitrobenzyl crosslinker for biochemical (E) and biophysical patterning using UV-Vis light (F). Reproduced from DeForest and Anseth with permission from Nature Publishing Group.¹²

In the last years, catechol-terminated PEGs have been used to form hydrogels. Mussel-inspired gels demonstrated potential in suture-less wound repair,^{13-14,15-19} sealing of fetal membranes,^{19, 20} cell engineering^{17,21} or local delivery of therapeutic drug particles.²² The adhesive and mechanical properties of PEG-catechol systems can be controlled by PEG architecture (i.e., linear, 4-, 6-, 8-arm), polymer molar mass (i.e., 10, 20 kDa), and PEG-catechol linker (i.e., ester, amide).^{23, 24} PEG-catechol adhesives have comparable properties, in terms of mechanical strength and tissue adhesion, to commercial PEG-based medical sealants (e.g., CoSeal and DuraSeal). These adhesives are used in clinical procedures as a two-component system delivered via a double-barrel syringe or similar medical device. This chemistry has also been transferred to mediate adhesion of hemostatic pads (InnoSEAL®, InnoTherapy). However, there is a limitation in the development of on demand photodegradable mussel-inspired adhesives which will be ideal for complex geometries, and light-modulated release of therapeutic acrgos, therefore adjusting material's degradation to the healing progress and contributing to the overall tissue regeneration.

So far, various versatile hydrogels have been reported, activated by triggers that are potentially unsuitable for biomedical applications (i.e., high pressure,²⁵ high temperature,²⁶ large change in pH^{27, 28} or redox environment).²⁹ Recently, a photoremoveable hydrogel has been commercialized as skin adhesive (Lumina™, CE marked).³⁰ Additionally, chitosan and NHS-terminated polyethylene glycol (PEG) hydrogels containing nitrobenzyl groups have been explored as *in situ* forming and photodegradable hydrogels that can adhere to skin tissue and be used for wound management.³¹ Designing a hydrogel which can be formed under mild physiological conditions, used as bioadhesive and degraded on demand; remains a challenge.

In this chapter, the photodegradation properties of derived gels (**PEG-NBt-c** and **PEG-NNPE**) were characterized by photorheology and compared to other photocleavable gels previously reported in the literature (**PEG-NDop**). The efficient photodegradability of novel hydrogels allows the modulation of material's stiffness and the creation of gel microenvironments. The PEG-based hydrogels containing a novel triazole nitrobenzyl linker (**PEG-NBt-c**) can attach to wet skin and photodegrade on-demand under cytocompatible irradiation doses. These findings

expand the functionality of previously reported hydrogel systems^{32, 33} for application scenarios in advanced wound management.

3.3 Results and Discussion

3.3.1 Characterization of crosslinking kinetics

The PEG-catechol precursors synthesized in Chapter 2 (**PEG-NBt-c**, **PEG-NNPE**, **PEG-NDop** and **PEG-Dop**) were used to formulate hydrogels via oxidative crosslinking. PEG polymeric precursors of 10 and 20 kDa were used since previous work demonstrated that such size range is relevant for 3D cell encapsulation applications.³⁴ Also, the oxidant (sodium periodate) concentration used in this formulation is within the range typically used for mussel-inspired hydrogels for cell encapsulation and *in vivo* tissue adhesion (ca 10-30 mM).^{17-19, 35, 36}

The oxidative crosslinking of the macromers was followed by rheology. A 40 µL volume of precursors solution (gel composition: 10 kDa, 10 wt% polymer, 9 mM oxidant, in water (pH≈6.8), (catechol groups to oxidant molar ratio= 2.1)) was placed between the rheometer plates and the changes in the shear storage (G') and loss (G'') moduli over time were followed as indication of the crosslinking kinetics until a stable plateau was reached in the rheological curves.

Representative rheological curves of the crosslinking of the PEG-catechol hydrogels are shown in Figure 3.2. The gradual increase of G' over time reflects the stiffening of the gel as the crosslinking reaction takes place. **PEG-NBt-c** and **PEG-NNPE** showed a sigmoidal shape, typical of processes with slow crosslinking kinetics. The control sample **PEG-Dop** showed a similar profile. **PEG-NDop** showed a different profile (Figure 3.2C), characteristic of crosslinking processes with two parallel crosslinking reactions with different kinetics. This profile has been reported previously.³⁷

The kinetics of the crosslinking was different for the different samples. The macromers containing a catechol group as crosslinker, **PEG-NBt-c** and **PEG-Dop** respectively, reached the plateau value of G' within 50 min. **PEG-NNPE** and **PEG-NDop** which contain nitrocatechol as

crosslinking functionality, showed a much slower kinetics at the same crosslinking conditions, and plateau values were reached at 200 min. This trend can be explained by the mechanism of self-condensation of nitrocatechols. Nitrocatechols (i.e. nitrodopamine and nitronorepinephrine) present an electron-withdrawing nitro group in the 6-position, which lowers the pK of the catechol hydroxyl groups ($pK_1 \sim 6.5$ and $pK_2 \sim 10$), decreasing the oxidation potential of the catechol ring and increasing the stability against oxidation.³⁸ Instead, the unsubstituted catechols participate in different crosslinking paths, forming oligomers through polymerization of the catechol (as exemplified in Figure 1.2 in Chapter 1). This alteration in the crosslinking mechanism contributes to the difference in NaIO₄ concentration-dependent curing behavior between PEG-nitrocatechol and PEG-catechol hydrogels.³⁹

The final values of G' differed among the different polymers. **PEG-NBt-c** reached a final G' of 339 Pa, **PEG-NNPE** reached the lowest G'= 200 Pa. **PEG-Dop** achieved the highest G' of 12800 Pa, and **PEG-NDop** reached G' of 2500 Pa. Higher G' of PEG-Dop hydrogels suggested higher crosslinking density which could be fully attributed to the difference in the degree of polymerization between the catechol and nitrocatechol species. It is known that nitrocatechols mostly form dimers through oxidative crosslinking while unsubstituted catechols can form oligomers with higher numbers of repeats as high as six,³⁹ therefore the latter present higher G' in the final PEG catechol gels.^{38, 39} The **PEG-Dop** stiffened and showed elevated G' values because of the long polymer chains between crosslinks which didn't have the possibility to reorganize themselves within the short time scale of the oscillatory deformation. This indicated that PEG-nitrocatechol hydrogels were more loosely crosslinked than PEG-catechol.³⁹ Mechanical strength is a relevant parameter for hydrogels designed for adhesive applications. Formation of the nitrocatechol dimers leads to reduced crosslinking density and lower bulk mechanical properties, which is typically reflected in lower adhesive performance.

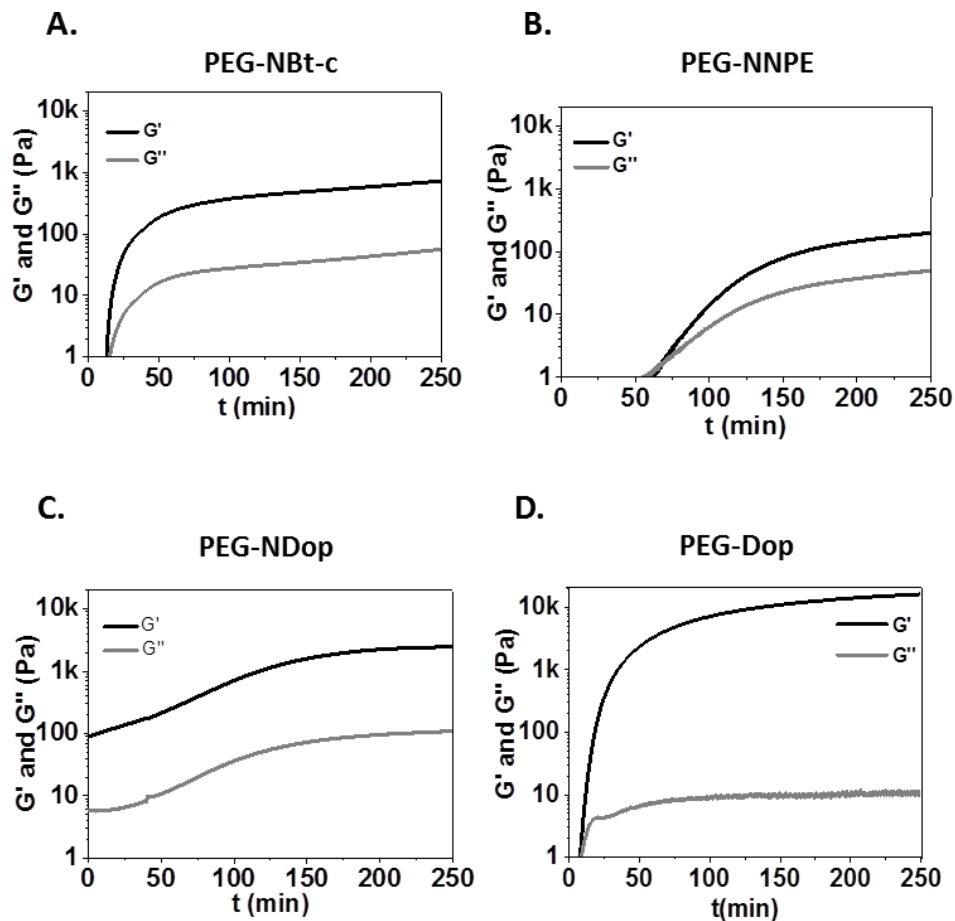


Figure 3.2 Rheological measurements of oxidative crosslinking of PEG-catechol hydrogels (**PEG-NBt-c** (A), **PEG-NNPE** (B), **PEG-NDop** (C) and **PEG-Dop** (D)). Final gel composition: 10 kDa macromer, 10 wt% polymer content, 9 mM NaIO₄, in water (pH≈6.8).

Table 3.1 Shear storage modulus (G'), loss modulus (G'') and gelation time of the different PEG-catechol gels, as measured by in situ oscillatory rheology

Hydrogel ^(a)	gelation time (min)	G' at t= 250 min	G'' at t= 250 min

PEG-NBt-c 	15	339 Pa	76 Pa
PEG-NNPE 	55	218 Pa	47 Pa
PEG-NDop 	< 2	2.5 kPa	401 Pa
PEG-Dop 	10	12.8 kPa	9 Pa

^(a) Gel composition: 10 kDa, 10 wt% polymer, 9 mM oxidant, in water (pH≈6.8), (catechol groups to oxidant molar ratio= 2.1), sample thickness= 250 μm.

In summary, the crosslinking kinetics, in order to reach the final plateau, of the PEG-catechol hydrogels followed the sequence: **PEG-Dop** > **PEG-NBt-c** >> **PEG-NDop** > **PEG-NNPE**. The crosslinking degree (i.e. the final G' and the cohesiveness of the material) followed the sequence: **PEG-Dop** >> **PEG-NDop** >> **PEG-NBt-c** > **PEG-NNPE** (Table 3.1). Note that the kinetics and final G' of catechol-crosslinked hydrogels can be significantly accelerated at higher pH or oxidant concentration.^{14, 40} This will be studied in the following section.

Study of the effect of pH and oxidant concentration on gelation

The possibility to obtain hydrogels with different mechanical properties was tested by preparing hydrogels at two different oxidant concentrations (9 mM and 18 mM) and within the pH range from 7.2 to 8.3. These gelation conditions are compatible with living cells, as will be shown in Chapter 4. Increasing the oxidant concentration and the pH leads to a higher crosslinking degree and higher storage modulus of the hydrogel (Tables 3.2 - 3.3) and also accelerates the crosslinking process, in agreement with previous studies.⁸ This is due to the oxidative crosslinking of catechol, which accelerates at higher pH and concentration of oxidant. The rate of crosslinking increases with increasing pH because of higher conversion of catechol to quinone. Additionally, crosslinking using an oxidant (NaIO_4) polymerizes the α,β -dehydro form of the catechol with a maximum rate of crosslinking occurring at oxidant: catechol molar ratios (0.5 – 1).⁴¹

Table 3.2 Effect of increasing pH over G' and gelation time of the model **PEG-Dop** gels, as measured by *in situ* oscillatory rheology, at constant 9 mM oxidant concentration.

pH ^(a)	gelation time (min)	G' at t= 500 min (kPa)	G'' at t= 500 min (Pa)
7.2	32	2	124
7.5	27	3	21
7.8	18	4	68
7.9	16	4	43
8.3	11	12	53

^(a) Gel composition: 10 kDa, 10 wt% polymer, 9 mM oxidant, in 50 mM HEPES, sample thickness= 250 μm .

Table 3.3 Effect of increasing pH over G' and gelation time of the model PEG-Dop gels, as measured by *in situ* oscillatory rheology at constant 18 mM oxidant concentration.

pH ^(a)	gelation time	G' at t= 500 min	G'' at t= 500 min

	(min)	(kPa)	(Pa)
7.2	28	3	135
7.5	23	4	25
7.8	14	6	75
7.9	12	9	44
8.3	8	15	100

^(a) Gel composition: 10 kDa, 10 wt% polymer, 18 mM oxidant, in 50 mM HEPES, sample thickness= 250 µm.

Reported studies show that cell encapsulation with star-PEG requires hydrogels with final G' ~ 0.03-10 kPa⁴². By adjusting the oxidant concentration (9-18 mM NaIO₄) and the pH (7.0-.7.5), G' in the gels fabricated in this Thesis ranged between 0.1 and 12 kPa.

3.3.2 Characterization of hydrogel's photodegradation

Photodegradation process was also followed by rheology. Hydrogel samples were formed between the rheometer plates and irradiated during measurements. An oil trap was used to prevent dehydration during the experiment. The composition of the precursor hydrogel solution was: 10 kDa, 10 wt% polymer, 9 mM NaIO₄ (catechol: oxidant molar ratio is 4.4), in PBS:water (1:1) at pH 7.0. A transparent lower plate was used for the measurements to allow illumination of the probe ($\lambda = 365$ nm, 10 mW cm⁻²). The light-exposure dose used for the experiments is calculated as:

$$\frac{\text{Irradiance}}{1,000} \times \text{time} = \text{Irradiation Dose}$$

The irradiance measured in mW cm⁻², the time in s and the irradiation dose in J cm⁻².⁴³

PEG-NBt-c and **PEG-NNPE** gels showed a rapid decay in G' when the light was turned on (Figure 3.3.), indicating immediate softening of the hydrogel due to photocleavage of the nitrobenzyl triazole unit. When the measurement was finished and the rheometer plates were detached, a liquid brownish solution was observed on the plates, confirming the degradation of the previously crosslinked network. **PEG-NBt-c** gels with initial $G' \sim 500$ Pa showed a 50% loss of mechanical properties after 3 min, and fluidization at > 7 min of exposure (irradiation dose = 3.6 J cm^{-2} , Fig. 3.3A). In comparison, the initial $G' \sim 2000$ Pa of **PEG-NNPE** was halved after 13 min and no longer measurable after 30 min of exposure (irradiation dose = 18 J cm^{-2} , Fig. 3.3B).

Similar experiments were conducted with control gels. **PEG-NDop** with initial $G' (\sim 2500 \text{ Pa})$ showed no changes in G' at the same irradiation power (10 mW cm^{-2} , Fig. 3.3C), which evidences the poor photodegradability of this control material. **PEG-Dop** gel with initial $G' \sim 10000$ Pa did not change either during exposure. This result confirms that the photocleavable character of **PEG-NBt-c** and **PEG-NNPE** is due to the presence of the nitrobenzyl triazole linker.

Figure 3.3.E compares the photodegradation kinetics of the different polymers, as measured by the decay of G' in time. In agreement with previous work, it was assumed that the softening process had a first-order kinetics, and the data were fitted to the equation⁴⁴:

$$G'(t) = G'_0 e^{-k_{obs} t}$$

where $G'(t)$ is the shear storage modulus as a function of time, G'_0 is the initial shear storage modulus, and t is the time. The $\ln(G'/G'_0)$ was plotted as a function of time (Figure 3.3F). Only values of $G'(t)$ corresponding to 90% to 50% of the initial G'_0 were used for calculation of the rate constant (Figure 3.3E).⁴⁵ The first-order rate constant (k_{obs}) of the photodegradation was estimated from the slope of the plot. **PEG-NBt-c** gels presented good fitting with the assumed kinetic law for a first-order process, which is observed from figure 3.3F, where the slope fits to the linear regression model. However, **PEG-NNPE** shows some deviation from the previously assumed first-order kinetic profile. This result suggest that photodegradation of **PEG-NNPE** could involve other secondary photochemical processes, which were not investigated further in this Thesis. Nevertheless, assuming that the determined values of k_{obs} can be compared, the photodegradation rate constant of **PEG-NBt-c** ($k_{obs} = 1.5 \pm 0.002 (\times 10^{-3}) \text{ s}^{-1}$) gels was 7.5 times

faster than that of **PEG-NNPE** ($k_{obs} = 0.2 \pm 0.001$ ($\times 10^{-3}$) s^{-1}). Note that G'_0 is different in both cases, being higher for **PEG-NNPE**, which could also explain the lower degradation efficiency of **PEG-NNPE**, (see figure 3.3B) as well as the possible secondary photochemical reactions taking place in PEG-NNPE, which may reduce its photodegradation efficiency.

The control **PEG-NDop** hydrogel showed slight stiffening instead of degradation during irradiation. At the used doses (Irradiation dose = 30 J cm^{-2} ; $I_0 = 10\text{ mW cm}^{-2}$) no significant photodegradation is expected for this gel. Reported work shows that **PEG-NDop** gels covalently crosslinked with 20 mM oxidant proved non-degradable at all because of too extensive crosslinking, even at high exposure doses= 400 J cm^{-2} ($\lambda = 360\text{ nm}$). **PEG-NDop** non-covalently crosslinked with Fe^{3+} ions required ca 85 J cm^{-2} exposure dose for degradation.⁴⁶ Since no drying of the hydrogel is expected to occur because the sample was sealed during the experiment with oil, the stiffening of this gel could be a consequence of side reactions triggered by light.

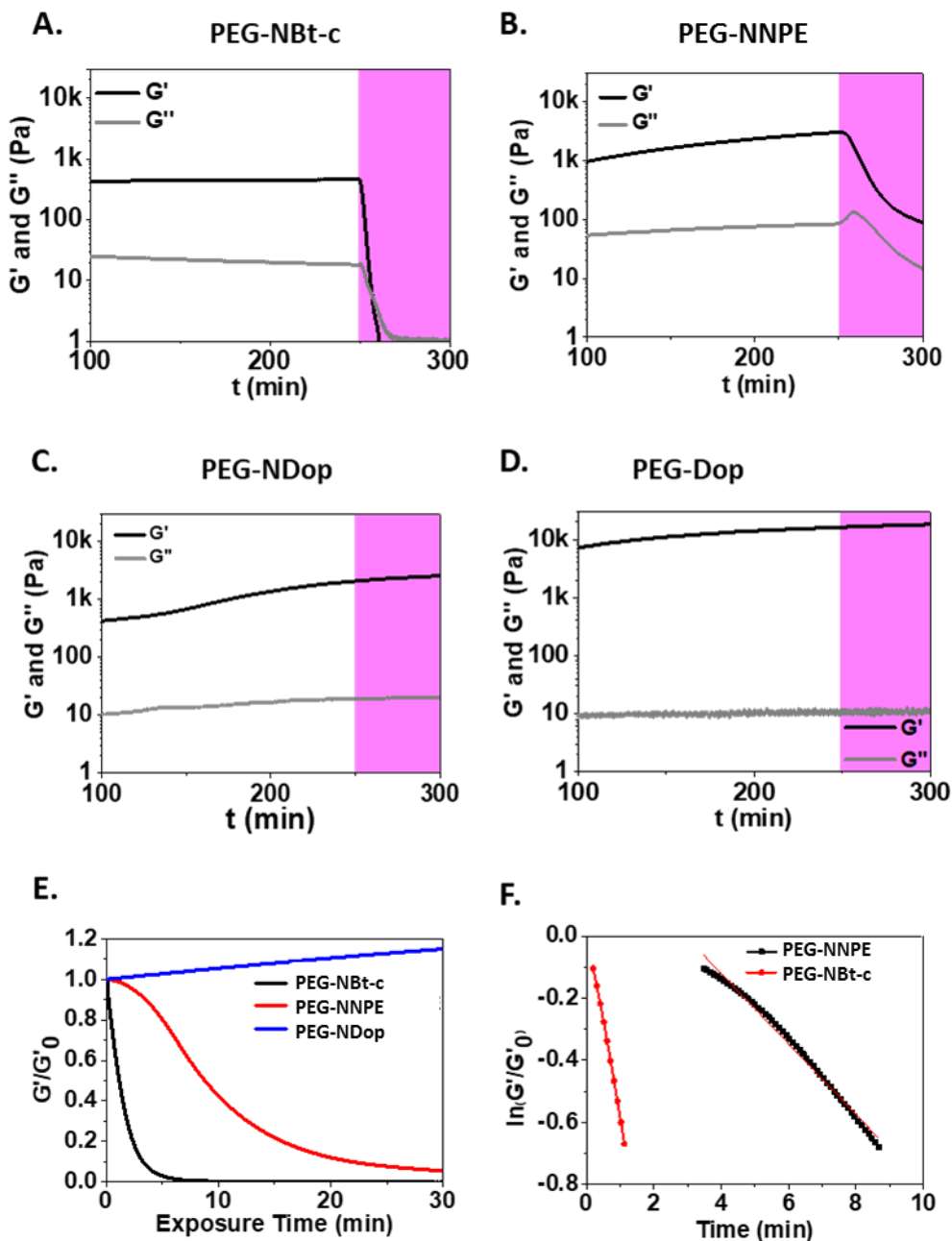


Figure 3.3 Study of photodegradation of different PEG-catechol hydrogels by in situ rheology (G' : black line and G'' : grey lines). (A-E) Gel Composition: 10 kDa, 10 wt% polymer, 9 mM NaIO₄ (catechol: oxidant molar ratio is 4.4), in PBS:water (1:1), pH 7.0. The photodegradation efficiency of **PEG-NBt-c** (A), **PEG-NNPE** (B) and **PEG-NDop** (C) was measured and compared in (E). (F) Kinetic parameters for the photodegradation reaction extracted from rheology data in (E). Curing samples were allowed to gelate in situ, followed by photoirradiation (indicated in pink color) at conditions: $\lambda = 320\text{-}550\text{ nm}$, 10 mW cm^{-2} .

Experiments with hydrogels at a lower polymer concentrations, i.e. 5 wt%, typically used for cell encapsulation, were performed. These experiments should estimate if reported cytocompatible irradiation doses ($5\text{--}10 \text{ J cm}^{-2}$)^{11, 45, 47, 48} are enough to photodegrade the new **PEG-NBt-c** hydrogels. The hydrogel composition was 10 kDa, 5 wt% polymer, 9 mM NaIO₄, PBS:water (1:1), pH 7.0. Irradiation conditions were: $\lambda = 320\text{--}550 \text{ nm}$, 10 mW cm^{-2} . Crosslinked **PEG-NBt-c** gels showed a $G'_{\text{0}} \sim 0.1 \text{ kPa}$ (Figure 3.4A), which softened to 0.05 kPa within 2.5 min exposure (corresponding to an irradiation dose of 1.5 J cm^{-2}). Full degradation was achieved after 7 min irradiation dose (4.2 J cm^{-2}). Control hydrogel **PEG-NDop**, with $G'_{\text{0}} \sim 0.4 \text{ kPa}$, showed a slower photodegradation rate. G' was halved after 36.5 min exposure (irradiation dose= 22 J cm^{-2}) and full degradation was not even achieved at long irradiation doses ($> 90 \text{ J cm}^{-2}$, 100 min) (Figure 3.4C). These results demonstrate that the photocleavable unit in **PEG-NBt-c** is much more efficient than **PEG-NDop**, in good agreement with the photolysis studies in solution shown in Chapter 2. For reference, typical exposure conditions used in reported studies for photodegradation of PEG-NB base hydrogels with $G'_{\text{0}} = 1.5$ to 5 kPa (10 - 20 kDa 5 wt% concentration)^{44, 48, 49} are $\lambda = 365 \text{ nm}$, $I = 5\text{--}20 \text{ mW cm}^{-2}$ and time = 2–30 min, corresponding to total exposure doses of $5\text{--}36 \text{ J cm}^{-2}$.^{11, 45, 47, 48} According to these results, the exposure doses required for photodegradation of **PEG-NBt-c** gels are expected to be within the cytocompatible range.

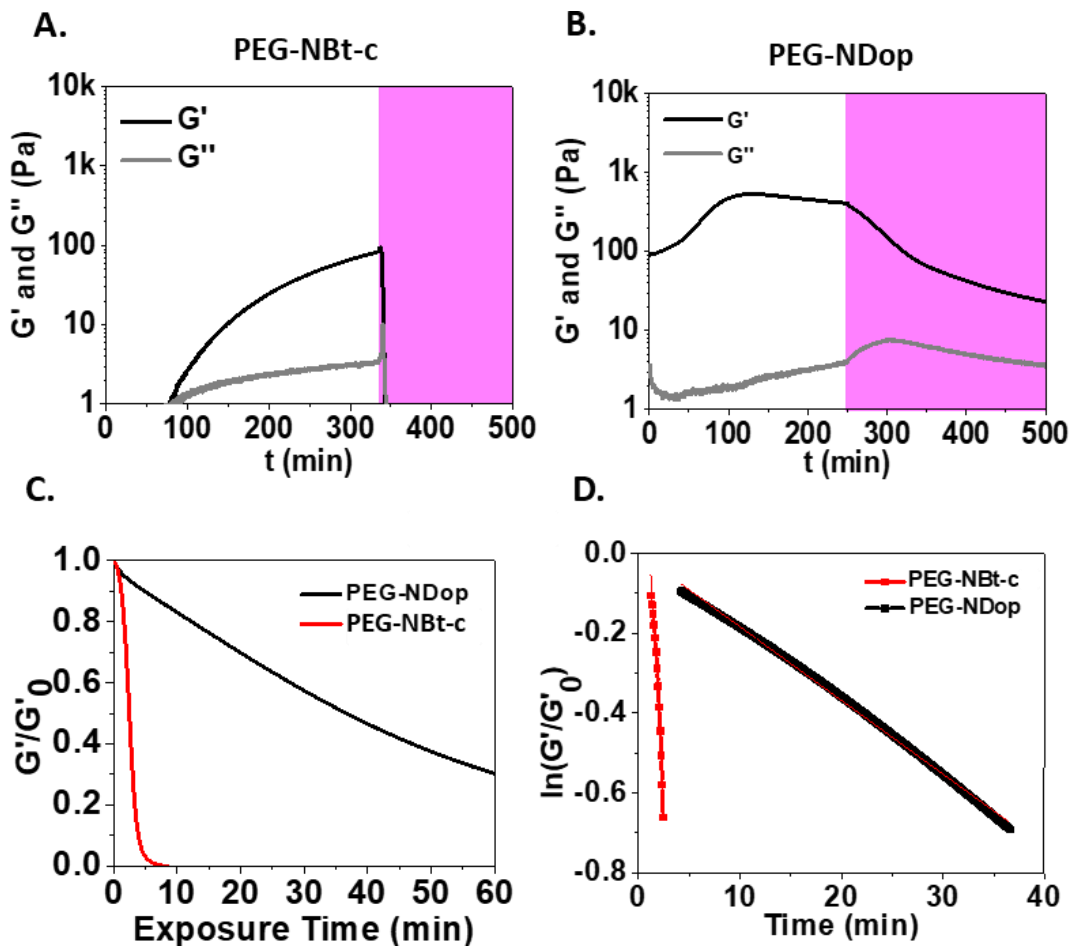
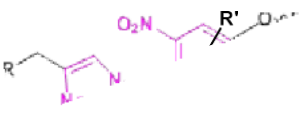
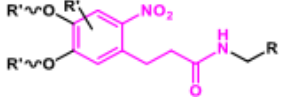


Figure 3.4 Study of the crosslinking and subsequent photodegradation of the different PEG-catechol hydrogels by rheology (G' : black line and G'' : grey lines). (A-C) Composition: 10 kDa, 5 wt% polymer, 9 mM oxidant (catechol: oxidant molar ratio is 2.2), in PBS:water (1:1), pH 7.0. The photodegradation efficiency of **PEG-NBt-c** (A) and **PEG-NDop** (B) was measured and compared in (C). (D) **PEG-NDop** required 36.5 min vs. **PEG-NBt-c** 2.5 min of exposure (dose= 22 vs. 1.5 J cm^{-2}) for 50% degradation of gel under same conditions (5 wt %, 10-kDa gels, with initial $G' \sim 0.4 \text{ kPa}$ and $G' \sim 0.1 \text{ kPa}$, respectively). Curing samples were allowed to gelate *in situ*, followed by photoirradiation (indicated in pink color) at conditions: $\lambda = 320\text{-}550 \text{ nm}$, 10 mW cm^{-2} .

Table 3.4 Comparison of the kinetics of photodegradation of **PEG-NBt-c** vs. **PEG-NDop** gels as measured by photorheology.^(a)

Hydrogel and photolabile group structure	k_{obs} [ms ⁻¹]	k_{obs} relative value
PEG-NBt-c 	7.4 ± 0.4	24.0
PEG-NDop 	0.31 ± 0.001	1.0

(a) $\lambda = 320\text{-}550$ nm (centered at 365 nm), $I_0 = 10$ mW cm⁻², T=25°C; k_{obs} calculated from the $\ln(G'/G'_0)$ vs. time plot. Gel composition: 4-arm PEG, 10 kDa, 5 wt%, 9 mM ox., in PBS:water (1:1) pH 7.0, sample thickness= 250 μm .

To further optimize the photodegradation of **PEG-NBt-c** for cell-encapsulation applications, experiments using PEG precursors of higher molar mass were performed. Hydrogels were prepared using 20 kDa PEG precursors, and compared with 10 kDa analogues. Precursor solutions with 10 wt% 20 kDa, 18 mM NaIO₄ in 50 mM HEPES buffer, pH 7.5 were prepared. Resulting **PEG-NBt-c** hydrogels showed a $G'_0 = 1$ kPa, which decayed to 0.5 kPa after 3.9 min exposure (irradiation dose = 2.3 J cm⁻², Fig. 3.5A), and was fully degraded after 30 min (18 J cm⁻², Fig. 3.5A). In comparison, a 10 kDa gel polymerized at comparable conditions formed gels with $G'_0 = 11$ kPa that required 7.2 min exposure (4.3 J cm⁻², Fig. 3.5A) for a 50% decay in G' value. The lower G'_0 and faster degradation of the 20 kDa hydrogel is explained by the lower number of crosslinking points per chain length. For the same polymer concentration in the hydrogel, the crosslinking density in the PEG gel from 20 kPa precursors is lower than from 10 kPa.

The same analysis was conducted with **PEG-NBt-c** hydrogels from 20 kDa and 10 kDa precursors that showed a similar initial $G'_0 = 1$ kPa after crosslinking. For this purpose hydrogels with the following composition were prepared: 10 wt% 20 kDa **PEG-NBt-c**, 18 mM NaIO₄, 50 mM

HEPES buffer at pH 7.5, and 10 wt% 10 kDa PEG-NBt-c, 9 mM NaIO₄, PBS:water (1:1), pH 7.0. The 10 kDa hydrogel lost 50% of mechanical stability after 1.5 min exposure (0.9 J cm^{-2} , Fig. 3.5B), whereas the 20 kDa required 3.5 min (2.1 J cm^{-2} , Fig. 3.5B). This result can be explained by the higher density of catechol crosslinks present in 10 kDa PEG network (final catechol: oxidant ratio = 4.4 vs 1.1). The higher the concentration of photodegradable crosslinks, the higher number of chemical bonds are cleaved during exposure, and the faster degradation at comparable dose.

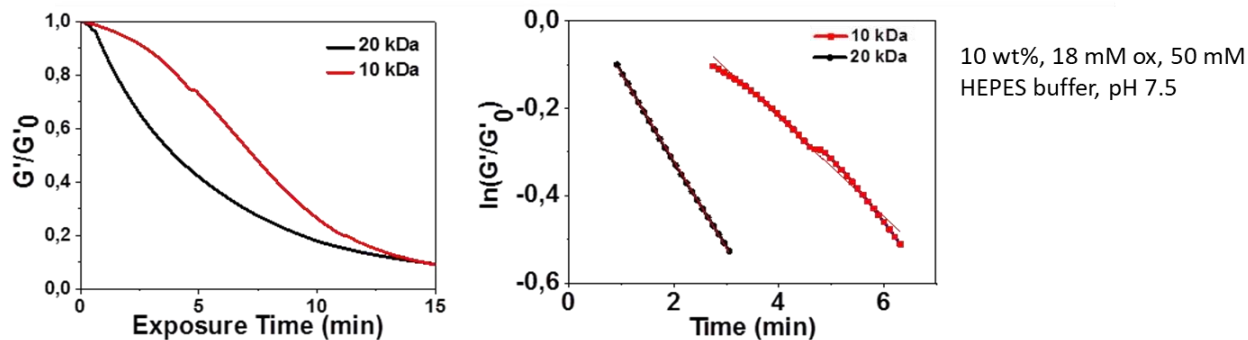
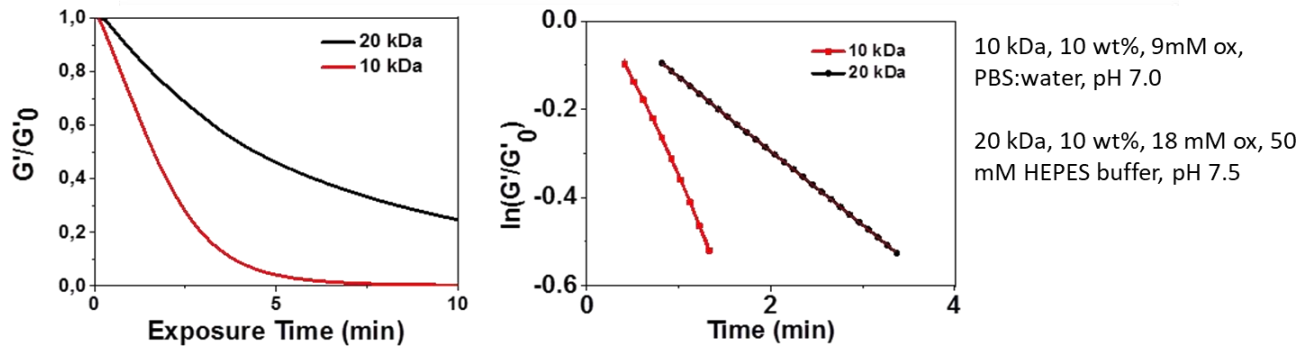
A.**B.**

Figure 3.5 Photodegradation kinetics of hydrogels with 10 kDa vs 20 kDa PEG-NBt-c precursor. (A-B) Normalized rheology curves during irradiation at $\lambda = 365 \text{ nm}$ (10 mW cm^{-2}).

Light-mediated degradation provides the opportunity of precise dose control.

Experiments were also performed to study the tunability of the photodegradation by exposing a

hydrogel to different pulses and to different irradiance values. Fig. 3.6B shows a hydrogel with initial $G' \sim 17$ kPa that is sequentially softened by 25% or 80% by applying successive illumination pulses of 3 min duration. Fig. 3.6D shows another hydrogel (initial $G' \sim 1$ kPa) softened by 25% or 50% through repetitive 2-min irradiation pulses. Figure 3.7 shows a hydrogel that is illuminated with light of decreasing irradiance, from 10 to 5 to 1 mW cm^{-2} . A slower degradation rate was seen with decreasing irradiance. A 50% softening required 1.7 min, 4.8 min and 17 min of illumination respectively.

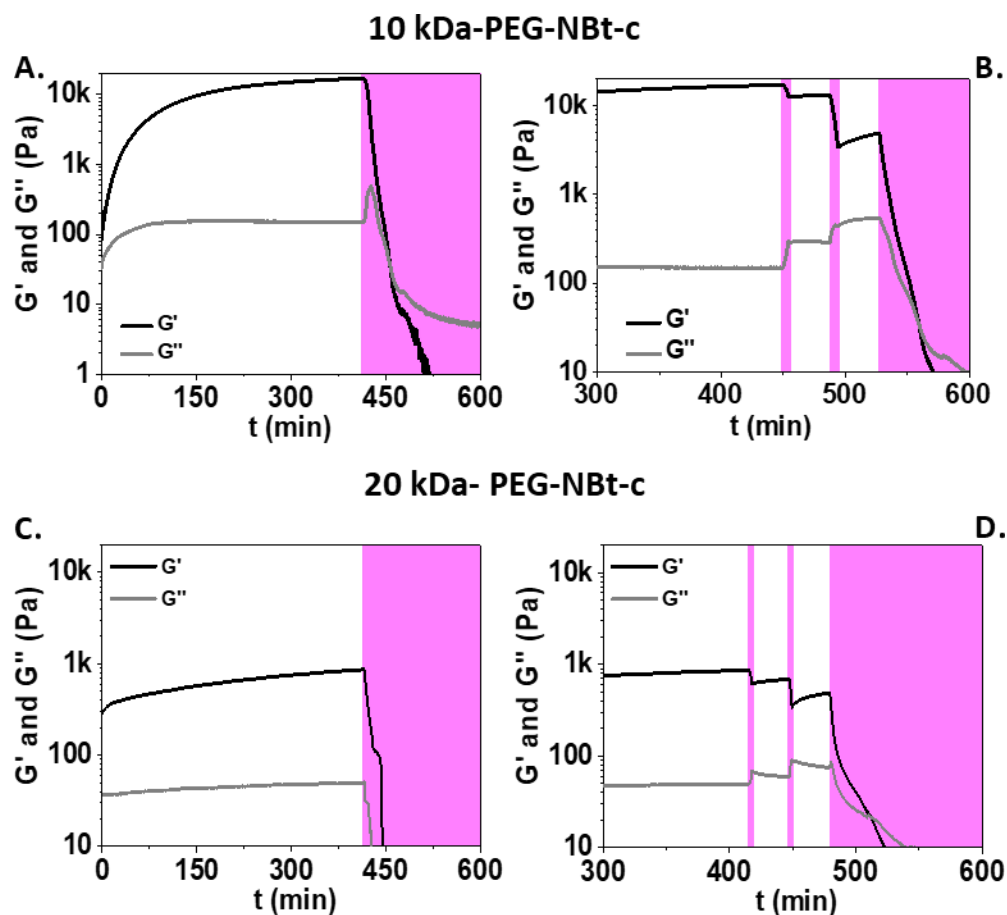


Figure 3.6 Oxidative curing and photodegradation of **PEG-NBt-c** hydrogels by in situ rheology. A-D) Time sweep measurements. Gels were allowed to cure for 400 min in the dark and then the illumination source was turned on ($\lambda = 365$ nm, 10 mW cm^{-2} , indicated in pink color in the plots). Composition of hydrogels: 10 kDa (A-B) or 20 kDa (C-D), 10 wt% polymer, 18 mM oxidant, 50 mM HEPES buffer, pH 7.5; cat: oxid. mol. ratio= 2.2. Photodegradation process applied was either continuous (A and C) or stepwise (B and D, pulsed irradiation of 180 s (B) and 120 s (D)).

To get a deeper insight on the photodegradation kinetics of **PEG-NBt-c** hydrogels, and to compare it to reported photocleavable hydrogels, time sweep experiments were used to estimate the rate constant of gel photodegradation (k_{obs} , see Fig. 3.7). A value $k_{obs} = 6.8 \times 10^{-3} \text{ s}^{-1}$ was obtained for **PEG-NBt-c**. The value $k_{obs} = 2.6 \times 10^{-3} \text{ s}^{-1}$ was obtained from the literature for a nitrobenzyl ester linker.^{44, 45, 48} The degradation kinetics obtained for Nbt is, therefore, within the same order of magnitude than the kinetics of reported systems based on nitrobenzyl ester systems, which ranged 2.2 to $3.3 \times 10^{-3} \text{ s}^{-1}$.^{12, 45} The kinetic parameter, defined as $k_{obs} / I_0 (\times 10^4) = 7 \text{ cm}^2 \text{ s}^{-1} \text{ mW}^{-1}$, indicates cleavage kinetics independently from the light intensity applied. Its value was in agreement with reported values of ester-nitro benzyl gels in the range 3.3 - $5.8 \text{ cm}^2 \text{ s}^{-1} \text{ mW}^{-1}$ (Table 3.5). These results demonstrate that the photodegradability of **PEG-NBt-c** gels is similar to other photodegradable gels used for cell therapy applications and serves as validation of our molecular design. Furthermore, as this is the first report on photolabile gels based on triazole nitrobenzyl linkages, these findings complement the toolbox of X-nitro benzyl cleavable linkers (X= ester, amide, carbonate, carbamate) recently investigated.⁴⁴

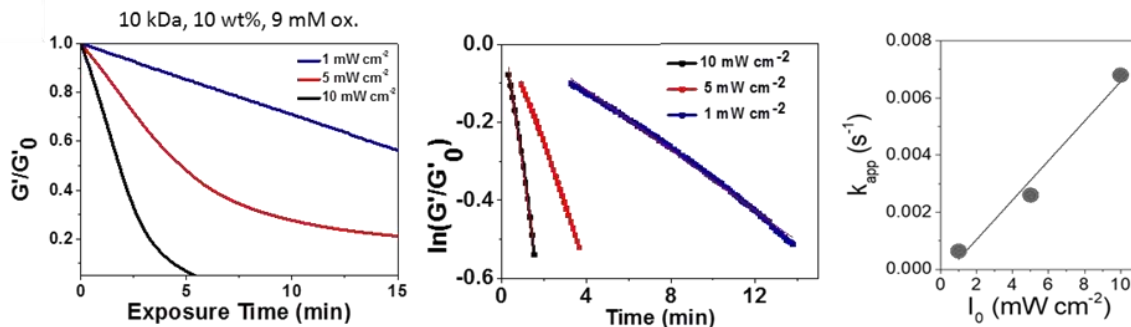


Figure 3.7 Kinetic parameters for the photodegradation reaction extracted from rheology data. Data correspond to 10 kDa **PEG-NBt-c** hydrogels exposed to different light intensities ($\lambda = 365 \text{ nm}$, irradiance = 1, 5 and 10 mW cm^{-2}).

Table 3.5 Kinetic parameters for the photodegradation reaction of nitrobenzyl triazole (**PEG-NBt-c**) and nitrobenzyl ester (**PEG-NBe-c**) units as obtained from photorheology measurements of the corresponding hydrogels.

Hydrogel and photolabile group structure	k_{obs} [ms ⁻¹]	$k^{obs} / I_0 (x 10^4)$ [cm ² s ⁻¹ mW ⁻¹] ^(b)
PEG-NBt-c ^(a) 	6.8 ± 0.2 ^(b)	7 ± 0.5 ^(c)
PEG-NBe-c ^(c) 	2.6-3.3 ^(d)	3.3-5.8 ^(d)

^(a) Gel composition: 4-arm PEG, 10 kDa, 10 wt%, 9 mM ox., in 50 mM HEPES buffer pH 7.5, sample thickness= 250 μ m. Irradiation conditions: λ = 365 nm, I_0 = 10 mW cm⁻², T=25°C. ^(b) Calculated from the $\ln(G'/G'_0)$ vs. t plot. ^(c) Calculated from k_{obs} vs. I_0 plot; I_0 = 1, 5 and 10 mW cm⁻². ^(d) λ = 365 nm, I_0 = 10 mW cm⁻², obtained from Refs. 44, 45, 48

To conclude this section, photorheology experiments were conducted over the novel photodegradable hydrogels **PEG-NBt-c** and **PEG-NNPE** and compared to the **PEG-Dop** and **PEG-NDop** control gels in order to confirm that the photodegradation response of these gels is solely due to the presence of the o-nitrobenzyl photo-cleavable linker. Under the same conditions, the photodegradation rate constant for **PEG-NBt-c** gels was found 7.5 times faster than that of **PEG-NNPE** and 24 times faster than that of **PEG-NDop**. These results indicate that the nitrobenzyl triazole units confer controlled photodegradability to new hydrogels (**PEG-NBt-c** and **PEG-NNPE**). The efficiency of the photodegradation reaction is similar to the efficiency of nitrobenzyl ester analogs that are typically used for dynamic cell culture.

3.3.3 Quantification of photodegradation by gravimetry

The photodegradation of **PEG-NBt-c** and **PEG-NNPE** hydrogels was also studied by gravimetric analysis of hydrogel discs fabricated in PDMS molds and subjected to light illumination. The gels, swollen in cell culture medium, were exposed to light ($\lambda = 365$ nm, 70 mW cm⁻²) and the degradation was analyzed by following the decay in the mass of the swollen gel as a function of the irradiation dose. Figures 3.8 show pictures of the different PEG-catechol hydrogels, before and after irradiation and their weight loss calculated by gravimetric method.

PEG-NBt-c gels showed 45% weight loss at 42 J cm⁻² (15 min of irradiation) and 70% at 63 J cm⁻² (20 min of irradiation) (Figure 3.8). A softening of the hydrogel and a yellowish coloring of the supernatant solution due to the release of photolysis products were visible (Figure 3.8). **PEG-NNPE** showed a 30% weight loss at 42 J cm⁻² (15 min of irradiation) and 50% at 63 J cm⁻² (20 min of irradiation). The control gel PEG-Dop showed negligible mass loss at the highest irradiation dose = 63 J cm⁻², and **PEG-NDop** lost ca 10 % at the same dose (Figure 3.8). The degradation of PEG-NDop was visible by the increased swelling and softer appearance. The observed trend is in agreement with the rheology results shown above and with the UV-Vis studies in solution (shown in chapter 2).

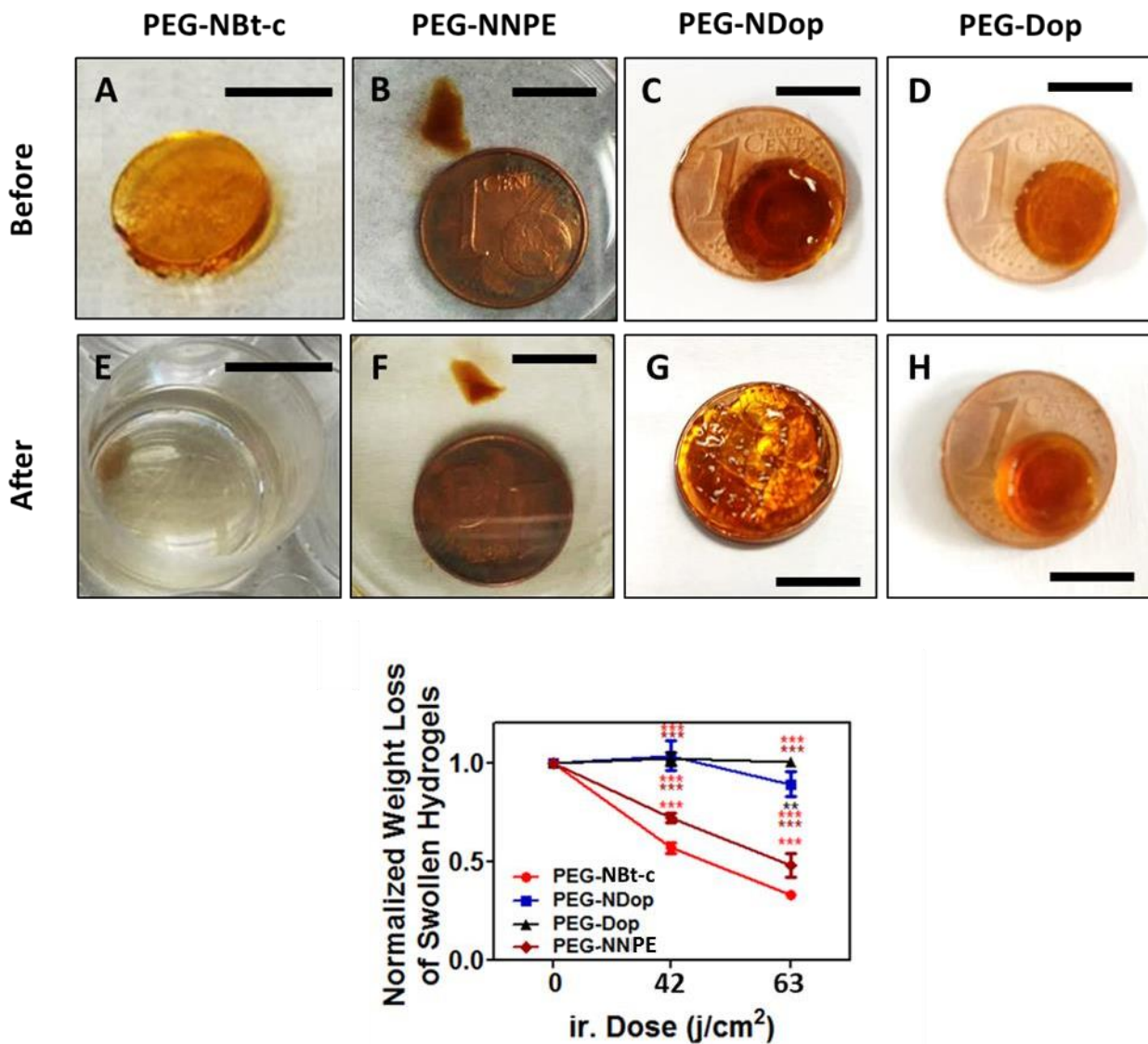


Figure 3.8 Photographs of PEG-catechol hydrogels, before and after light irradiation; scale bar: 10 mm. Gel composition: 10 kDa, 10 wt% PEG polymer, 9 mM oxidant, in PBS:water (1:1), pH 7.0. Hydrogel before irradiation (A-D), and after 20 min of irradiation, at 63 J cm⁻² (E-H). Weight loss of the swollen hydrogels upon light irradiation (I). Irradiation conditions: at $\lambda = 365$ nm, 70 mW cm⁻², in cell culture media; n = 3). Statistical significance analysis was conducted by ANOVA followed by post-hoc Tukey test (mean \pm SD; *p < 0.05, **p < 0.01, ***p < 0.001 used for statistical significance).

3.3.4 Photopatterning of PEG-catechol gels

The selective light illumination of a photoresponsive hydrogel enables the modification of specific volumes of the biomaterial⁵⁰ (i.e., some degree of 3D patterning is possible). To demonstrate the spatial degradation of hydrogels upon focused illumination, the following experiment was conducted. Using a single-photon laser scanning microscope (LSM), selected regions of the **PEG-NBt-c** gels were scanned with focused light of $\lambda = 405$ nm. This process localized the photo-cleavage reaction to occur in regions near the focal point of the laser and specifically degraded the material.

In order to visualize the illuminated regions, **PEG-NBt-c** gels were covalently labeled with the photoactivatable 5-carboxymethoxy-2-nitrobenzyl ether (CMNB)-succinimidyl ester fluorescein. Following an adapted protocol from del Campo and coworkers,⁵¹ the succinimidyl ester group of this molecule was coupled to the amine moiety of an amine-PEG-thiol bifunctional linker and subsequently mixed with a solution of **PEG-NBt-c** precursor. Upon addition of the oxidant, the catechol groups of the macromer are oxidized to quinones, which undergo nucleophilic attack by the pendant thiol group of the thiol-PEG-CMNB-fluorescein obtained in the previous step (see details in the Appendix, section 3.5). Resulting hydrogels contained CMNB-fluorescein which is non-fluorescent. However, upon light exposure, the CMNB photoprotecting group is cleaved from the molecule (Fig. 3.9A) and yields a green-fluorescent fluorescein-labeled hydrogel. The fluorescent and bright field images were analyzed to verify the photodegraded region and the resulting 3D feature.

First experiments were carried out to work out irradiation conditions on CMNB-fluorescein gels. A torus of dimensions inner radius/outer radius/height 150 μm /600 μm /250 μm was scanned into **PEG-NBt-c** hydrogels and increase of fluorescence intensity within the illuminated volume was observed (Fig. 3.9B). The efficiency of the photolytic removal of CMNB group can be regulated by irradiation dose; therefore, the resulting increase of fluorescence intensity on labeled gels was expected to be dose-dependent. CMNB-labeled **PEG-NBt-c** gels were exposed to light of increasing power 10-100% (in our microscope settings, this corresponds to an increase of irradiation dose in the range of 0.02-1.6 mW, 2.6-211 nJ per voxel (scan speed = 1), 1.3-105 nJ per voxel (scan speed = 2)) that led accordingly to an increase of the normalized fluorescence intensity as demonstrated in Fig. 3.9C. A square 2D pattern of 200 μm size was scanned on the gels with a

1% laser power (irradiation dose = 2.6 nJ per voxel, 0.02 mW), and was visualized either by an increase of the fluorescence intensity (fluorescent patterns due to fluorescein) or by a very low decrease of the bright field intensity (that appear as slightly darker features due to local degradation of the illuminated matrix) (Fig. 3.9D). Note that visualization in both modes is complementary. At low irradiation dose, fluorescence intensity due to fluorescein uncaging is developed. Patterns drawn with longer irradiation dose showed higher fluorescence, demonstrating the dose-dependent uncaging of the fluorophore with 3D resolution. At higher irradiation doses, decrease of bright field intensity becomes more useful than fluorescent detection.

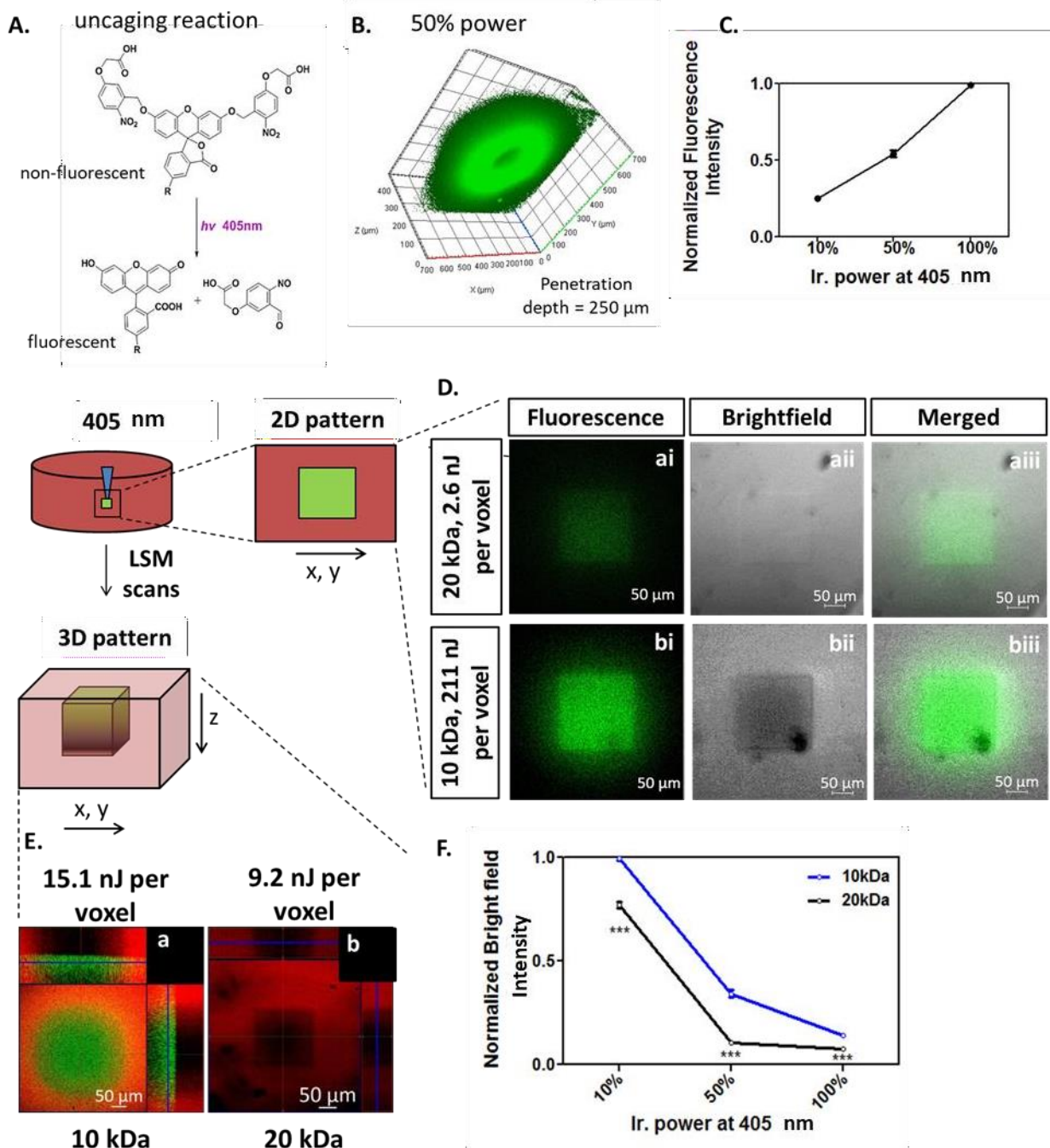


Figure 3.9 2D and 3D patterning by single-photon activation ($\lambda= 405 \text{ nm}$) of photodegradable PEG-NBt-c hydrogels (gel composition: 10 or 20 kDa, 10 wt% polymer, 18 mM oxidant, 50 mM HEPES buffer pH 7.5; labeled with 1 mM CMNB-fluorescein). Upon light irradiation, the CMNB groups of fluorescein are cleaved (A) and the fluorescence intensity at the illuminated region increases (B, a torus (150 μm /600 μm /250 μm) scanned at laser power 50%). C) The increase in the

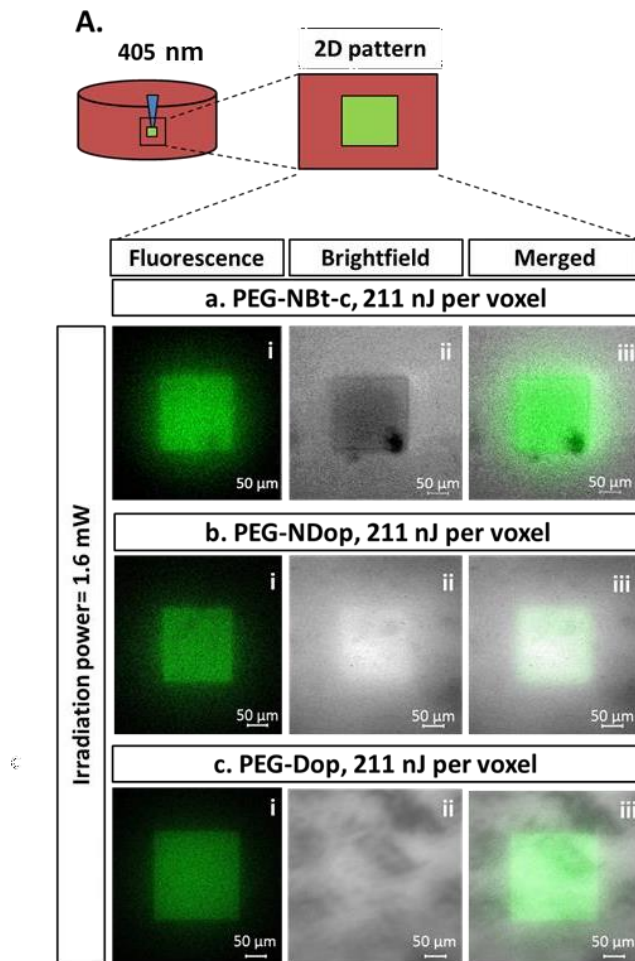
fluorescence intensity is dose dependent. D) 2D square patterns ($200 \times 200 \mu\text{m}^2$) scanned at laser power 1% (2.6 nJ per voxel) or 100% (211 nJ per voxel). E) 3D patterns showing a cylinder (diameter/height $300 \mu\text{m}/150 \mu\text{m}$) and a rectangular prism ($200 \times 200 \times 100 \mu\text{m}^3$) scanned at different laser power: 15 % (15.1 nJ per voxel) and 8 % power (9.2 nJ per voxel). F) The dose dependent degradation of 10 kDa vs. 20 kDa hydrogels is followed by decrease in the bright field intensity.

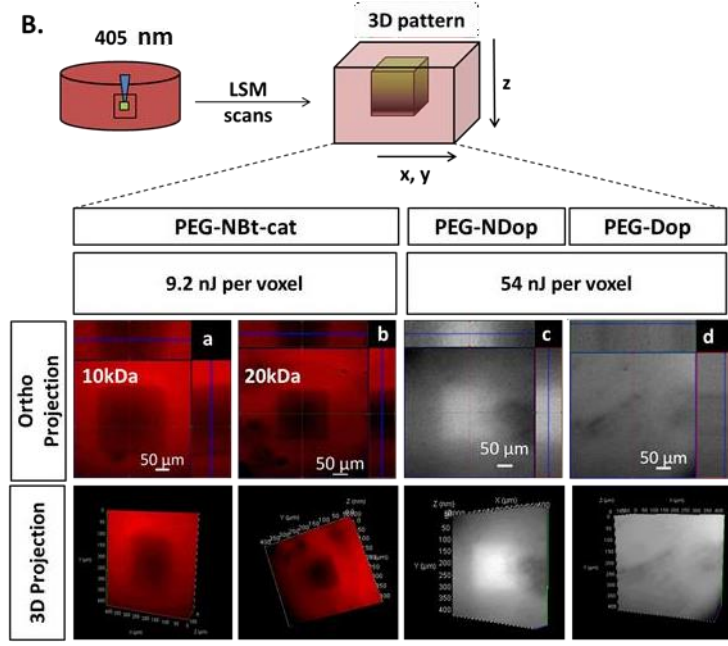
Following a similar procedure, 3D patterns of a cylinder (diameter/height $300 \mu\text{m}/150 \mu\text{m}$) and a rectangular prism ($200 \times 200 \times 100 \mu\text{m}^3$) were scanned into **PEG-NBt-c** gels (Figure 3.9E). Hydrogel formulation and illumination parameters were optimized. Taking into account the results previously obtained by rheology, different gel formulations (polymer concentration 10 %, 10 vs 20 kDa molar mass, oxidant concentrations 18 mM) were prepared to obtain a gel within $G' = 1-10 \text{ kPa}$ stiffness values. Matrices prepared from 10 kDa and 20 kDa, exposed to same irradiation dose (9.2 nJ per voxel, 0.14 mW) were compared by analyzing the change in the bright field intensity through a line across the exposed region (Figure 3.9Ba-b). Higher gel degradation (signed as lower value of the normalized intensity) was observed for the 20 kDa-gel, in accordance to the rheology results shown above. The lower crosslinking degree of the 20 kDa-gel permits to use a lower irradiation dose for gel photodegradation. Furthermore, the following illumination parameters were adjusted to optimize light exposure and visualization conditions: laser power (1-100 %), scan speed (1-2), number of scan repetitions (i.e. number of passing laser) (1-16). The combination of these three parameters results in a irradiation dose which value in nJ per voxel was calculated following the protocol described by García-López et al.,⁵² using the following equation:

$$\text{Ir. Dose} = \text{Ir. Power(for specific objective)} * P. \text{Dwell(for specific scanning settings)}.$$

Adjustment of the irradiation dose within the range of 9.2 – 211 nJ per voxel was performed and representative results are shown in figure 3.9. To validate this methodology, similar experiments were performed over **PEG-Dop** and **PEG-NDop** control gels labeled with CMNB-fluorescein. At comparable doses used in the previous case (211 nJ per voxel), illuminated

regions in **PEG-Dop** and **PEG-NDop** gels showed increased fluorescence intensity but no decrease in bright field intensity, sign of either absent or poor photodegradability (Figure 3.10). Only at high exposure doses (105-211 nJ per voxel) **PEG-NDop** gels showed swelling of the illuminated area, which suggests some decrease of the network's crosslinking degree due to photodegradation.





C. 10 vs. 20 kDa, PEG-NBt-cat hydrogels; 9.1 nJ per voxel

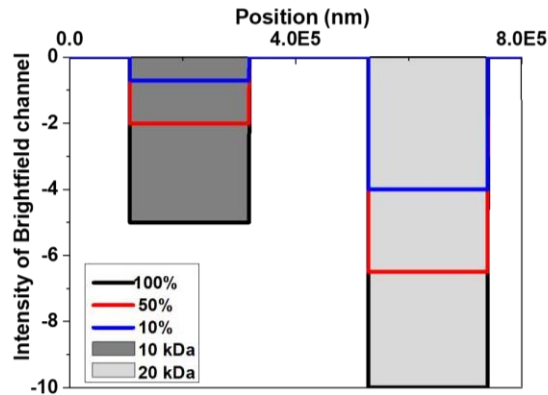


Figure 3.10 2D (A) and 3D (B) patterning by single-photon activation ($\lambda = 405$ nm, LSM) of the different hydrogels **PEG-NBt-c**, **PEG-NDop** and **PEG-Dop** (gel composition: 10 kDa, 10 wt % polymer, 18 mM oxidant, in HEPES buffer pH 7.5, labeled with 1 mM caged fluorescein). A) Square patterned at laser power = 100% (211 nJ per voxel). B) Rectangular prisms drawn on the gels at laser power 8% (9.2 nJ per voxel) and 50% (54 nJ per voxel). C) Comparison of the decrease in brightfield intensity at increasing illumination dose (laser power of 10, 50 and 100%) over 10 kDa vs 20 kDa, PEG-NBt-c gels.

In order to better visualize the local change in the mechanical properties of hydrogels upon selective irradiation of a defined volume, polystyrene particles (PSPs) of around 30 µm diameter were encapsulated into the **PEG-NBt-c** gels. The PSPs, labeled with a red fluorophore, were mixed with the precursor solution followed by addition of the oxidant. The resulting **PEG- NBt-c** gel with embedded PSPs was placed in buffer until equilibrium swelling and then subjected to focused exposure as explained above. Localized erosion of the gel results in material's softening and embedded PSPs located within the exposed region are expected to move out of their original position. This enables a clear visualization of the local gel degradation and allows optimization of irradiation dosage prior to experiment with cells.

Encapsulated PSPs within **PEG-NBt-c** gels illuminated with a dose as low as 22 nJ per voxel were displaced from their original location inside of the material and completely released out of the exposed region at dose = 44.8 nJ per voxel (Figure 3.11). This demonstrates the possibility to erode the gel locally and to release particles embedded within. Conversely, PSPs embedded in the control **PEG-NDop** gels did not change their position at illumination doses up to 422 nJ per voxel. PSPs release was only observed at high doses = 1688 nJ per voxel, suggesting poor release efficiency that is connected to the poor photodegradability of this material. Exposing **PEG-Dop** control gels to the same high dose proved ineffective to release embedded PSPs, in line with the previous results. Altogether, these results prove the efficient photodegradation of **PEG-NBt-c** hydrogels under low illumination doses and support their use for cell experiments.

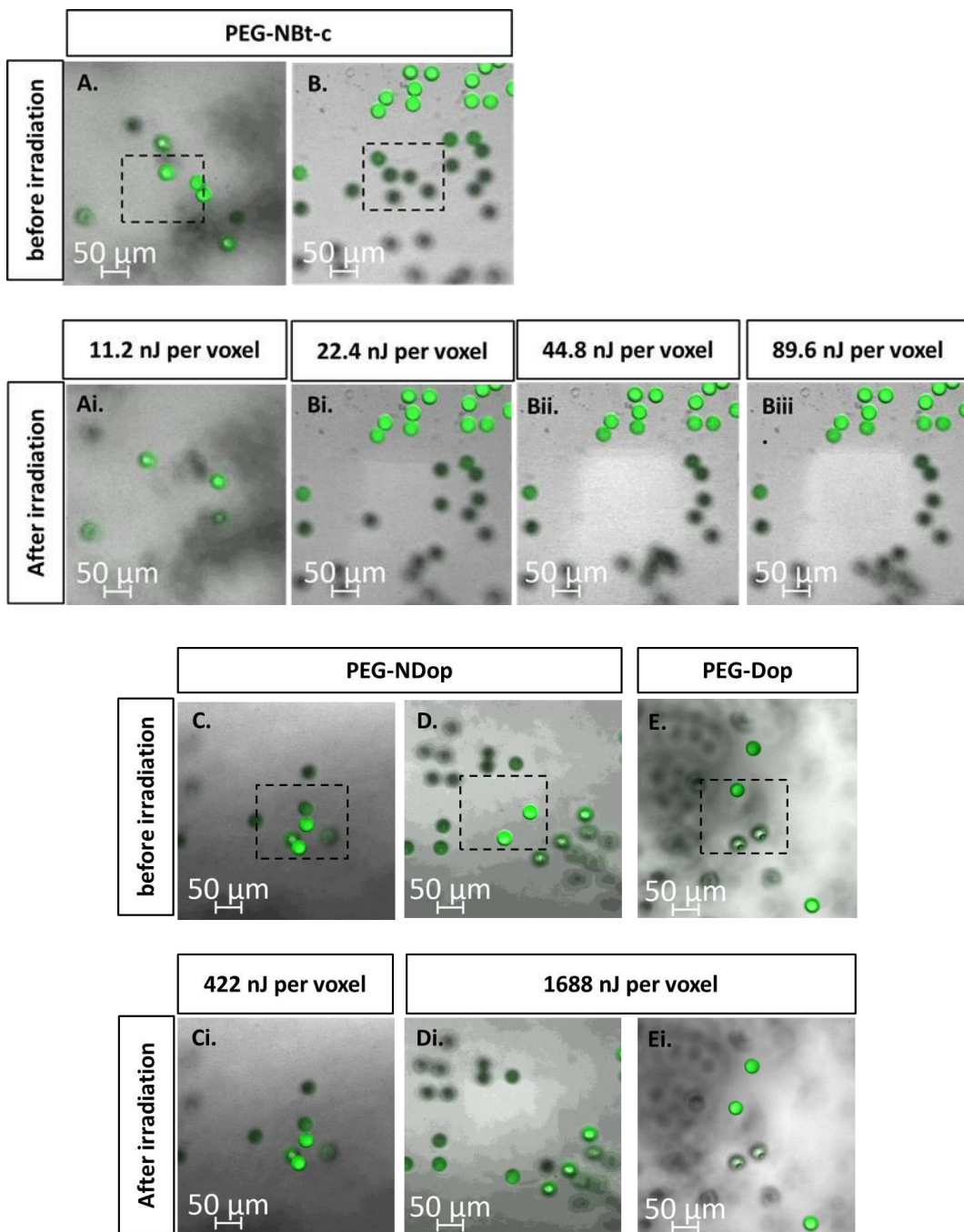


Figure 3.11 Release of polystyrene particles (PSPs) that were encapsulated in PEG hydrogels (gel composition: 10kDa, 10 wt% PEG polymers, 18 mM oxidant, 50 mM HEPES buffer, pH 7.5) by single-photon LSM irradiation (405 nm): (A-E) Before Irradiation; F-J) after irradiation (exposure area marked with rectangles and conditions denoted in each case); scale bars = 50 μ m. In **PEG-NBt-c** (F-G), local degradation of the material under low exposure doses (laser power = 5% (0,085 mW), scan passing number ($n = 1$ (11,2 nJ per voxel), $n = 2$ (22,4 nJ per voxel), $n = 4$ (44,8 nJ per

voxel)) leads to PSPs release. In **PEG-NDop** (H-I) high irradiation doses (laser power = 100% (1,6 mW), scan passing number ($n = 2$ (422 nJ per voxel), $n = 8$ (1688 nJ per voxel)) are required for photo-triggered release, while in **PEG-Dop** (J) no material degradation was observed even at high irradiation doses.

In summary, the photodegradation efficiency found followed the sequence: **PEG-NBt-c** > **PEG-NDop** >> **PEG-Dop**.

3.3.5 Adhesion of PEG-NBt-c hydrogels to tissue and light-mediated debonding

The tissue adhesion properties of **PEG-NBt-c** hydrogels on natural tissue (chicken skin) under wet conditions were studied, and the possibility to trigger debonding by light exposure was explored.¹⁴⁻¹⁹ A final composition of 10 wt% PEG-NBt-c, 18 mM NaIO₄, 50 mM HEPES buffer pH 7.5 was used. In order to facilitate imaging of the transparent hydrogel, fluorescent beads were also added to the precursor mixture. The mixture was applied on the skin surface and cured for 1 h in humid atmosphere at 37°C. These conditions should simulate the application scenario of medical tissue adhesives. After curing, the hydrogel proved to be adhesive and remained firmly bonded to tissue even after 30 min of vigorous shaking of the substrate underwater (see Appendix figure 3).

Fluorescence imaging of the outer layer of the hydrogel bonded to tissue was performed. The visualization of the embedded fluorescent PSPs included in the formulation confirmed the presence of the adhesive hydrogel on the tissue (Figure 3.12B). PSPs were homogeneously distributed into all PEG-catechol skin-adhesives (Figure 3.12). This was as well supported by ESEM imaging of the cross-section of the bonded tissue, revealing continuous and intimate contact between the tissue surface and the adhesive hydrogel in both wet and dry states (Figure 3.14B). According to a previous report, this likely suggests the presence of strong, covalent bonding at the interface.¹⁷ In comparison, **PEG-NDop** and **PEG-Dop** control gels proved tissue adhesive as well (Figure 3.12, 3.14). This was in contrast to a non-adhesive control, **PEG-thiol-Maleimide** gel, which did not attach to tissue and showed absence of PSPs on top of tissue, at the microscopic level (Figure 3.13-3.14).

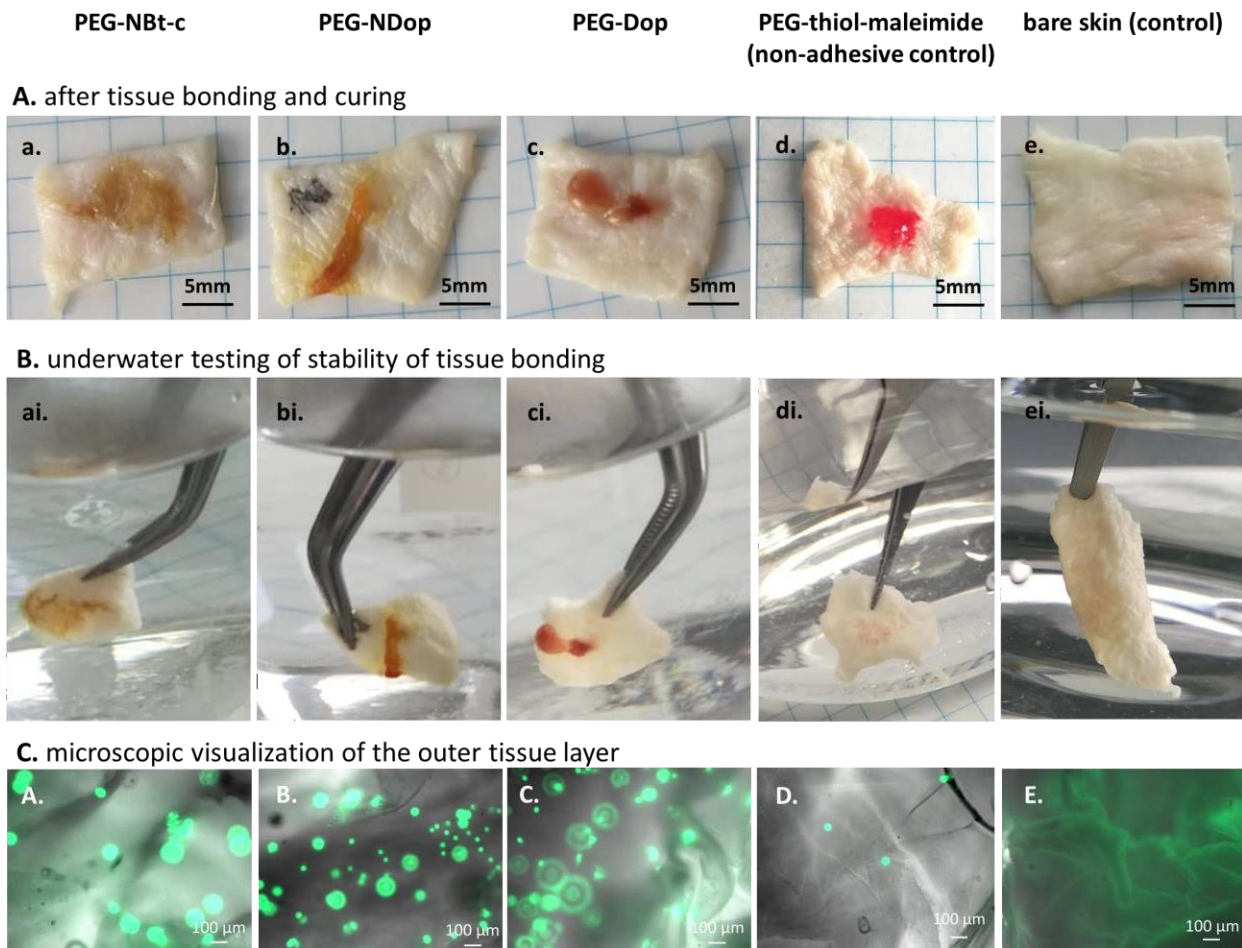


Figure 3.12 Representative adhesive hydrogels attached to chicken skin. Final polymer composition = 10 kDa, 10 wt% PEG-catechol derivatives, 18 mM oxidant-PSPs, 50 mM HEPES buffer, pH 7.5. Scale bar A-E = 100 μ m; scale bar a-e = 5 mm.

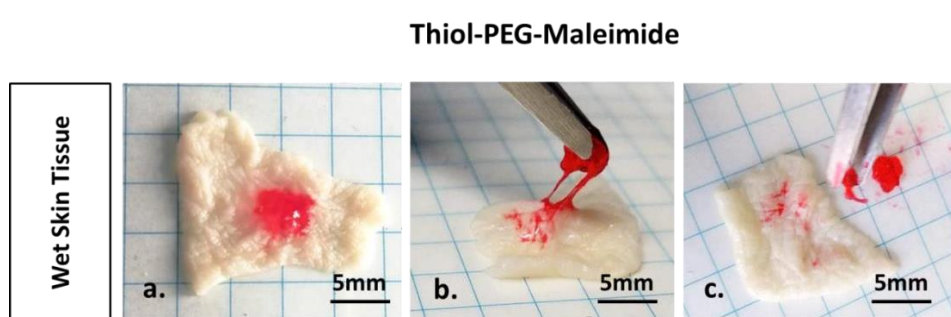


Figure 3.13 Representative non-adhesive hydrogel. Final polymer composition = 20kDa, 10 wt% PEG-thiol mixed with 10 wt% PEG-Maleimide, 50 mM HEPES buffer, pH 7.5. (a-c) Thiol-PEG-Maleimide adhesive is not attached to the chicken skin. Scale bar a-c = 5 mm.

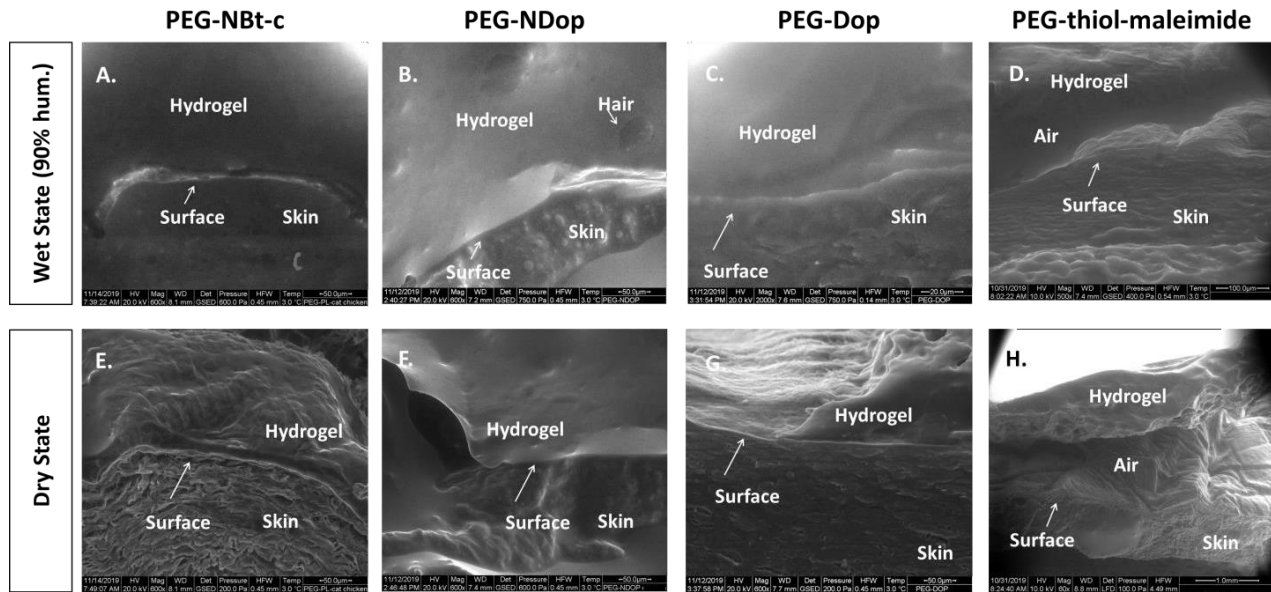


Figure 3.14 Microscopic visualization of the hydrogel attachment on the skin surface (wet (A-C) vs dry state (E-G)). In **Thiol-PEG-Maleimide**, there is no connection between the tissue and the skin (D,H). Scale bar B,E-F = 50 μ m; scale bar C = 20 μ m; scale bar D = 100 μ m; scale bar H = 1 mm.

Finally, to test the possibility of light-triggered debonding, the bonded tissue was light-exposed (irradiation conditions: $\lambda = 365$ nm, $I = 70$ mW cm $^{-2}$ for 6 min; dose = 25 J cm $^{-2}$) and soaked again in water. Light-triggered debonding of the **PEG-NBt-c** hydrogel from tissue was clearly observed macroscopically and microscopically (see Appendix, Figure 4). In contrast, **PEG-NDop** and **PEG-Dop** control gels did not show light-debonding from tissue (Figure 3.15). At same exposure dose, **PEG-NDop** only swelled slightly but did not show any visible photo-degradation or debonding, reflecting the poor light responsiveness of the system; while **PEG-Dop** remained firmly attached regardless. These results are in a good agreement with the previous photodegradation studies in bulk (by gravimetric study).

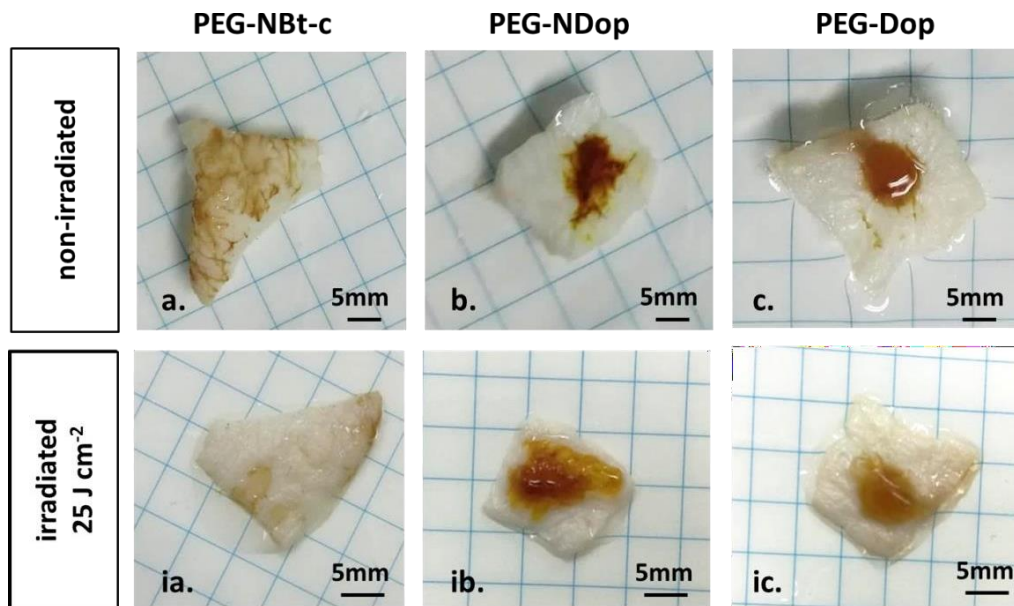


Figure 3.15 Representative adhesive hydrogels attached on chicken skin (before and after exposure at UV-vis irradiation, 365 nm). Final polymer composition = 10kDa, 10 wt% PEG-catechol derivatives, 18 mM oxidant-PSPs, 50 mM HEPES buffer, pH 7.5. (a-c) Strong adhesion; (ia-ic) Hydrogels were exposed to light (400 W, Irradiance = 70 mW cm⁻² for 6 min (25 J cm⁻²). Scale bar = 5 mm.

The above results confirm the properties of tissue adhesiveness combined with light-triggered detachment of **PEG-NBt-c** gels on natural tissue. This opens up exciting possibilities for the application of this material towards cell therapies, wound management and tissue repair.

3.4 Conclusions

In this chapter, the mechanical strength and curing kinetics of different PEG-catechol hydrogels were characterized via rheology. Crosslinking kinetics followed the sequence: **PEG-NDop** > **PEG-Dop** > **PEG-NBt-c** > **PEG-NNPE**. Also, their degradation kinetics in response to low-intensity irradiation was characterized via photorheology. Photodegradation kinetics followed the sequence: **PEG-NBt-c** > **PEG-NNPE** >> **PEG-NDop**. **PEG-Dop** did not photodegrade at all.

PEG-NBt-c and **PEG>NNPE** hydrogels were demonstrated to be photodegradable under UV irradiation at 365 nm by incorporation of the nitrobenzyl-triazole moiety within the gel structure. The photodegradation kinetics of the two new hydrogels was very rapid compared to previous gel design, **PEG-NDop**. Especially, **PEG-NBt-c** gel was completely degraded during photorheology measurements within 6 minutes upon irradiation of UV light at an intensity of 10 mW cm⁻² (Irradiation dose = 3.6 J cm⁻²). For reference, typical biocompatible exposure doses (at $\lambda = 365$ nm) are 5–36 J cm⁻².^{11, 45, 47, 48} A gravimetric method demonstrated that **PEG-NBt-c** degraded faster than all the other tested photodegradable gels (**PEG>NNPE** and **PEG-NDop**).

The higher photodegradability of **PEG-NBt-c** gel was exploited for photopatterning with high precision and low light dosage. **PEG-NBt-c** was degraded under cytocompatible irradiation conditions to create z- or xy-direction property gradients, as well as to erode hydrogels for controlled depolymerisation at any point in time and in three dimensions. PSPs were successfully released from **PEG-NBt-c** gel, with a xy-direction degradation gradient.

The tissue-adhesive property of **PEG-NBt-c** hydrogels was demonstrated to wet natural tissue. Importantly, the photodegradation property of **PEG-NBt-c** gel can be used for tissue debonding “on demand”. This kind of hydrogel that can respond to external stimulus are attractive in biomedical community, allowing the gel properties to be manipulated by the use of external cues, such as light. For the future work the combination of tissue adhesives and drug delivery will be promoted in surgeries, for faster healing rates and tissue regeneration.

3.5 References

1. Drury, J. L.; Mooney, D. J., Hydrogels for tissue engineering: scaffold design variables and applications. *Biomaterials* 2003, 24 (24), 4337-4351.
2. Liu, W.; Deng, C.; McLaughlin, C. R.; Fagerholm, P.; Lagali, N. S.; Heyne, B.; Scaiano, J. C.; Watsky, M. A.; Kato, Y.; Munger, R., Collagen–phosphorylcholine interpenetrating network hydrogels as corneal substitutes. *Biomaterials* 2009, 30 (8), 1551-1559.
3. Torres-Rendon, J. G.; Femmer, T.; De Laporte, L.; Tigges, T.; Rahimi, K.; Gremse, F.; Zafarnia, S.; Lederle, W.; Ifuku, S.; Wessling, M., Bioactive gyroid scaffolds formed by sacrificial

- templating of nanocellulose and nanochitin hydrogels as instructive platforms for biomimetic tissue engineering. *Advanced materials* 2015, 27 (19), 2989-2995.
4. Lee, K. Y.; Mooney, D. J., Hydrogels for tissue engineering. *Chemical reviews* 2001, 101 (7), 1869-1880.
 5. Murphy, J. L.; Vollenweider, L.; Xu, F.; Lee, B. P., Adhesive performance of biomimetic adhesive-coated biologic scaffolds. *Biomacromolecules* 2010, 11 (11), 2976-2984.
 6. Liu, X. J.; Li, H. Q.; Zhang, B. Y.; Wang, Y. J.; Ren, X. Y.; Guan, S.; Gao, G. H., Highly stretchable and tough pH-sensitive hydrogels with reversible swelling and recoverable deformation. *Rsc Advances* 2016, 6 (6), 4850-4857.
 7. Malmsten, M.; Bysell, H.; Hansson, P., Biomacromolecules in microgels—Opportunities and challenges for drug delivery. *Current Opinion in Colloid & Interface Science* 2010, 15 (6), 435-444.
 8. Ruskowitz, E. R.; DeForest, C. A., Photoresponsive biomaterials for targeted drug delivery and 4D cell culture. *Nature Reviews Materials* 2018, 3.
 9. Luo, Y.; Shoichet, M. S., A photolabile hydrogel for guided three-dimensional cell growth and migration. *Nature materials* 2004, 3 (4), 249.
 10. Frey, M. T.; Wang, Y.-I., A photo-modulatable material for probing cellular responses to substrate rigidity. *Soft matter* 2009, 5 (9), 1918-1924.
 11. Kloxin, A. M.; Kasko, A. M.; Salinas, C. N.; Anseth, K. S., Photodegradable Hydrogels for Dynamic Tuning of Physical and Chemical Properties. *Science* 2009, 324 (5923), 59-63.
 12. DeForest, C. A.; Anseth, K. S., Cytocompatible click-based hydrogels with dynamically tunable properties through orthogonal photoconjugation and photocleavage reactions. *Nature chemistry* 2011, 3 (12), 925.
 13. Mehdizadeh, M.; Weng, H.; Gyawali, D.; Tang, L.; Yang, J., Injectable citrate-based mussel-inspired tissue bioadhesives with high wet strength for sutureless wound closure. *Biomaterials* 2012, 33 (32), 7972-7983.
 14. Feng, J.; Ton, X.-A.; Zhao, S.; Paez, J. I.; del Campo, A., Mechanically Reinforced Catechol-Containing Hydrogels with Improved Tissue Gluing Performance. *Biomimetics* 2017, 2 (4), 23.
 15. Kivelio, A.; DeKoninck, P.; Perrini, M.; Brubaker, C. E.; Messersmith, P. B.; Mazza, E.; Deprest, J.; Zimmermann, R.; Ehrbar, M.; Ochsenbein-Koelble, N., Mussel mimetic tissue

- adhesive for fetal membrane repair: initial in vivo investigation in rabbits. *European Journal of Obstetrics & Gynecology and Reproductive Biology* 2013, 171 (2), 240-245.
16. Perrini, M.; Barrett, D.; Ochsenbein-Koelble, N.; Zimmermann, R.; Messersmith, P.; Ehrbar, M., A comparative investigation of mussel-mimetic sealants for fetal membrane repair. *Journal of the mechanical behavior of biomedical materials* 2016, 58, 57-64.
17. Brubaker, C. E.; Kissler, H.; Wang, L.-J.; Kaufman, D. B.; Messersmith, P. B., Biological performance of mussel-inspired adhesive in extrahepatic islet transplantation. *Biomaterials* 2010, 31 (3), 420-427.
18. Liu, Y.; Meng, H.; Konst, S.; Sarmiento, R.; Rajachar, R.; Lee, B. P., Injectable dopamine-modified poly (ethylene glycol) nanocomposite hydrogel with enhanced adhesive property and bioactivity. *ACS applied materials & interfaces* 2014, 6 (19), 16982-16992.
19. Bilic, G.; Brubaker, C.; Messersmith, P. B.; Mallik, A. S.; Quinn, T. M.; Haller, C.; Done, E.; Guciardo, L.; Zeisberger, S. M.; Zimmermann, R., Injectable candidate sealants for fetal membrane repair: bonding and toxicity in vitro. *American journal of obstetrics and gynecology* 2010, 202 (1), 85. e1-85. e9.
20. Haller, C.; Buerzle, W.; Kivelio, A.; Perrini, M.; Brubaker, C.; Gubeli, R.; Mallik, A.; Weber, W.; Messersmith, P.; Mazza, E., Mussel-mimetic tissue adhesive for fetal membrane repair: An ex vivo evaluation. *Acta biomaterialia* 2012, 8 (12), 4365-4370.
21. Hong, S.; Yang, K.; Kang, B.; Lee, C.; Song, I. T.; Byun, E.; Park, K. I.; Cho, S. W.; Lee, H., Hyaluronic acid catechol: a biopolymer exhibiting a pH-dependent adhesive or cohesive property for human neural stem cell engineering. *Advanced Functional Materials* 2013, 23 (14), 1774-1780.
22. Kastrup, C. J.; Nahrendorf, M.; Figueiredo, J. L.; Lee, H.; Kambhampati, S.; Lee, T.; Cho, S.-W.; Gorbatov, R.; Iwamoto, Y.; Dang, T. T., Painting blood vessels and atherosclerotic plaques with an adhesive drug depot. *Proceedings of the National Academy of Sciences* 2012, 109 (52), 21444-21449.
23. Dalsin, J. L.; Lee, B. P.; Vollenweider, L.; Silvary, S.; Murphy, J. L.; Xu, F.; Spitz, A.; Lyman, A., Multi-armed catechol compound blends. Google Patents: 2012.
24. Messersmith, P. B.; Dalsin, J. L.; Lee, B. P.; Burke, S. A., DOPA-functionalized, branched, poly (aklylene oxide) adhesives. Google Patents: 2014.

25. Lei, Z. Q.; Xiang, H. P.; Yuan, Y. J.; Rong, M. Z.; Zhang, M. Q., Room-temperature self-healable and remoldable cross-linked polymer based on the dynamic exchange of disulfide bonds. *Chemistry of Materials* 2014, 26 (6), 2038-2046.
26. Dai, X.; Zhang, Y.; Gao, L.; Bai, T.; Wang, W.; Cui, Y.; Liu, W., A Mechanically Strong, Highly Stable, Thermoplastic, and self-healable supramolecular polymer hydrogel. *Advanced Materials* 2015, 27 (23), 3566-3571.
27. Hu, Y.; Guo, W.; Kahn, J. S.; Aleman-Garcia, M. A.; Willner, I., A Shape-Memory DNA-Based Hydrogel Exhibiting Two Internal Memories. *Angewandte Chemie International Edition* 2016, 55 (13), 4210-4214.
28. Phadke, A.; Zhang, C.; Arman, B.; Hsu, C.-C.; Mashelkar, R. A.; Lele, A. K.; Tauber, M. J.; Arya, G.; Varghese, S., Rapid self-healing hydrogels. *Proceedings of the National Academy of Sciences* 2012, 109 (12), 4383-4388.
29. Nakahata, M.; Takashima, Y.; Yamaguchi, H.; Harada, A., Redox-responsive self-healing materials formed from host-guest polymers. *Nature communications* 2011, 2, 511.
30. Website: <https://www.lumina.se>; accessed on April 2020
31. Wu, H.; Qin, Z.; Yu, X.; Li, J.; Lv, H.; Yang, X., On-demand removable hydrogels based on photolabile cross-linkings as wound dressing materials. *Journal of Materials Chemistry B* 2019, 7 (37), 5669-5676.
32. Antonio, F.; Petya, P.; Tzanko, T., Hydrogel Dressings for Advanced Wound Management. *Current Medicinal Chemistry* 2018, 25 (41), 5782-5797.
33. Op 't Veld, R. C.; Walboomers, X. F.; Jansen, J. A.; Wagener, F. A. D. T. G., Design Considerations for Hydrogel Wound Dressings: Strategic and Molecular Advances. *Tissue Engineering Part B: Reviews* 2020, *in press*.
34. Phelps, E. A.; Enemchukwu, N. O.; Fiore, V. F.; Sy, J. C.; Murthy, N.; Sulchek, T. A.; Barker, T. H.; García, A. J., Maleimide cross-linked bioactive peg hydrogel exhibits improved reaction kinetics and cross-linking for cell encapsulation and in situ delivery. *Advanced materials* 2012, 24 (1), 64-70.
35. Hong, S.; Yang, K.; Kang, B.; Lee, C.; Song, I. T.; Byun, E.; Park, K. I.; Cho, S.-W.; Lee, H., Hyaluronic Acid Catechol: A Biopolymer Exhibiting a pH-Dependent Adhesive or Cohesive

Property for Human Neural Stem Cell Engineering. *Advanced Functional Materials* 2013, 23 (14), 1774-1780.

36. Kastrup, C. J.; Nahrendorf, M.; Figueiredo, J. L.; Lee, H.; Kambhampati, S.; Lee, T.; Cho, S.-W.; Gorbatov, R.; Iwamoto, Y.; Dang, T. T.; Dutta, P.; Yeon, J. H.; Cheng, H.; Pritchard, C. D.; Vegas, A. J.; Siegel, C. D.; MacDougall, S.; Okonkwo, M.; Thai, A.; Stone, J. R.; Coury, A. J.; Weissleder, R.; Langer, R.; Anderson, D. G., Painting blood vessels and atherosclerotic plaques with an adhesive drug depot. *Proceedings of the National Academy of Sciences* 2012, 109 (52), 21444-21449.

37. Paez, J. I.; Ustahüseyin, O.; Serrano, C.; Ton, X.-A.; Shafiq, Z.; Auernhammer, G. K.; d'Ischia, M.; del Campo, A., Gauging and Tuning Cross-Linking Kinetics of Catechol-PEG Adhesives via Catecholamine Functionalization. *Biomacromolecules* 2015, 16 (12), 3811-3818.

38. Paez, J. I.; Ustahüseyin, O.; Serrano, C.; Ton, X.-A.; Shafiq, Z.; Auernhammer, G. n. K.; d'Ischia, M.; del Campo, A. n., Gauging and tuning cross-linking kinetics of catechol-PEG adhesives via catecholamine functionalization. *Biomacromolecules* 2015, 16 (12), 3811-3818.

39. Cencer, M.; Murley, M.; Liu, Y.; Lee, B. P., Effect of nitro-functionalization on the cross-linking and bioadhesion of biomimetic adhesive moiety. *Biomacromolecules* 2015, 16 (1), 404-410.

40. Cencer, M.; Liu, Y.; Winter, A.; Murley, M.; Meng, H.; Lee, B. P., Effect of pH on the Rate of Curing and Bioadhesive Properties of Dopamine Functionalized Poly(ethylene glycol) Hydrogels. *Biomacromolecules* 2014, 15 (8), 2861-2869.

41. Kord Forooshani, P.; Lee, B. P., Recent approaches in designing bioadhesive materials inspired by mussel adhesive protein. *Journal of Polymer Science Part A: Polymer Chemistry* 2017, 55 (1), 9-33.

42. Yang, J.; Bai, R.; Chen, B.; Suo, Z., Hydrogel adhesion: A supramolecular synergy of chemistry, topology, and mechanics. *Advanced Functional Materials* 2020, 30 (2), 1901693.

43.

https://www.dymax.com/images/pdf/technical_bulletins/lit135_intensity_conversion_chart_tb.pdf

44. LeValley, P. J.; Neelarapu, R.; Sutherland, B. P.; Dasgupta, S.; Kloxin, C. J.; Kloxin, A. M., Photolabile Linkers: Exploiting Labile Bond Chemistry to Control Mode and Rate of Hydrogel

- Degradation and Protein Release. *Journal of the American Chemical Society* 2020, 142 (10), 4671-4679.
45. Griffin, D. R.; Kasko, A. M., Photodegradable Macromers and Hydrogels for Live Cell Encapsulation and Release. *Journal of the American Chemical Society* 2012, 134 (31), 13103-13107.
46. Shafiq, Z.; Cui, J.; Pastor-Pérez, L.; San Miguel, V.; Gropeanu, R. A.; Serrano, C.; del Campo, A., Bioinspired Underwater Bonding and Debonding on Demand. *Angewandte Chemie International Edition* 2012, 51 (18), 4332-4335.
47. Wong, D. Y.; Ranganath, T.; Kasko, A. M., Low-Dose, Long-Wave UV Light Does Not Affect Gene Expression of Human Mesenchymal Stem Cells. *PLOS ONE* 2015, 10 (9), e0139307.
48. DeForest, C. A.; Anseth, K. S., Cytocompatible click-based hydrogels with dynamically tunable properties through orthogonal photoconjugation and photocleavage reactions. *Nat. Chem.* 2011, 3 (12), 925-931.
49. Truong, V. X.; Li, F.; Forsythe, J. S., Photolabile Hydrogels Responsive to Broad Spectrum Visible Light for Selective Cell Release. *ACS Applied Materials & Interfaces* 2017, 9 (38), 32441-32445.
50. Caliari, S. R.; Burdick, J. A., A practical guide to hydrogels for cell culture. *Nature methods* 2016, 13 (5), 405.
51. Farrukh, A.; Paez, J. I.; del Campo, A., 4D Biomaterials for Light-Guided Angiogenesis. *Advanced Functional Materials* 2019, 29 (6), 1807734.
52. García-López, V.; Chen, F.; Nilewski, L. G.; Duret, G.; Aliyan, A.; Kolomeisky, A. B.; Robinson, J. T.; Wang, G.; Pal, R.; Tour, J. M., Molecular machines open cell membranes. *Nature* 2017, 548 (7669), 567.

Chapter 4: Cytocompatibility of photodegradable PEG-catechol hydrogels

4.1 Abstract

Hydrogels are considered good mimics of the natural cellular microenvironment and are thus widely utilized as 3D carriers and scaffolds for cell growth and encapsulation. In this chapter, the cytocompatibility of photodegradable hydrogels fabricated and physicochemically characterized in Chapter 3 was explored. For this purpose, cells were encapsulated into **PEG-NBt-c** and **PEG-NNPE** gels and cultured. Light-induced degradation of the hydrogel scaffold allowed encapsulated cells to migrate.

4.2 Introduction

Cell culture systems should mimic the biological milieu considering that cells inside the organism are likely to receive biosignals in all three dimensions, filling the gap between traditional cultures and complex native *in vivo* microenvironment. 3D cell culture models provide similar morphology, signaling, and metabolic microenvironment to encapsulated cells to the native organism. 3D cultures support cell-type and tissue specific function, gene expression and physiological cell-cell and cell- extracellular matrix (ECM) interactions. Cell-cell communication as well as cell-ECM interactions play a crucial role in the sensing and response to external stimuli.

Degradable hydrogels are used widely as biomaterials for 3D cell encapsulation and cell based therapies for tissue regeneration.^{1, 2} Hydrogels mimic the properties of the ECM and can support cell viability and functionality. Relevant parameters for hydrogel design include porosity for exchange of nutrients and waste products, mechanical stability for cell support, degradability for cell migration, and the functionalization with binding motifs for cell attachment and spreading.³

Poly(ethylene glycol) (PEG) is frequently used for cell encapsulation.⁴⁻⁸ It is FDA approved for clinical use and has low toxicity. PEG is a non-degradable polymer and does not interact with biological molecules or cells. In order to be used for cell encapsulation, PEG needs to be crosslinked with degradable functional groups. Light-induced depolymerization is an interesting

strategy for spatiotemporal manipulation of hydrogel degradation.⁸⁻¹³ Reported examples incorporate photocleavable moieties into the polymer network, mainly o-nitrobenzyl (o-NB) groups.¹⁴ For example, Kloxin et al. incorporated o-NB ester to a PEG diacrylate network and obtained an “on demand” photodegradable hydrogel for cell encapsulation.⁵ The storage modulus of the hydrogel could be decreased during cell culture just by UV light exposure (unfortunately, there is no report of the mechanical strength of the gel before illumination). In such study, fibrosarcoma cells were encapsulated into PEG based gels utilizing o-NBe moieties and channels were degraded within the hydrogels by using two-photon laser scanning microscope. Encapsulated cells migrated into the degraded channel (Figure 4.1).

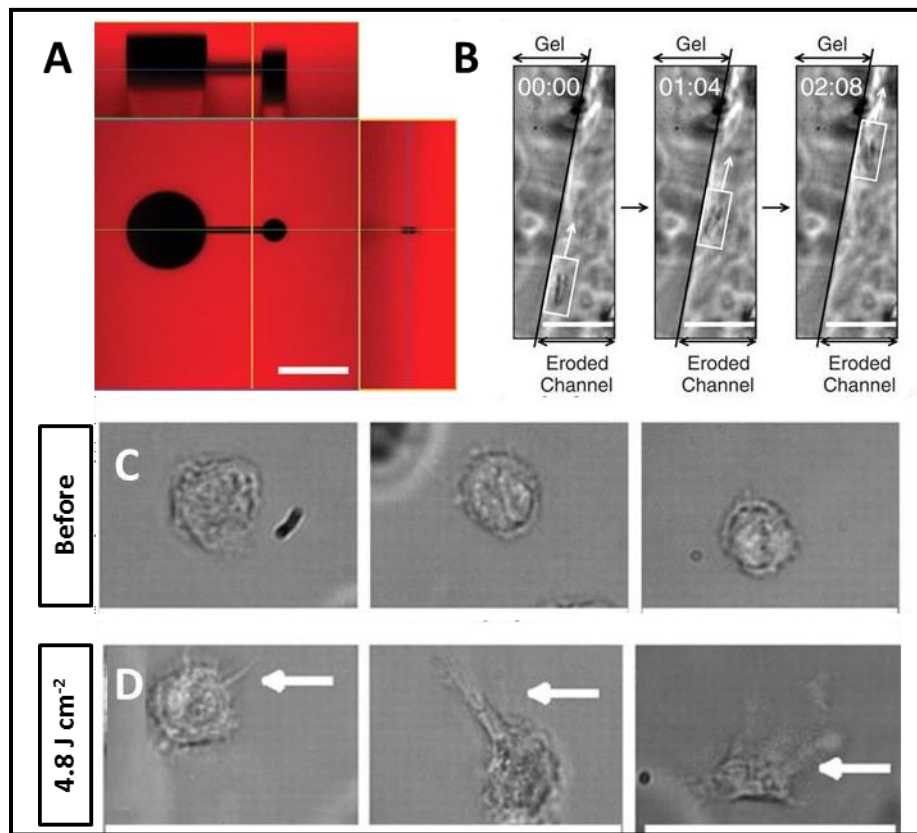


Figure 4.1 Patterning in 3D were demonstrated in a PEG based hydrogel utilizing o-NBe moieties. (A) 3D Channels were created in the photodegradable hydrogel using a confocal scanning two-photon laser microscope. (B) Encapsulating fibrosarcoma cells were released and migrated into the degraded channel, shown in time-lapsed bright field images. (C) Encapsulated human

mesenchymal stem cells (hMSCs) in dense hydrogels presented round morphology. (D) Upon irradiation (for 480 s, at 365 nm at 10 mW cm^{-2}) and gel's degradation, hMSC spread after 3 days of culture, shown with arrows. (A) Scale bar: 100 μm ; (B-D) Scale bars: 50 μm . Reproduced from Kloxin et al. with permission from The American Association for the Advancement of Science. Copyright 2009.⁵

In a similar study, Anseth et al.⁶ opened channels with light exposure within a o-NB and RGD-functionalized PEG hydrogel. The authors demonstrated the possibility to guide cell migration to specific regions of the hydrogel (Figure 4.2). Light of different wavelengths was used to independently control the functionality and architecture of the hydrogel network. Additionally, the same group used photodegradable PEG hydrogels to guide and direct axonal outgrowth in photodegraded channels (Figure 4.2.C-D). Specifically, embryonic stem cell-derived motor neurons (ESMNs) and myotubes were co-encapsulated and the formation of user-directed neural networks was demonstrated.⁸

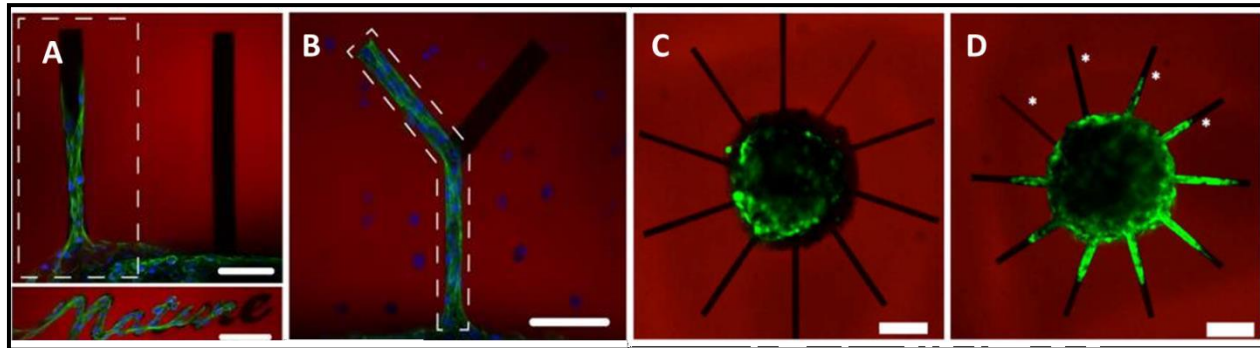


Figure 4.2 Light-directed cell migration within specific regions of the hydrogel. (A-B) Encapsulated 3T3 fibroblasts migrated to photodegraded channels functionalized with RGD (white stripes marked on the left). The control channel with no RGD (right) did not lead to cell migration. (A-B) Scale bars: 100 μm . Reproduced from DeForest and Anseth with permission from Nature Publishing Group.⁶ Copyright 2011. (C-D) Encapsulated ESMN embryo in PEG hydrogel incorporating YIGSR binding peptide, immediately after degradation of channels (C) and 48 h after

(D). Axons extend into channels that have been exposed to sufficient light to erode the material. Each channel represents different degradation where the power was varied from 15 to 110 mW μm^{-3} . (C-D) Scale bars: 100 μm . Reproduced from McKinnon et al. with permission from American Chemical Society.⁸ Copyright 2014.

In this chapter, PEG catechol gels (**PEG-NBt-c**, **PEG-NNPE**, **PEG-NDop** and **PEG-Dop**) will be tested for cell encapsulation. Fibroblasts and retinal pigment epithelium (RPE1) cells were chosen because they are robust cells and easy to culture. The gels' cytocompatibility and their use for *in situ* softening and degradation of the synthetic cellular microenvironment is demonstrated.

4.3 Results and Discussion

4.3.1 Cytocompatibility study of PEG-catechol hydrogels

L929 fibroblasts cultured on a plastic culture plate were brought in contact with **PEG-NBt-c**, **PEG-NNPE**, **PEG-NDop** and **PEG-Dop** hydrogels and cultured for 1 d. A live/dead assay was performed to assess cell viability after 48 h of cell-hydrogel contact. Cell viability of 97% was observed (Figure 6, Appendix). This result indicated that crosslinked PEG-catechol hydrogels show good cytocompatibility.

Next, the suitability of PEG-catechol hydrogels to encapsulate cells and as scaffolds for cell culture was tested. Several hydrogel formulations were tested and their effect over cell viability was quantified. Studied parameters involved the oxidant concentration (1 – 18 mM, Figure 4.3), polymer content (5 % or 10 %), encapsulation medium (cell culture medium, PBS, water: PBS, HEPES buffer (10 to 50 mM)) and pH (6 - 8.3), (Figure 4.3A-D). Note that the oxidant concentration used in this formulation is within the range used for mussel-inspired hydrogels for cell encapsulation and *in vivo* tissue adhesion (ca 10-30 mM).¹⁵⁻¹⁹

The oxidant concentration affected the pH of the solution. NaIO₄ concentration from 1 to 18 mM lead to acidic solutions in water or PBS (pH 2 - 6.5), which were not favorable for cell

viability (Figure 4.3b-d). An oxidant concentration of 1 mM was acceptable for the cells, but too low to lead to a mechanically stable hydrogel. Oxidant concentrations between 9 mM and 18 mM were necessary to trigger sufficient crosslinking degree and obtain stable hydrogels.

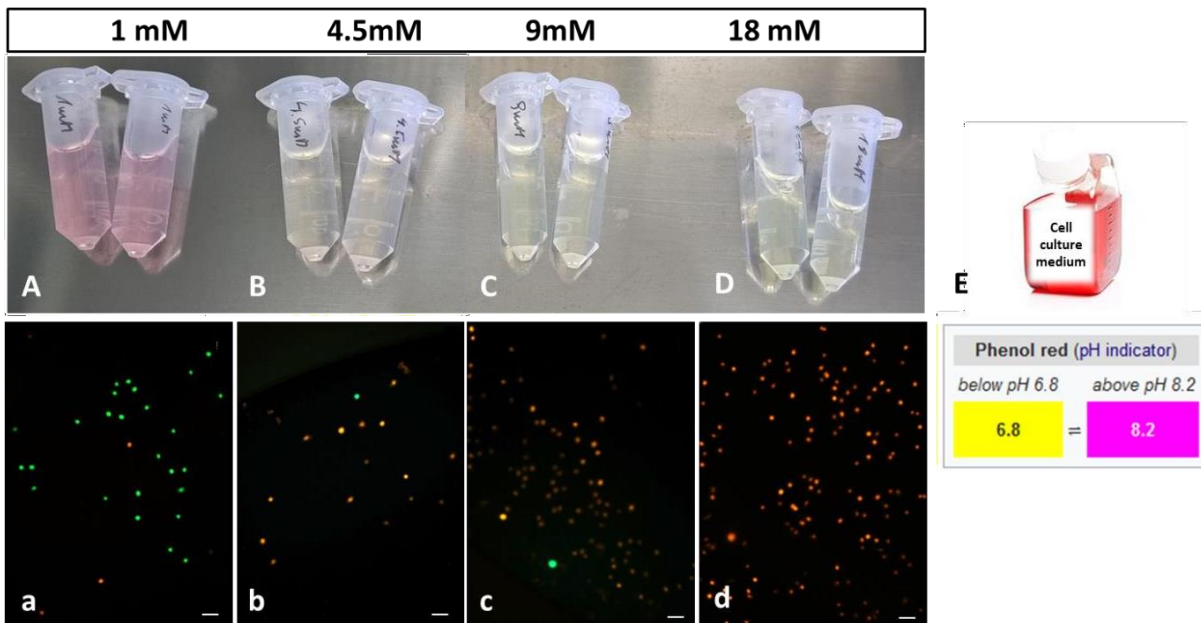


Figure 4.3 (A-D) Adjustment of oxidant concentration and resulting pH for high cell viability. Higher oxidant concentration gives more acidic pH. (E) Phenol red is a pH indicator. Its color exhibits a gradual transition from white-yellow to pink over the pH range 6.8 to 8.2. (a-d) Live (green)/ dead (red) assay was performed after 1 h of culture. Low cell viability in 3D (< 4 %) was observed in all cases (c-d) except in 1 mM NaIO₄ (a). (a-d) Scale bars: 100 µm. Gel composition: 10 kDa, 10 wt% polymer, 1-18 mM oxidant, pH = 2-6 in cell culture medium.

Using HEPES buffer, commonly used for cell culture, the pH of the oxidant solution could be maintained around the physiological value = 7.4. Increasing concentrations of HEPES buffer (10, 20 or 50 mM) could stabilize the pH in the range 6 - 8.3 (Figure 4.4). 50 mM HEPES buffer allowed a stable pH in the range 7.3 - 8.3 and was not toxic to cells.²⁰ At pH ~ 7.5, cell viability around 90 % was observed.

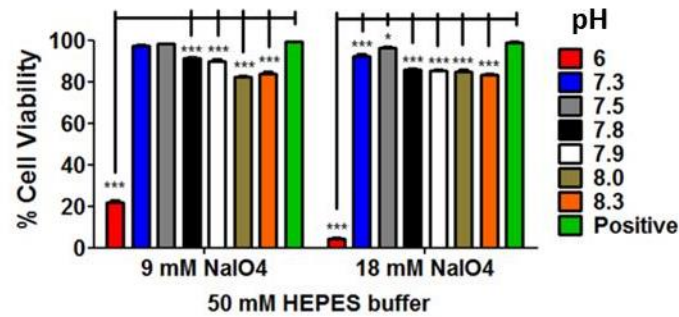
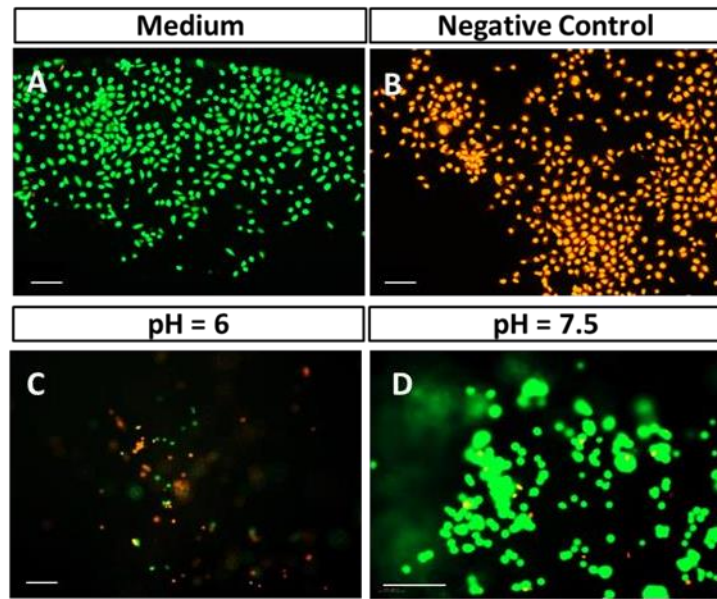


Figure 4.4 pH effect over cell viability. L929 fibroblasts were encapsulated in PEG-catechol hydrogels (conditions: 10kDa, 10 wt% polymer, 9 or 18 mM oxidant, 50 mM HEPES buffer, different pH). Live (green)/ dead (red) assay was performed after 1 h of culture. (A) Positive control: untreated cells (B), negative control: killed cells, (C, D) representative pictures from **PEG-Dop** hydrogels. Scale bars: 100 μ m.

The compatibility of PEG-catechol hydrogels modified with the cell-adhesive ligand cyclo(RGDfC) was also tested. Fibroblasts were mixed with the hydrogel precursors (final gel composition: 10 kDa, 10 wt % PEG polymers, 18 mM oxidant, 1 mM cyclo(RGDfC) peptide, 50 mM

HEPES buffer, pH 7.5) and the mixture was left to cure for 30 min at 37 °C. At this point the cell culture medium was replaced. The cell culture medium was exchanged every day. The viability of the cells in the 3D culture was tested after 3 d of culture. Viability ratios of ~91% (Fig. 4.5) were observed in all PEG-catechol gels tested. These data corroborate the cytocompatibility of PEG-catechol hydrogels as materials for cell encapsulation.

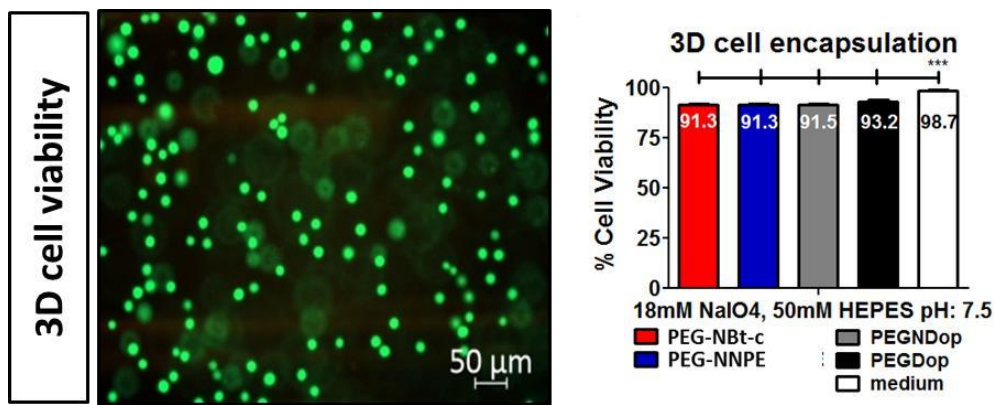


Figure 4.5 3D culture cell culture (L929 fibroblasts) performed on non-irradiated PEG-catechol hydrogels (conditions: 10 kDa, 10 wt % PEG polymers, 18 mM oxidant, 1 mM cyclo(RGDfC) peptide, in 50 mM HEPES buffer, pH 7.5). Live (green)/ dead (red) assay was performed after 3 d of culture. High cell viability (> 90 % in 3D) was observed for all tested conditions. Statistical significance analysis was conducted by ANOVA followed by post-hoc Tukey test (mean ± SD; ***p < 0.001 used for statistical significance).

4.3.2 Analysis of toxicity of photolysis products

The toxicity of the photolysis products from the photocleavage of **PEG-NBt-c**, **PEG-NNPE** and **PEG-NDop** hydrogels was tested. Hydrogel discs soaked in cell culture medium were irradiated at different doses (10 min = 42 J cm⁻², 15 min = 63 J cm⁻², 20 min = 84 J cm⁻² and 30 min = 126 J cm⁻²). Irradiation degrades the hydrogels and the low molecular photolysis products are expected to diffuse to the solution. The supernatant was collected after exposure, and brought into contact with cultured cells for 24 h. Then, cell viability was quantified.

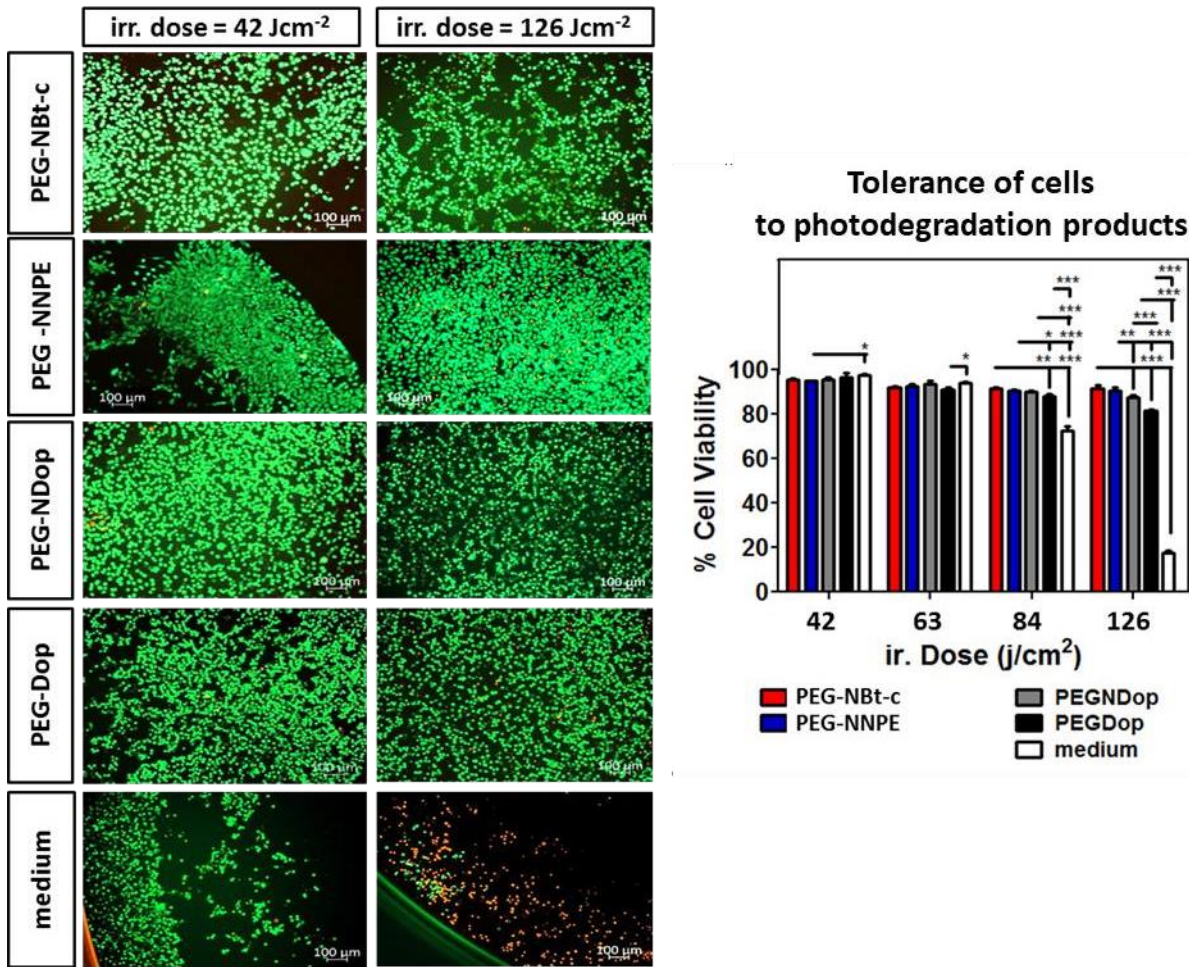


Figure 4.6 Viability of L929 fibroblasts cultured in the presence of soluble photolysis products of irradiated **PEG-Nbt-C**, **PEG-NNPE**, **PEG-NDop** and **PEG-Dop** gels. Gel composition: 10 kDa, 10 wt % PEG polymers, 18 mM oxidant, 50 mM HEPES buffer, pH 7.5.

High cell viability (> 90 %) was observed for all the photolyzed PEG-catechol hydrogels at irradiation doses 42 to 126 J cm^{-2} . This result proofs that the photolysis products of the gel degradation are non-cytotoxic within the concentrations used for this experiment.

4.3.3 Cell encapsulation in PEG-NBt-c gels and light-triggered cell release

PEG-NBt-c hydrogels were tested as substrates for cell encapsulation and photorelease (Fig. 4.7). Initial experiments were performed to prove that the gel could be degraded at cell compatible doses in 2D cell cultures. Thin films of **PEG-NBt-c** gels were fabricated in a culture plate and coated with the matrix protein collagen I to mediate cell attachment (Figure 4.7A). L929 fibroblast cells attached to the collagen coated hydrogel already at 4 h after seeding. After 4 days of culture, cells remained alive (viability 99%, Fig. 3.3.1.D), spread and covered the gel surface (Fig. 4.7B). This result indicates that **PEG-NBt-c** hydrogels biofunctionalized with cell adhesive molecules can support cell culture. The cell culture was exposed to light ($\lambda = 365$ nm, $I = 2.6$ mW cm⁻²) at given light doses (0, 0.5, 0.6, 0.8 and 1.1 J cm⁻²) expected to degrade the hydrogel. After illumination, most cells remained attached to the hydrogel surface, and some cells detached from the substrate and remained in the supernatant, presumably due to light-mediated erosion of the hydrogel. Remaining cells on the hydrogel were trypsinized²¹ and counted. The number of cells decreased with increasing illumination dose to reach 57% after illumination with 1.1 J cm⁻² (Fig. 4.8G). Remarkably, cell viability was high in all cases (97%, Fig. 4.7D). Cell viability was confirmed independently by LDH assay (Fig. 4.8F). These results suggest that neither the illumination dose nor the photolysis products resulting from gel erosion were cytotoxic. The partial photodegradation of the **PEG-NBt-c** gel surface removes the cell adhesive collagen coating and this causes detachment of the cells from the hydrogel.

The released cells after illumination were collected and seeded in a cell culture plate for 12 h. Cell viability and cell number were analyzed. Cell viability remained high (90 %) when cells were exposed to irradiation doses ≤ 1.1 mJ cm⁻². Within this irradiation range, the number of released cells increased with increasing irradiation dose, and reached 47% at 1.1 mJ cm⁻². These results demonstrate that irradiated cells remain viable and can be cultured for at least 12 h. It is important to point out that these are simple and short term tests to investigate cell functionality. Differentiation tests and long-term culture would be important to rule out photodamage and demonstrate the absence of damage in the genetic components²².

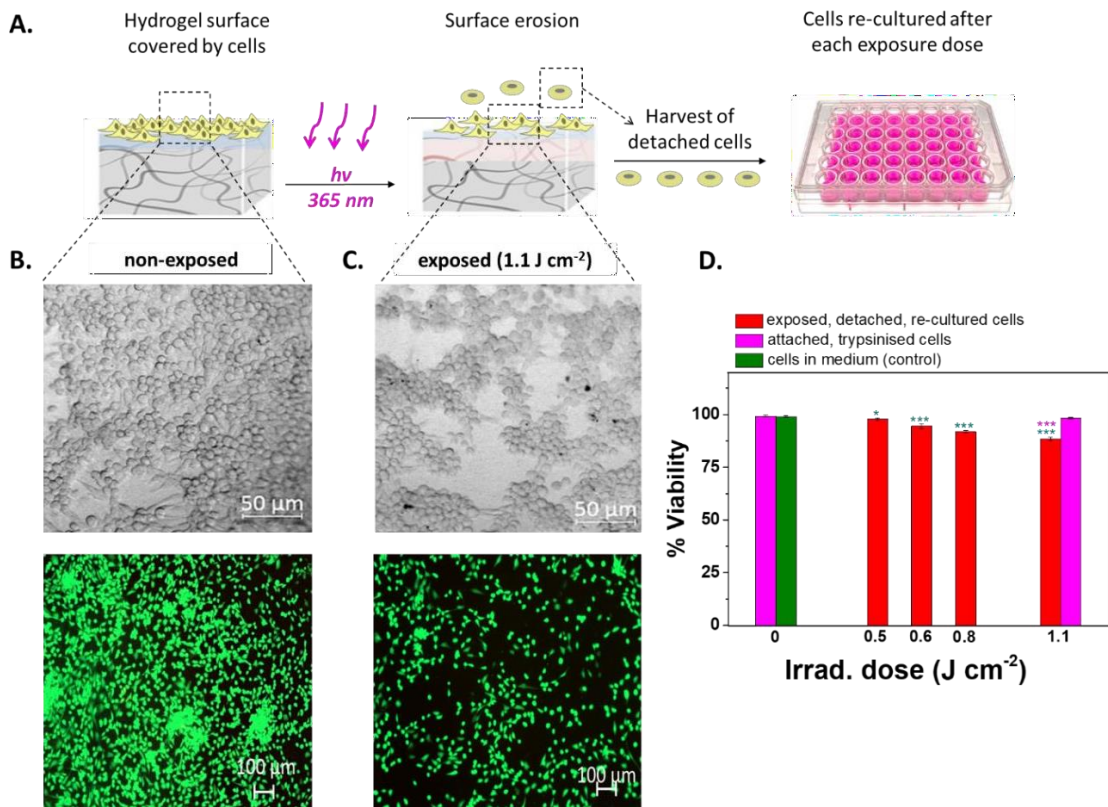
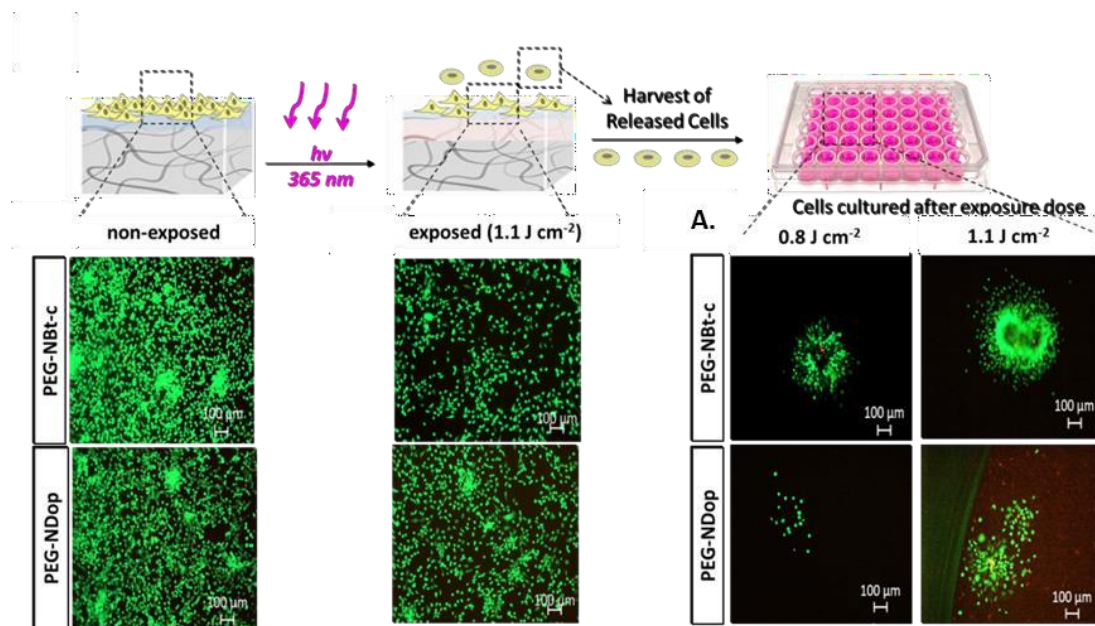


Figure 4.7 Photodegradation of **PEG-NBt-c** gels in 2D cell culture format A) Schematics of preparation of cell-adhesive gels and their use for cell culture (composition: 10 kDa, 10 wt% polymer, 18 mM oxidant, in 50 mM HEPES buffer, pH 7.5, coated with collagen I). L929 Fibroblasts were cultured on the top of the hydrogels for 4 days, and viability and spreading were checked (B). The complete hydrogel surface covered by cells was light exposed (LED lamp, $\lambda = 365 \text{ nm}$, $I = 2.6 \text{ mW cm}^{-2}$) for increasing doses. Cells remaining adherent atop the gel surface were analyzed (C), while detached cells were harvested, re-cultured separately for 12 h and analyzed for viability (D). At each stage, cell viability was evaluated by live (green)/dead (red) assay. Scale bars: 50 μm for bright field, 100 μm for fluorescence channel. Statistical significance analysis was performed by ANOVA followed by post-hoc Tukey test (mean \pm SD; * $p < 0.05$, *** $p < 0.001$ used for statistical significance).

Control experiments were performed on **PEG-NDop** gels prepared in the same way (Fig. 4.8). After 7 min exposure (dose = 1.1 J cm^{-2}), cells left on the hydrogel surface remained highly

viable (>95 %) while cells that were harvested and re-cultured for 12 h showed slightly but significantly decreased viability (83%) in relation to **PEG-NBt-c** (90%). Noticeably, at the same irradiation dose (= 18 mJ cm⁻²) the amount of cells remaining attached atop **PEG-NDop** gels decreased only to 87% (vs. 57% for **PEG-NBt-c**). Moreover, the number of harvested and re-cultured cells increased as well with increasing irradiation dose, although 3-fold fewer cells were released in comparison to **PEG-NBt-c** gels. These results reflect the higher photodegradation efficiency of **PEG-NBt-c** gels in relation to the control **PEG-NDop**.



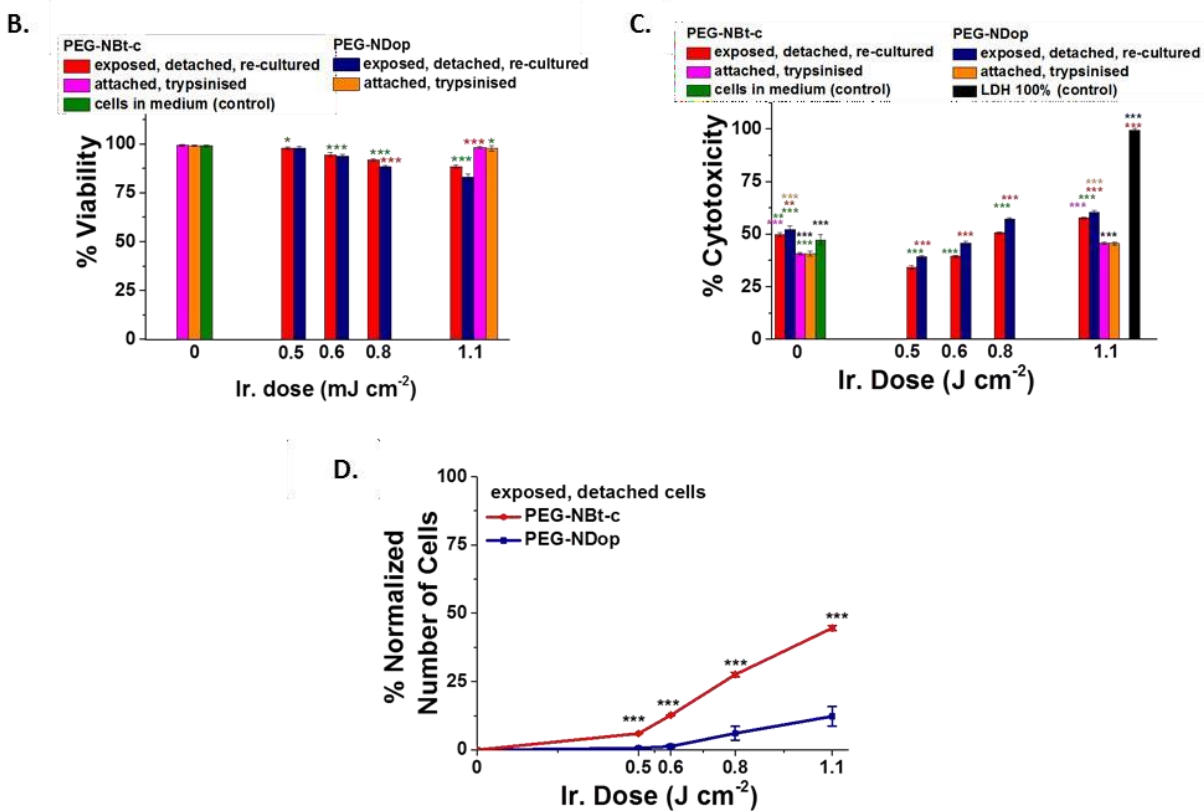


Figure 4.8 Comparison of **PEG-NBt-c** and **PEG-NDop** photodegradable gels for cell culture and light-triggered cell detachment (fibroblasts L929). The hydrogel surface covered by cells was exposed (LED lamp, $\lambda = 365 \text{ nm}$) for selected doses (5 min = 0.8 J cm^{-2} and 7 min = 1.1 J cm^{-2}) and live/dead assay performed. The cells detached at increasing light exposure were harvested, cultured separately for 12 h, stained and imaged (A). The tolerance of cells to exposure was evaluated by measuring cell viability by live (green)/dead (red) assay (B), and by LDH assay (C). Cells detached at increasing exposure doses, harvested and re-cultured were trypsinized and counted (D). Statistical significance analysis was performed by ANOVA followed by post-hoc Tukey test (mean \pm SD; * $p < 0.05$, *** $p < 0.001$ used for statistical significance).

These findings indicate the possibility of using **PEG-NBt-c** as biomaterials for 2D cell culture and subsequent light-triggered release, useful for applications in several technologies like cell-sheet harvesting and patterning as well as tunable surface topography or designing biointerfaces for cell cultures.²³⁻²⁵

4.3.4 3D cell encapsulation with PEG-NBt-c gels and *in situ* photodegradation

PEG-NBt-c gels were used to encapsulate cells and study cell migration and invasiveness as consequence of gel degradation by light. These are important cellular functions that need to be supported by polymeric matrices for cell culture and tissue regeneration, and are typically achieved by a balanced contribution of adhesion and proteolysis.²⁶ The introduction of photocleavable units in the hydrogel allows external control over degradation and, therefore, over cell fate.

Single RPE1 cells were encapsulated in **PEG-NBt-c** gels (gel composition: 10 kDa, 10 wt% polymer, 18 mM oxidant, pH 7.5, containing 1.5 mM cell adhesive RGD peptide) and cultured for one day. RPE1 cells clustered in their typical cobblestone morphology and did not spread or move through the hydrogel matrix. The lack of proteolytically cleavable bonds and the high stiffness of the matrix ($G' = 15$ kPa) explain the absence of cell invasiveness. Selected regions of the hydrogel were scanned with a laser at $\lambda = 405$ nm and the position of the cells after exposure was tracked. Cells within illuminated regions moved from their original location due to the local degradation of the material (Figure 4.9). This effect was visible at low irradiation doses (11.2 nJ per voxel). This result shows the possibility to control hydrogel degradation and consequently cell migration within a 3D construct just by using the laser of a microscope as external stimulus.

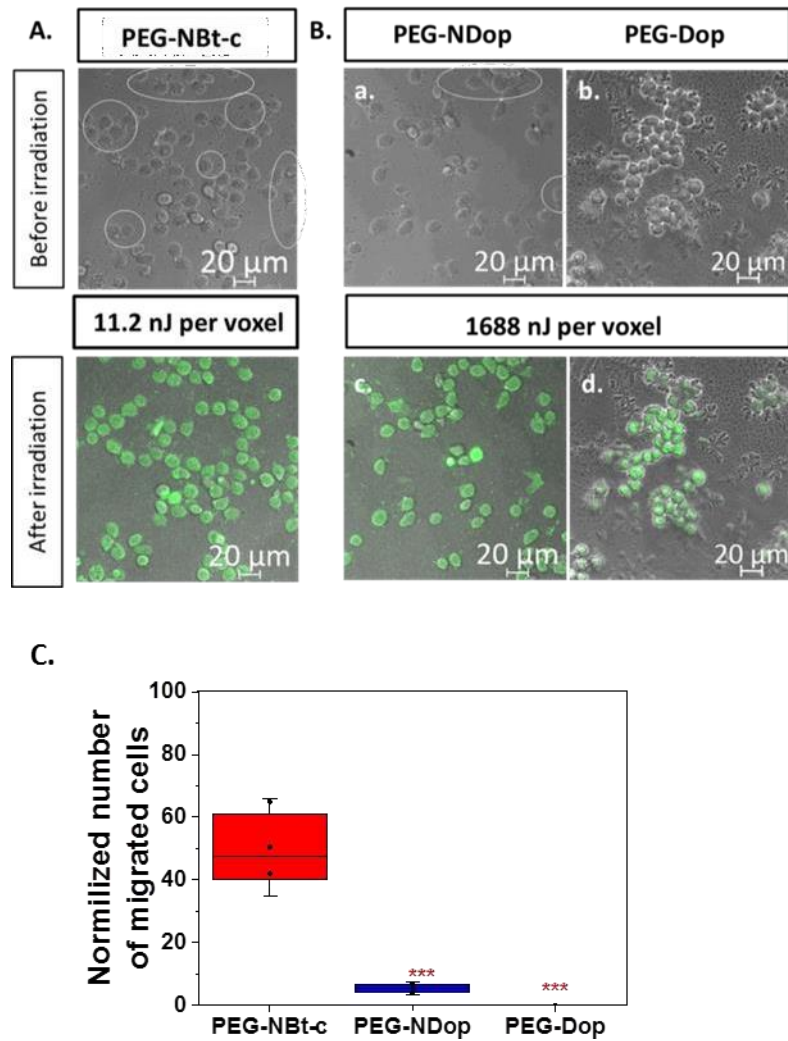


Figure 4.9 RPE1 cells encapsulated in PEG-catechol hydrogels (10 kDa, 10 wt% PEG polymers, 18 mM oxidant, 1 mM cyclo(RGDfC) peptide) after light exposure (scanning laser at $\lambda = 405 \text{ nm}$). (a-c) before irradiation, (d-f) after irradiation. White ovals mark the regions where cell displacement was observed upon irradiation. Irradiation conditions: d) laser power = 5 %, scan speed = 1, passing number = 1 (0.085 mW and 11.2 nJ per voxel). e-f) laser power = 100 %, scan speed = 1, passing number = 8 (1.6 mW and 1688 nJ per voxel). (B) Normalized number of migrated cells after irradiation. Scale bar: 20 μm . Statistical significance analysis was performed by ANOVA followed by post-hoc Tukey test (mean \pm SD; *** $p < 0.001$ used for statistical significance).

The possibility to spatiotemporally modulate the photocleavage of **PEG-NBt-c** gels and control 3D invasion from fibroblast spheroids was tested. The spheroids were embedded in **PEG-NBt-c** gels modified with cell-adhesive RGD peptide without presenting any enzymatically cleavable sequence. The timing for the addition of the spheroids to the gel precursors mixture was optimized to avoid sedimentation of spheroids during crosslinking (see details in the Appendix). Embedded spheroids remained confined within the hydrogel and highly viable (>90%, see Fig. 7 Appendix). After 7 h of encapsulation, an area at the periphery of the spheroid was illuminated (18.4 nJ per voxel) to locally degrade the material and allow cell invasion. Cell migration out of the spheroid was analyzed over time. After 2 d of culture, cells migrated out of the spheroid following the irradiated area (migrated distance was 15 μm), and this process became more evident after 5 d of culture, reaching a migrated distance of 75 μm at the irradiated regions of the hydrogel. Cells located in non-irradiated areas remained confined (migrated distance $\sim 0 \mu\text{m}$) (Fig. 4.10b-c). At day 9 after irradiation, spheroids could be connected by scanning a “bridge” between them, through which fibroblasts moved and came into contact (Figure 4.10d, dose= 23.7 nJ per voxel and distance of migration 100 μm). Collectively, these results show that **PEG-NBt-c** gels can be partially degraded to hydrogels that allow invasion inside the gel, but maintain stability in the cell culture. Such materials are interesting for areas such as study of cancer invasiveness and progression, development of angiogenesis models, and for mechanics-controlled stem cell differentiation.^{4, 5, 27-30}

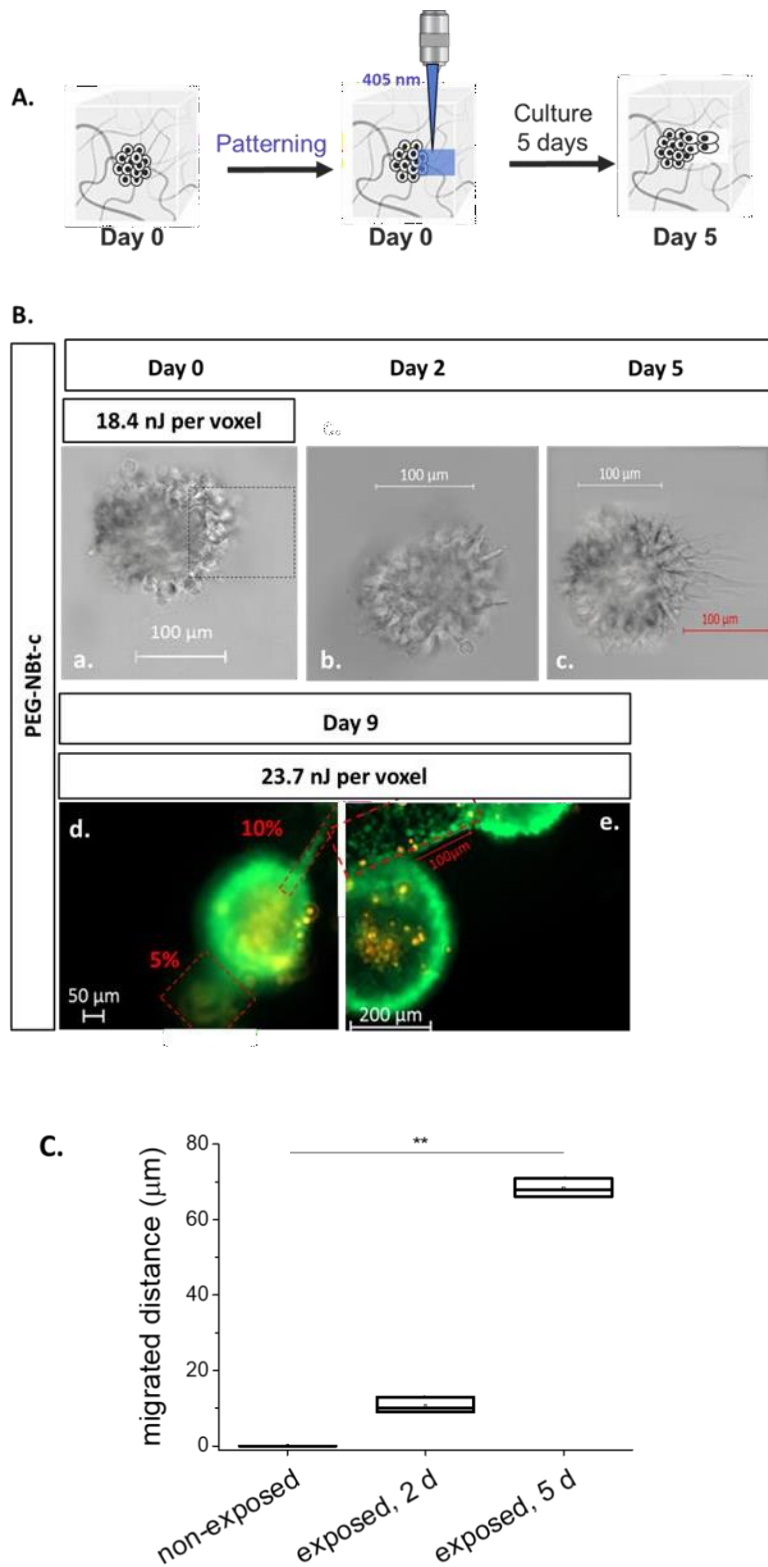


Figure 4.10 Light-triggered migration from fibroblast spheroids encapsulated in PEG-NBT-c hydrogels (gel composition: 10 kDa, 10 wt% polymer, 18 mM oxidant, 1 mM cyclo(RGDfC)

peptide). A) Schematics of the photo-activatable control of cell invasion on the matrices 3D Fibroblast spheroids. B) Spheroids were encapsulated in PEG-NBt-c hydrogel and cultured for 7 h. An area on the end of spheroid was irradiated (indicated by dashed rectangles, laser power denoted (for 8% laser power : 0.14 mW and 18.4 nJ per voxel, 5% : 0.085 mW and 12.2 nJ per voxel and 10% : 0.18 and 23.7 nJ per voxel) and cell migration out of the spheroid was analyzed over 5 d of culture and cell viability over 9 d of culture. C) Distance of migrated cells (μm) at different days of culture (day 2, 5: laser power denoted 8% : 0.14 mW and 18.4 nJ per voxel). Scale bar: a-c = 100 μm ; d = 200 μm ; e = 50 μm . Statistical significance analysis was performed by ANOVA followed by post-hoc Tukey test (mean \pm SD; * p < 0.05, *** p < 0.001 used for statistical significance).

Similar experiments performed with control **PEG-NDop** and **PEG-Dop** gels showed that spheroids remained viable after encapsulation, but gel illumination did not trigger cell migration, even when high irradiation doses were used (see Figure 4.11, dose= 211 nJ per voxel, >9 times higher than the dose used for **PEG-NBt-c**). This proves the value of **PEG-NBt-c** gel as a platform for 3D-regulated degradation and control of cell invasiveness and migration inside the hydrogel, which is not possible in **PEG-NDop** and **PEG-Dop** controls.

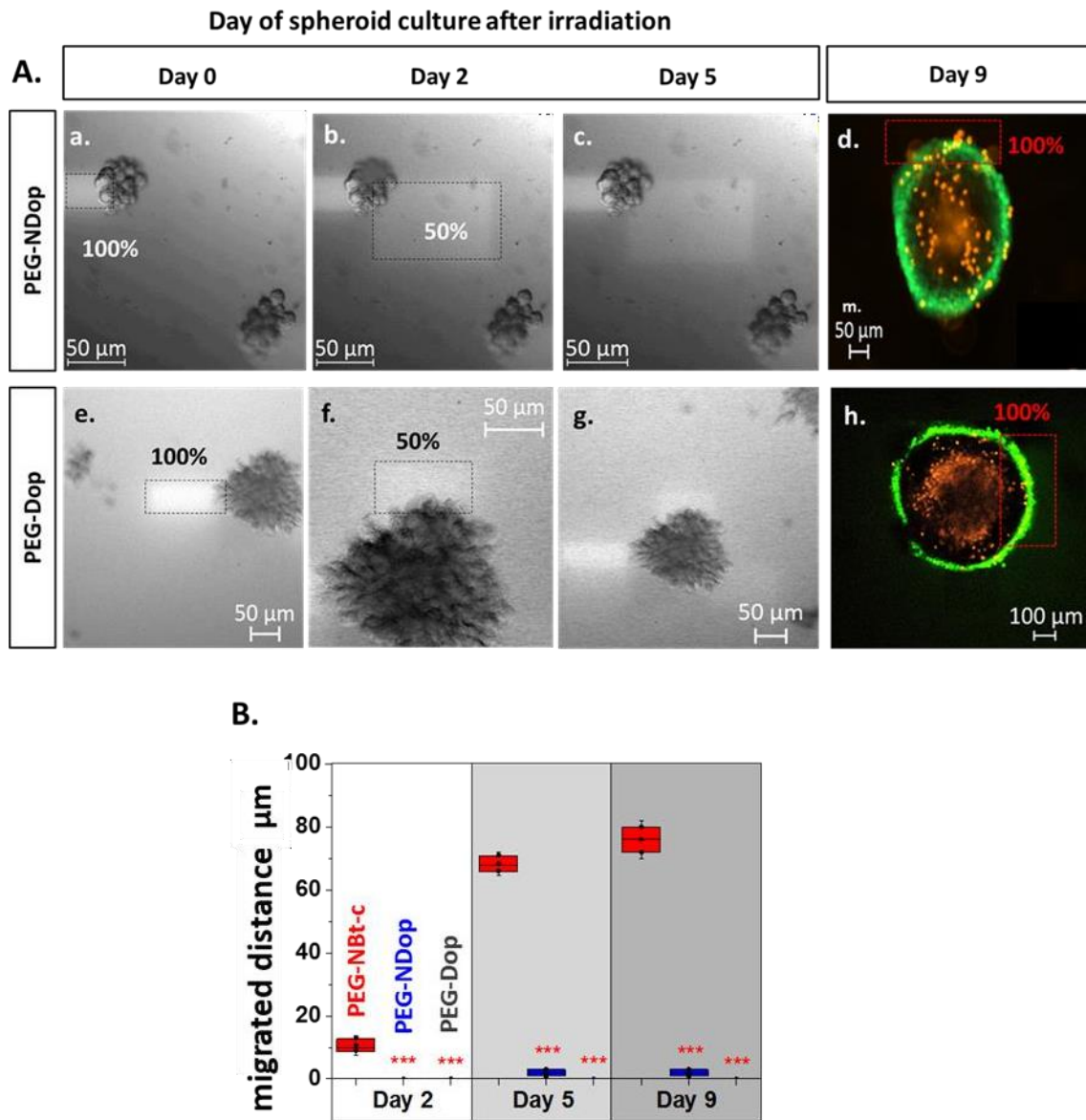


Figure 4.11 Fibroblast spheroids encapsulated in **PEG-NDop** and **PEG-Dop** hydrogels and cultured for 7 h. An area at the periphery of the spheroid was irradiated (indicated by dashed rectangles, laser power denoted (for 50% : 0,82 mW and 104 nJ per voxel and 100% : 1,6 mW and 211 nJ per voxel). Final polymer composition = 10 kDa, 10 wt% PEG, 18 mM oxidant, 1 mM cyclo(RGDfC)peptide, 50 mM HEPES buffer, pH 7.5. Live (green)/Dead (orange) assay was performed in 9 days of culture. B) Distance of migrated cells (μm) at different hydrogels (**PEG-NBt-c**: red; **PEG-NDop**: blue; **PEG-Dop**: grey), at different days of culture (day 2, 5, 9). Scale bar:

a-c = 100 µm, d-h = 50 µm. Statistical significance analysis was performed by ANOVA followed by post-hoc Tukey test (mean ± SD; ***p < 0.001 used for statistical significance).

4.4 Conclusions

PEG-catechol hydrogels synthesized in this Thesis were characterized and successfully used as biocompatible matrices for 2D and 3D cell culture. Gel formulation conditions were optimized by varying experimental parameters such as the oxidant concentration, polymer content, culture medium and pH. The optimal conditions for cell encapsulation were 10 kDa, 10 wt % PEG polymers, 18 mM oxidant, 1 mM cyclo(RGDfC) peptide, 50 mM HEPES buffer, pH 7.5. At these conditions, encapsulated fibroblasts proliferated and showed high viability (> 90%) after 3 days of encapsulation. Importantly, the products of the photolysis at irradiation doses up to 126 J cm⁻² are not toxic for cells.

The possibility to regulate cellular release by the responsiveness of **PEG-NBt-c** hydrogels to light was tested. L929 fibroblast cells cultured on the top of **PEG-NBt-c** gel coated with collagen I were released on-demand by light irradiation at 4 day of culture, and the released cells had high viability (90 %). Released cells remained functional and were able to reattach and proliferate on 96-well plate. These results indicate the possibility to use **PEG-NBt-c** as biomaterials for 2D cell culture and subsequent light-triggered release, useful for applications like cell harvesting, cell-sheet patterning as well as tunable surface topography or designing biointerfaces for dynamic cell cultures.²³⁻²⁵

PEG-NBt-c gels were also used as biomaterials for 3D cell encapsulation. Upon irradiation at 405 nm, the illuminated region of the hydrogel was degraded and crosslinking density decreased, thereby opening pores to facilitate cell movement across the hydrogel. This light-controlled dynamic modulation of the cell microenvironments was demonstrated through the release of RPE1 cells and the matrix invasion out of fibroblast L929 spheroids. RPE1 were released on-demand at low irradiation dose (11.2 nJ per voxel at λ = 405 nm) at 1 day post encapsulation. Fibroblast migration was triggered at 18.4 nJ per voxel. Such biomaterials that enable light-guided

invasion could be valuable for applications such as study of cancer invasiveness and progression, development of angiogenesis models, and for mechanics-controlled stem cell differentiation.^{4, 5, 27-30}

PEG-NBt-c photodegradable hydrogel represents a useful material for cell encapsulation and 3D cultures, and potential as a cell expansion substrate or a smart material for guiding, and regulating cell migration.

4.5 References

1. Nicodemus, G. D.; Bryant, S. J., Cell encapsulation in biodegradable hydrogels for tissue engineering applications. *Tissue Engineering Part B: Reviews* 2008, 14 (2), 149-165.
2. Slaughter, B. V.; Khurshid, S. S.; Fisher, O. Z.; Khademhosseini, A.; Peppas, N. A., Hydrogels in regenerative medicine. *Advanced materials* 2009, 21 (32-33), 3307-3329.
3. Khademhosseini, A.; Langer, R.; Borenstein, J.; Vacanti, J. P., Microscale technologies for tissue engineering and biology. *Proceedings of the National Academy of Sciences* 2006, 103 (8), 2480-2487.
4. Kloxin, A. M.; Kasko, A. M.; Salinas, C. N.; Anseth, K. S., Photodegradable hydrogels for dynamic tuning of physical and chemical properties. *Science* 2009, 324 (5923), 59-63.
5. Kloxin, A. M. Photolabile hydrogels for dynamic tuning of physical and chemical properties to probe cell-cell and cell-material interactions. University of Colorado at Boulder, 2009.
6. DeForest, C. A.; Anseth, K. S., Cytocompatible click-based hydrogels with dynamically tunable properties through orthogonal photoconjugation and photocleavage reactions. *Nature chemistry* 2011, 3 (12), 925.
7. Truong, V. X.; Ablett, M. P.; Gilbert, H. T.; Bowen, J.; Richardson, S. M.; Hoyland, J. A.; Dove, A. P., In situ-forming robust chitosan-poly (ethylene glycol) hydrogels prepared by copper-free azide–alkyne click reaction for tissue engineering. *Biomaterials Science* 2014, 2 (2), 167-175.
8. McKinnon, D. D.; Brown, T. E.; Kyburz, K. A.; Kiyotake, E.; Anseth, K. S., Design and characterization of a synthetically accessible, photodegradable hydrogel for user-directed formation of neural networks. *Biomacromolecules* 2014, 15 (7), 2808-2816.

9. Kloxin, A. M.; Tibbitt, M. W.; Anseth, K. S., Synthesis of photodegradable hydrogels as dynamically tunable cell culture platforms. *Nature protocols* 2010, 5 (12), 1867.
10. Griffin, D. R.; Kasko, A. M., Photodegradable macromers and hydrogels for live cell encapsulation and release. *Journal of the American chemical society* 2012, 134 (31), 13103-13107.
11. Kirschner, C. M.; Alge, D. L.; Gould, S. T.; Anseth, K. S., Clickable, photodegradable hydrogels to dynamically modulate valvular interstitial cell phenotype. *Advanced healthcare materials* 2014, 3 (5), 649-657.
12. Kirschner, C. M.; Anseth, K. S., In situ control of cell substrate microtopographies using photolabile hydrogels. *Small* 2013, 9 (4), 578-584.
13. Lee, T. T.; García, J. R.; Paez, J. I.; Singh, A.; Phelps, E. A.; Weis, S.; Shafiq, Z.; Shekaran, A.; Del Campo, A.; García, A. J., Light-triggered in vivo activation of adhesive peptides regulates cell adhesion, inflammation and vascularization of biomaterials. *Nature materials* 2015, 14 (3), 352.
14. Hansen, M. J.; Velema, W. A.; Lerch, M. M.; Szymanski, W.; Feringa, B. L., Wavelength-selective cleavage of photoprotecting groups: strategies and applications in dynamic systems. *Chemical Society Reviews* 2015, 44 (11), 3358-3377.
15. Brubaker, C. E.; Kissler, H.; Wang, L.-J.; Kaufman, D. B.; Messersmith, P. B., Biological performance of mussel-inspired adhesive in extrahepatic islet transplantation. *Biomaterials* 2010, 31 (3), 420-427.
16. Hong, S.; Yang, K.; Kang, B.; Lee, C.; Song, I. T.; Byun, E.; Park, K. I.; Cho, S.-W.; Lee, H., Hyaluronic Acid Catechol: A Biopolymer Exhibiting a pH-Dependent Adhesive or Cohesive Property for Human Neural Stem Cell Engineering. *Advanced Functional Materials* 2013, 23 (14), 1774-1780.
17. Liu, Y.; Meng, H.; Konst, S.; Sarmiento, R.; Rajachar, R.; Lee, B. P., Injectable dopamine-modified poly (ethylene glycol) nanocomposite hydrogel with enhanced adhesive property and bioactivity. *ACS applied materials & interfaces* 2014, 6 (19), 16982-16992.
18. Bilic, G.; Brubaker, C.; Messersmith, P. B.; Mallik, A. S.; Quinn, T. M.; Haller, C.; Done, E.; Gucciardo, L.; Zeisberger, S. M.; Zimmermann, R., Injectable candidate sealants for fetal membrane repair: bonding and toxicity in vitro. *American journal of obstetrics and gynecology* 2010, 202 (1), 85. e1-85. e9.

19. Kastrup, C. J.; Nahrendorf, M.; Figueiredo, J. L.; Lee, H.; Kambhampati, S.; Lee, T.; Cho, S.-W.; Gorbatov, R.; Iwamoto, Y.; Dang, T. T.; Dutta, P.; Yeon, J. H.; Cheng, H.; Pritchard, C. D.; Vegas, A. J.; Siegel, C. D.; MacDougall, S.; Okonkwo, M.; Thai, A.; Stone, J. R.; Coury, A. J.; Weissleder, R.; Langer, R.; Anderson, D. G., Painting blood vessels and atherosclerotic plaques with an adhesive drug depot. *Proceedings of the National Academy of Sciences* 2012, 109 (52), 21444-21449.
20. <https://www.thermofisher.com/de/de/home/life-science/cell-culture/mammalian-cell-culture/reagents/hepes.html>
21. <https://www.sigmaaldrich.com/technical-documents/articles/biology/cell-dissociation-with-trypsin.html>; access date: January 2020.
22. Wong, D. Y.; Ranganath, T.; Kasko, A. M., Low-Dose, Long-Wave UV Light Does Not Affect Gene Expression of Human Mesenchymal Stem Cells. *PLOS ONE* 2015, 10 (9), e0139307.
23. Pasparakis, G.; Manouras, T.; Selimis, A.; Vamvakaki, M.; Argitis, P., Laser-induced cell detachment and patterning with photodegradable polymer substrates. *Angewandte Chemie International Edition* 2011, 50 (18), 4142-4145.
24. Uto, K.; Tsui, J. H.; DeForest, C. A.; Kim, D.-H., Dynamically tunable cell culture platforms for tissue engineering and mechanobiology. *Progress in polymer science* 2017, 65, 53-82.
25. Kolesnikova, T. A.; Kohler, D.; Skirtach, A. G.; Mohwald, H., Laser-induced cell detachment, patterning, and regrowth on gold nanoparticle functionalized surfaces. *ACS nano* 2012, 6 (11), 9585-9595.
26. Qin, X.-H.; Wang, X.; Rottmar, M.; Nelson, B. J.; Maniura-Weber, K., Near-Infrared Light-Sensitive Polyvinyl Alcohol Hydrogel Photoresist for Spatiotemporal Control of Cell-Instructive 3D Microenvironments. *Advanced Materials* 2018, 30 (10), 1705564.
27. Lutolf, M.; Lauer-Fields, J.; Schmoekel, H.; Metters, A. T.; Weber, F.; Fields, G.; Hubbell, J. A., Synthetic matrix metalloproteinase-sensitive hydrogels for the conduction of tissue regeneration: engineering cell-invasion characteristics. *Proceedings of the National Academy of Sciences* 2003, 100 (9), 5413-5418.
28. Phelps, E. A.; Enemchukwu, N. O.; Fiore, V. F.; Sy, J. C.; Murthy, N.; Sulchek, T. A.; Barker, T. H.; García, A. J., Maleimide cross-linked bioactive peg hydrogel exhibits improved reaction

- kinetics and cross-linking for cell encapsulation and in situ delivery. *Advanced materials* 2012, 24 (1), 64-70.
29. Moon, J. J.; Saik, J. E.; Poche, R. A.; Leslie-Barbick, J. E.; Lee, S.-H.; Smith, A. A.; Dickinson, M. E.; West, J. L., Biomimetic hydrogels with pro-angiogenic properties. *Biomaterials* 2010, 31 (14), 3840-3847.
30. Bryant, S. J.; Anseth, K. S.; Lee, D. A.; Bader, D. L., Crosslinking density influences the morphology of chondrocytes photoencapsulated in PEG hydrogels during the application of compressive strain. *Journal of Orthopaedic Research* 2004, 22 (5), 1143-1149.

Conclusions & Outlook

In this PhD thesis, bioinspired hydrogels for tissue adhesion and cell encapsulation were developed and complemented with the possibility of light-mediated degradation and cell release at cytocompatible exposure doses. This work expands previous reports on hydrogels for tissue adhesion and cell culture,¹ for tissue adhesion and photodegradability², or for cell culture and photodegradability for controlled release.³ The developed hydrogels in this PhD work unify the three properties (tissue adhesion, photodegradability, as well as suitability for cell culture) in a single material. These properties are relevant in biomaterials for advanced wound dressings and cell therapies.

The following are the major conclusions from this work:

1. Mussel-inspired **PEG-NBt-c** hydrogel precursors based on star 4-arm PEG (10 and 20 kDa) terminated with catechol groups as crosslinking units and photocleavable o-nitrobenzyl triazole can be synthesized and polymerized to form photodegradable hydrogels. Polymerization occurs at mild conditions and the final mechanical properties of the hydrogels can be controlled with pH or oxidant concentration to obtain hydrogels within relevant physiological ranges for cell encapsulation.
2. The NBt unit proved to be advantageous vs. reported ester analogue (NBe⁴) in terms of hydrolytic stability of the hydrogel, without compromising the photolytic efficiency. This makes PEG-NBt-c more suitable as material for long term tissue adhesion and cell encapsulation.
3. The conditions for photodegradation of PEG-NBt-c are compatible with living cells encapsulated in the material. This property makes this system interesting for on-demand release of cargos (cells) and customized debonding from tissue.

The modular design of the hydrogel precursors enables variations to fine tune hydrogel properties. For example, the PEG polymer backbone can be replaced by other backbones such

Conclusions & Outlook

as gelatin or hyaluronic acid to increase bioactivity of the system (cell-adhesion, degradability). Additionally, the incorporation of substituted catechol moieties like chloro-catechol instead of catechol could allow faster crosslinking kinetics, while not altering the adhesion strength⁵ of the formulation. This is particularly relevant towards the development of minimally invasive cell therapies, by providing a comfortable time frame for the handling of cell-containing hydrogel solution and its administration.⁶

Photodegradable biomaterials that can respond to external stimulus are useful in biomedical community, allowing the gel properties to be manipulated by light. They represent useful formulations for cell encapsulation and 3D cultures, and potential as a cell expansion substrate or a smart material for guiding, and regulating cell migration. For future work the combination of tissue adhesives and drug delivery will be promoted in surgeries, for faster healing rates and tissue regeneration.⁷

References

1. Brubaker, C. E.; Kissler, H.; Wang, L.-J.; Kaufman, D. B.; Messersmith, P. B., Biological performance of mussel-inspired adhesive in extrahepatic islet transplantation. *Biomaterials* **2010**, *31* (3), 420-427.
2. Wu, H.; Qin, Z.; Yu, X.; Li, J.; Lv, H.; Yang, X., On-demand removable hydrogels based on photolabile cross-linkings as wound dressing materials. *Journal of Materials Chemistry B* **2019**, *7* (37), 5669-5676.
3. Griffin, D. R.; Kasko, A. M., Photodegradable Macromers and Hydrogels for Live Cell Encapsulation and Release. *Journal of the American Chemical Society* **2012**, *134* (31), 13103-13107.
4. Ruskowitz, E. R.; DeForest, C. A., Photoresponsive biomaterials for targeted drug delivery and 4D cell culture. *Nature Reviews Materials* **2018**, *3* (2), 17087.
5. Paez, J. I.; Ustahüseyin, O.; Serrano, C.; Ton, X.-A.; Shafiq, Z.; Auernhammer, G. K.; d'Ischia, M.; del Campo, A., Gauging and Tuning Cross-Linking Kinetics of Catechol-PEG Adhesives via Catecholamine Functionalization. *Biomacromolecules* **2015**, *16* (12), 3811-3818.

6. Shin, J.; Lee, J. S.; Lee, C.; Park, H.-J.; Yang, K.; Jin, Y.; Ryu, J. H.; Hong, K. S.; Moon, S.-H.; Chung, H.-M.; Yang, H. S.; Um, S. H.; Oh, J.-W.; Kim, D.-I.; Lee, H.; Cho, S.-W., Tissue Adhesive Catechol-Modified Hyaluronic Acid Hydrogel for Effective, Minimally Invasive Cell Therapy. *Advanced Functional Materials* **2015**, *25* (25), 3814-3824.
7. Khanlari, S.; Dubé, M. A., Bioadhesives: a review. *Macromolecular Reaction Engineering* **2013**, *7* (11), 573-587.

Appendix

Table of contents

Appendix Section	Page
1. Materials and Instrumentation	131
2. Chapter 2: Synthesis and physicochemical characterization of Photodegradable PEG-catechol precursors	134
3. Chapter 3: Preparation & Characterization of Photodegradable Adhesive PEG-catechol hydrogels	183
4 .Chapter 4: Photodegradable PEG-catechol hydrogels as cell culture scaffolds	189
5. References	198

Experimental Section

1. Materials and instrumentation

10 and 20 kDa, 4-arm PEG succinimidyl carboxymethyl ester (PEG-NHS) and Thiol PEG Amine, 10 and 20 kDa, 4-arm PEG Acetic Acid (PEG-COOH) and HCl Salt (HS-PEG-NH₂HCl) were purchased from JenKem Technology, USA. HOBr (1-hydroxybenzotriazole hydrate), NaN₃ (sodium azide), DIPEA (N,N-diisopropylethylamine), DMF (dimethylformamide), N-Boc-ethylenediamine, MgSO₄ (magnesium sulfate), EtOAc (ethyl acetate), DCM (dichloromethane), Ms-Cl (methanesulfonyl chloride), TEA (triethylamine), DCC (N,N'-dicyclohexylcarbodiimide), DMAP (4-dimethylaminopyridine), SA (sulfuric acid), Dop (dopamine hydrochloride), NaNO₂ (Sodium nitrite), MeOH (methanol), NaIO₄ (sodium periodate), NMM (N-methylmorpholine) and NE (DL-Norepinephrine hydrochloride) were purchased from Sigma-Aldrich. The photocleavable linker, denoted as NB (4-[4-(1-Hydroxyethyl)-2-methoxy-5-nitrophenoxy]butyric acid), was purchased either from Sigma-Aldrich or from Santa Cruz Biotechnology. PBS (Phosphate-buffered saline) and CMNB-caged fluorescein was purchased from Thermo Fisher GmbH, Life Technologies. HBTU (N,N,N',N'-Tetramethyl-O-(1H-benzotriazol-1-yl)uronium hexafluoro-phosphate) was

purchased from Carbolution Chemicals GmbH. Na₂CO₃ (sodium carbonate), DHCA (3-(3,4-dihydroxyphenyl)propionic acid), DBCO-NH₂ (DBCO-amine) and diethylether were purchased from Alfa Aesar. NMP (N-methyl-2-pyrrolidone), piperidine and 1,4-Dioxane were purchased from Acros Organics. The cell adhesive peptide cyclo (Arg-Gly-Asp-D-phenylalanine-Cys) (cyclo(RGDfC)) was purchased from Peptides International (Kentucky, USA). 6-nitro-dopamine (NDop), 6-nitro-dopamine benzamide (NDop-benzamide), PEG-Dop and PEG-NDop macromer were synthesized following protocols previously reported by del Campo's group.^{1,2}

Synthesis and manipulation of photo-sensitive compounds were performed in the dark. The course of the reactions was typically monitored by thin layer chromatography (TLC) of 0.20 mm silica gel 60 with fluorescent indicator (Macherey-Nagel GmbH & Co.KG, Germany) or via analytical HPLC (see below).

Silica gel column chromatography was performed with 0.04 -0.063 mm silica 60 M (Macherey-Nagel GmbH & Co.KG, Germany). Dialysis purification of substituted PEG polymers was performed using membrane tubing (molecular weight cut-off of 3.5 kDa; Spectrum Laboratoried, Canada), against acetone, methanol or water, typically for at least 48 h (dialysate was changed 2-3 times per day).

Analytical and semi-preparative reverse phase high performance liquid chromatography (HPLC) was performed with a HPLC JASCO 4000 (Japan) equipped with a diode array UV/Vis detector and fraction collector. Elution solvents used were solvent A (water + 0.1%TFA) and solvent B (acetonitrile + 5 % water + 0.1% TFA). Reprosil C18 columns were used for semi-preparative (250 × 25 mm) and analytical (250 × 5 mm) runs. Typically, a run was performed over 40 min of duration and consisted in a isocratic pre-run at 30%B for 3 min, followed by a gradient increase of 30%B to 95%B for 30 min and isocratic run at 95 %B for 7 min. Detection of the compounds was performed at triple wavelengths λ = 210, 254 and 360 nm. Retention time of the compounds is reported in min.

¹H-NMR spectra (300 MHz) were recorded using a Bruker Avance 300 spectrometer. Chemical shifts are reported in parts per million (ppm) using the residual non-deuterated solvent signal of CDCl₃ (δ = 7.26 ppm), D₂O (δ = 4.79 ppm), DCM-d₂ (δ = 5.32 ppm) or acetone-d₆ (δ = 2.05 ppm) as internal reference. Multiplicities are reported by using the following abbreviations; s: singlet; bs: broad singlet; d: doublet; dd: doublet of doublets; t: triplet; q: quartet; quint: quintet; m: multiplet. The

degree of substitution during polymer modification reactions was obtained by ^1H NMR end-group determination method. The integral of the signal corresponding to the PEG backbone (4.2–3.9 ppm) was set to 220 or 440 protons, corresponding to 4-arm PEG polymers of 10 or 20 kDa, respectively; and compared with the integral of the protons or the new expected signals. Functionalization degrees of 80–90% and yields of 60–90% were obtained in all cases.

UV/VIS Spectra were recorded with a Varian Cary 4000 UV/VIS spectrometer (Varian Inc. Palo Alto, USA). ESI-MS+ mass spectrometry were recorded using a LC/ESI- Q-TOF 6545 and LC/ESI-MSD SL 1260 Infinity (Agilent). AB Sciex 4800 MALDI-TOF mass spectrometry (Sciex-Company, Darmstadt, Germany) were performed in linear mode in the mass range from 4000-40000 Da. About 4000 single shots were accumulated for one spectrum for each sample. 50% of aqueous tetrahydrofuran containing 10 mg/mL Dithranol was used to solve solid samples or to dilute liquids. About 1 μL of sample solution containing Dithranol was pipetted onto a 384 sample steel plate and dried according to dried-droplet method.⁸

Light irradiation experiments in solution were carried out as follows. Photolysis in solution was performed at $\lambda=365\text{nm}$, with a LUMOS 43 lamp (100 W, Irradiance: 1.2mW cm^{-2}) (Atlas Photonics, Switzerland). Ex situ photolysis of hydrogels was done at $\lambda=365\text{ nm}$, under ECE 2000 standard metal halide UV curing bulb (400W, Irradiance = 70mW/cm^2)(DYMAX).

2. Chapter 2

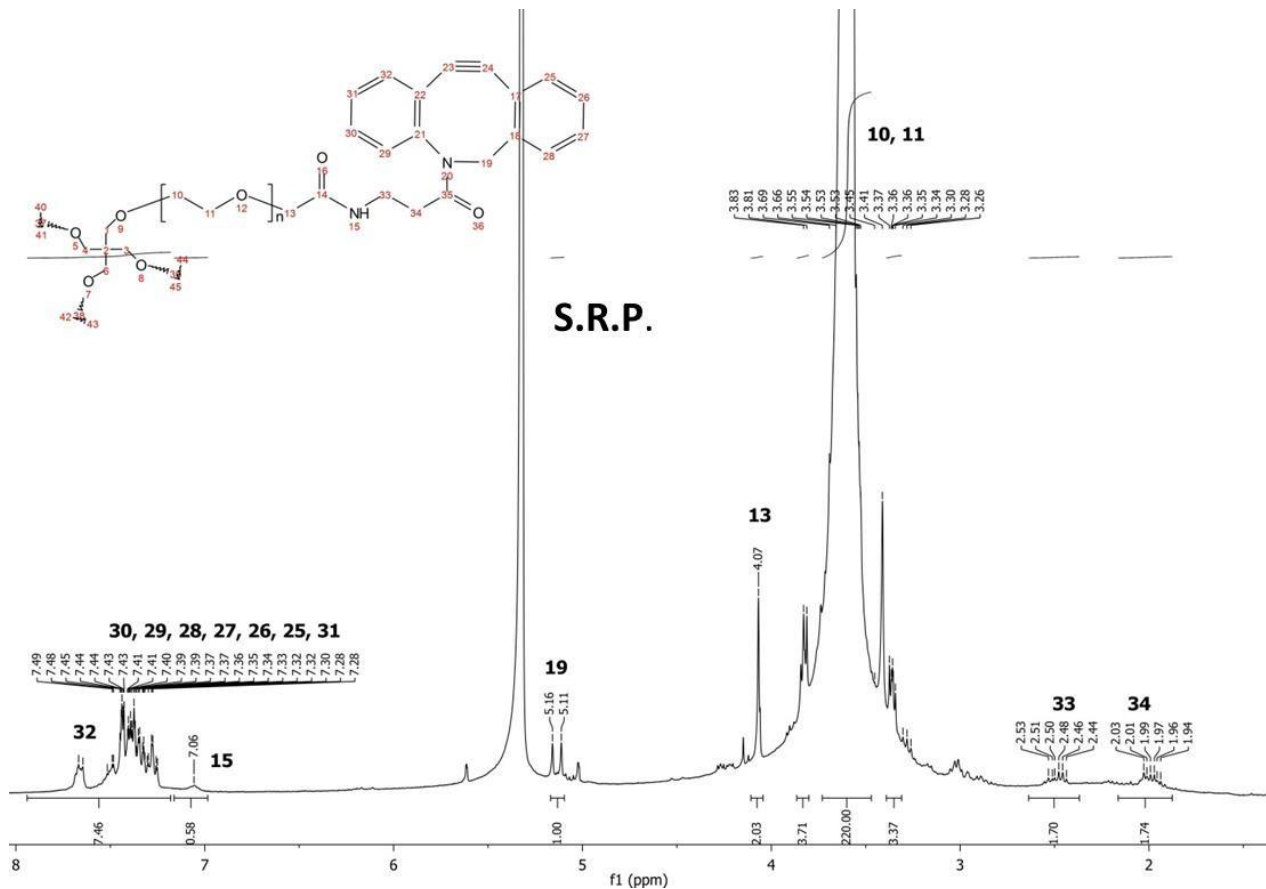
Synthesis and physicochemical characterization of Photodegradable PEG-catechol precursors

2.1 Synthesis of PEG-DBCO

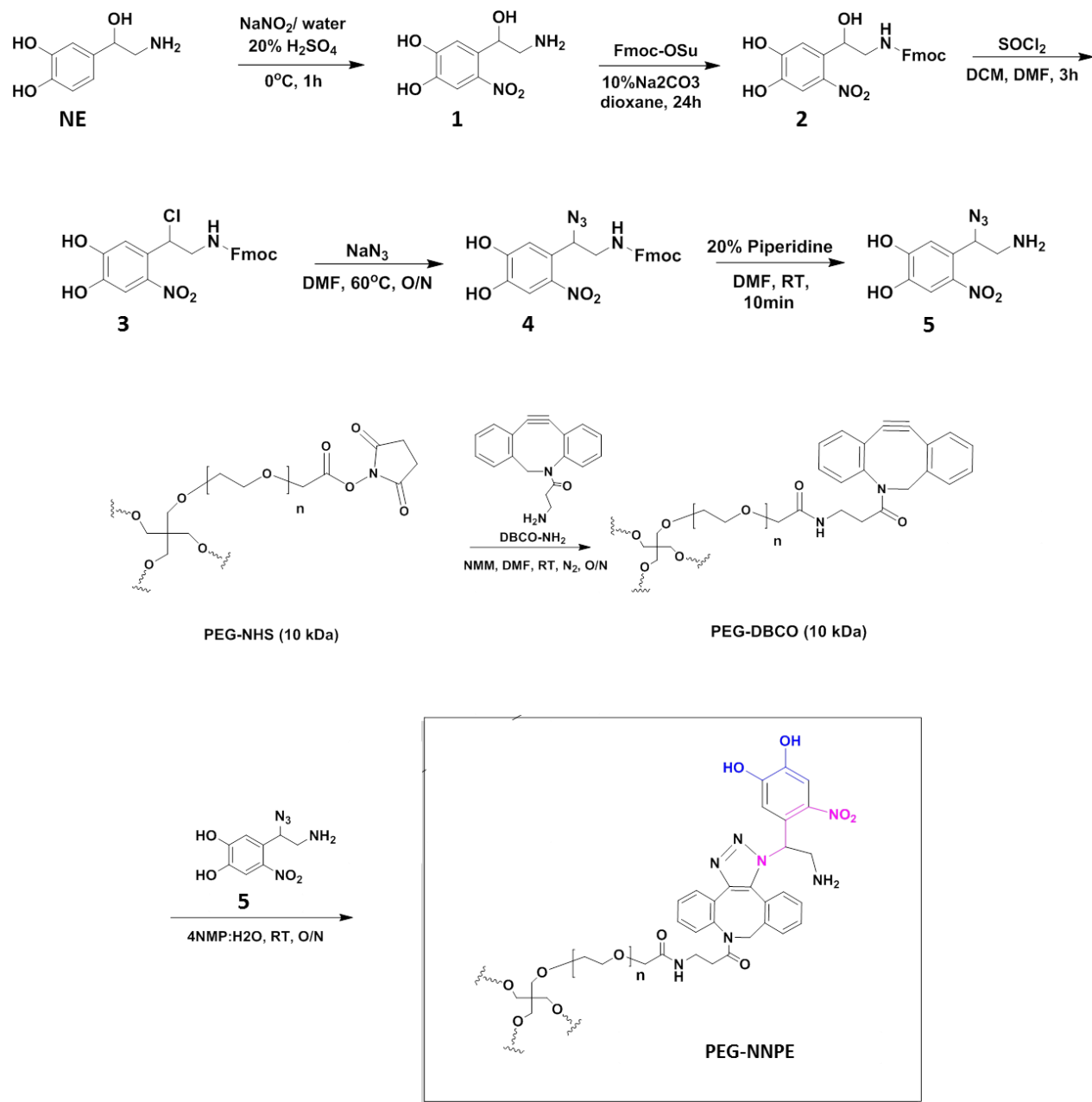
PEG-NHS (200 mg, 0.020 mmol polymer, 0.08 mmol succinimide ester groups, 1 equiv.) was dissolved in DMF (2 mL). Separately, DBCO-NH₂ (33 mg, 0.12 mmol, 6 equiv.) was dissolved in DMF (2 mL) and added to PEG-NHS solution followed by NMM (22 μL , 0.2 mmol, 10 equiv.) under N₂ atmosphere. The reaction was stirred at room temperature, under Ar atmosphere

overnight. The yellow solution was purified by dialysis against MeOH and MeOH-H₂O for 24 h, filtered and evaporated in rotavap, then dissolved in H₂O and freeze dried. An off-white product was obtained (yield= 87%), which was characterized by ¹H-NMR. Integration of signals corresponding to DBCO vs PEG-core gave around 88% of functionalization degree.

¹H-NMR (300 MHz, DCM, δ): 7.49-7.28(m, 8H, DBCO), 7.06 (bs, 1H, NHCH₂), 5.16-5.11 (d, 1H, CH₂NC₀), 4.07 (s, 1H, CH₂CONH), 3.63 (bs, 4H, O(CH₂CH₂O)_n), 2.53-2.44 (m, 2H, NHCH₂CH₂DBCO), 2.03-1.94 (m, 2H, NHCH₂CH₂DBCO).



2.2 Synthesis of photodegradable polymer PEG-NNPE macromere



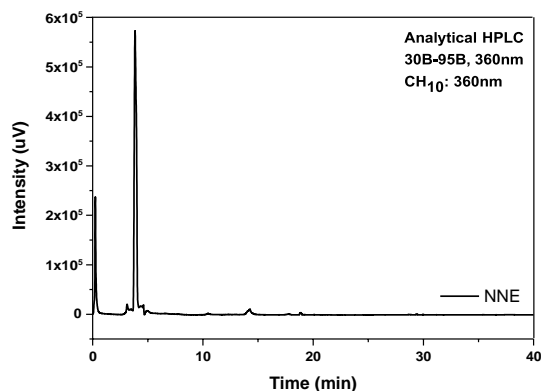
Synthesis of 4-(2-amino-1-hydroxyethyl)-5-nitrobenzene-1,2-diol (**1**)

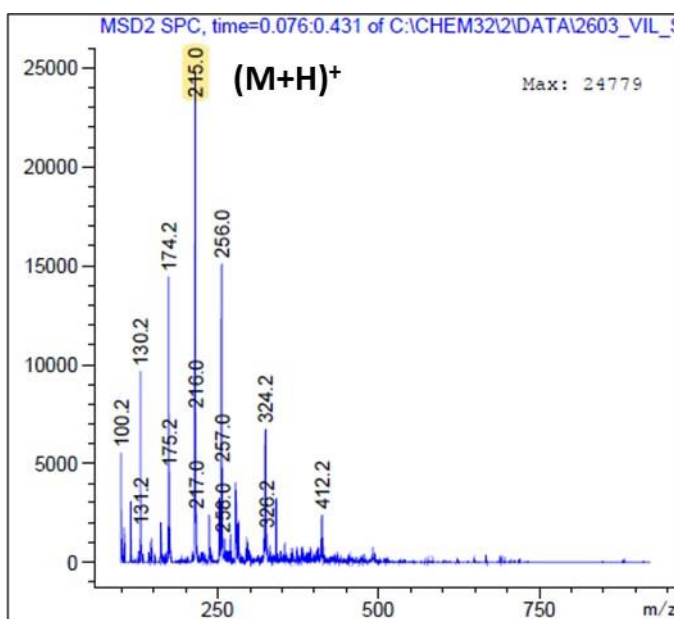
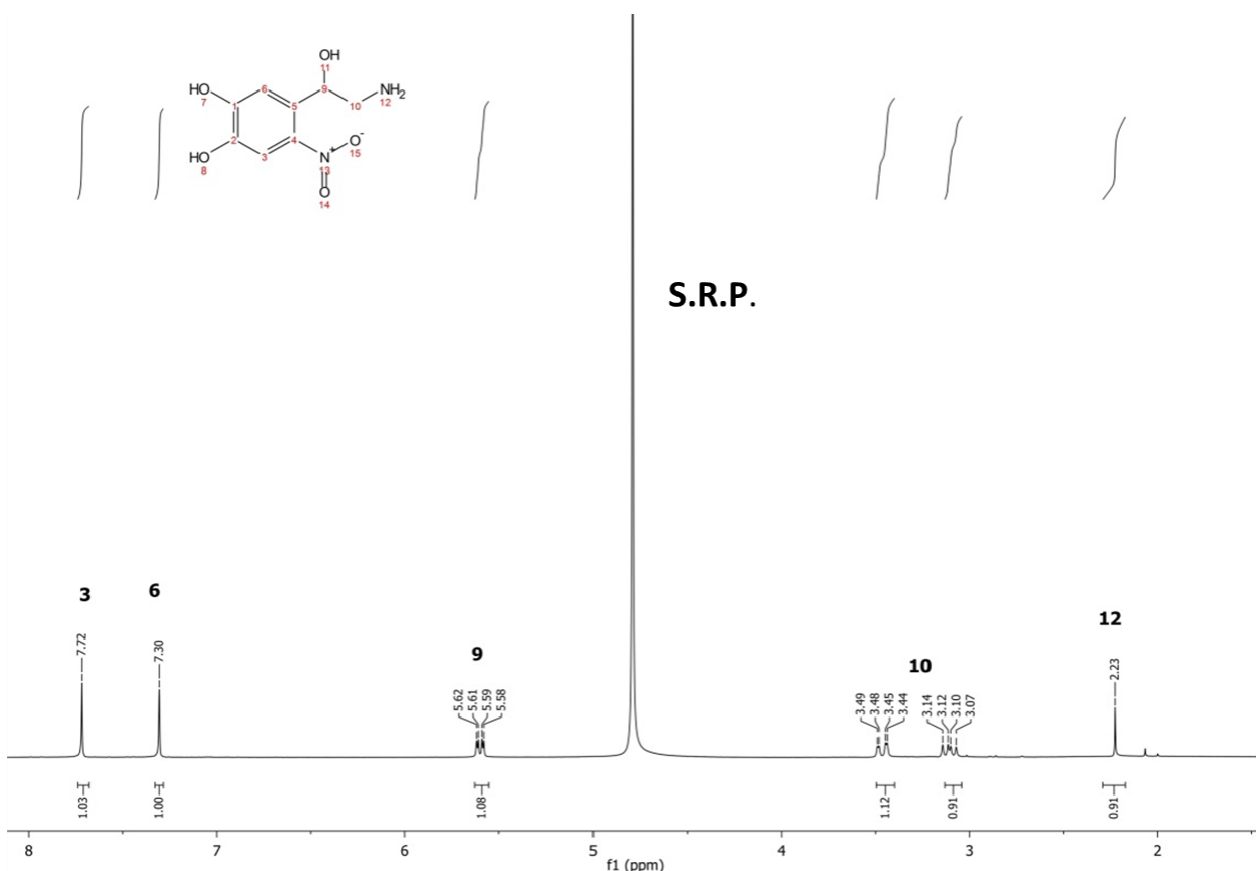
A general procedure reported for nitration of catecholic compounds was followed.^{1, 3} NE (1 g, 5.91 mmol, 1 equiv.) was dissolved in H₂O (30 mL) and 3-5 drops of HCl were added to ensure complete solubilization of the compound. To this solution, NaNO₂ (1.25 g, 18 mmol, 3 equiv.) was added as solid, the system was purged with N₂ and cooled down to 0°C with an ice

bath. 20 % v/v H₂SO₄ solution in H₂O (5 mL) was added carefully and the mixture was stirred at 0°C for 80 min. The reaction crude was neutralized until pH 5-6 by adding NaHCO₃. The completion of the reaction was monitored by TLC (35%Hex: 65% EtOAc), and HPLC (method: 30 %B- 95 %B 360 nm, retention time = 4 min). After neutralization, the supernatant was freeze-dried and full conversion was proven by ¹H-NMR. The product obtained was directly used for the next reaction.

ESI-MS⁺: 215.0 (M+H)⁺.

¹H-NMR (300 MHz, D₂O, δ): 7.72 (s, 1H, Aromatic-H), 7.30 (s, 1H, Aromatic-H), 5.62-5.58 (q, 1H, Ar-CH₂-OH), 3.49-3.44 (q, 1H, NH₂CH₂), 3.14-3.05 (q, 1H, NH₂CH₂), 2.23 (s, 2H, NH₂).



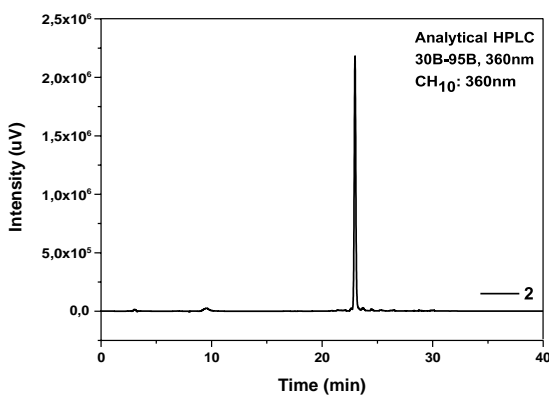


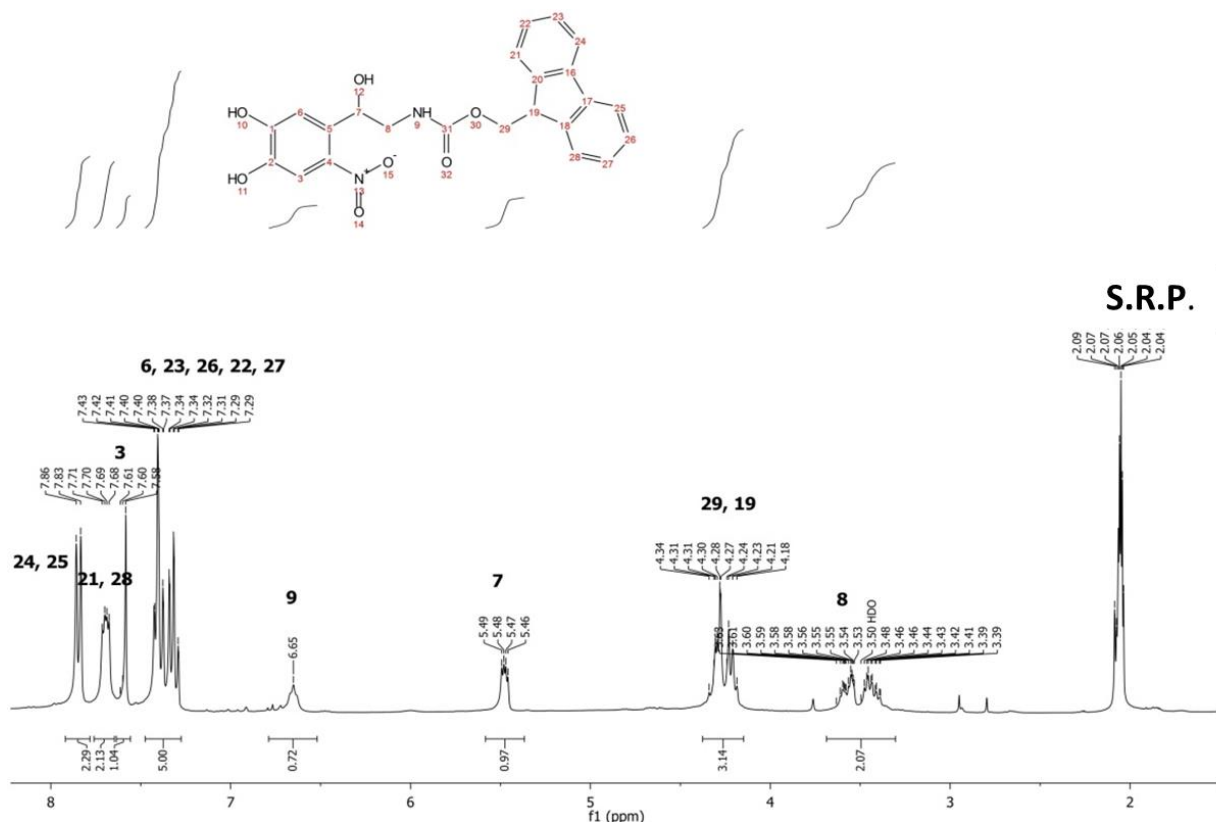
Synthesis of (9H-fluoren-9-yl)methyl (2-(4,5-dihydroxy-2-nitrophenyl)-2-hydroxyethyl)carbamate (2)

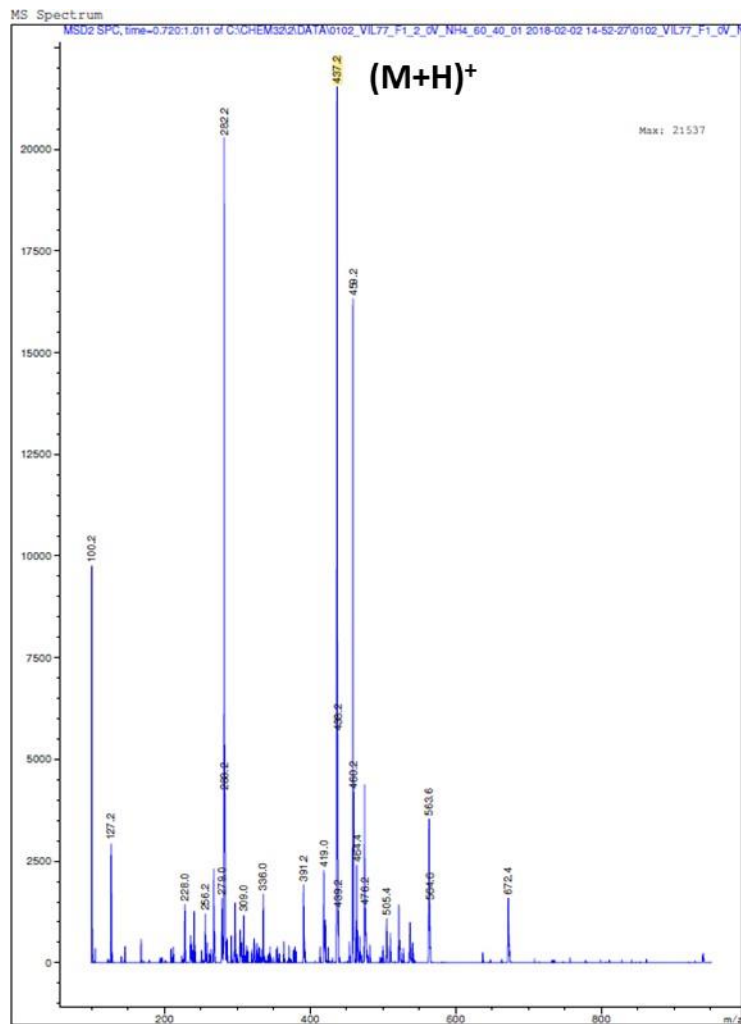
A procedure from Carpino et al was followed.⁴ **1** (ca 1 g, 5.91 mmol, 1 equiv.) obtained in the previous step was dissolved in 10 % Na₂CO₃ solution in H₂O: 1,4-dioxane (20 mL), purged with N₂ and cooled down to 0°C with ice bath. Separately, Fmoc-Osu was dissolved in 10% Na₂CO₃ solution in H₂O: dioxane (10 mL) and purged with N₂ and carefully added to the first solution. The mixture was stirred for 4 h at 0°C and then for 24 h at room temperature. The crude was extracted with diethylether three times and partitioned twice between EtOAc and water; the combined organic layers washed three times with water and brine and dried over MgSO₄, evaporated and checked by TLC at 20 %Hex: 80 % EtOAc. The crude product was purified by silica gel column chromatography (65 % EtOAc: 35 %Hex). The product was obtained with 40 % yield (815 mg) and characterized by HPLC (method: 30 %B- 95 %B 360 nm, retention time = 23- 24 min), and ¹H-NMR.

ESI-MS⁺: 437.2 (M+H)⁺.

¹H-NMR (300 MHz, C₃D₆O-d6, δ): 7.85-7.83 (m, 2H, Fmoc), 7.71-7.68 (m, 2H, Fmoc), 7.58 (s, 1H, Aromatic-H), 7.43-7.29 (m, 5H, Fmoc & Aromatic-H), 6.65 (bs, 1H, NH), 5.49-5.46 (q, 1H, Ar-CH-OH), 4.31-4.18 (m, 3H, NHOCH₂CH) 3.61-3.53 (m, 1H, NH₂CH₂), 3.48-3.39 (m, 1H, NH₂CH₂).



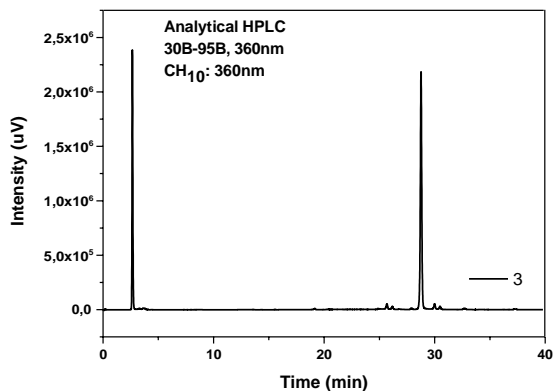
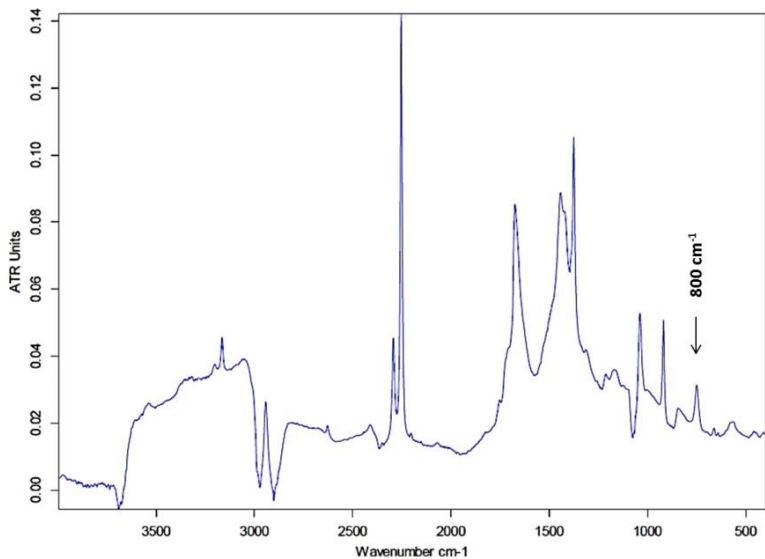




Synthesis of (9H-fluoren-9-yl)methyl (2-chloro-2-(4,5-dihydroxy-2-nitrophenyl)ethyl)carbamate (3)

2 (30 mg, 69 µmol, 1 equiv.) was dissolved in dry DCM (6 mL) purged with N₂ and 2-3 drops of dry DMF were added as catalyst. The mixture was cooled down to 0°C and SOCl₂ (1 mL) was carefully added against N₂ dropwisely and the mixture was stirred at 0°C for 4h. The course of the reaction was monitored by HPLC (method: 30 %B- 95 %B 360 nm, retention time 28 min). The solvent was evaporated under stream of N₂. Due to its high sensitivity, the product was used directly for the next reaction.

FT-IR: $\nu = 800 \text{ cm}^{-1}$ (Cl-C bond stretching).



Synthesis of (9H-fluoren-9-yl)methyl (2-azido-2-(4,5-dihydroxy-2-nitrophenyl)ethyl)carbamate (**4**)

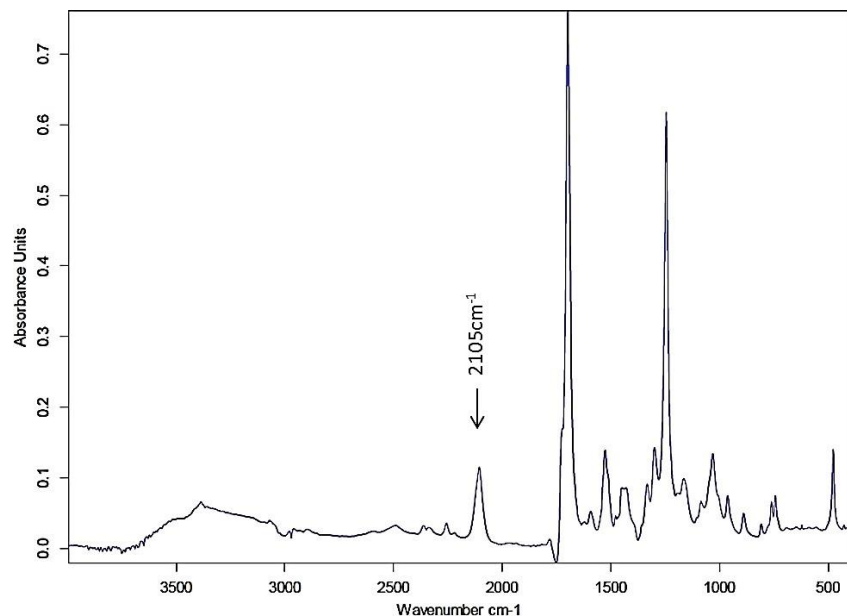
Freshly prepared compound **3** obtained in the previous step (ca 31 mg, 69 µmol, 1 equiv.) was dissolved in dry DMF (5 mL) and purged with N₂. NaN₃ (20 mg, 137 µmol, 2 equiv.) was added as solid and purged with N₂ for 5 min. The mixture was stirred at 60°C overnight. The reaction was quenched with HCl (5 %, 0.2 mL). The crude was partitioned three times between EtOAc and water, the combined organic layers washed three times with water and brine, dried over

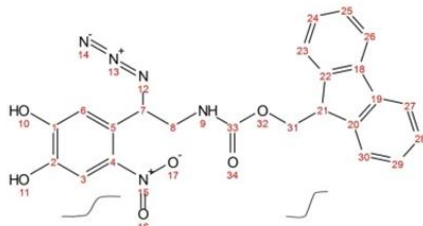
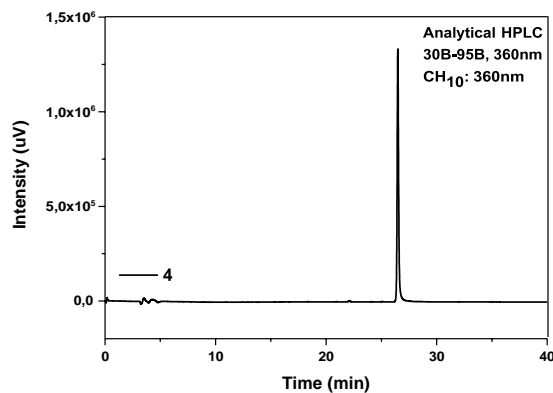
MgSO₄, evaporated and purified by preparative HPLC (30 %B- 95 %B 365 nm, retention time 26-27 min). The pure product was obtained as a yellow solid with 70 % yield (22 mg).

FT-IR: $\nu = 2105\text{cm}^{-1}$ (azide stretching).

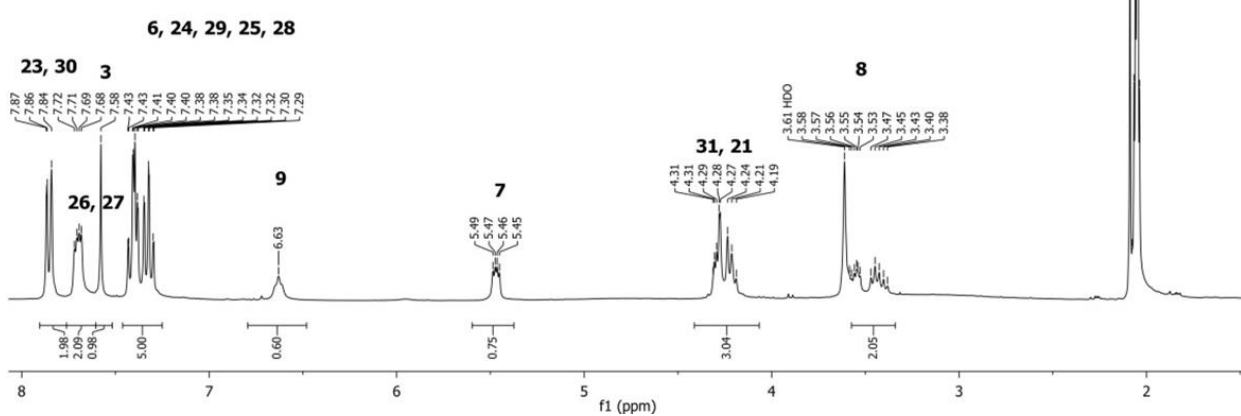
ESI-MS⁺: 462.2 ($\text{M}+\text{H}$)⁺, 479.2 ($\text{M}+\text{NH}_4$)⁺.

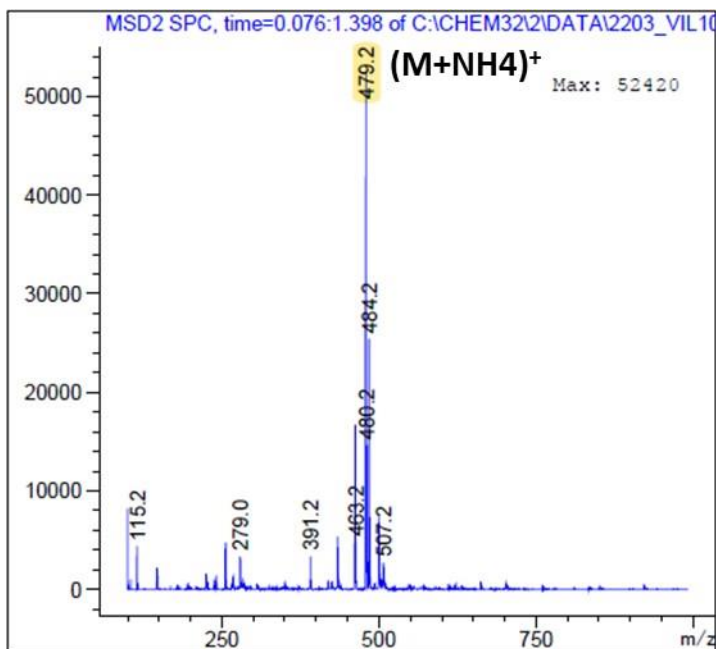
¹H-NMR (300 MHz, C₃D₆O-d6, δ): 7.87-7.84 (m, 2H, Fmoc), 7.72-7.68 (m, 2H, Fmoc), 7.58 (s, 1H, Aromatic-H), 7.43-7.29 (m, 5H, Fmoc & Aromatic-H), 6.63 (bs, 1H, NH), 5.49-5.45 (q, 1H, Ar-CH-N₃), 4.31-4.19 (m, 3H, NHOCH₂CH) 3.59-3.54 (m, 1H, NH₂CH₂), 3.53-3.38 (m, 1H, NH₂CH₂).





S.R.P.





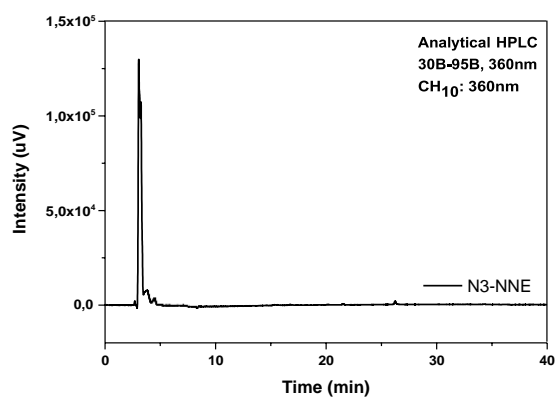
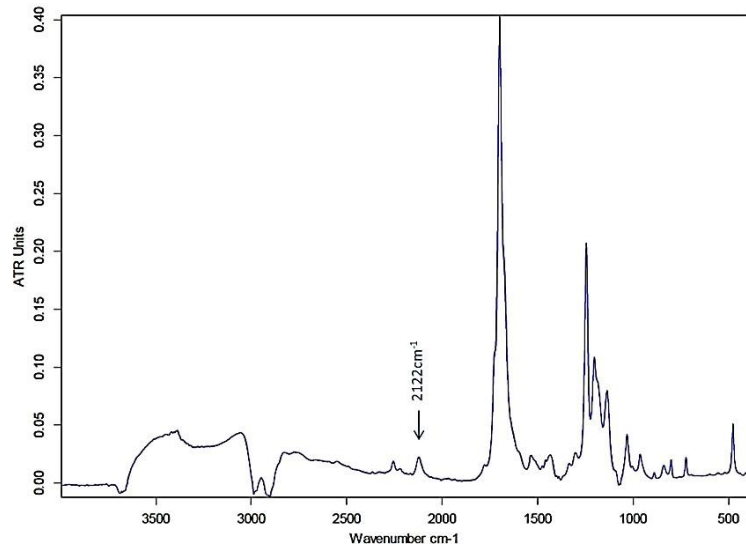
Synthesis of 4-(2-amino-1-azidoethyl)-5-nitrobenzene-1,2-diol (**5**)

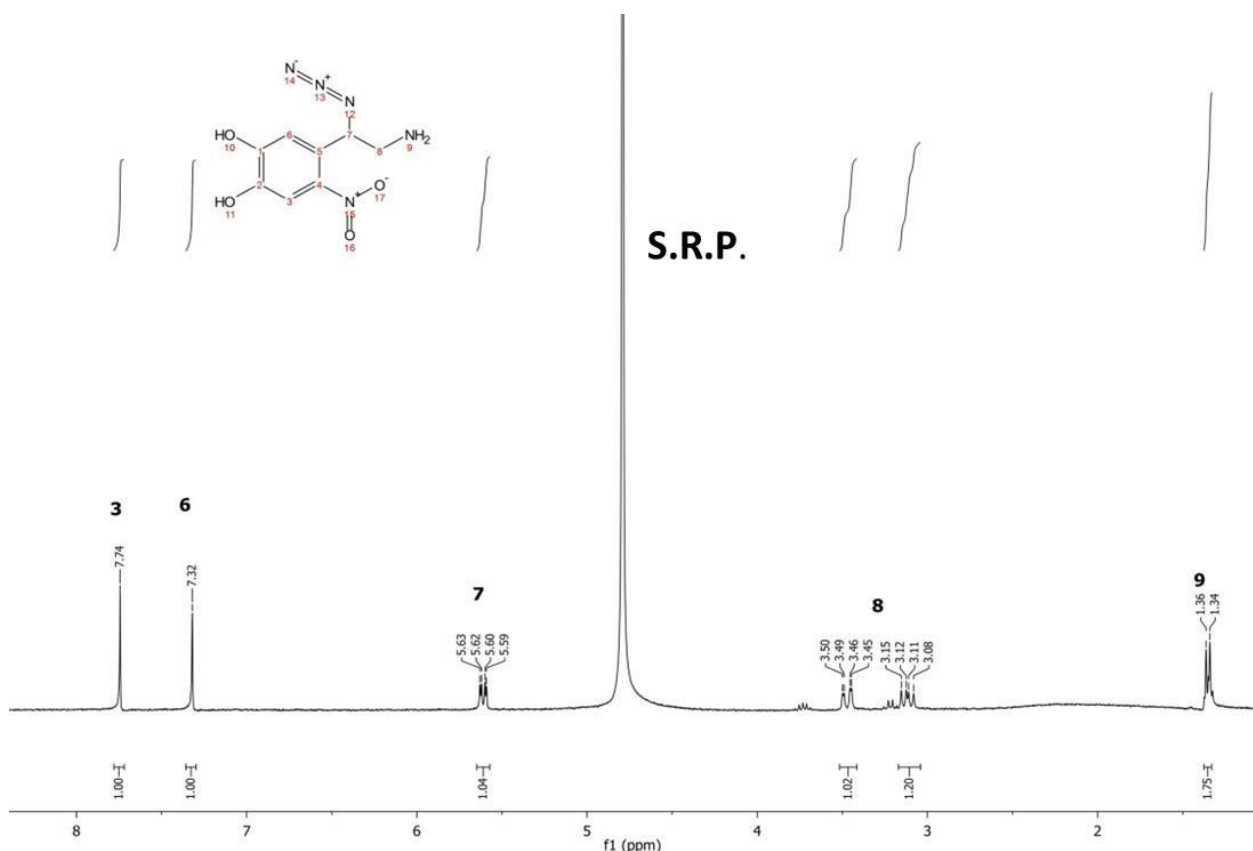
Compound **4** (28 mg, 0.11mmol, 1 equiv.) was dissolved in dry DMF (800 uL) and purged with N₂. Piperidine (200 uL, 0.172 mg, 0.002 mmol, 0.02 equiv.) was added and the color of the solution changed from yellow to orange. The deprotection took place for 10 min, as judged from analytic HPLC (30 %B- 95 %B 360 nm, retention time = 3-4 min). The crude product was purified by preparative HPLC (30 %B- 95 %B 360 nm) and obtained as a yellow solid with 65 % yield (10 mg).

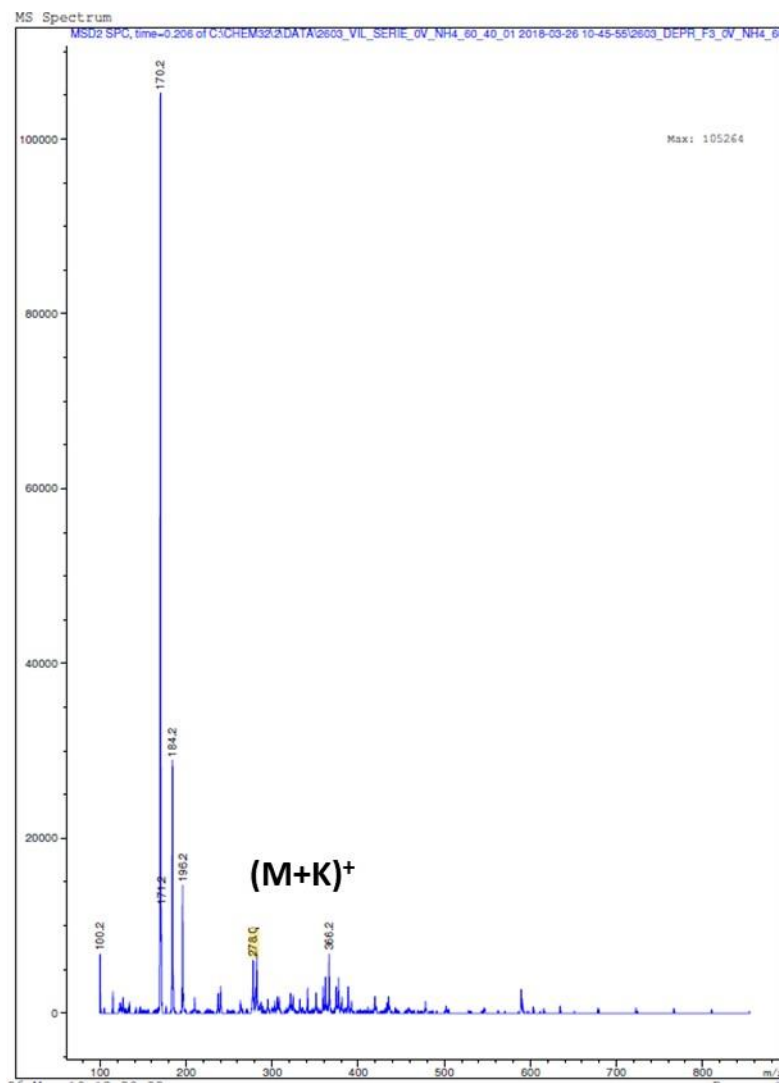
FT-IR: ν = 2122 cm⁻¹ (azide stretching).

ESI-MS⁺: 278.0 (M+K)⁺.

¹H-NMR (300 MHz, D₂O, δ): 7.74 (s, 1H, Aromatic-H), 7.32 (s, 1H, Aromatic-H), 5.63-5.59 (q, 1H, Ar-CH-OH), 3.50-3.45 (q, 1H, NH₂CH₂), 3.15-3.08 (q, 1H, NH₂CH₂), 1.36-1.34 (m, 2H, NH₂).



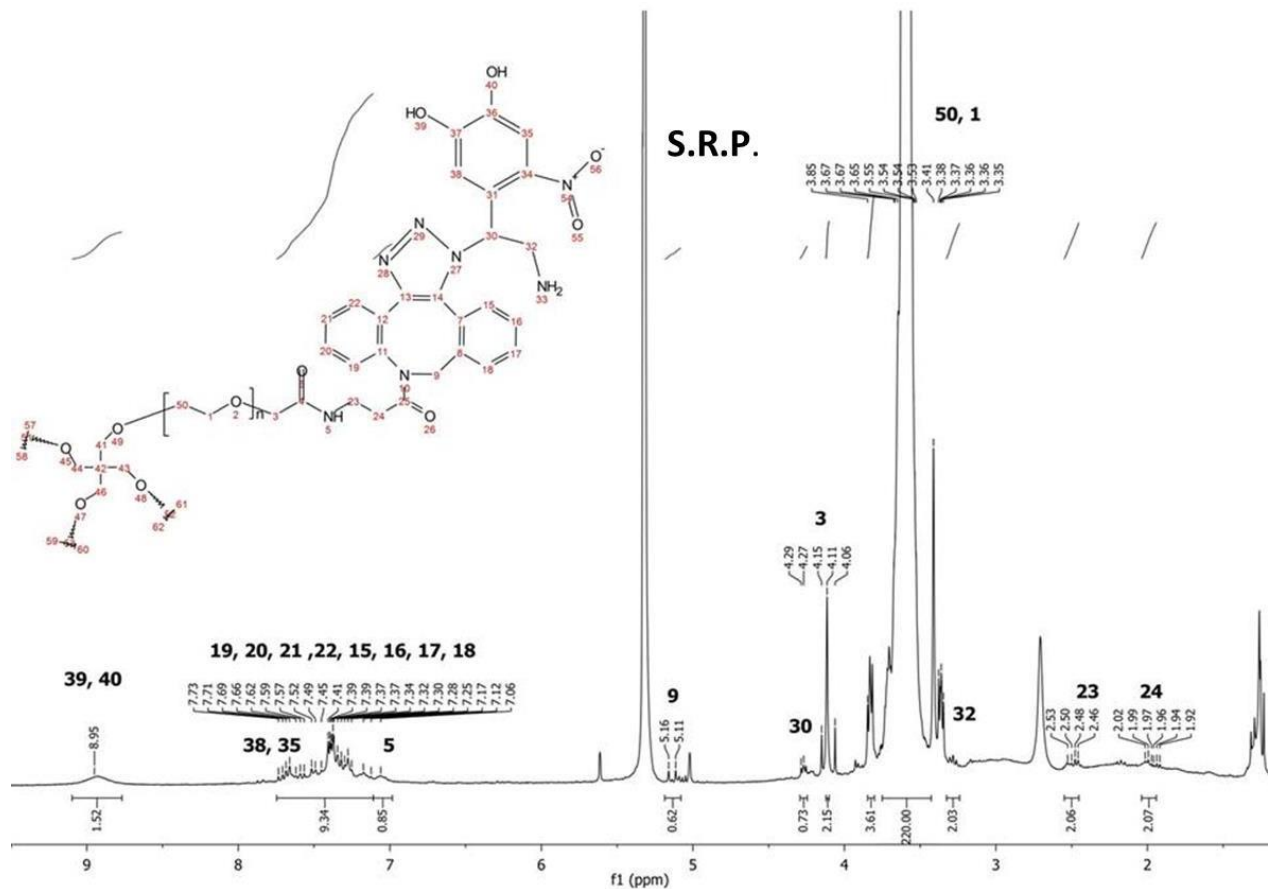




Synthesis of PEG-NNPE

Compound **5** (6.6 mg, 0.005 mmol, 6 equiv.) was dissolved in 4:1 NMP:H₂O (2 mL). Separately, PEG-DBCO (35 mg, 0.03 mmol, 1 equiv.) was dissolved in 4:1 NMP:H₂O (2 mL) and added to the prior solution, purged with N₂ for 15 min and the mixture was stirred under N₂ atmosphere, overnight. The crude was purified by dialysis against MeOH and MeOH-H₂O for 24 h twice, evaporated in rotavap, dissolved in H₂O and freeze dried. White-yellowish product was obtained (yield = 85%, 30 mg), which was characterized by ¹H-NMR. Substitution degree was > 84% as calculated via ¹H-NMR.

¹H-NMR (300 MHz, DCM, δ): 8.95 (bs, 2H, -OH), 7.73-7.12(m, 10H, DBCO, C₂H₂C₂(OH)₂), 7.06 (bs, 1H, NHCH₂), 5.16-5.11 (CH₂NC0), 4.29-4.27 (m, 1H, CHCH₂NH₂), 4.11 (s, 1H, CH₂C0NH), 3.54 (bs, 4H, O(CH₂CH₂O)_n), 3.37-3.35 (m, 2H, CHCH₂NH₂), 2.53-2.46 (m, 2H, NHCH₂CH₂DBCO), 2.02-1.92 (m, 2H, NHCH₂CH₂DBCO).



2.3 Synthesis of photodegradable polymer PEG-NBt-c macromer

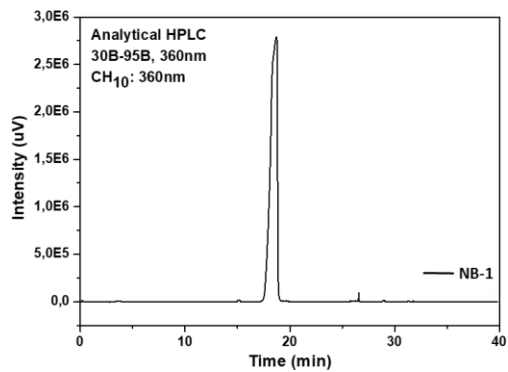
Synthesis of tert-butyl (2-(4-(1-hydroxyethyl)-2-methoxy-5-nitrophenoxy)-butanamido)ethyl carbamate (NB-1)

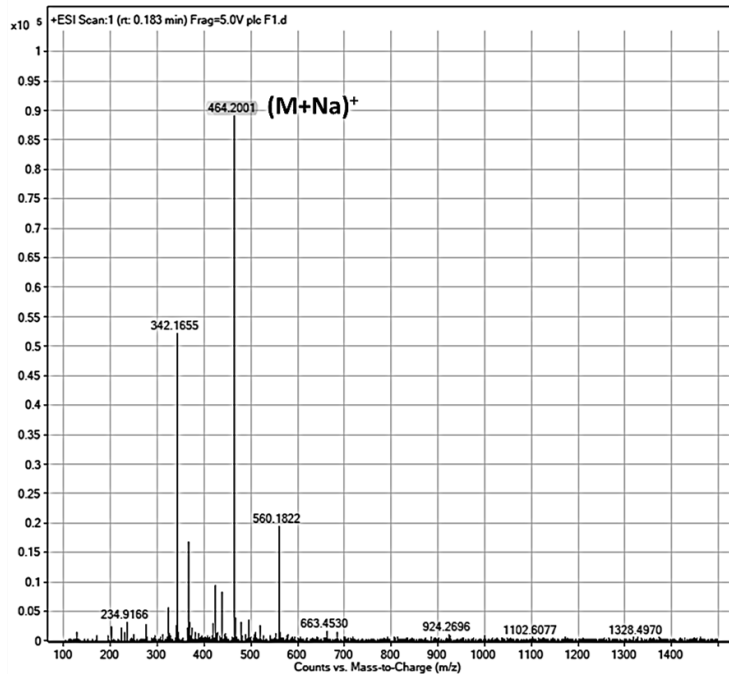
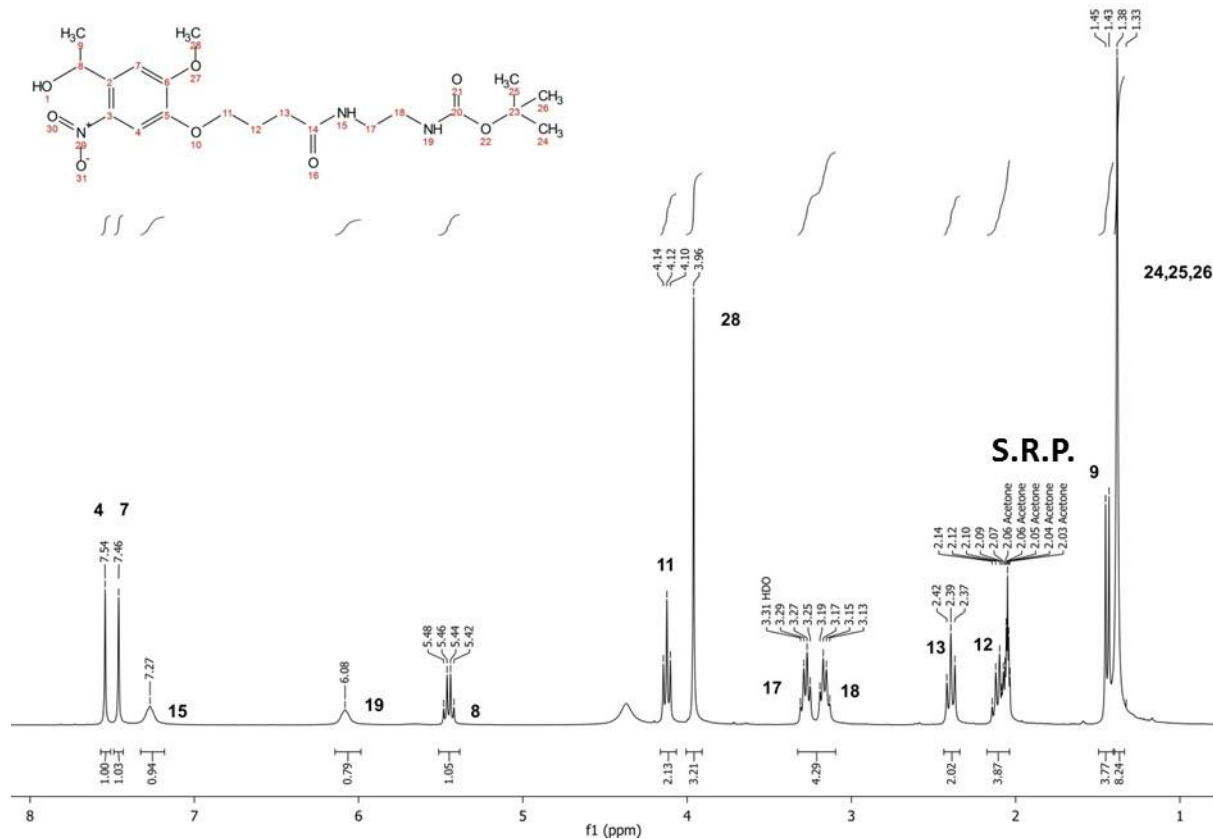
HOBt (150 mg, 1.1 mmol, 1.1 equiv.), HBTU (417 mg, 1.1 mmol, 1.1 equiv.) and DIPEA (0.5 mL, 3 mmol, 3 equiv.) were dissolved in dry DMF (5.0 mL) and then NB (300 mg, 1 mmol, 1 equiv.) was added. Then, N-Boc-ethylendiamine (190 mg, 1.2 mmol, 1.2 equiv) was added. The solution was stirred for 6 h at room temperature, followed by quenching with water and extraction with EtOAc, twice. The combined organic layers were washed 3 times with brine and dried over MgSO₄. The crude product was purified by HPLC (method: 30 %B- 95 %B, $\lambda_{\text{det}} = 360$ nm,

retention time= 16-18 min), evaporated, and freeze-dried. A yellow product was obtained (274 mg) with 62 % yield.

ESI-MS⁺: 464.2 (M+Na)⁺.

¹H-NMR (300 MHz, acetone-d₆, δ): 7.54-7.45 (m, 2H, aromatic-H), 7.27 (bs, 1H, NHCH₂CH₂NHBoc), 6.08 (bs, 1H, NH_{Boc}), 5.48-5.42 (q, 1H, Ar-CH-OH), 4.14-4.10 (t, 2H, CH₂O-Ar), 3.95 (s, 3H, Ar-O-CH₃), 3.31-3.25 (m, 2H, NHCH₂CH₂NHBoc), 3.19-3.13 (m, 2H, CH₂NHBoc), 2.42-2.37 (t, 2H, CH₂CONH), 2.14-2.07 (m, 2H, CH₂CH₂CH₂CONH), 1.45-1.43 (d, J= 6Hz, 3H, CH₃CH-OH), 1.38 (s, 9H, Boc).



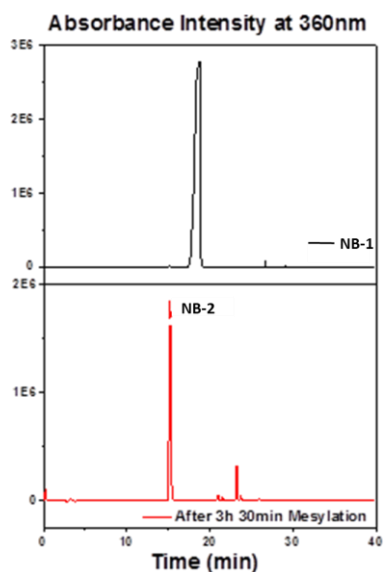


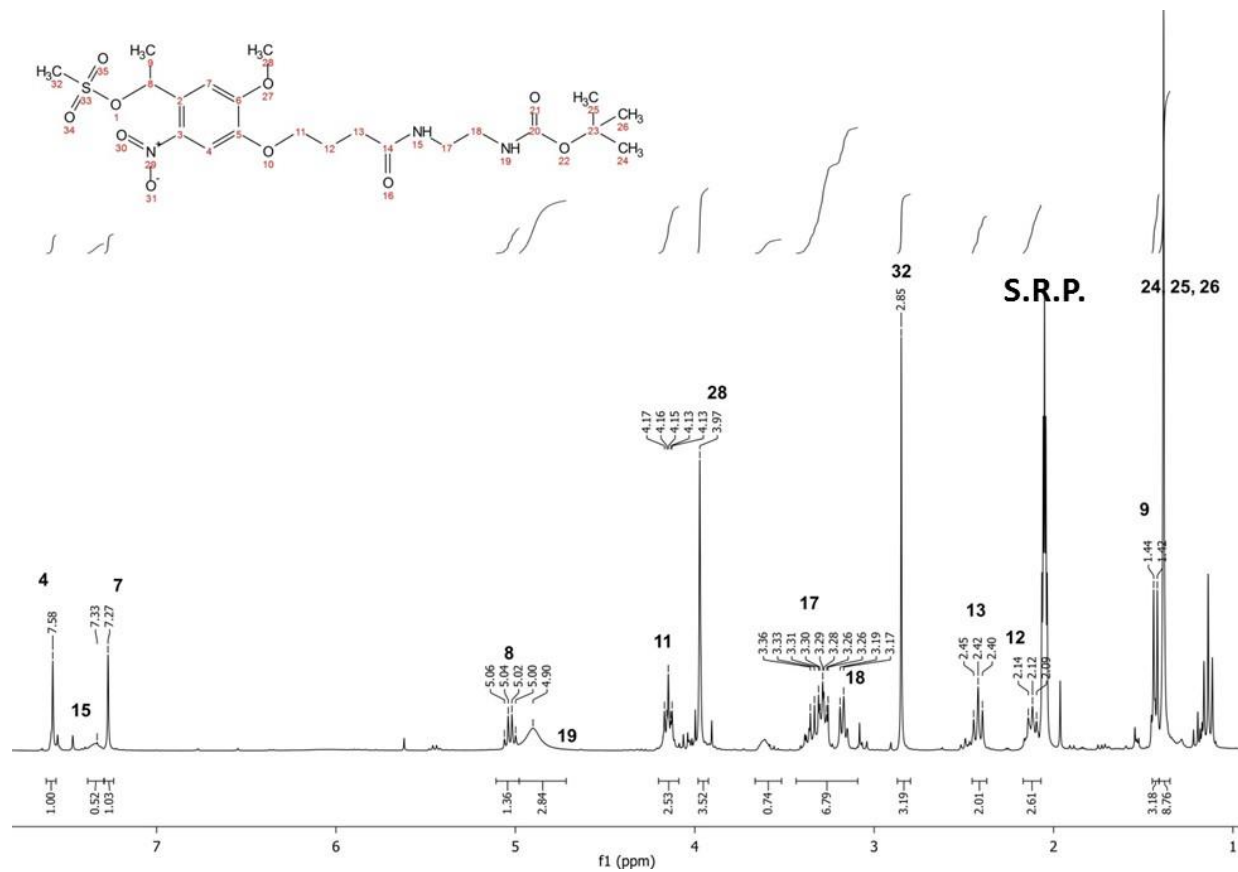
Synthesis of 1-(4-((2-((tert-butoxycarbonyl)amino)ethyl)amino)-4-oxobutoxy)-5-methoxy-2-nitrophenyl)ethyl methanesulfonate (NB-2)

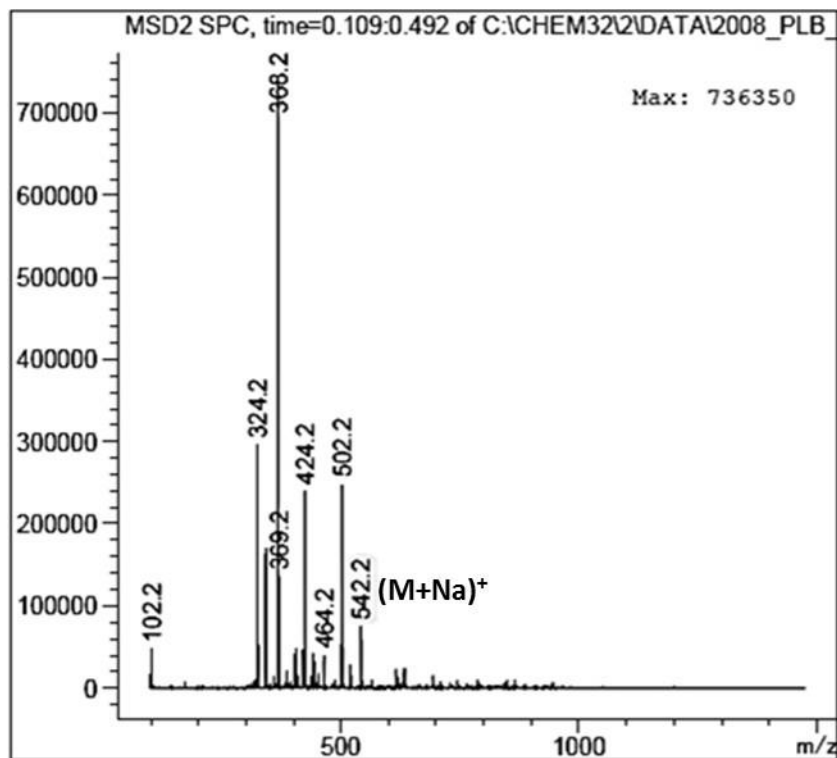
Compound **NB-1** (100 mg, 0.23 mmol, 1 equiv.) was dissolved in dry DCM (5 mL) and cooled down to 0°C with ice bath. Under N₂ atmosphere, TEA (96 µL, 0.69 mmol, 3 equiv.) was added followed by Ms-Cl (27 µL, 0.34 mmol, 1.5 equiv.) dropwise. The reaction was stirred at room temperature and completion was followed by TLC and analytical HPLC (method: 30 %B- 95 %B, $\lambda_{\text{det}} = 360$ nm), observing complete consumption of starting material after 3 h. The crude was partitioned twice between EtOAc and water; the combined organic layers were washed 3 times with water and brine and dried over MgSO₄. The product was characterized by ¹H-NMR (conversion was calculated to be 97%) and used immediately for next reaction without further purification.

ESI-MS⁺: 542.2 (M+Na)⁺.

¹H-NMR (300 MHz, acetone-d₆, δ): 7.58 (s, 1H, aromatic-H), 7.33 (bs, 1H, NHCH₂CH₂NHBoc), 7.27 (s, 1H, aromatic-H), 5.06-5.00 (q, 1H, Ar-CH-Ms), 4.90 (bs, 1H, NH₂Boc), 4.17-4.13 (t, 2H, CH₂O-Ar), 3.97 (s, 3H, Ar-O-CH₃), 3.36-3.28 (m, 2H, NHCH₂CH₂NHBoc), 3.26-3.17 (m, 2H, CH₂NHBoc), 2.85 (s, 3H, Ms) 2.45-2.40 (t, 2H, CH₂CONH), 2.14-2.09 (m, 2H, CH₂CH₂CH₂CONH), 1.44-1.42 (d, J= 6Hz, 3H, CH₃CH-Ms), 1.39 (s, 9H, Boc).







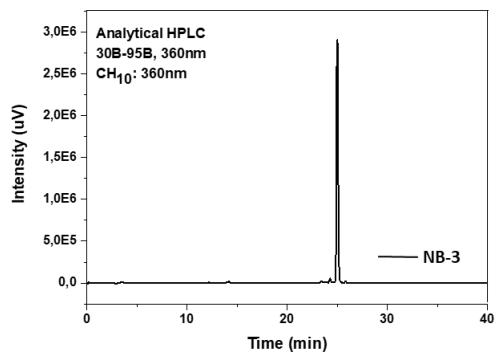
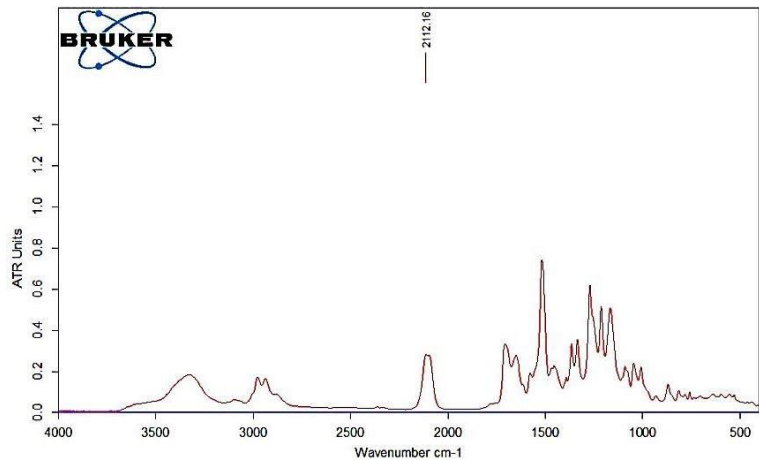
Synthesis of tert-butyl (2-(4-(4-(1-azidoethyl)-2-methoxy-5-nitrophenoxy)butanamido)-ethyl)carbamate (NB-3**)**

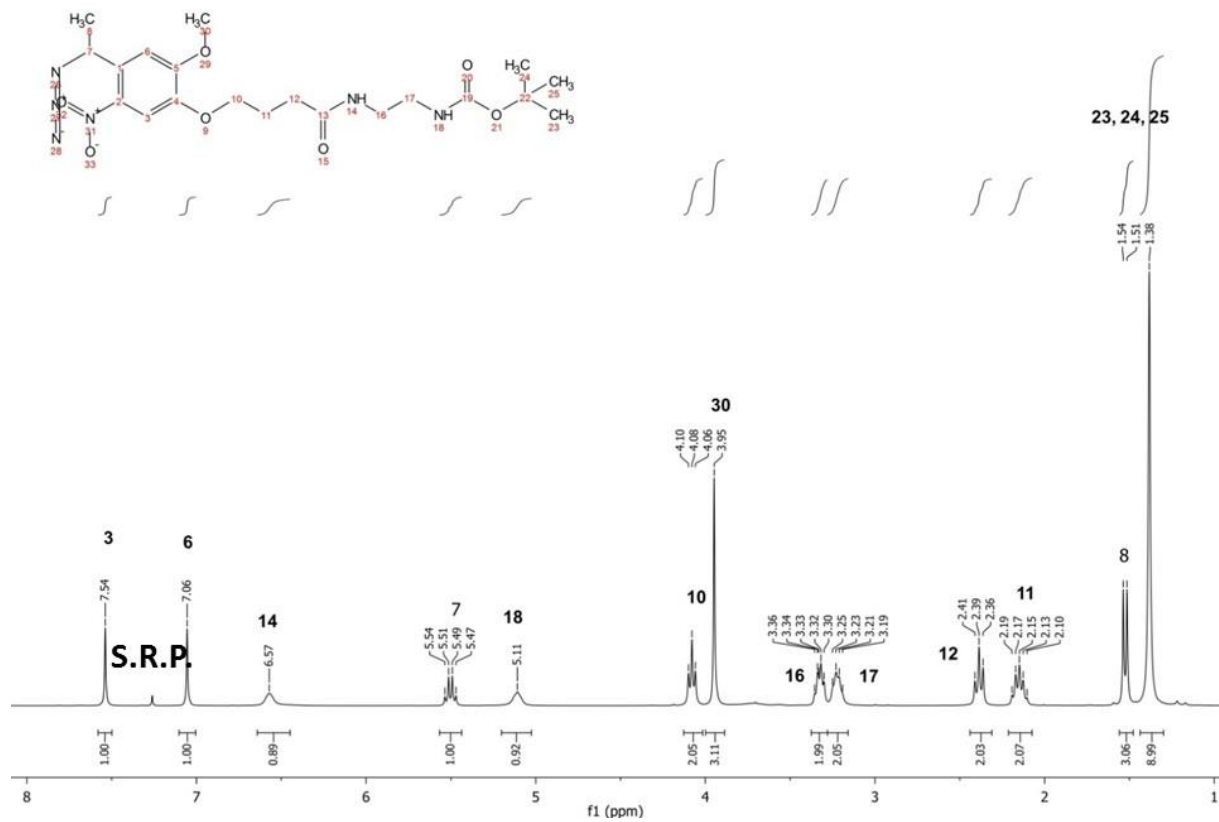
Freshly prepared compound **NB-2** (100 mg, 0.23 mmol, 1 equiv.) was dissolved in dry DMF (3 mL) in a flask and purged under N₂. Then, NaN₃ (29 mg, 0.46 mmol, 2 equiv.) was added at room temperature, and the reaction was heated overnight at 80°C. The crude was partitioned twice between EtOAc and water, the combined organic phase were washed three times with water and brine, dried over MgSO₄ and evaporated. The crude product (an orange viscous oil) was purified by RP-HPLC (30 %B- 95 %B, λ_{det} = 360 nm, retention time = 25 min), evaporated and freeze-dried. The pure yellow product was obtained with 47 % yield (46.6 mg).

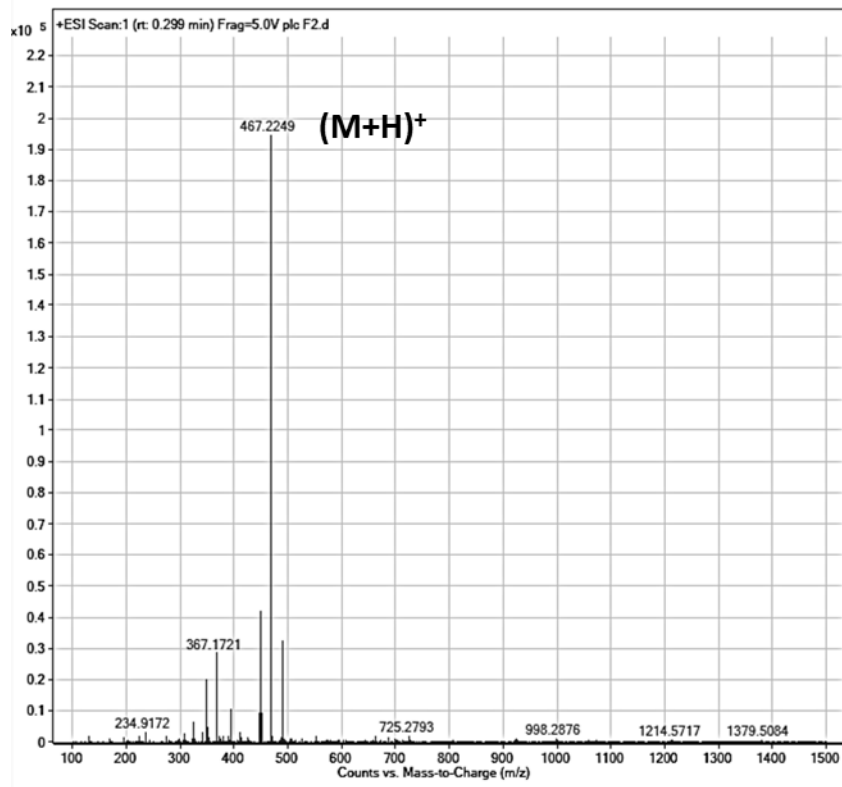
FT-IR: ν = 2112 cm⁻¹ (azide stretching)

ESI-MS⁺: 467.2 (M+H)⁺.

¹H-NMR (300 MHz, CDCl₃, δ): 7.54 (s, 1H, aromatic-H), 7.06 (s, 1H, aromatic-H), 6.57 (bs, 1H, NHCH₂CH₂NHBoc), 5.54-5.47 (q, 1H, Ar-CH-N₃), 5.11 (bs, 1H, NH₂Boc), 4.10-4.06 (t, 2H, CH₂-O-Ar), 3.95 (s, 3H, Ar-O-CH₃), 3.36-3.30 (m, 2H, NHCH₂CH₂NHBoc), 3.25-3.19 (m, 2H, CH₂NHBoc), 2.41-2.36 (t, 2H, CH₂CONH), 2.19-2.10 (m, 2H, CH₂CH₂CH₂CONH), 1.54-1.51 (d, J= 6Hz, 3H, CH₃CH-N₃), 1.38 (s, 9H, Boc).







General protocol for the synthesis of 4-arm PEG-NBt-c macromers

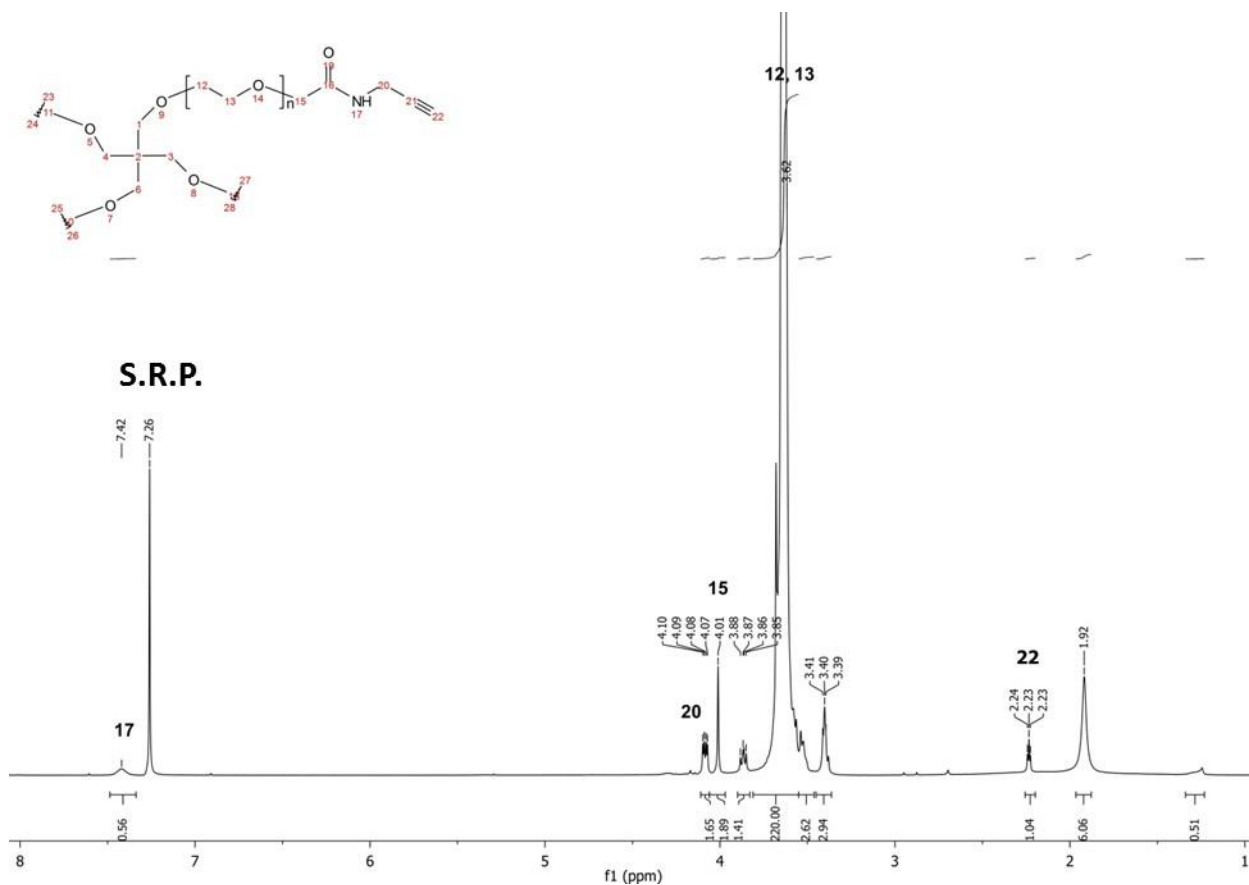
The polymers were synthesized by coupling the intermediate **NB-3** to a 4-arm PEG alkyne (10 or 20 kDa) via a copper-catalyzed azide-alkyne cycloaddition, followed by acidic Boc deprotection and coupling to the catechol compound. In the following sections, a typical procedure for polymer modification is described for a 10 kDa PEG polymer. Similar procedure was followed for preparation of the 20 kDa PEG.

Synthesis of PEG-alkyne

Propargylamine (255 μ L, 4 mmol, 10 equiv.) was dissolved in DMF (5 mL) and NMM (220 μ L, 2 mmol, 5 equiv.) was added. The mixture was stirred for 15 min under N_2 atmosphere. Then, PEG-NHS (1.0 g, 0.10 mmol polymer, 0.4 mmol succinimide ester groups, 1 equiv.) was added as solid in small portions, the solution was purged with N_2 , and left stirring overnight at room

temperature. The crude product was evaporated in rotavap to reduce solvent. The remaining solution (ca. 1.5 mL) was precipitated by dropping it into cold diethylether (50 mL at 0°C), the precipitate was isolated by centrifugation was redissolved in DCM (2 mL), and precipitated in cold diethylether again twice. The resulting product was dried under vacuum. An off-white to pale yellow solid was obtained (0.96 g, yield = 96%). The success of the polymer modification was confirmed by ¹H-NMR (substitution degree was > 90%).

¹H-NMR (300 MHz, CDCl₃, δ): 7.42 (bs, 1H, NHCH₂CH), 4.10-4.07 (q, 2H, NHCH₂CH), 4.01 (bs, 1H, CH₂NHC₀), 3.63 (bs, 4H, O(CH₂CH₂O)_n), 2.24-2.23 (t, 1H, NHCH₂CH).

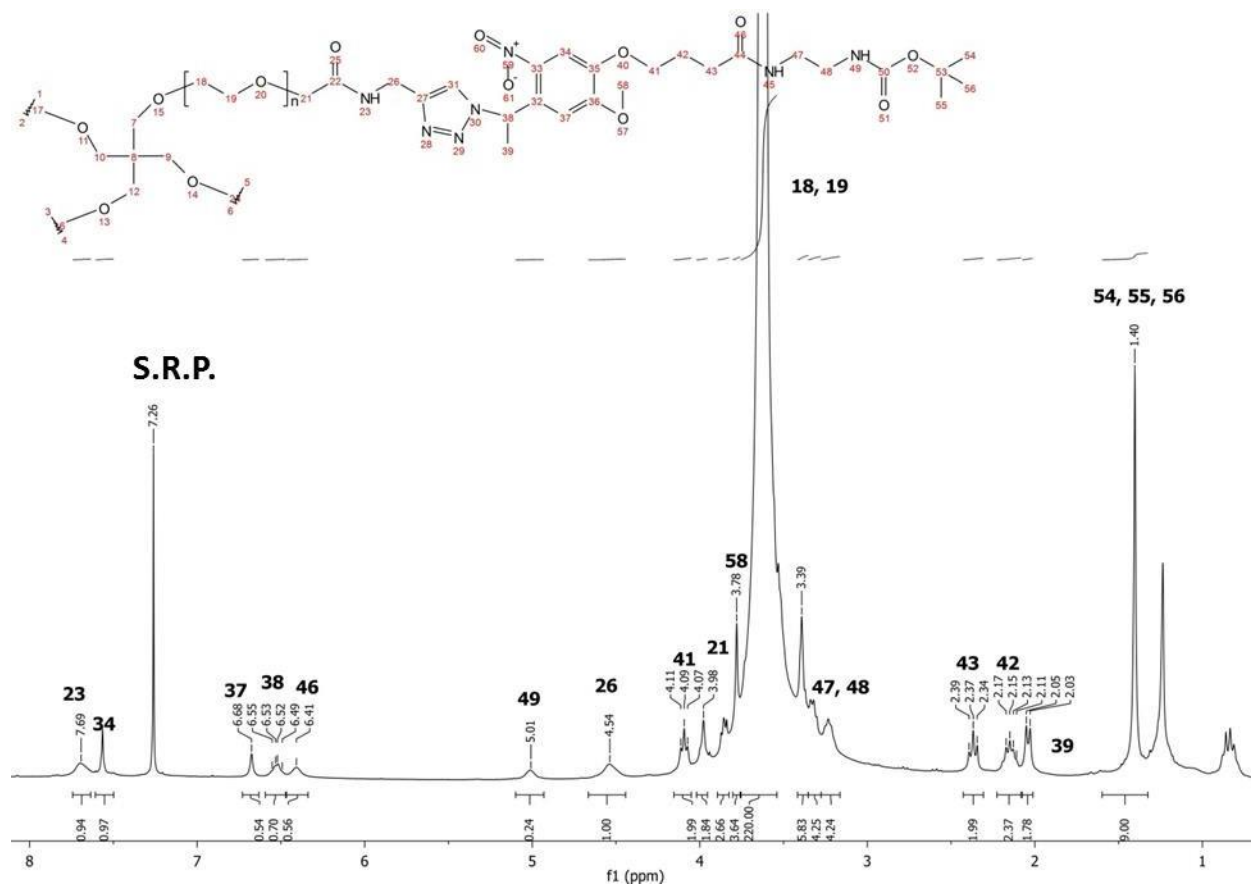


Synthesis of PEG-Nbt-Boc macromer

An adapted protocol reported by Nielsen *et al.*³ was used. CuI (210 mg, 1.12 mmol, 4 equiv.) sodium ascorbate (224 mg, 1.12 mmol, 4 equiv.) and of 2,6-lutidine (266 μL, 2.24 mmol, 8

equiv.) were mixed in NMP/H₂O (4:1) (22 mL) and shaken for 30 min before adding compound **NB-3** (385 mg, 0.84 mmol, 3 equiv.), followed by addition 10 kDa PEG-alkyne (696 mg, 0.07 mmol polymer, 0.28 mmol alkyne groups, 1 equiv.) as solid. The reaction mixture (a brownish-yellow solution with a grey-bluish precipitate) was shaken overnight at room temperature (a brownish suspension was obtained). The crude product was centrifuged twice in order to remove inorganics (grey-blueish solid) and the supernatant solution was purified by dialysis against acetone and water. An aqueous solution of EDTA (20 wt%) was used once during the dialysis in order to remove the inorganics. After dialysis, the solution was freeze-dried. A dark brown solid polymer was obtained (620 mg, yield = 89%). The success of the polymer modification was confirmed by ¹H-NMR (substitution degree was > 90%). The purified product was stored at -20°C and protected from light exposure until use.

¹H-NMR (300 MHz, CDCl₃, δ): 7.69 (bs, 1H, NHCH₂CH), 7.56 (s, 1H, aromatic-H), 6.68 (s, 1H, aromatic-H), 6.55-6.49 (q, 1H, Ar-CH-triazole), 6.41 (bs, 1H, NHCH₂CH₂NHBoc), 5.01(bs, 1H, NH_{Boc}), 4.54 (bs, 1H, CH₂NHCOC₂CH₂-PEG_{core}), 4.11-4.07 (t, 2H, CH₂-O-Ar), 3.98 (bs, 1H, COCH₂-PEG_{core}), 3.78 (s, 3H, Ar-O-CH₃), 3.62 (bs, 4H, O(CH₂CH₂O)_n), 3.37-3.30 (m, 2H, NHCH₂CH₂NHBoc), 3.25-3.22 (m, 2H, CH₂NHBoc), 2.39-2.34 (t, 2H, CH₂CONH), 2.17-2.11 (m, 2H, CH₂CH₂CH₂CONH), 2.05-2.03 (d, J= 6Hz, 3H, CH₃CH-triazole), 1.40 (s, 9H, Boc)

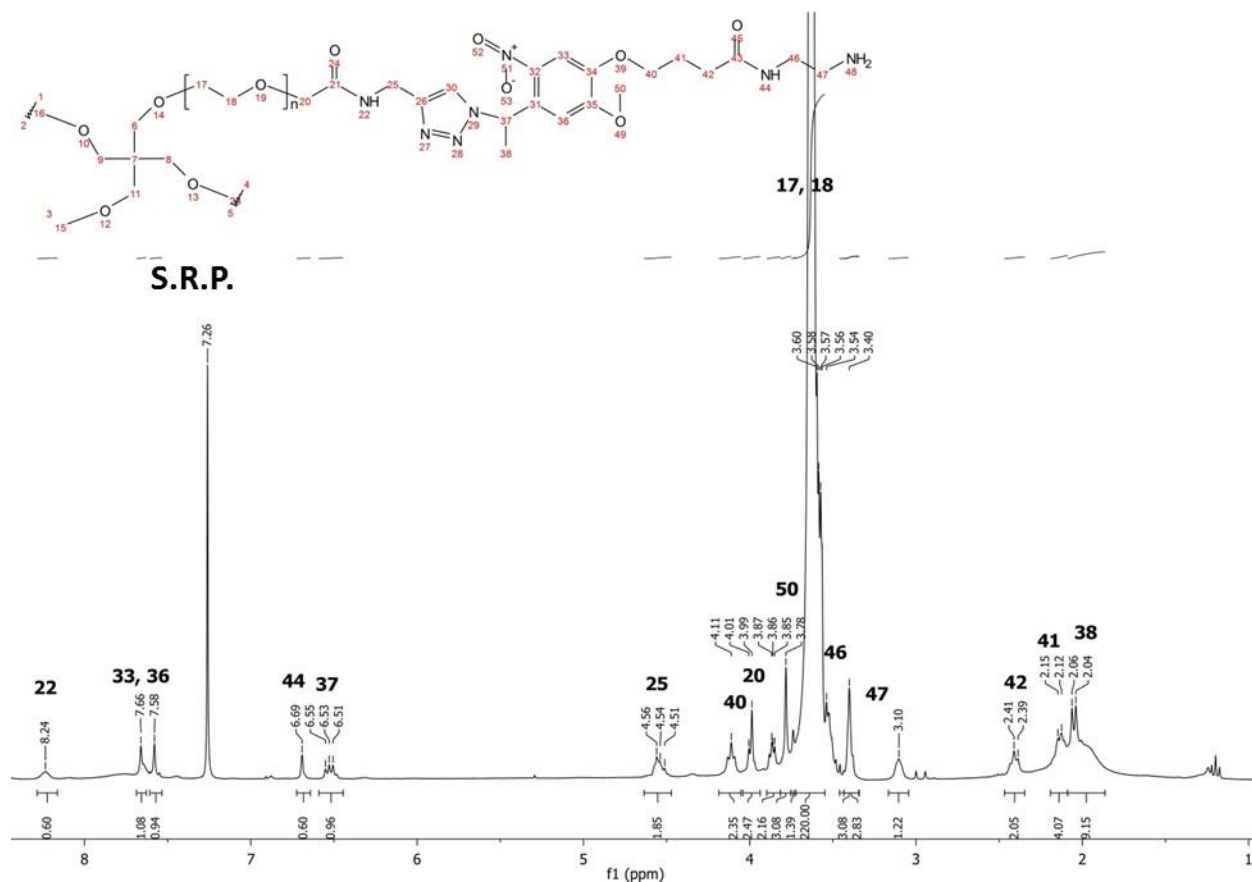


Synthesis of PEG-NBt-amine

10 kDa **PEG-NBt-Boc** (597 mg, 0.06 mmol polymer, 0.24 mmol Boc groups) was dissolved in TFA:water (95:5) (3 mL) and reacted for 1 h at room temperature. After reduction of solvent under N₂ stream, the crude product (ca 0.75 mL left) was precipitated twice in cold diethylether, isolated by centrifugation and dried under vacuum. The product was an off white- brownish solid (430 mg, yield = 72%) was characterized by ¹H-NMR showing complete Boc cleavage, indicated by the complete disappearance of the signal at 1.40 ppm (-tBu groups of Bocgroup).

¹H-NMR (300 MHz, CDCl₃, δ): 8.24 (bs, 1H, NHCH₂CH), 7.66-7.58 (m, 2H, aromatic-H), 6.69 (s, 1H, NHCH₂CH₂NH₂), 6.55-6.51 (q, 1H, Ar-CH-triazole), 4.54 (bs, 1H, CH₂NHCOC₂-PEG_{core}), 4.13-4.09 (t, 2H, CH₂-O-Ar), 4.01 (bs, 1H, COCH₂-PEG_{core}), 3.78 (s, 3H, Ar-O-CH₃), 3.63 (bs, 4H,

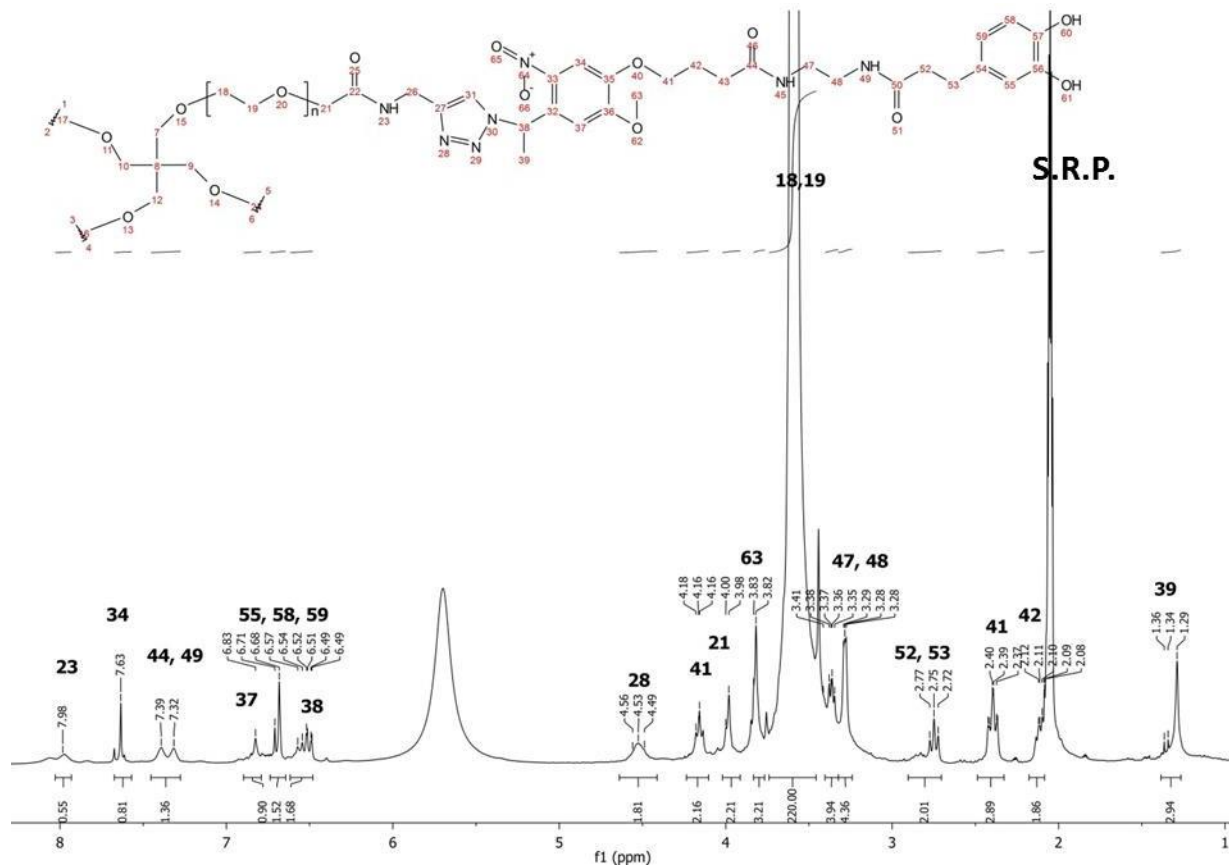
$\text{O}(\text{CH}_2\text{CH}_2\text{O})_n$, 3.54-3.47 (m, 2H, $\text{NHCH}_2\text{CH}_2\text{NH}_2$), 3.41-3.38 (m, 2H, CH_2NH_2), 2.40-2.39 (t, 2H, CH_2CONH), 2.14-2.13 (m, 2H, $\text{CH}_2\text{CH}_2\text{CH}_2\text{CONH}$), 2.06-2.0 (d, $J=6\text{Hz}$, 3H, CH_3CH -triazole).



Synthesis of PEG-NBt-c

10 kDa **PEG-NBt-amine** (410 mg, 0.04 mmol polymer, 0.16 mmol amine groups, 1 equiv.) was dissolved in dry DMF (3 mL) and purged with N_2 for 10 min. Separately, DHCA (120 mg, 0.64 mmol, 4 equiv.), HBTU (240 mg, 0.64 mmol, 4 equiv.), HOBT (88 mg, 0.64 mmol, 4 equiv.) and DIPEA (88 μL , 0.8 mmol, 5 equiv.) were dissolved in dry DMF (3 mL) and degassed for 5 min, and subsequently added to above PEG solution. The reaction mixture was stirred under N_2 at room temperature overnight, then precipitated in diethylether and isolated by centrifugation. The crude product was purified by dialysis against acetone and water. The obtained solution was freeze-dried. An off white-yellowish solid product (250 mg, yield= 61 %) was obtained, and the identity of the product was confirmed by $^1\text{H-NMR}$, showing a substitution degree >85 %.

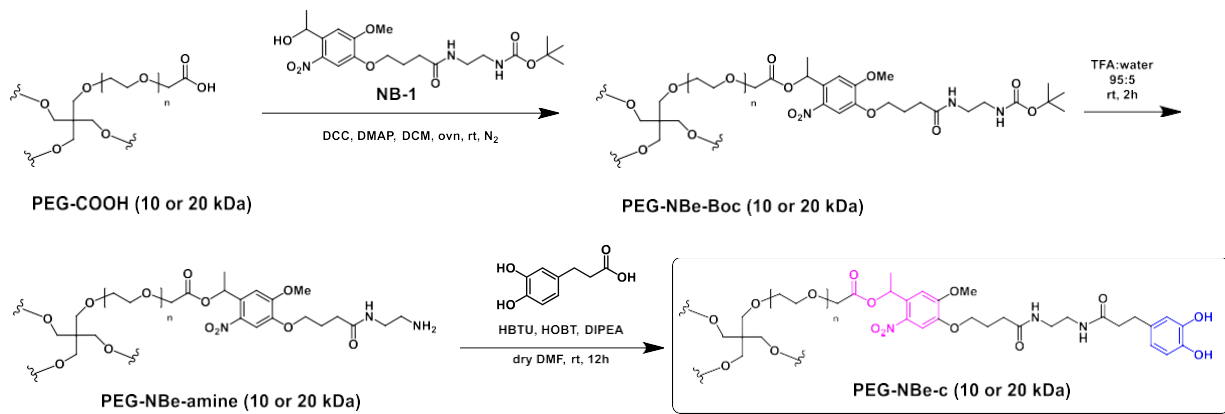
¹H-NMR (300 MHz, acetone-d₆, δ): 7.98 (s, 1H, aromatic-H), 7.63 (s, 1H, aromatic-H), 7.39 (bs, 1H, NHCH₂CH), 7.32 (bs, 1H, NHCH₂CH₂NHBoc), 6.83 (s, 1H, Ar-OH), 6.71-6.68 (m, 2H, Ar-OH), 6.54 (bs, 1H, NHCOCH₂-PEG_{core}), 6.52-6.49 (q, 1H, Ar-CH-triazole), 4.53 (bs, 1H, CH₂NHCOCOCH₂-PEG_{core}), 4.18-4.06 (t, 2H, CH₂-O-Ar), 4.00 (bs, 1H, COCH₂-PEG_{core}), 3.83 (s, 3H, Ar-O-CH₃) 3.60 (bs, 4H, O(CH₂CH₂O)_n), 3.40-3.36 (m, 2H, NHCH₂CH₂NHBoc), 3.29-3.28 (m, 2H, CH₂NHBoc), 2.77-2.72 (t, 4H, CH₂CH₂CO-Ar(OH)₂) 2.41-2.39 (t, 2H, CH₂CONH), 2.11-2.08 (m, 2H, CH₂CH₂CH₂CONH), 2.36-2.34 (d, J= 6Hz, 3H, CH₃CH-triazole).



2.4 Synthesis of photodegradable polymer PEG-NBe-c macromer

The polymers were synthesized by coupling the intermediate **NB-1** to a 4-arm PEG-COOH (10 or 20 kDa) via an esterification reaction, followed by acidic Boc deprotection and coupling to the

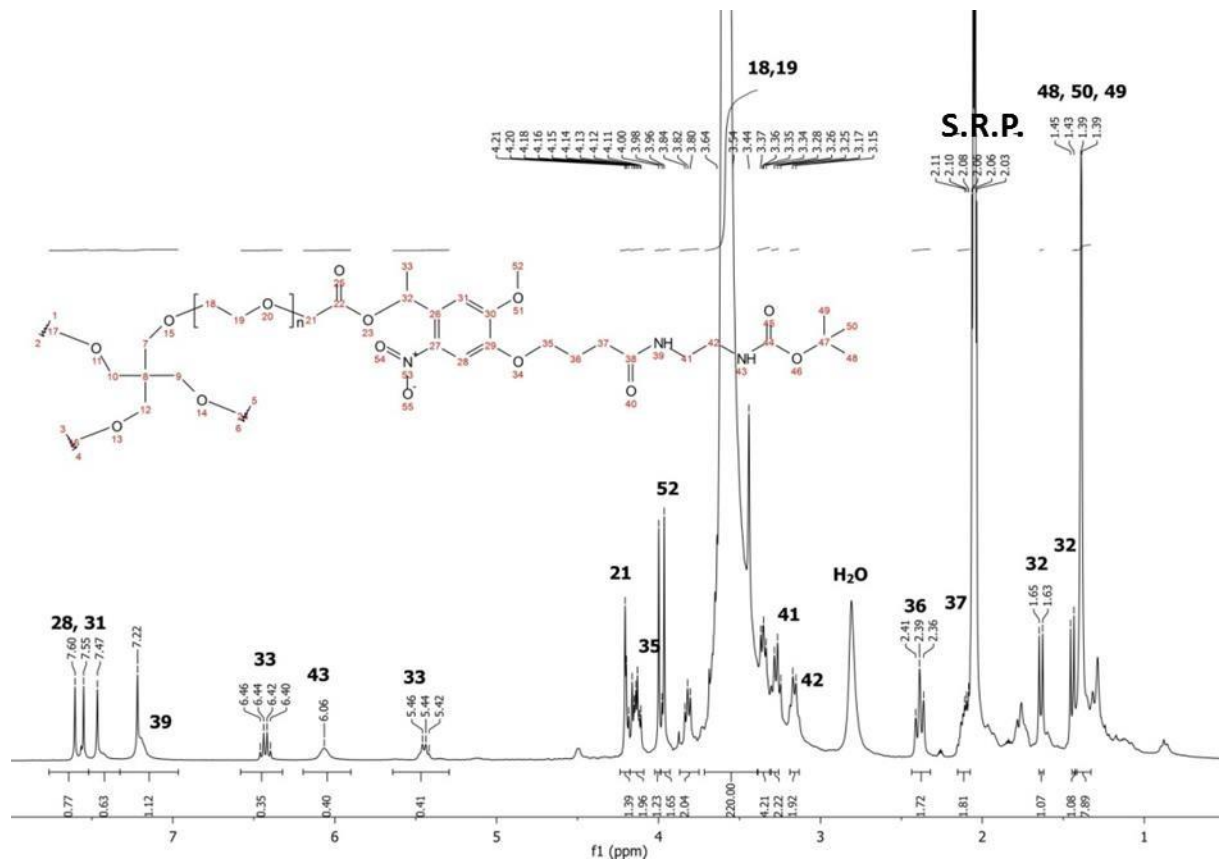
catechol compound. In the following sections, a typical procedure for polymer modification is described for a 10 kDa PEG polymer. Similar procedure was followed for preparation of the 20 kDa PEG.



Synthesis of PEG-NBe-Boc macromer

An adapted protocol reported by Wirkner et al.⁵ was used. **NB-1** (60 mg, 0.12 mmol, 3 equiv.) was dissolved in DCM (6 mL) and followed by addition of 10 kDa PEG-COOH (100 mg, 0.01 mmol polymer, 0.04 mmol alkyne groups, 1 equiv.), DCC (50mg, 0.24mmol, 6 equiv.), DMAP (3mg, 0.025mmol, 0.6 equiv.) as solids. The reaction mixture was shaken overnight at room temperature under N₂ atmosphere. The crude product was purified by dialysis against EtOH and water. After dialysis, the solution was concentrated in the rotavap and freeze-dried. A solid polymer was obtained (89 mg, yield= 89 %). The success of the polymer modification was confirmed by ¹H-NMR (substitution degree was >80 %). The purified product was stored at -20°C until use.

¹H-NMR (300 MHz, acetone-d6, δ): 7.60-7.55 (d, 1H, aromatic-H), 7.47(s, 1H, aromatic-H), 7.22 (bs, 1H, NHCH₂CH₂NHBoc), 6.45-6.40 (q, 3H, Ar-CH₂-CH₃), 6.06 (bs, 1H, NH₂Boc), 4.54 (bs, 1H, CH₂NHCOC₂-PEG_{core}), 5.45-5.42 (m, 3H, Ar-CH₂-CH₃), 4.21 (s, 1H, COCH₂-PEG_{core}), 4.20-4.15 (m, 2H, CH₂-O-Ar), 4.00 (s, 3H, Ar-O-CH₃), 3.98 (s, 3H, Ar-O-CH₃), 3.35-3.28 (m, 2H, NHCH₂CH₂NHBoc), 3.26-3.15 (m, 2H, CH₂NHBoc), 2.41-2.36 (m, 2H, CH₂CONH), 2.11-2.08 (m, 2H, CH₂CH₂CH₂CONH), 1.65-1.45 (m, 2H, COOCH₂-Ar), 1.39 (s, 9H, Boc).

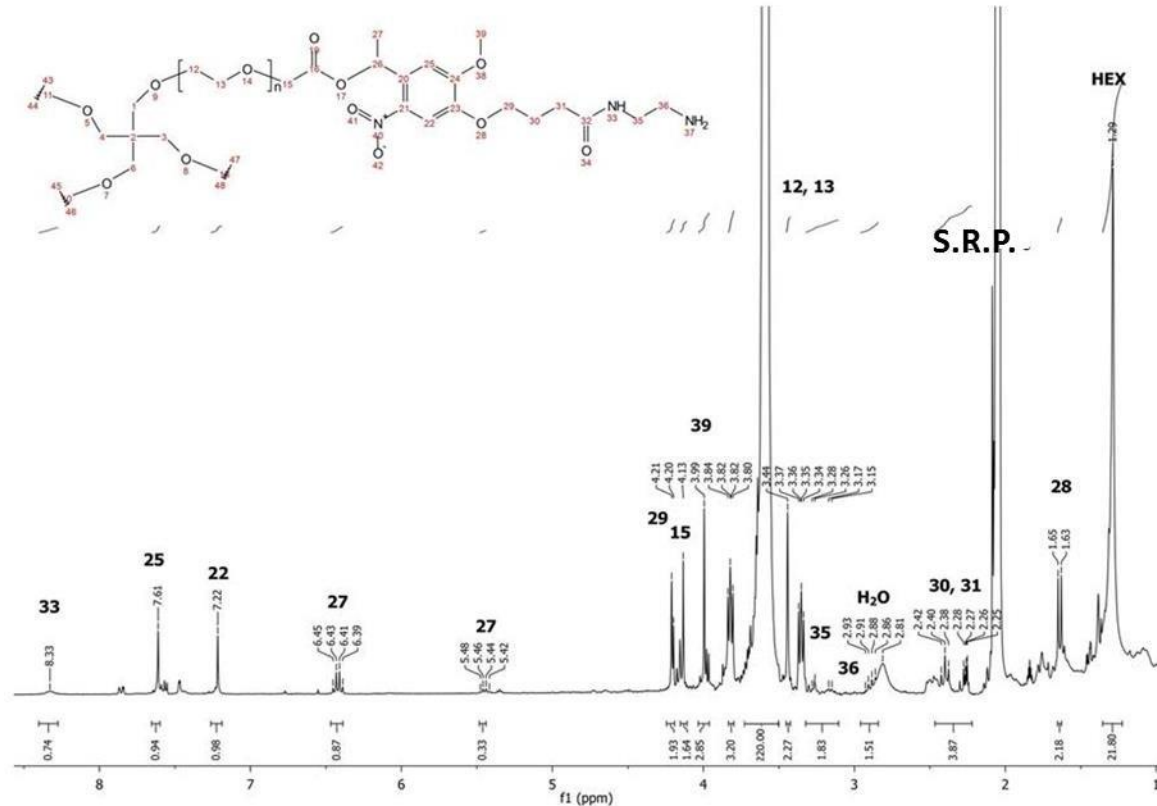


Synthesis of PEG-NBe -amine

10 kDa PEG-NBe-Boc (100 mg, 0.01 mmol polymer, 0.04 mmol Boc groups) was dissolved in TFA:water (95:5) (1 mL) and reacted for 1 h at room temperature. After reduction of solvent under N₂ stream, the crude product (ca 0.5 mL left) was precipitated twice in cold diethylether, isolated by centrifugation and dried under vacuum. The product was an off white-brownish solid(75.3 mg, yield= 75%) was characterized by ¹H-NMR showing complete Boc deprotection, indicated by the complete disappearance of the signal at 1.39 ppm (-tBu groups of Boc protecting group).

¹H-NMR (300 MHz, acetone-d₆, δ): 8.33 (1H, NHCH₂CH₂NH₂) 7.61(s, 1H, aromatic-H), 7.22(s, 1H, aromatic-H), 6.45-6.39 (q, 3H, Ar-CH₂-CH₃), 5.48-5.42 (q, 3H, Ar-CH₂-CH₃), 4.21 (s, 1H, COCH₂-PEG_{core}), 4.20-4.13 (m, 2H, CH₂-O-Ar), 3.99 (s, 3H, Ar-O-CH₃), 3.34-3.28 (m, 2H, NHCH₂CH₂NH₂),

3.26-3.15 (m, 2H, CH_2NH_2), 2.42-2.38 (m, 2H, CH_2CONH), 2.28-2.25 (m, 2H, $\text{CH}_2\text{CH}_2\text{CH}_2\text{CONH}$), 1.65-1.63 (m, 2H, $\text{COOCH}_2\text{-Ar}$).

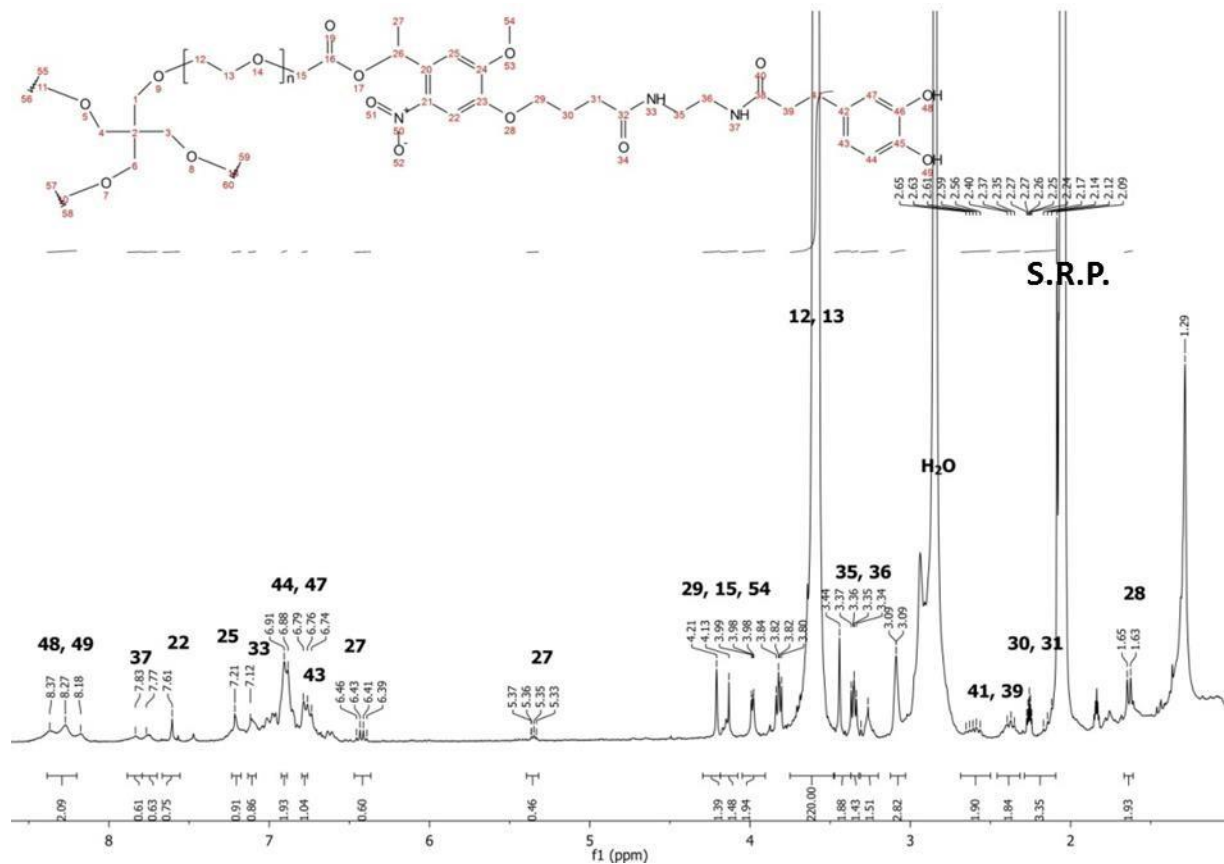


Synthesis of PEG-NBe-c

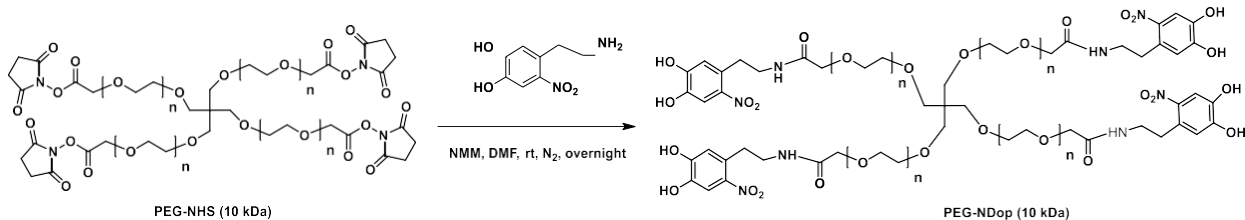
10 kDa **PEG-NBe-amine** (100 mg, 0.01 mmol polymer, 0.04 mmol amine groups, 1 equiv.) was dissolved in dry DMF (1 mL) and purged with N_2 for 10 min. Separately, DHCA (30 mg, 0.16 mmol, 4 equiv.), HBTU (60 mg, 0.16 mmol, 4 equiv.), HOBT (22 mg, 0.16 mmol, 4 equiv.) and DIPEA (70 μL , 0.2 mmol, 5 equiv.) were dissolved in dry DMF (1.5 mL) and degassed for 5 min, and subsequently added to above PEG solution. The reaction mixture was stirred under N_2 at room temperature overnight, then precipitated in diethylether and isolated by centrifugation. The crude product was purified by dialysis against acetone and water. The obtained solution

was freeze-dried. An off white-yellowish solid product (70.9 mg, yield= 71 %) was obtained, and the identity of the product was confirmed by $^1\text{H-NMR}$, showing a substitution degree >85 %.

$^1\text{H-NMR}$ (300 MHz, acetone-d6, δ): 8.37-8.18 (catechol-Ar), 7.83-7.77 (1H, NHCO-Ar), 7.83-7.61 (s, 1H, aromatic-H), 7.21(s, 1H, aromatic-H), 7.12 (1H, NHCH2CH2NHCO), 6.91-6.88(m, 2H, aromatic-H), 6.79-6.74 (m, 1H, aromatic-H), 6.46-6.39 (q, 3H, Ar- CH_2-CH_3), 5.37-5.33 (q, 3H, Ar- CH_2-CH_3), 4.21 (s, 1H, $\text{COCH}_2\text{-PEG}_{\text{core}}$), 4.13-3.99 (m, 2H, $\text{CH}_2\text{-O-Ar}$), 3.99-3.98 (m, 3H, Ar-O- CH_3), 3.37-3.34 (m, 2H, $\text{NHCH}_2\text{CH}_2\text{NHCO}$), 3.099 (m, 2H, CH_2NHCO), 2.63-2.56 (m, 2H, CH_2CONH), 2.40-2.35 (m, 2H, $\text{CH}_2\text{CH}_2\text{CH}_2\text{CONH}$), 2.27-2.25 (m, 2H, $\text{COCH}_2\text{CH}_2\text{-Ar}$), 2.24-2.09 (m, 2H, $\text{COCH}_2\text{CH}_2\text{-Ar}$), 1.65-1.63(m, 2H, $\text{OCH}_2\text{-Ar}$)

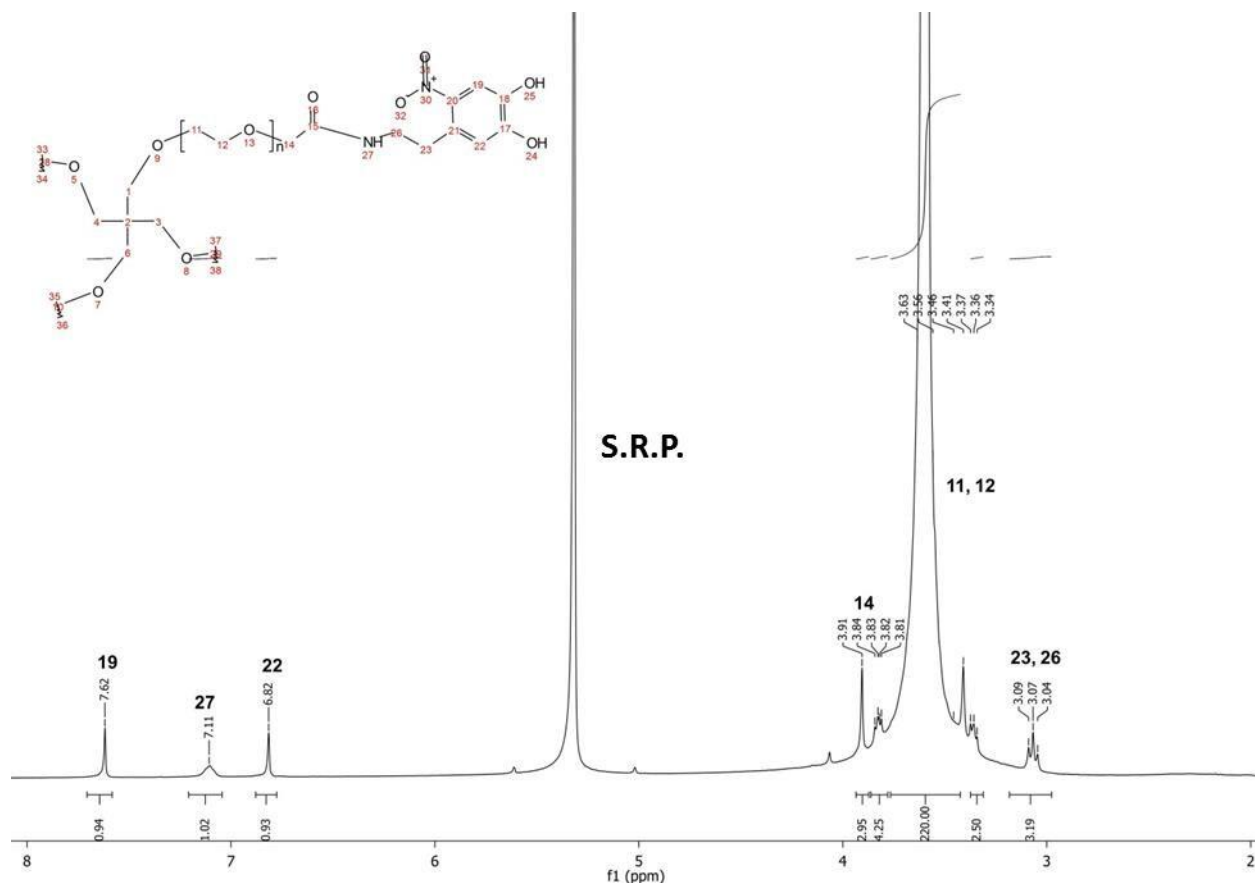


2.5 Synthesis of control macromer PEG-NDop

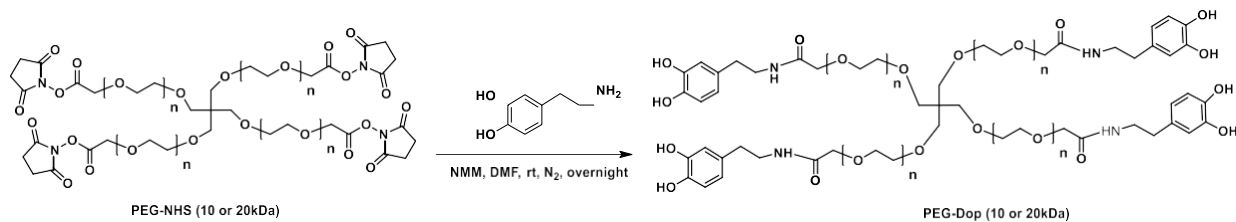


A previously reported protocol¹ was followed. NDop (44.4 mg, 0.15 mmol, 1.5 equiv.) and NMM (27.5 μ L, 0.25 mmol, 2.5 equiv.) were dissolved dry DMF (1.0 mL) and purged with N₂ for 20 min. 10 kDa, 4-arm PEG-NHS (250 mg, 0.025 mmol polymer, 0.1 mmol succinimide ester groups, 1 equiv.) was dissolved in dry DMF (1 mL) and then added dropwise into above mixture. The reaction was performed for 24 h at room temperature under N₂ atmosphere, with constant stirring. After evaporation of DMF at reduced pressure, the crude product was re-dissolved in deionized water (pH 6.0) and dialyzed against water (pH 6.0) for 2 d (dialysate was changed three times per day). The purified product was freeze-dried and stored under -20 °C until use. ¹H-NMR characterization matched the values reported in the literature. The substitution degree was >85 %.

¹H-NMR (300 MHz, DCM, δ): 7.62 (s, 1H, Ar-H), 7.11 (bs, 1H, NHCH₂), 6.82 (s, 1H, Ar-H), 3.91 (s, 2H, CH₂C(=O)NH), 3.41 (bs, 4H, O(CH₂CH₂O)_n), 3.09-3.04 (m, 4H, Ar-CHCH₂NH).



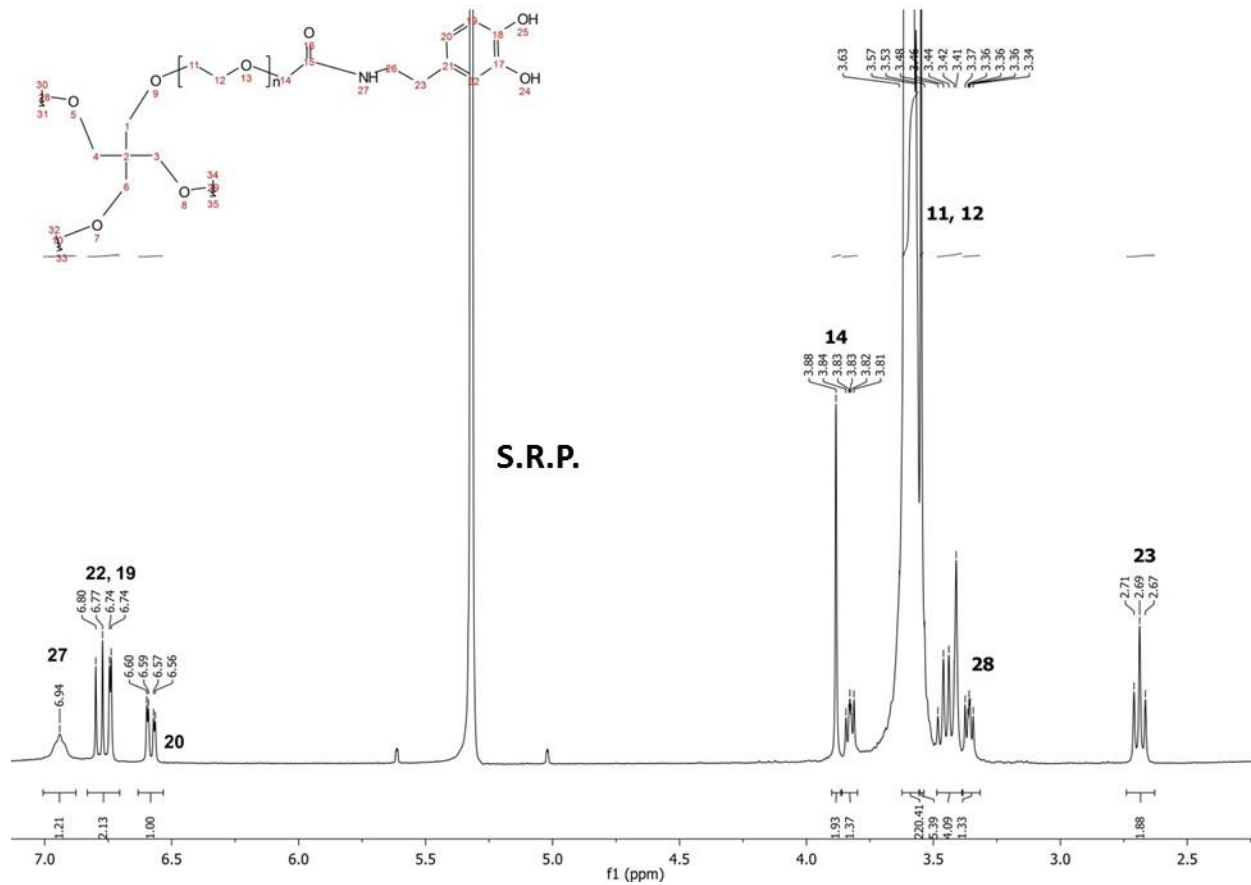
2.6 Synthesis of control PEG-Dop macromer



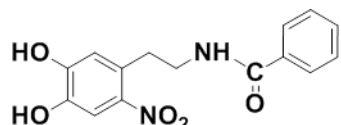
A previously reported protocol² was followed. Dop (114 mg, 0.6 mmol, 1.5 equiv.) and NMM (110 μ L, 1.0 mmol, 2.5 equiv.) were dissolved dry DMF (5.0 mL) and purged with N_2 for 20 min. 10 kDa, 4-arm PEG-NHS (1 g, 0.1 mmol polymer, 0.4 mmol succinimide ester groups, 1 equiv.) was dissolved in dry DMF (5 mL) and then added dropwise into above mixture. The reaction was performed for 24 h at room temperature under N_2 atmosphere, with constant stirring. After

evaporation of DMF at reduced pressure, the crude product was re-dissolved in deionized water (pH 6.0) and dialyzed against water (pH 6.0). The purified product was freeze-dried and stored under -20 °C until use. ¹H-NMR characterization matched the values reported in the literature. The substitution degree was >90 %.

¹H-NMR (300 MHz, DCM, δ): 6.94 (bs, 1H, NHCH₂), 6.80-6.77 (m, 1H, Ar-H), 6.74 (s, 1H, Ar-H), 6.60-6.59 (m, 1H, Ar-H) 3.88 (s, 2H, CH₂CONH), 3.41 (bs, 4H, O(CH₂CH₂O)_n), 3.37-3.34 (m, 2H, Ar-CH₂CH₂NH) 2.71-2.67 (m, 2H, Ar-CH₂).



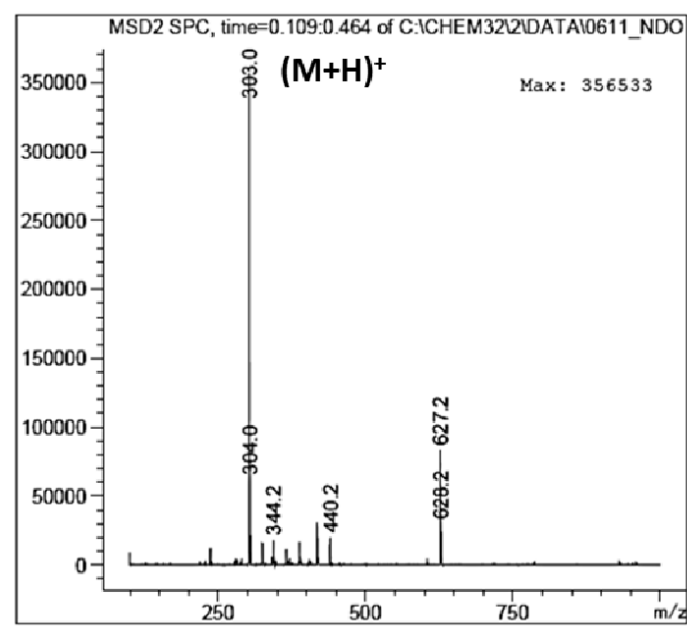
2.7 Synthesis of small model compounds for photodegradation studies

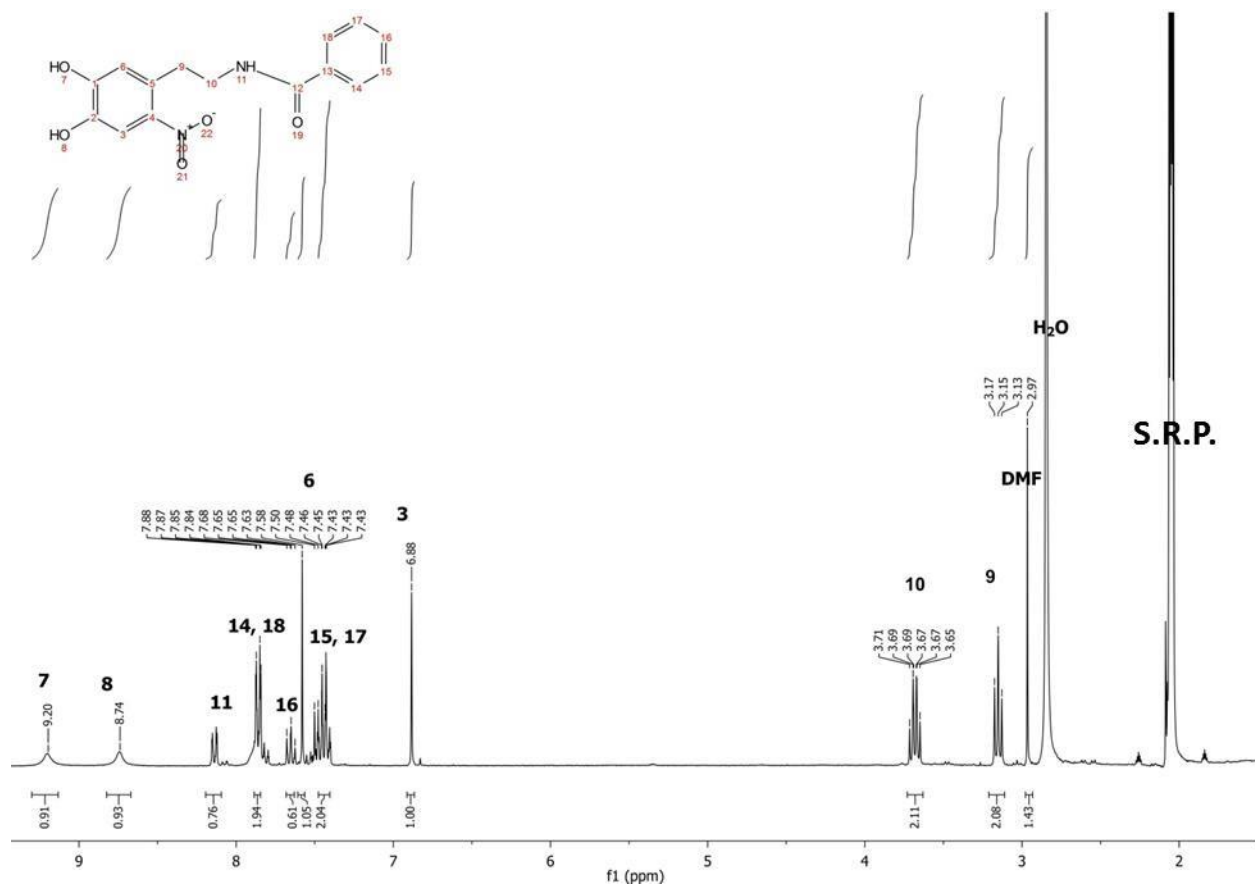
*Synthesis of N-(4,5-dihydroxy-2-nitrophenethyl)benzamide (**1**)***1**

This compound was synthesized by following a previously reported protocol.¹ Spectroscopic characterization matched the expected values.

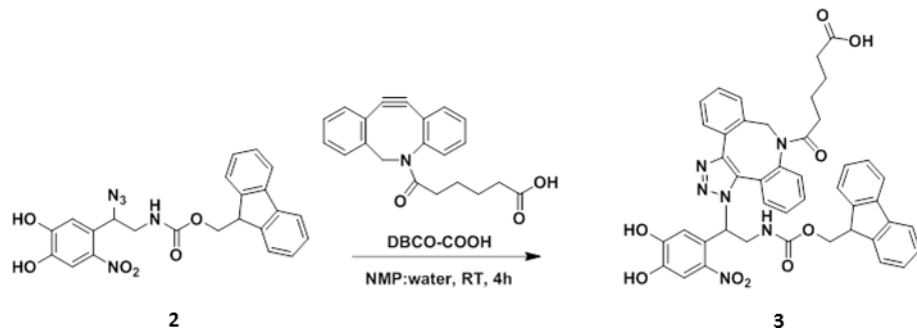
ESI-MS⁺: 303.0 (M+H)⁺

¹H-NMR (300 MHz, CD₃COCD₃, δ): 9.20 (bs, 1H, -OH), 8.74 (bs, 1H, -OH), 7.68-7.88 (m, 2H, aromatic-H), 7.65-7.63 (m, 1H, aromatic-H), 7.58 (s, 1H, aromatic-H), 7.45-7.43 (m, 2H, aromatic-H), 6.88 (s, 1H, aromatic-H), 3.71-3.65 (m, 2H, CH₂NH), 3.17-3.13 (t, 2H, CH₂-CH₂NH₂).





Synthesis of 6-(3-((3-(2-(((9H-fluoren-9-yl)methoxy)carbonyl)amino)-1-(4,5-dihydroxy-2-nitrophenyl)ethyl)-3,9-dihydro-8H-dibenzo[b,f][1,2,3]triazolo[4,5-d]azocin-8-yl)-6-oxohexanoic acid (3)

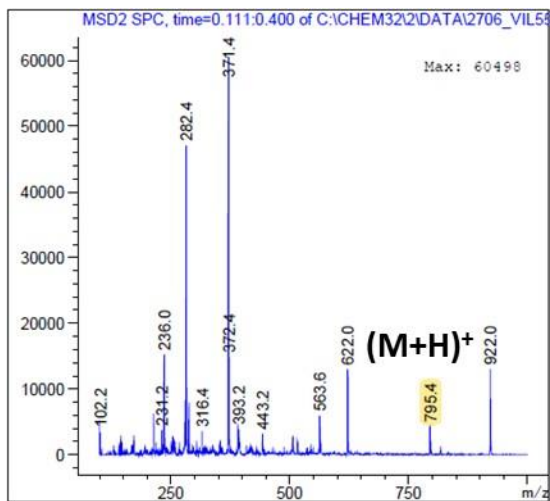


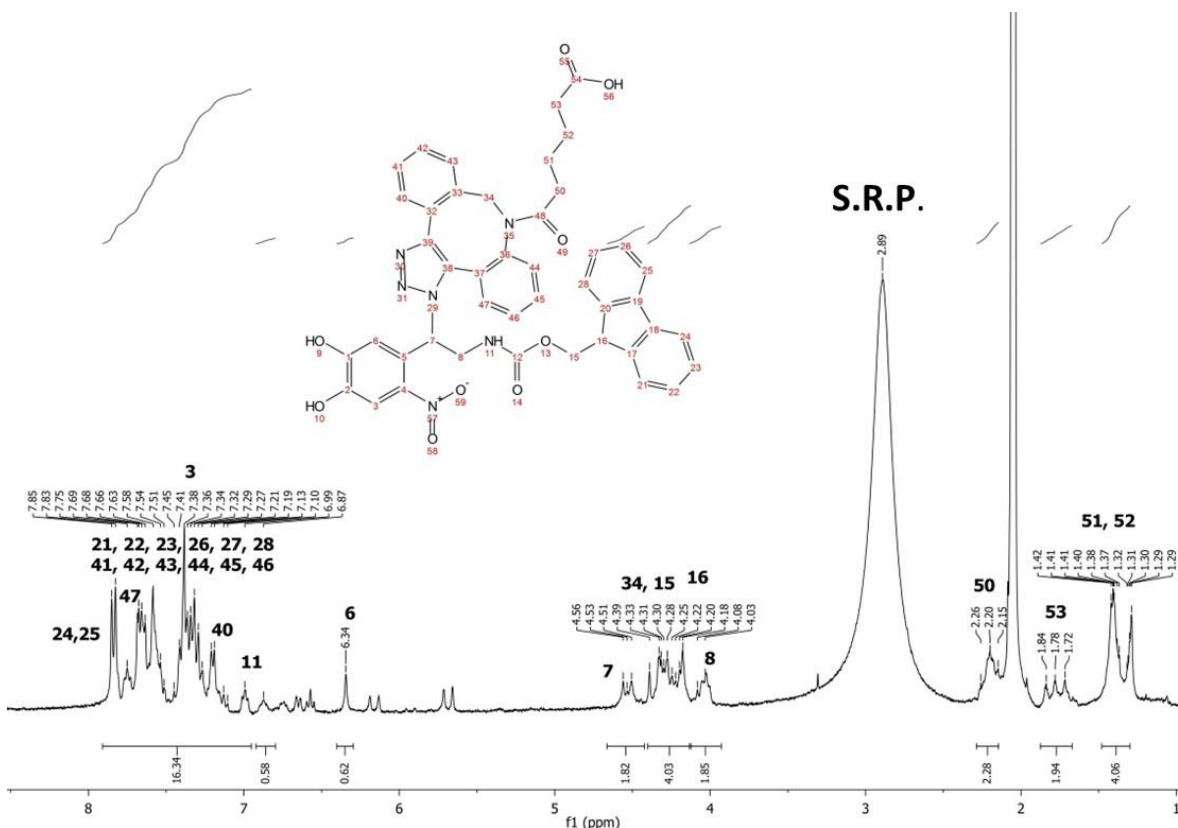
2 (5 mg, 10.8 µmol, 1 equiv.) was dissolved in NMP:water (4:1) (2mL) and DBCO-COOH (4.3 mg, 13 µmol, 1.2 equiv.) was added. The reaction mixture was stirred at room temperature for 4 h.

The course of the reaction was monitored by analytic HPLC until complete consumption of the starting material. The crude product was purified with by RP-HPLC (50% B- 95% B $\lambda_{\text{det}} = 360 \text{ nm}$, retention time = 18.5-21 min. Yield = 82% (15 mg yellowish product).

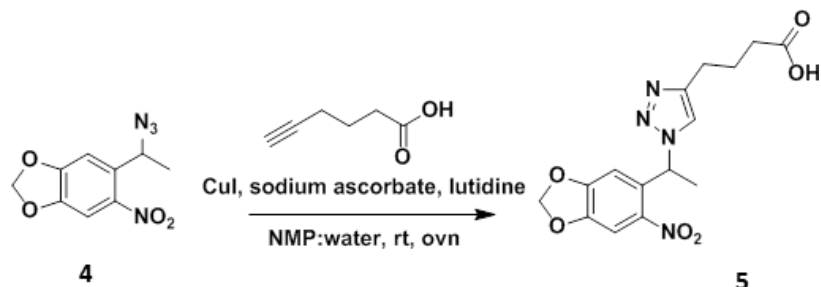
ESI-MS⁺: 795.4 ($\text{M}+\text{H}$)⁺.

¹H-NMR (300 MHz, CD₃COCD₃, δ): 7.85-7.83 (m, 2H, Fmoc), 7.69-7.68 (m, 2H, DBCO), 7.66-7.51 (m, 6H, DBCO), 7.45-7.27 (m, 5H, Fmoc), 7.38 (s, 1H, Aromatic-H), 7.10-6.99 (m, 2H, DBCO), 6.87 (bs, 1H, NH), 6.64 (bs, 1H, NH), 4.56-4.51 (NHCH₂CH), 4.33-4.28 (m, 4H, NHCOOCH₂ & CH₂NCO), 4.25-4.20 (t, 1H, NHCOOCH₂CH), 4.18-40.3 (m, 2H, CONHCH₂), 2.26-2.15 (t, 2H, COCH₂CH₂CH₂COOH), 1.84-1.72 (t, 2H, CH₂COOH), 1.42-1.37 (m, 2H, CH₂CH₂CH₂COOH), 1.32-1.29 (m, 2H, CH₂CH₂COOH).





Synthesis of 4-(1-(1-(6-nitrobenzo[d][1,3]dioxol-5-yl)ethyl)-1*H*-1,2,3-triazol-4-yl)butanoic acid (5)

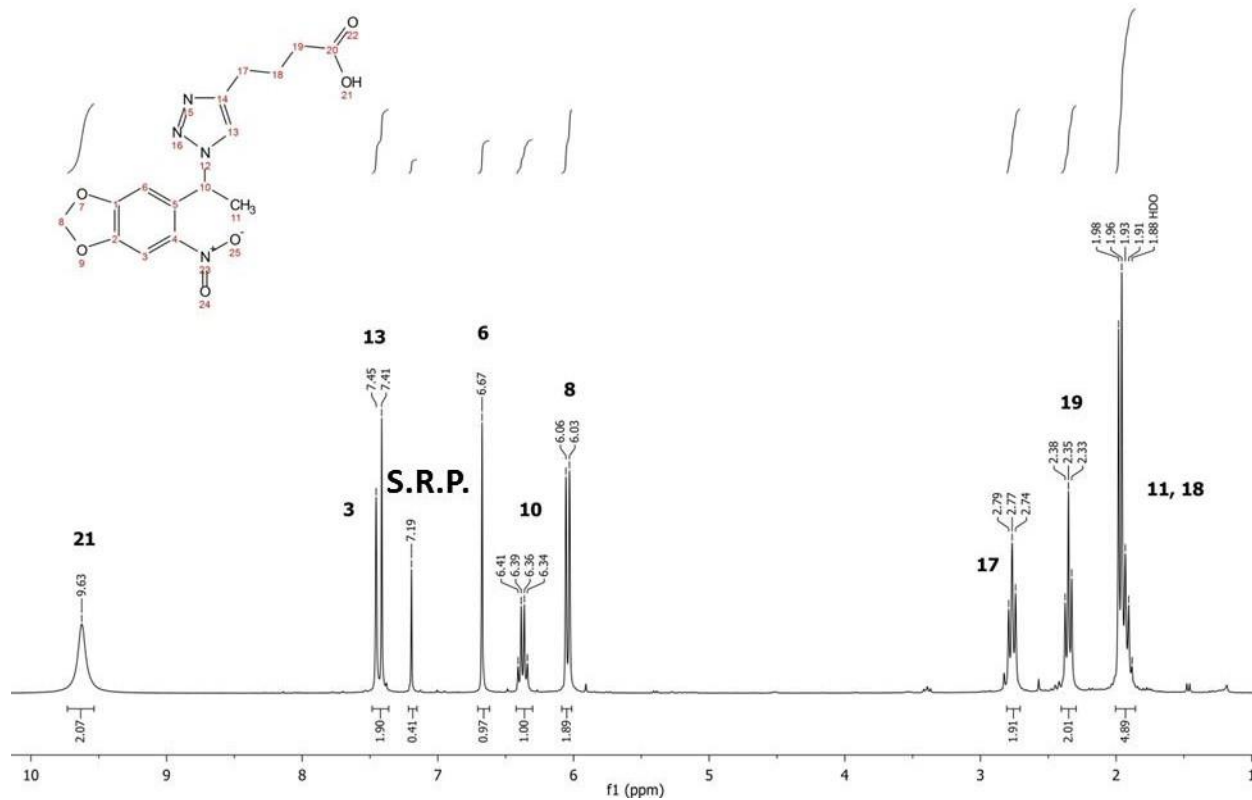


A previously reported protocol⁶ was followed. CuI (8 mg, 42 μmol , 1 equiv.), sodium ascorbate (8.3 mg, 42 μmol , 1 equiv.), and 2,6-lutidine (10 μL , 84 μmol , 2 equiv.) were mixed in 5mL NMP/H₂O (4:1) and shaken for 30 min before adding pip-azide, followed by addition of hexynoic acid (10 μL , 11.2 mg, 84 μmol , 2 equiv.). The reaction mixture was shaken at room temperature for 12 h, centrifuged to remove the precipitate and partitioned twice between EtOAc and water, dried over MgSO_4 and evaporated. The crude product was purified with RP-HPLC (30% B-

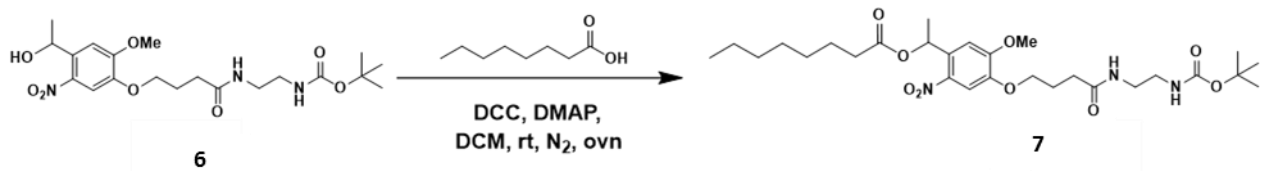
95% B $\lambda_{\text{det}} = 360 \text{ nm}$), evaporated and freeze-dried. A pure yellowish product was obtained with 62% yield (9 mg).

ESI-MS⁺: 349,2 (M+H)⁺, 317.2 (M+Na)⁺.

¹H-NMR (300 MHz, CDCl₃, δ): 9.63 (bs, 1H, -COOH), 7.45 (s, 1H, aromatic-H), 7.41 (s, 1H, CH-triazol), 6.67 (s, 1H, aromatic-H), 6.41-6.34 (q, 1H, Ar-CH-triazol), 6.06-6.03 (d, 2H, O-CH₂-O), 2.79-2.74 (t, 2H, CH₂-triazol), 2.38-2.33 (t, 2H, CH₂-COOH), 1.98-1.91 (M, 5H, CH₂-CH₂COOH, -CH₃).



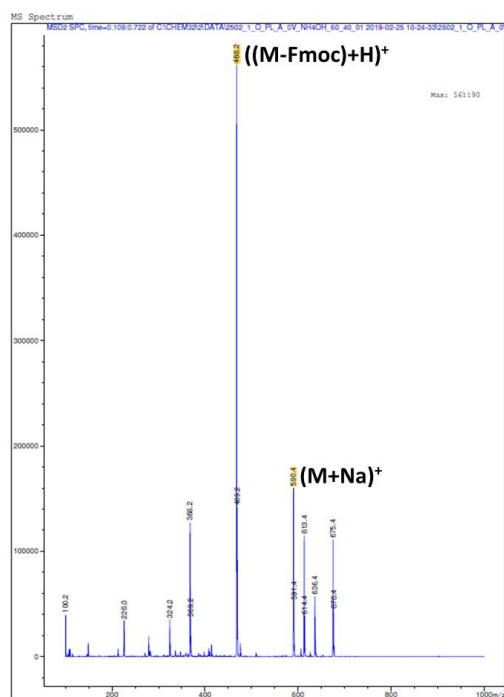
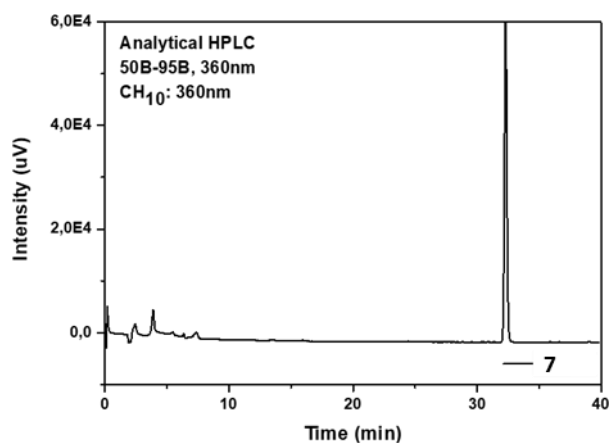
Synthesis of 1-(4-((2-((tert-butoxycarbonyl)amino)ethyl)amino)-4-oxobutoxy)-5-methoxy-2-nitrophenyl)ethyl octanoate (**7**)

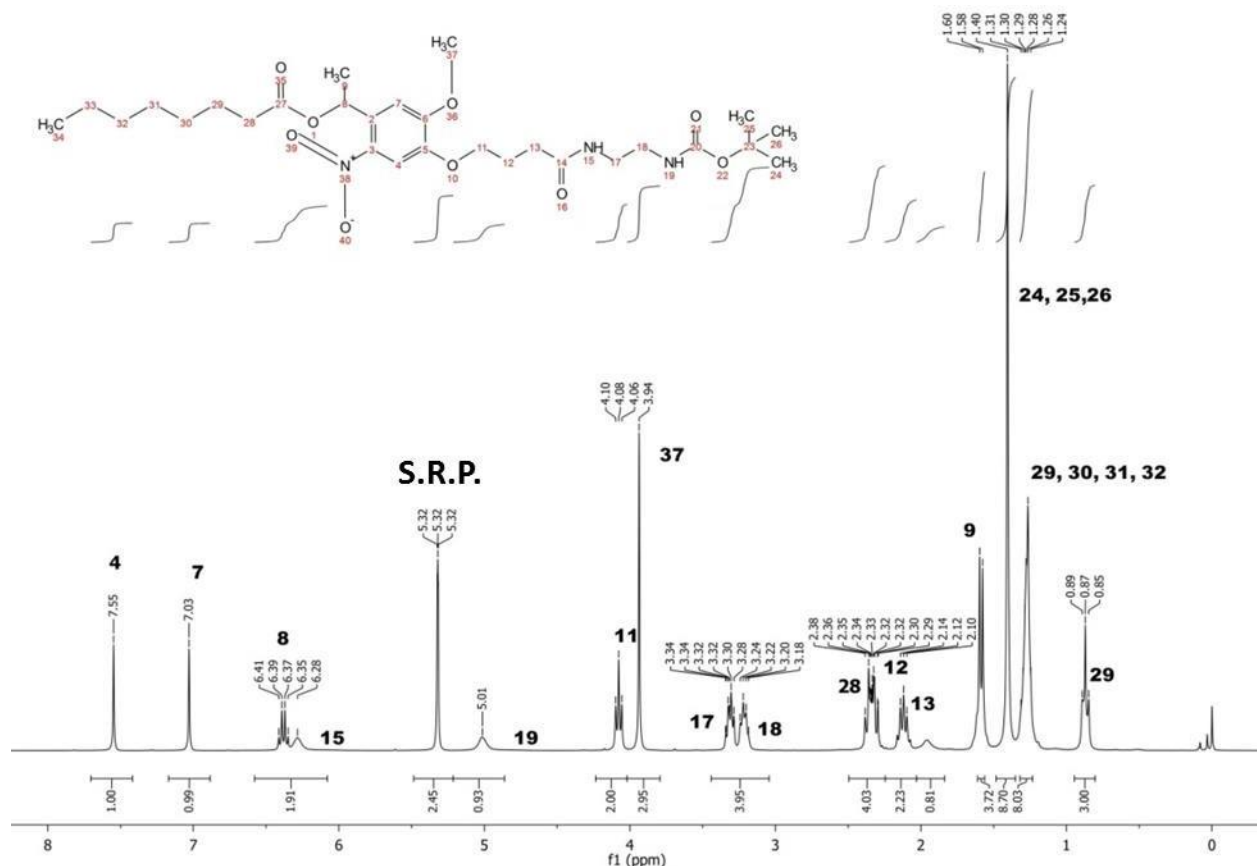


A previously reported protocol was followed.⁵ **6** (30 mg, 0.068 mmol, 0.068 equiv.) was dissolved in DCM (6 mL) followed by addition of octatonic acid (9.8 mg, 1 mmol polymer, 1 equiv.), DCC (14 mg, 1 mmol, 6 equiv.), DMAP (0.66 mg, 0.8 mmol, 0.8 equiv.) as solids. The reaction mixture was shaken overnight at room temperature under N₂ atmosphere. The crude product was quenched with Na₂CO₃ and partitioned twice between EtOAc and water, dried over MgSO₄ and evaporated. The crude product was purified with by HPLC (5%B- 95%B $\lambda_{\text{det}} = 360$ nm, rt=32 min), evaporated and freeze-dried. A pure yellowish product was obtained with 90% yield (35 mg).

ESI-MS⁺: 590.4 (M+Na)⁺, 468.2 ((M-Boc)+H)⁺.

¹H-NMR (300 MHz, CDCl₂, δ): 7.55 (s, 1H, Aromatic-H), 7.03(s, 1H, Aromatic-H), 6.41-6.35 (q, 1H, Ar-CH-OH), 6.28 (bs, 1H, NHCH₂CH₂NHBoc), 5.01 (bs, 1H, NH₂Boc), 4.10-4.05 (t, 2H, CH₂-O-Ar), 3.94 (s, 3H, Ar-O-CH₃), 3.34-3.28 (m, 2H, NHCH₂CH₂NHBoc), 3.24-3.18 (m, 2H, CH₂NHBoc), 2.38-2.32 (m, 2H, CH₂CONH & 2H, CH₂COOCH), 2.30-2.10 (m, 2H, CH₂CH₂CH₂CONH), 1.60-1.58 (d, J=6Hz, 3H, CH₃CH-OH), 1.40 (s, 9H, Boc), 1.26 (bs, 8H, CH₃CH₂CH₂CH₂CH₂), 0.89-0.85 (t, 3H, CH₃CH₂CH₂CH₂CH₂).





2.8 Photolysis studies of model compounds and macromers in solution

Photolysis experiments were performed over either 1 μM solution of the 4-Arm PEG-derivatives in water or 1 mM solution of the small molecules in acetonitrile, all freshly prepared. The sample (1 mL) was irradiated at different time points and spectral evolution was followed by UV/Vis spectroscopy measurement until the spectrum did not change further. At selected time points, aliquots were taken and analyzed by ESI-MS, in search for m/z peaks indicative of starting material consumption and/or appearance of the expected photolysis products.

Light-exposure doses will be informed, as calculated from the following equation:

$$\frac{\text{Irradiance}}{1,000} \times \text{time} = \text{Irradiation Dose}$$

The irradiance expressed in mW cm^{-2} , the time in s and the irradiation dose in J cm^{-2} .⁷

3. Chapter 3

Preparation & Characterization of Photodegradable Adhesive PEG-catechol hydrogels

3.1 Hydrogel formation in a PDMS mold

The precursor mixture solutions of the hydrogel precursor were prepared in 50 mM HEPES buffer, pH 7.5. In a typical experiment, hydrogels were formed under mild oxidative conditions by mixing 20 wt % 4-arm PEG-catechol derivatives with the oxidant solution of 36 mM (or 18 mM) NaIO₄ in a polymer: oxidant (1:1) volume ratio. The final composition of the hydrogel was 10 wt % PEG-catechol (10 or 20 kDa) and 18 mM (or 9 mM) oxidant. Under these conditions the catechol group is expected to oxidize and self-polymerize to form a crosslinked network.² Immediately after mixing the two precursors, the resulting solution (20-100 µL) was quickly poured to the center of a PDMS mold (1 cm diameter) and incubated in a humidified chamber at 25°C. The hydrogels were cured in the incubator for 6 h to achieve complete crosslinking and kept in water or PBS for 12-72 h. The obtained hydrogels were transparent, homogeneous and brownish orange (Figure 1). When needed for cell studies (chapter 4), the prepared hydrogels were washed thoroughly with 70 % ethanol and sterile PBS solution for several times before use.

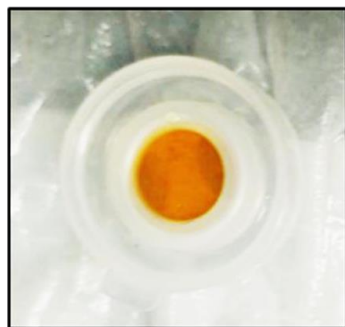


Figure 1 Hydrogel formation into the polypropylene mold: 10 wt% 4-arm PEG-catechol gel (10 kDa, **PEG-NBt-c**) and 9 mM oxidant (NaIO₄).

3.2 Photo-degradation studies of fully swollen hydrogels by a gravimetric method

Experiments of hydrogel photodegradation were performed over fully swollen gels, by following a gravimetric method. Hydrogel precursor solutions were prepared in water:PBS (1:1), pH 7.0 by mixing 20 wt % 4-Arm PEG-polymers (20 µL) with 18 mM NaIO₄ oxidant solution (20 µL). The gels were let cure for 6 h at 25°C and then swollen until equilibrium by immersing them in cell culture medium for 24 h at room temperature. The thickness of the swollen gel was about 5 mm. The mass of the swollen gels was measured (M_0). The swelling solution was replaced by fresh medium (2 mL) and the hydrogels were exposed to light under ECE 2000 standard metal halide UV curing bulb (400W, Irradiance = 70 mW cm⁻², DYMAX) for selected time points (10 min = 42 J cm⁻², 15 min = 63 J cm⁻², 20 min = 84 J cm⁻² and 30 min = 126 J cm⁻²). After selected irradiation doses, the irradiated swollen hydrogel was weighted (M_i). The normalized weight loss of the swollen hydrogels over time was calculated according to the following equation:

$$\text{Normalized weight loss} = \frac{M_0}{M_i}$$

The experiment was performed in triplicate (three individual experiments). During the irradiation, the color of the supernatant solutions where the hydrogels were placed turned yellowish, indicating the formation of colored photolysis products. The irradiated medium at different time points was collected and used for the cytotoxicity studies.

3.3 Rheological characterization of PEG hydrogels *in situ*: curing kinetics, degradation kinetics and shear moduli

To determine the rheological properties and curing kinetics of PEG-catechol based hydrogels, storage modulus (G') and loss modulus (G'') were measured using a rotational rheometer (DHR3, TA Instruments, USA) equipped with a 12 mm parallel plate geometry. A mixture of gel precursors of 40 µL (containing 20 µL polymer solution and 20 µL oxidant) was placed on the rheometer for the measurements. An initial measuring gap of 250 µm was set and the experiments were performed at strain= 5 %, frequency= 1 Hz and controlled temperature of

23°C (Peltier lower plate). To avoid drying of the sample during testing, paraffin oil was applied around the samples after setting measuring gap and metal cap was installed (to prevent evaporation). All rheological experiments were performed at least in triplicate.

Rheological analysis was also used as a direct measurement of the PEG hydrogels degradation upon irradiation at $\lambda= 365$ nm. A mixture of gel precursors of 40 μL (containing 20 μL polymer solution and 20 μL oxidant) was placed on the rheometer and allowed to crosslink for 250 min or until G' reached a plateau. The cured gel was subsequently degraded by exposing it to light irradiation (typically, at $\lambda= 365$ nm, Irradiance= 10 mW cm^{-2}). Irradiation was performed either continuously or stepwisely (irradiation pulses of 6-8 min).

3.4 Analysis of photodegradation kinetics as measured by in situ photorheology

A methodology previously described in the literature⁸⁻¹¹ was followed, using as starting point the results obtained from the time sweep experiments during irradiation. The photodegradation of the hydrogel was considered to be a first-order process, therefore the plot of decaying shear storage modulus was fit to the following equation:

$$G'(t) = G'_0 e^{-k_{obs} t}$$

where $G'(t)$ is the shear storage modulus as a function of time, G'_0 is the initial shear storage modulus, and t is the time. This generalization can be utilized to calculate the first-order degradation rate constant (k_{obs}) by linear regression using the linearized change in storage modulus over time upon hydrogel light irradiation. To this end, the normalized decay of the storage modulus, (G'/G'_0), as a function of time was plotted and only values of $G'(t)$ corresponding to 90% to 50% of the initial G'_0 were used for calculation of the rate constant.⁹ The $\ln(G'/G'_0)$ was plotted as a function of time. The first-order rate constant (k_{obs}) of the photodegradation of the network was estimated from the slope of such plot, after a linear fitting according to the equation:

$$\ln(\frac{G'}{G'_0}) = -k_{obst} t$$

$$G'_0$$

Analysis of a representative data set is shown as follows. Gel composition and irradiation conditions are indicated in the plot.

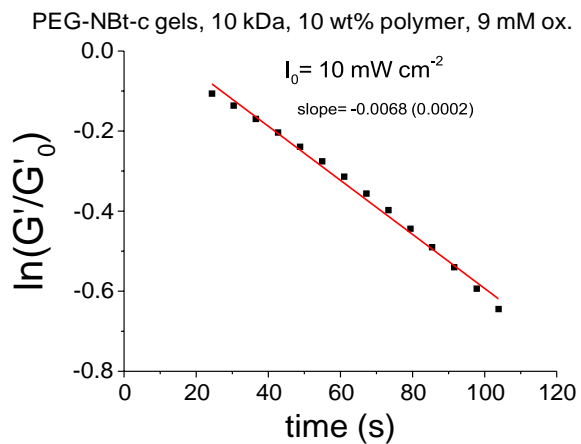
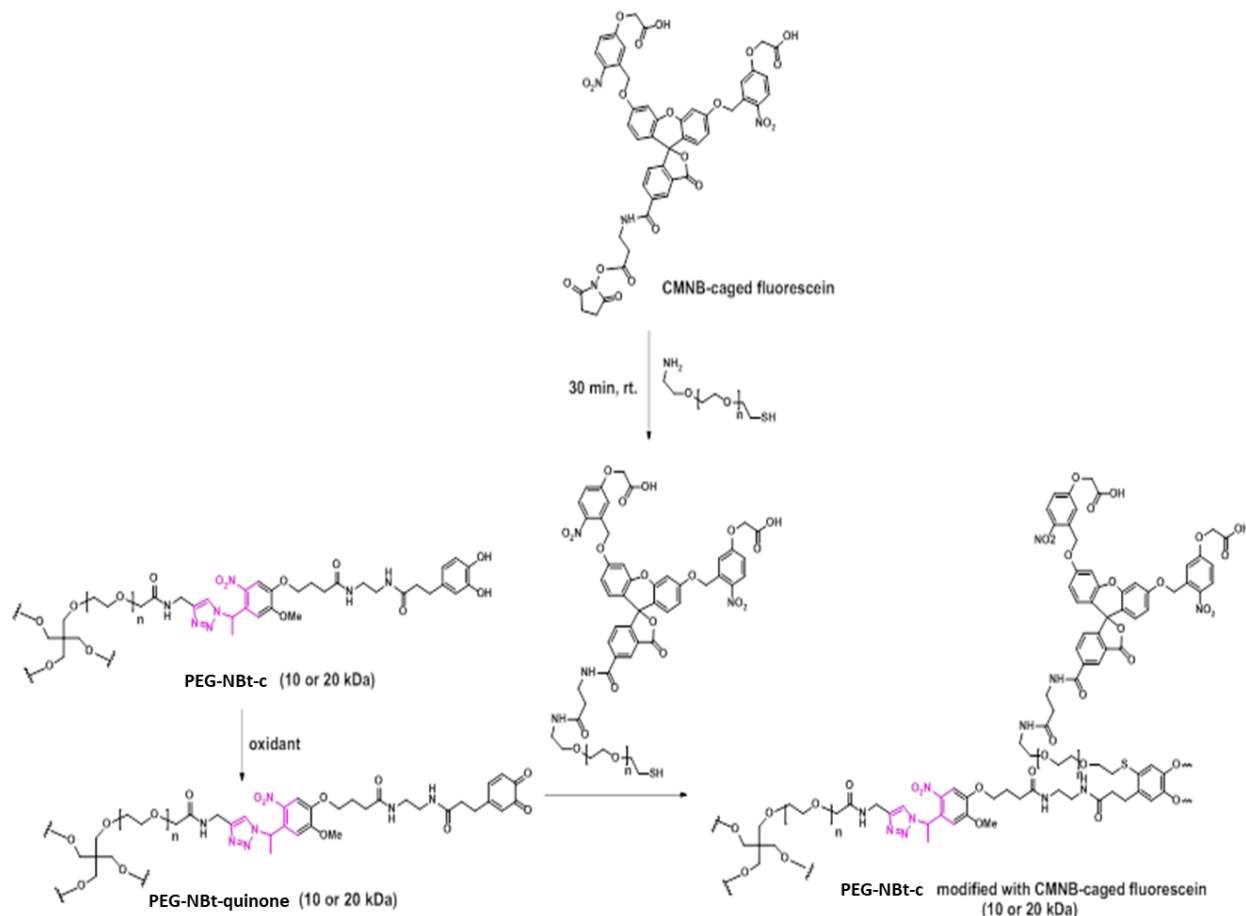


Figure 2 The $\ln(G'/G'_0)$ was plotted as a function of time.

3.5 2D and 3D patterning of acellular photodegradable hydrogels

Preparation of PEG-catechol hydrogels labeled with CMNB-fluorescein



An adapted protocol previously reported by our group was followed.⁵ Amine-PEG-thiol solution (3.5kDa, 1 mM in 50 mM HEPES buffer, pH 7.5, 1 μ L) was mixed with CMNB-caged fluorescein (2.5 mM in 50 mM HEPES buffer, pH 7.5, 2 μ L) and incubated for 30 min at 37°C. 2 μ L of above solution was mixed with 20 wt% 4-Arm PEG-catechol solution (4 μ L) and placed in an Ibidi® 15-well angiogenesis slide, mixed with NaIO₄ solution (36 mM in 50 mM HEPES buffer, pH 7.5, 4 μ L) and allow to crosslink for 6 h at 25 °C.

Note that, during photoirradiation, CMNB-fluoresceine is uncaged: the cleavage of the CMNB-photoprotecting group results in increased fluorescence intensity in the irradiated region of the gel.

The labeled hydrogels were exposed to focused light using a single-photon confocal LSM (LSM 880 AxioObserver, Zeiss). The gel was submerged in water in an Ibidi® 15-well

angiogenesis slide. Zeiss Region of Interest (ROI) software was then used to draw and subsequently scan a square shape within an x-y plane of the gel with a single-photon laser (30W, at $\lambda = 405$ nm) to create a local void. Subsequently, these shapes were scanned in the z- direction to achieve stacked 3D voids within the gel. To demonstrate this concept, squares were scanned in zoom 2.5 (pixel size = 0.11 μm) with the laser (20x objective NA ~ 617.6 nm, $\sim 5.34\mu\text{m}$ scan intervals over ~ 180 μm thickness, scan speed setting = 2 (P.Dwell = 65.94 μsec) or 1 (P.Dwell = 131.88 μsec)). The following irradiation parameters were optimized for the different samples to adjust the irradiation dose: irradiance power (1-100 %), scan speed (1-2), scan number repetitions (i.e. number of passing laser) (1-16). The resulting features were visualized with confocal LSM imaging at zoom 1 (0.83 $\mu\text{m} \times 0.83 \mu\text{m} \times 5.34 \mu\text{m}$), where the irradiated patterned displays increased green fluorescence intensity. These pattern features were also imaged in bright field. These fluorescent and bright field raw images allow verification of the photodegraded region and the resulting 3D feature. Patterns drawn with longer irradiation doses showed higher fluorescence, demonstrating the dose-dependent uncaging of the fluorophore with 3D resolution.

3.6 Encapsulation of polystyrene particles (PSPs) into PEG-catechol hydrogels and their release upon light irradiation

For this experiment, red-fluorescently labelled polystyrene particles with a mean diameter= 28.61 μm , abs/em: 530/607 nm were used (microParticlesGmbH, Germany).

Stock solutions of 10 kDa, 40 wt % polymer and 36 mM oxidant solution were prepared in 50 mM HEPES buffer, pH 7.5. 40 wt % polymer solution (10 μL) was mixed with 2.5% w/v aqueous suspension of PS-NPs (10 μL), in order to have a final stock composition of 20 wt% polymer with PS-NPs. These two stock solutions (20 wt% polymer with PS-NPs and 36 mM oxidant) were mixed (5.5 μL each) in order to form a hydrogel with a final composition of 10 wt% PEG-derivatives and 9 mM oxidant. The PSP-laden hydrogels were equilibrated in water for 12 h before irradiation in the microscope.

Release of encapsulated PSPs during in situ photodegradation was followed by LSM confocal microscopy. To release the red-fluorescently labelled polystyrene particles from the gel, the hydrogels were exposed to focused light using a single-photon confocal LSM (LSM 880 AxioObserver, Zeiss) at $\lambda = 405$ nm. The gel was submerged in water in Ibidi® 15-well angiogenesis slide. Zeiss Region of Interest (ROI) software was then used to draw and subsequently scan a square shape within an x-y plane of the gel with the laser to degrade the material locally. The degradation of the hydrogel was observed by the displacement of the encapsulated PSPs, which are following the change in the local gel architecture. To demonstrate this concept, squares were scanned with the laser (30W laser, 20x objective NA ~617.6 nm, zoom 2.5, laser power = 2-100 %, scan speed setting = 1-2, scan number repetitions = 1-8). The resulting features were imaged in bright field.

3.7 Adhesion tests of PEG hydrogels on natural tissue

For this experiment, red-fluorescently labelled polystyrene particles with a mean diameter= 28.61 μm , abs/em: 530/607 nm were used (microParticlesGmbH, Germany).

PEG-catechol hydrogels with high substitution degree (>90%) were used for adhesion testing. 20 wt % polymer solution in 50 mM HEPES buffer, pH 7.5 (10 μL) was mixed with 36 mM of oxidant – PSPs (10 μL), in order to form a hydrogels with final composition of 10 wt% PEG-derivatives and 18 mM oxidant.

3.8 Adhesion tests of PEG-cat hydrogels on skin tissue

Fresh chicken skin was obtained from a local butcher and stored at 4°C overnight. For the adhesion measurements, a portion of tissue was kept at room temperature in aluminum paper to prevent from drying.

For the adhesion measurements, chicken skin was cut into square pieces of 15*20 mm and the fat was removed with a scalpel. The remaining tissue was clean under cold tap water

using hand soap once and then washed with water. The skin was immersed in ethanol for 2 min and washed with fresh tap water. The skin was kept in water until use (within the same day). For adhesion measurements on wet skin, skin samples were immersed in 10 mM HEPES buffer, pH 7.5 for 30 min before adding the tissue glue on the skin, which was covered by a thin layer of HEPES buffer.

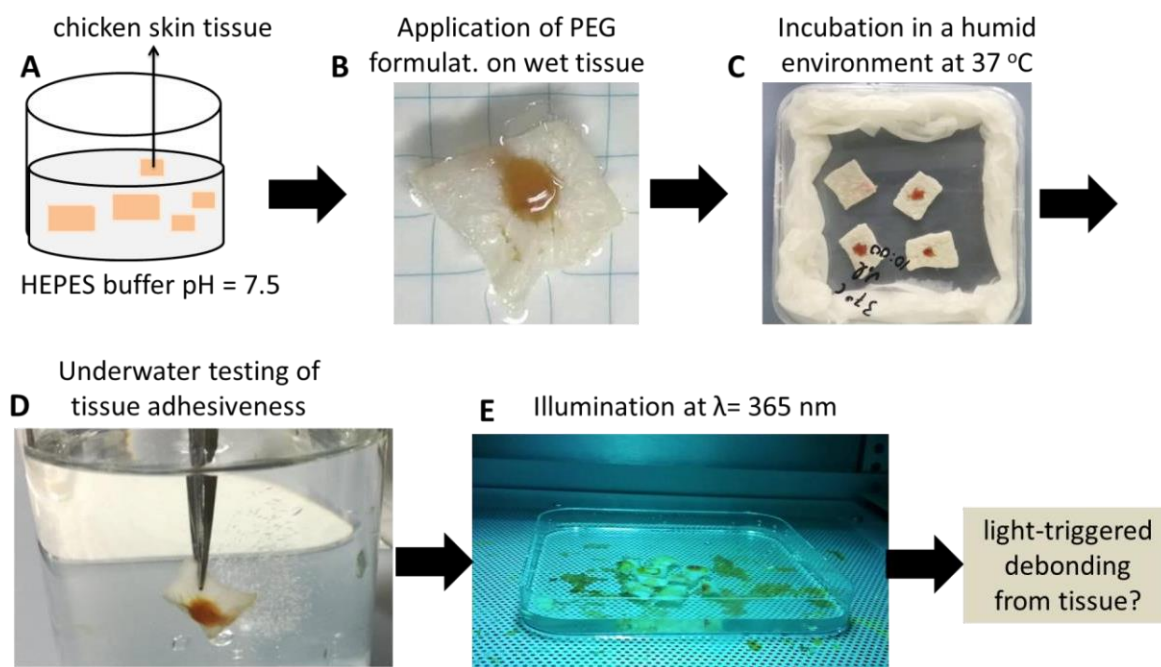


Figure 3 Schematic representation of the preparation of samples for tissue adhesive testing, before and after light exposure.

3.9 Fluorescence imaging of outer layer of bonded tissue

Tissue samples, with bonded PSPs-laden-hydrogels on top, were prepared as explained above, washed with MilliQ water and imaged by fluorescence microscopy before and after light illumination. During ex situ photodegradation, light-triggered release of encapsulated PSPs (irradiation conditions: $\lambda = 365 \text{ nm}$, $I = 70 \text{ mW cm}^{-2}$ for 6 min; dose = 25 J cm^{-2}), was imaged by fluorescence microscopy (see Appendix. Figure 4).

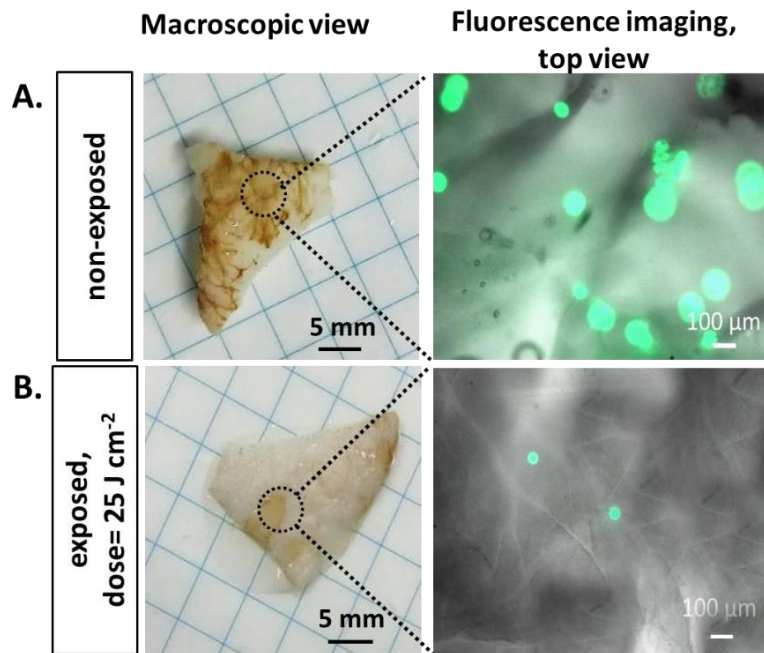


Figure 4 Macroscopic and microscopic visualization of the tissue adhesiveness of PEG-NBt-c hydrogel tested on chicken skin, before (A) and after (B) light exposure. The left panel shows the macroscopic view of the bonded tissue. The right panel displays the fluorescence imaging of the outer tissue layer; where embedded fluorescent PSPs in the adhesive hydrogel facilitate the visualization of the presence of hydrogel material bond to the tissue. Final gel composition: 10 kDa, 10 wt % PEG-NBt-c, 18 mM oxidant containing fluorescent PSPs, in 50 mM HEPES buffer, pH 7.5. Irradiation conditions: $\lambda = 365$ nm, irradiance = 70 mW cm^{-2} , for exposure time= 6 min (dose= 25 J cm^{-2}). Scale bars= 5 mm (left) and 100 μm (right).

3.10 Environmental scanning electron microscopy (ESEM) imaging of cross-section of bonded tissue

The samples (hydrogel on skin) were washed with demineralized water and cut in pieces of approximately 10 mm x 10mm. Then a cross-section was made by cutting the samples using a sharp blade (GEM stainless steel uncoated type 62-0167) to get a sample size of 5 mm x 10 mm.

The wet samples were mounted onto a slit sample holder to investigate the cross-section from top view using an FEI Quanta 400 operating in ESEM mode ($T=3^\circ\text{C}$, $p=800 \text{ Pa}$).

Therefore the samples were precooled for 10 minutes at T=3°C before starting ESEM investigation at 20 kV accelerating voltage. Secondary electron micrographs were acquired using the GSE detector at 70% detector contrast settings. After imaging in wet state the samples were continuously dried inside the ESEM chamber at T=3°C ending at a pressure of p=200 Pa.

3.11 Light-triggered debonding of PEG-catechol hydrogels from skin tissue

Tissue samples with bonded PEG-NBt-c, PEG-NDop and PEG-Dop gels were prepared as explained above, , then immersed in water in an open square Petri dish and subjected to light illumination for selected time periods. Illumination conditions: $\lambda = 365$ nm, ECE 2000 standard metal halide UV curing bulb, 400 W, Irradiance = 70 mW cm⁻² (DYMAX). After selected exposure dose, the sample was again immersed in MilliQ water for 5 min and the stability of the bonded gel layer on the tissue was observed. The higher efficiency of PEG-NBt-c of light-mediated debonding from tissue in comparison to the other PEG gels is shown in figure 5 (Appendix).

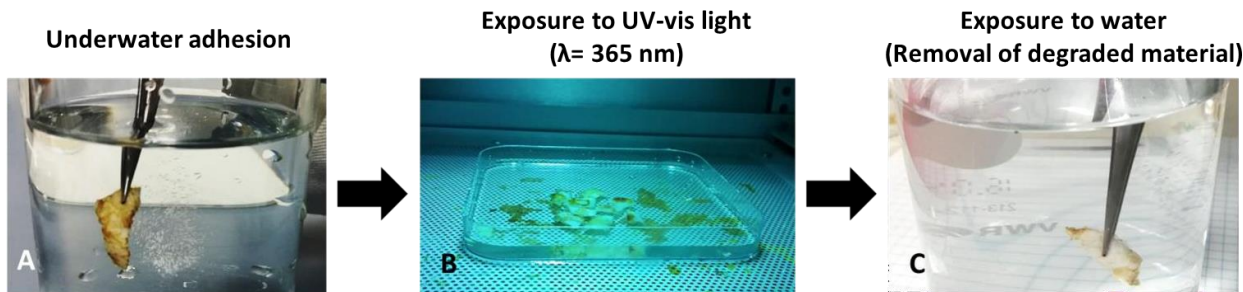


Figure 5 “On demand”, light-triggered degradation of tissue-adhesives on natural skin tissue, (A) Adhesive bound to tissue is placed in water. (B) The adhesive on the skin is exposed to light (wavelength = 365 nm) in order to photodegrade the material. (C) After each time point of irradiation, exposed sample is placed in water to remove the degraded (depolymerized) material.

3.12 LSM Irradiation Parameters¹²

Laser power (30W) 405nm	Irradiation Power (mW) (20x objective)	Irradiation Dose per voxel Passing number: 1 $P. Dwell = 131,88 \mu\text{sec}$	Irradiation Dose per voxel Passing number: 1 $P. Dwell = 65.94 \mu\text{sec}$
100%	1.6	211 nJ	105 nJ
50%	0.82	108 nJ	54 nJ
20%	0.32	42.2 nJ	21.1 nJ
15%	0.23	30 nJ	15.1 nJ
10%	0.18	23.7 nJ	11.8 nJ
8%	0.14	18.4 nJ	9.2 nJ
5%	0.085	11.2 nJ	5.6 nJ
1%	0.02	2.6 nJ	1.3 nJ

3.13 LSM Scanning Information

Zoom (20x objective)	Pixel Size (20x objective)
1x	0.83 μm
2.5x	0.33 μm

Scan Speed	Pixel Dwell (20x objective)
1	131.88 μsec
2	65.94 μsec

Scan Speed: 1	
Scan Number repetitions	Scan Time
1	40.51 sec
2	1 min 21 sec

4	2 min 42 sec
8	5 min 24 sec
12	10 min 48 sec

Scan Speed: 2	
Scan Number repetitions	Scan Time
1	20.26 sec

3.14 Statistical analysis

All the results are reported as the mean \pm standard deviation. Statistical differences were analyzed based on one-way Analysis of Variance (ANOVA) together with Tukey's range test and Bonferroni Procedure, performed using Excel Data Analysis, Prism or Origin software. Differences of * $p < 0.05$, ** $p < 0.01$ and *** $p < 0.01$ values were used for significance.

4. Chapter 4

Photodegradable PEG-catechol hydrogels as cell culture scaffolds

4.1 Cell culture

L929 fibroblasts (ATCC, Germany) were cultured in RPMI 1640 medium (Gibco, 61870-010) supplemented with 10% Fetal Bovine Serum (Gibco, 10270) and 1% antibiotics (penicillin/streptomycin) (Invitrogen), at 37°C under a humidified atmosphere containing 5% CO₂. Cell culture media was changed every second day. Cells from passage 8-11 were used. RPE1 (Retinal Pigmented Epithelial Cells) (ATCC, Germany) were cultured in DMEM/F-12 (1:1)(1x) (Gibco) supplemented with 10% Fetal Bovine Serum (Gibco, 10270), 1% antibiotics

(penicillin/streptomycin) (Invitrogen) and Glutamax (Gibco, 35050-061) at 37°C under a humidified atmosphere containing 5% CO₂. Cell culture media was changed every second day. Cells from passage 4-8 were used.

4.2 Spheroids Preparation

Subconfluent L929 fibroblast cell cultures were passaged by trypsin digestion. Cells (20,000 per well) were placed in 96-well microplate (U-bottom) with cell-repellent surface and cultured overnight at 37 °C under a humidified atmosphere containing 5 % CO₂. Next day, spheroids with different volumes were formed. In order to use them for encapsulation, the extra cell culture medium was removed. The smallest possible amount of medium containing the spheroids was transferred into an Eppendorf tube and centrifuged for 30 s at 500 rpm. The supernatant was removed and the precipitated spheroids were used for following experiment.

4.3 3D encapsulation of spheroids in PEG hydrogels

PEG polymer solution (40 wt%, 2.75 µL) and cyclo(RGDfC) peptide (6 mM, 1.8 µL) were mixed in an Ibidi® 15-well angiogenesis slide. L929 fibroblast spheroids prepared in the previous step (2.64 µL) were added, followed by addition of the oxidant (72 mM, 2.57 µL) and allowed to crosslink. In systems with slow gelation kinetics, spheroids were seeded around 15 to 30 min after oxidant addition, to avoid spheroid sedimentation during crosslinking. The obtained spheroid-laden hydrogels were kept in cell culture medium total for 9 days at 37 °C under a humidified atmosphere containing 5 % CO₂.

4.4 Live/dead assay

Live/dead cell assay Double Staining (Sigma-Aldrich) based on fluorescein diacetate (FDA) and propidium iodide (PI) was carried out by following the manufacturer's protocol, where live cells are stained green (excitation/emission ≈490/515 nm) while dead cells appeared

in red color (excitation/emission \approx 535/617 nm). As control experiments, untreated cells (cells incubated in the absence of the hydrogel) were used as PI negative control (viable cells), and 0.1% Triton X-100 (TX) treated cells for 5 min were used as PI positive control (dead cells). The cells were counted by fluorescence microscopy, using imageJ software. The cell viability was calculated by the following equation:

$$\% \text{Viability} = \left(\frac{\text{total n}^{\circ} \text{ of cells} - \text{n}^{\circ} \text{ of stained cells}}{\text{total n}^{\circ} \text{ of cells}} \right) \times 100.$$

4.5 Cytocompatibility studies of PEG gels

Cytocompatibility over 2D cell culture

A previously reported protocol from our group was followed.¹³ Solutions of hydrogel precursors (4-arm, 10 kDa, 20 wt % PEG polymers and 36 mM oxidant NaIO₄) were freshly prepared in sterile 50 mM HEPES buffer, pH 7.5. PEG gels were prepared in PDMS molds as above specified with the following final formulation: 10 kDa, 10 wt % PEG polymers, 18 mM oxidant. The prepared hydrogels were washed thoroughly with 70% ethanol and sterile PBS solution 3 times before use. L929 fibroblast cells, previously cultured on plastic culture plates for 1 d, were cultured in the presence of PEG gels for 1 d, followed by live/dead assay. Cell viability was compared for the different PEG gels. Figure 6 shows that high cell viability (>96%) was observed for all cases.

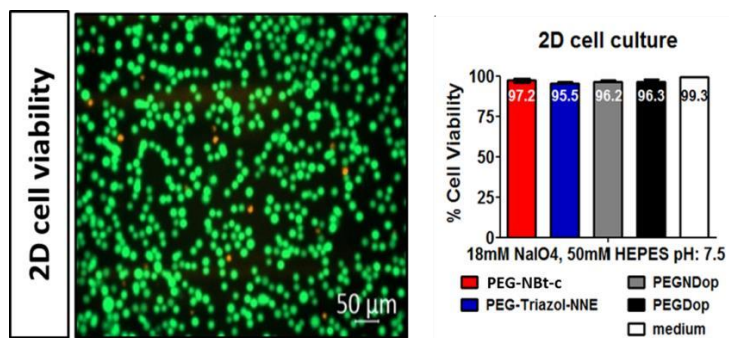


Figure 6 2D culture cell culture (L929 fibroblasts) performed in contact with non-irradiated PEG-catechol hydrogels (conditions: 10kDa, 10 wt% PEG polymers, 18 mM oxidant, 50 mM HEPES buffer, pH 7.5). Live (green)/ dead (red) assay was performed. High cell viability (> 95 % in 2D) was observed in all cases. Scale bar: 50 µm.

Cytocompatibility over 3D encapsulated cells

Solutions of 40 wt% PEGs, 72 mM oxidant, and 6 mM cyclo(RGDfC), were prepared in sterile 50 mM HEPES Buffer, pH 7.5. Note that cyclo(RGDfC) peptide promotes cell adhesion. 40 wt % polymer solution (2.5 µL) and cyclo(RGDfC) (1.8 µL) were mixed and placed in Ibidi® 15-well angiogenesis slide. L929 fibroblast cells (2.7 µL, 5,000 per well) were added, followed by the oxidant (2.5 µL) and the mixture was allowed to crosslink in incubator at 37 °C. Final formulation was: 10 kDa, 10 wt % PEG polymers, 18 mM oxidant, 1 mM cyclo(RGDfC). The obtained cell-laden hydrogels were kept in cell culture medium for 3 d. The cell culture medium was removed and the gels were washed once with PBS. Live/dead assay was performed. The experiment was conducted at least in triplicate. High cell viability was observed in cell-laden 3D gels (> 90%) for all cases, corroborating the non-cytotoxicity of the different materials (chapter 4, Figure 4.5). Despite the presence of 1 mM cyclo(RGDfC) peptide on the composition, cell remained rounded and did not spread, probably due to the high stiffness and no degradability of the matrix.

Cytocompatibility of cell spheroids encapsulated in PEG hydrogels

Spheroid-laden gels were prepared as in the previous section except that cell spheroids instead of single cells were used. Final formulation was: 10 kDa, 10 wt % PEG polymers, 18 mM oxidant, 1 mM cyclo(RGDfC). The gels were let cure for 30 min in the incubator at 37 °C and cell culture medium was replaced. The cell culture medium was exchanged every day. After 3 d of culture, live/dead assay was performed. Spheroid-laden gels from 10 vs 20 kDa precursors, and PEG-NBt-c vs PEG-NDop vs PEG-Dop were prepared and also studied for comparison (Figure 7). Cell viability was > 90% in all cases, indicating the good cytocompatibility of all PEG-gel

formulations. Interestingly, higher cell viability (> 95%) was observed for 20 kDa gels. Cells remained confined and did not show migration out of the spheroid, probably due to the high stiffness and no degradability of the matrix.

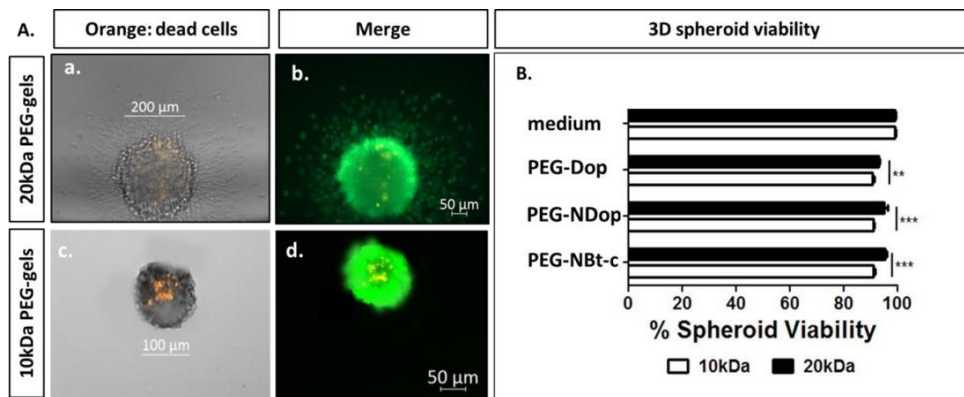
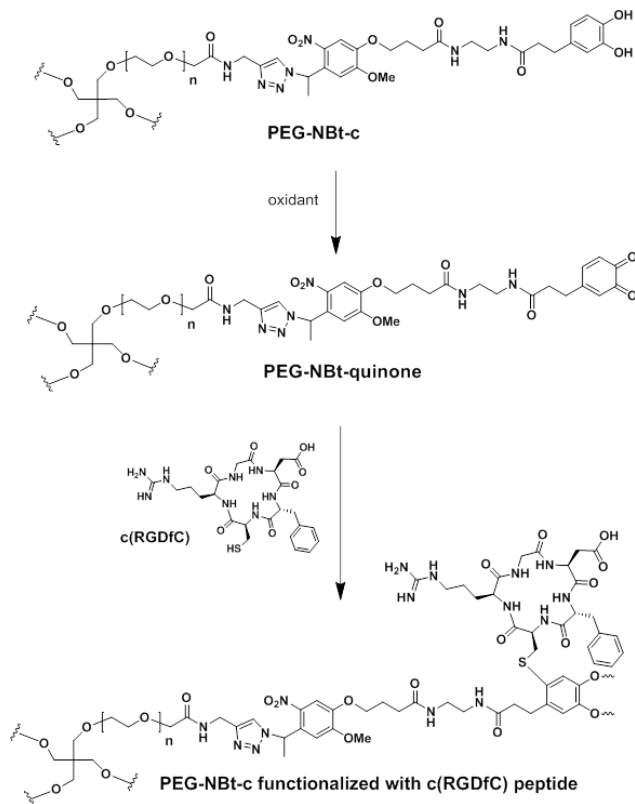


Figure 7 Cell viability and cell migration. Final polymer composition of 10 kDa PEG polymers, 18 mM NaIO4, 1 mM cyclo(RGDfC) (in 50mMHEPES buffer, pH:7.5) were used. (A, B) Cell viability of 3D spheroid culture was performed in PEG hydrogel derivatives, without any irradiation, with Live/Dead assay (which stains the dead cells orange color and the alive green color). The Fibroblast L929 cells and spheroids cultured for 72 h. (A, B) show the encapsulation of spheroids in different polymer concentration. (Aa, b) The material is softer than (Ac, d) and the cells start to migrate from the spheroid to the gel. (B) We observed higher cell viability in 20 kDa PEG polymers than in 10 kDa. Although in both cases we have cell viability above 90%.

4.6 3D cell encapsulation in PEG-catechol hydrogels



Solutions of 40 wt% PEG-catechol derivatives, 72 mM oxidant, and 6 mM cyclo((RGDfC) were prepared in 50mM HEPES Buffer, pH 7.5.

40 wt% polymer solution (2.75 μ L) and cyclo(RGDfC) (6 mM, 1.8 μ L) were mixed and placed in Ibidi® 15-well angiogenesis slide. L929 fibroblast cells (2.64 μ L, 5,000 per well) were added, followed by the oxidant (72 mM, 2.57 μ L) and allowed to crosslink in incubator at 37 °C. In systems with slow gelation kinetics, the timing for the inclusion of cells was adjusted to avoid cell sedimentation during crosslinking. In such cases, cells were added around 15 to 30 min after oxidant addition. The obtained cell-laden hydrogels were kept in cell culture medium for 2 d at 37°C under a humidified atmosphere containing 5 % CO₂.

4.7 Cytotoxicity study of the photolysis products of the different PEG-catechol hydrogels

Fibroblast L929 cells (30,000 per well) were cultured overnight at 37 °C under a humidified atmosphere containing 5 % CO₂. The irradiated medium, which was collected during

bulk irradiation of acellular gels (see above) at different irradiation doses (10 min = 42 J cm^{-2} , 13 min = 90 J cm^{-2} , 20 min = 84 J cm^{-2} and 30 min = 126 J cm^{-2}), was placed on the cultured cells ($250 \mu\text{L}$). Pure cell culture medium that was not in contact with the hydrogels was irradiated for the same time and used as internal control. Cells were then incubated (in the presence of the added photolysis products) for 24 h at 37°C under a humidified atmosphere containing 5 % CO_2 . Live/dead assay was performed (see procedure below) in order to check the tolerance of cells to the photodegradation products. The experiment was performed in triplicate (three individual experiments).

4.8 2D cell culture and release on PEG-catechol hydrogels

Preparation of 2D PEG-gels coated with collagen and cell adhesion

PEG hydrogels (10 kDa, 10 wt % polymer and 18 mM NaIO_4 in 50 mM HEPES buffer, pH 7.5) were prepared in Ibidi® 15-μwell angiogenesis slides, cured for 6 h at room temperature and swelled in water overnight. The hydrogels were washed thoroughly with 70% ethanol and sterile PBS solution for several times before using them for further studies. The hydrogel was coated with collagen I ($60 \mu\text{g mL}^{-1}$, at 4°C overnight)¹⁴ and washed with PBS sterile for three times in order to remove the excess of protein. Fibroblast cells (5,000 per well) were seeded on top of the gels and incubated overnight at 37°C under a humidified atmosphere containing 5 % CO_2 . Cell adhesion was observed at 4 h. The cell culture was kept for 4 d. During this time, the cell culture medium was exchanged twice.

2D cell release from PEG hydrogels during photodegradation

2D fibroblast cultured on the top of hydrogels were subjected to light radiation for different exposure times using a LED lamp (100 mW, operated at $\lambda = 365 \text{ nm}$, irradiance = 2.6 mW cm^{-2} , RoHS Compliant). UV exposure was performed for selected radiation doses: 3 min = 0.5 J cm^{-2} , 4 min = 0.6 J cm^{-2} , 5 min = 0.8 J cm^{-2} and 7 min = 1.1 J cm^{-2} . At every irradiation time

point (t_i), the irradiated medium (30 μL , containing or not any released cells) was collected and placed (with extra 30 μL fresh medium) in new 96-well plates, in triplicates. Before starting the irradiation experiment, medium was collected after 2 d of culture and used as internal control. These cells are not released due to irradiation but instead correspond to loosely bound cells that did not attach to the collagen coating. Very few cells (<3 cells) were observed in such medium, indicating that a considerable number of cells in only released upon light irradiation. After each irradiation point, fresh cell culture medium was added to the irradiated wells and irradiation was continued further. When the irradiation experiment was finished (7 min = 1.1 J cm^{-2} irradiation dose), the remaining irradiated cells were trypsinised and counted. Non-irradiated cells (irradiation dose = 0 J cm^{-2}) were cultured on PEG gels, trypsinised and counted to be used as internal positive control.

The two 96-well plates with the non-irradiated and irradiated medium containing the released cells were incubated for 24 h at 37 °C under a humidified atmosphere containing 5 % CO_2 .

Cytotoxicity study of the harvested cells after 2D irradiation

The cells released at different irradiation doses were harvested and placed in two different 96-well plates. After 12 h of incubation at 37 °C under a humidified atmosphere containing 5% CO_2 , live/dead assay was performed in order to check the tolerance of cells to light exposure.

In parallel, the number of released cells at different irradiation doses was counted, in order to evaluate the photodegradation efficiency of the polymers. Extra controls were the trypsinised cells from gels after irradiation and trypsinised cells from gels without irradiation. Trypsin digestion took place for 40 s on the top of the gels. The number of released cells was counted with imageJ software and normalized with the equation 3:

$$\% \text{ cell released} = \frac{\text{number of cells released at } t_i}{\text{total trypsinised cells without irradiation}} \times 100.$$

The experiment was performed in sextuplicate within two individual experiments.

LDH assay of the harvested released cells after 2D irradiation

This assay measures lactate dehydrogenase (LDH), a stable cytosolic enzyme that is released upon cell lysis due to cell damage. Released LDH in culture supernatants is measured with a 30-minute coupled enzymatic assay, which results in conversion of a tetrazolium salt (INT) into a red formazan product.

The cells released at different irradiation doses were harvested and their vitality was analyzed by a LDH assay, following the manufacturer's protocol (CytoTox® Non-Radioactive). After 6 h of the 2D irradiation experiment, the supernatant (irradiated medium that contains the released cells, 50 µL) was collected and placed in a new 96-well plate. An equal volume of CytoTox 96® Reagent was added to each well and incubated for 30 min, in the dark at room temperature. Stop Solution was added, and the absorbance signal was measured at 490 nm in a plate reader (SpectraMax 190 Microplate Reader, Molecular Devices, USA). The intensity of the absorbance at the mentioned wavelength is proportional to the number of lysed cells. As a non-cell control, cell culture medium with fetal bovine serum background but without cells was used as the negative control. As a vehicle-only cells control, cell culture medium containing untreated cells was used. As a maximum LDH release control, 10µL of 9% Triton X-100 (TX) per 100 µL of vehicle-only cells control were added 30 min before adding CytoTox 96® Reagent. In order to determine the background of the culture medium with fetal bovine serum and 9% Triton X-100 (TX). The cell cytotoxicity was calculated according to the equation 4:

$$\% \text{Cytotoxicity} = \left(\frac{\text{OD}_{490\text{nm}}, \text{experimental LDH released control}}{\text{OD}_{490\text{nm}}, \text{maximum LDH released}} \right) \times 100.$$

The experiment was performed in sextuplicate within two individual experiments. The experiment was performed in sextuplicate within two individual experiments. According to the manufacturer's protocol (CytoTox® Non-Radioactive), cells showing cytotoxicity < 60% are

considered to remain “healthy” comparable to control (cells in medium without exposure) which shows cytotoxicity $\sim 50\%$.

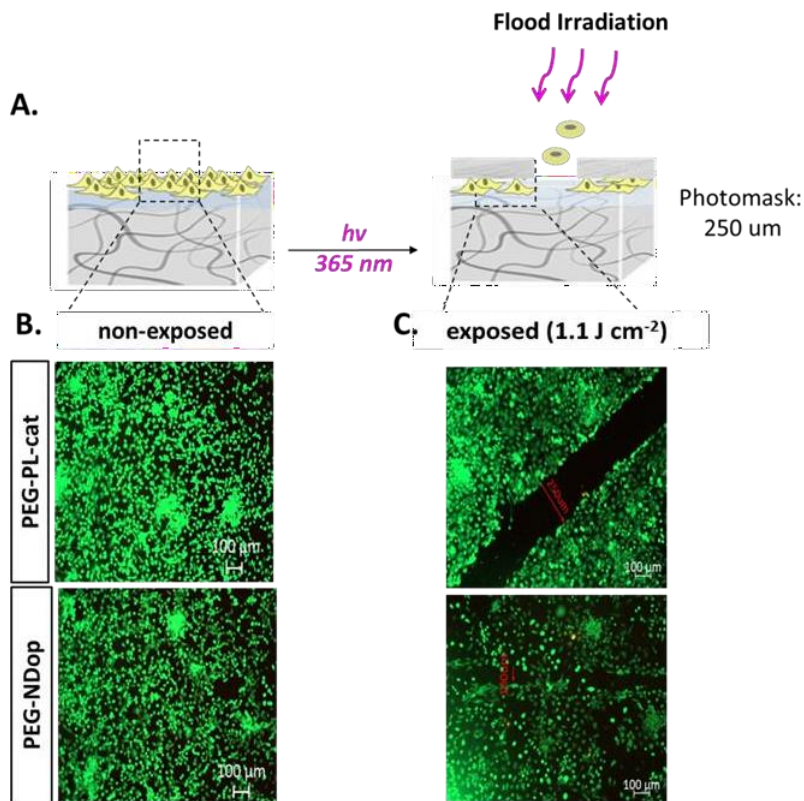


Figure 8 Comparison of PEG-NBt-c and PEG-NDop photodegradable gels for cell culture and light-triggered cell patterning (fibroblasts L929). A) Schematics of 2D cell culture on photocleavable PEG hydrogels (composition: 10 kDa, 10 wt% PEG, 18 mM oxidant, in 50 mM HEPES buffer, pH 7.5, coated with collagen I). Cells cultured for 4 d before exposure (B). The hydrogel surface covered by cells was exposed (LED lamp, $\lambda = 365$ nm) for 7 min = 1.1 mJ cm^{-2} and live/dead assay performed (C).

5. References

1. Shafiq, Z.; Cui, J.; Pastor-Pérez, L.; San Miguel, V.; Gropeanu, R. A.; Serrano, C.; del Campo, A., Bioinspired Underwater Bonding and Debonding on Demand. *Angewandte Chemie International Edition* **2012**, *51* (18), 4332-4335.
2. Paez, J. I.; Ustahüseyin, O.; Serrano, C.; Ton, X.-A.; Shafiq, Z.; Auernhammer, G. K.; d'Ischia, M.; del Campo, A., Gauging and Tuning Cross-Linking Kinetics of Catechol-PEG Adhesives via Catecholamine Functionalization. *Biomacromolecules* **2015**, *16* (12), 3811-3818.
3. Napolitano, A.; d'Ischia, M.; Costantini, C.; Prota, G., A new oxidation pathway of the neurotoxin 6-aminodopamine. Isolation and characterisation of a dimer with a tetrahydro [3, 4a] iminoethanophenoxazine ring system. *Tetrahedron* **1992**, *48* (39), 8515-8522.
4. Carpino, L. A.; Han, G. Y., 9-Fluorenylmethoxycarbonyl amino-protecting group. *The Journal of Organic Chemistry* **1972**, *37* (22), 3404-3409.
5. Wirkner, M.; Weis, S.; San Miguel, V.; Álvarez, M.; Gropeanu, R. A.; Salierno, M.; Sartoris, A.; Unger, R. E.; Kirkpatrick, C. J.; del Campo, A., Photoactivatable caged cyclic RGD peptide for triggering integrin binding and cell adhesion to surfaces. *ChemBioChem* **2011**, *12* (17), 2623-2629.
6. Qvortrup, K.; Nielsen, T. E., A photolabile linker for the solid-phase synthesis of 4-substituted NH-1,2,3-triazoles. *Chemical Communications* **2011**, *47* (11), 3278-3280.
7.
[https://www.dymax.com/images/pdf/technical_bulletins/lit135_intensity_conversion_c
hart_tb.pdf](https://www.dymax.com/images/pdf/technical_bulletins/lit135_intensity_conversion_chart_tb.pdf)
8. DeForest, C. A.; Anseth, K. S., Cytocompatible click-based hydrogels with dynamically tunable properties through orthogonal photoconjugation and photocleavage reactions. *Nature Chemistry* **2011**, *3* (12), 925-931.
9. Griffin, D. R.; Kasko, A. M., Photodegradable Macromers and Hydrogels for Live Cell Encapsulation and Release. *Journal of the American Chemical Society* **2012**, *134* (31), 13103-13107.
10. LeValley, P. J.; Neelarapu, R.; Sutherland, B. P.; Dasgupta, S.; Kloxin, C. J.; Kloxin, A. M., Photolabile Linkers: Exploiting Labile Bond Chemistry to Control Mode and Rate of Hydrogel Degradation and Protein Release. *Journal of the American Chemical Society* **2020**, *142* (10), 4671-4679.

11. Truong, V. X.; Li, F.; Forsythe, J. S., Photolabile Hydrogels Responsive to Broad Spectrum Visible Light for Selective Cell Release. *ACS Applied Materials & Interfaces* 2017, 9 (38), 32441-32445.
12. García-López, V.; Chen, F.; Nilewski, L. G.; Duret, G.; Aliyan, A.; Kolomeisky, A. B.; Robinson, J. T.; Wang, G.; Pal, R.; Tour, J. M., Molecular machines open cell membranes. *Nature* 2017, 548 (7669), 567.
13. Feng, J.; Ton, X.-A.; Zhao, S.; Paez, J. I.; del Campo, A., Mechanically Reinforced Catechol-Containing Hydrogels with Improved Tissue Gluing Performance. *Biomimetics* 2017, 2 (4), 23.
14. Chaudhuri, T.; Rehfeldt, F.; Sweeney, H. L.; Discher, D. E., Preparation of Collagen-Coated Gels that Maximize In Vitro Myogenesis of Stem Cells by Matching the Lateral Elasticity of In Vivo Muscle. In *Protocols for Adult Stem Cells*, Conboy, I. M.; Schaffer, D. V.; Barcellos-Hoff, M. H.; Li, S., Eds. Humana Press: Totowa, NJ, 2010; pp 185-202.

List of Scientific Contributions

Articles

1. Villiou, M.; Paez, J.I.; Del Campo, A. Photodegradable hydrogels for cell encapsulation and tissue adhesion. *ACS Appl. Mater. Interfaces* **2020**, *12*, 34, 37862–37872. M.V. conducted most experimental work. This article contains results shown in Chapters 2, 3 and 4.
2. Włodarczyk-Bieguna, M. K.; Paez, J. I.; Villiou, M.; Feng, J.; Del Campo, A. Printability study of metal ion crosslinked PEG-catechol based inks. *Biofabrication* **2020**, *12* (3), 035009. M.V. contributed with the cell and microscopy experiments.
3. Feng, J.; Zheng, Y.; Bhusari, S.; Villiou, M.; Pearson, S.; Del Campo, A. Printed degradable optical waveguides for guiding light into tissue. *Adv. Func. Mater.* **2020**, *200427*. M.V. contributed with the cell and microscopy experiments.
4. Włodarczyk-Bieguna, M. K.; Villiou, M.; Koch, M.; Muth, C.; Del Campo. Meltelecrtowriting of patterned scaffolds for human trabecular meshwork reconstruction. **Manuscript in preparation.** M.V. contributed with the cell and microscopy experiments.
5. Włodarczyk-Bieguna, M. K.; Villiou, M.; Herbeck-Engel, P.; Puertas, M.; Del Campo. Printing of alginate/gelatin ink into chitosan bath solution for printing with improved shape fidelity. **Manuscript in preparation.** M.V. contributed with the cell and microscopy experiments.

Scientific Talks

1. Villiou, M.; Paez, J.I.; Del Campo, A. Mussel-inspired photodegradable tissue adhesives. *International Conference on Adhesion in Aqueous Media: From Biology to Synthetic Materials, AAM2019, 09.10.2019*, Dresden, Germany
2. Villiou, M.; Paez, J.I.; Del Campo, A. Photodegradable Bioadhesives for 3d cell encapsulation. **08-12.10.2018**, URGO company, URGO Dijon, France
3. Villiou, M.; Paez, J.I.; Del Campo, A. Design of Bioinspired Adhesives for Soft Tissue Engineering. *4th Training School on Technology Transfer and Career Development, 06.03.2018*, BASF, Ludwigshafen, Germany

4. Villiou, M.; Paez, J.I.; Del Campo, A. Bioinspired Adhesives for Soft Tissue Engineering. *Doctoral Colloquia*, March **2018**, INM-Leibniz Institute for New Materials, Saarbrücken, Germany
5. Villiou, M.; Paez, J.I.; Del Campo, A. Bioinspired Adhesives for Tissue Regeneration. *3rd Training School on Advances in Mechanics and Chemistry of Adhesion*, **14.09.2017**, CNRS/ESPCI, Paris, France
6. Villiou, M.; Paez, J.I.; Włodarczyk-Biegum, M. K.; Del Campo, A. Bioinspired Medical Adhesives. *Doctoral Colloquia*, July **2017**, INM-Leibniz Institute for New Materials, Saarbrücken, Germany
7. Villiou, M.; Paez, J.I.; Włodarczyk-Biegum, M. K.; Del Campo, A. Bioinspired Medical Adhesives. *Mid Term Meeting of the Marie Skłodowska-Curie actions (ETN) on BioSmartTrainee project*, **12.09.2017**, CNRS/ESPCI, Paris, France
8. Włodarczyk-Biegum, M. K.; Paez, J. I.; Villiou, M.; Del Campo, A. Medical adhesives for 3D printing. *Engineering Conferences International on Biofabrication for Hierarchical in Vitro Tissue Models* **07.06.2017**, Schloss Hernstein Hernstein, Austria
9. Villiou, M.; Paez, J.I.; Del Campo, A. Bioinspired Adhesives for Tissue Regeneration. *2nd Training School on Training in Bio-Inspired Design of Smart Adhesive Materials*, **23.03.2017**, Leibniz-Institut für Polymerforschung Dresden e.V., IPF Dresden, Germany
10. Villiou, M.; Paez, J.I.; Del Campo, A. Bioinspired Medical Adhesives. *1st Training School on Fundamental Aspects in Polymer Synthesis, Adhesion and Modelling*, **15.09.2019**, University of Patras, UPATRAS, Greece

Poster Presentations

1. Villiou, M.; Paez, J.I.; Włodarczyk-Biegum, M. K.; Del Campo, A. Photodegradable Bioadhesive Hydrogels for 3D Cell Encapsulation. *International Conference on Living Materials*, date February **2020**, Universität des Saarlandes, Saarbrücken, Germany
2. Villiou, M.; Paez, J.I.; Del Campo, A. Photodegradable Biomedical Adhesives for 3D Cell Encapsulation. *Doktorandentag "Doktorandinnen/Doktoranden der Naturwissenschaftlich-*

*Technischen Fakultät stellen ihre Promotionsthemen vor, date November **2018**, Universität des Saarlandes,Saarbrücken, Germany*

3. Paez, J. I.; Villiou, M.; Feng, J.; Włodarczyk-Biegum, M. K.; Del Campo, A. Mild chemistries for photodegradable bioinspired hydrogels: opportunities for cell encapsulation, soft tissue adhesion and 3D bioprinting. *Gordon Research Conference on Bioinspired Multifunctional Dynamic Materials*, June **2018**, Les Diablerets Conference Center, Eurotel Victoria, Les Diablerets, Switzerland
4. Paez, J. I.; Villiou, M.; Feng, J.; Włodarczyk-Biegum, M. K.; Del Campo, A. Bioinspired multifunctional dynamic materials. *Gordon Research Seminar on Leveraging Bio-Molecular Complexity in Multi-Functional Synthetic Materials*, June **2018**, Les Diablerets Conference Center, Eurotel Victoria, Les Diablerets, Switzerland
5. Villiou, M.; Paez, J.I.; Del Campo, A. Bioinspired Adhesives for Soft Tissue Engineering. *First INTERREG – 6th TERMIS Winterschool on Mechanobiology in Musculoskeletal Tissue Regeneration – In Vitro/In Vivo Preclinical Models and Imaging*, January **2018**, Radstadt, Salzburg, Austria
6. Villiou, M.; Paez, J.I.; Włodarczyk-Biegum, M. K.; Del Campo, A. Design of Bioinspired Adhesives for Soft Tissue Engineering. *Doktorandentag "Doktorandinnen/Doktoranden der Naturwissenschaftlich-Technischen Fakultät stellen ihre Promotionsthemen vor, November **2017***, Universität des Saarlandes,Saarbrücken, Germany
7. Villiou, M.; Paez, J.I.; Włodarczyk-Biegum, M. K.; Del Campo, A. Bioinspired Adhesives for Soft Tissue Engineering. *Gordon Research Conference on Molecular Insight to Understand Fracture and Adhesion*, July **2017**, Mount Holyoke College South Hadley, MA, USA
8. Villiou, M.; Paez, J.I.; Włodarczyk-Biegum, M. K.; Del Campo, A. Bioinspired Adhesives for Tissue Regeneration. *Gordon Research Seminar on Molecular Insight to Understand Fracture and Adhesion*, July **2017**, Mount Holyoke College South Hadley, MA, USA

Studentships

1. From Gordon Research Conference on Molecular Insight to Understand Fracture and Adhesion, July **2017**, to participate with a poster presentation

2. European Fellowship from Marie Skłodowska-Curie, Horizon 2020, Early Stage Researcher Fellowship (ITN- project on BioSmartTrainee), **2016 – 2019**, to conduct PhD project

Participation in seminars

1. Virtual Mini-Symposium on Materials for the Digital Environment, June **2020**, INM-Leibniz Institute for new Materials, Saarbrücken, Germany
2. Weekly INM scientific seminars (Colloquia), **2016 - 2019**, INM-Leibniz Institute for new Materials, Saarbrücken, Germany
3. Monthly Biointerface lectures, **2016 - 2019**, INM-Leibniz Institute for new Materials, Universität des Saarlandes, Saarbrücken, Germany
4. Monthly GdCh seminars (Colloquia), **2016 - 2019**, Universität des Saarlandes, Saarbrücken, Germany
5. Annual genetic engineering and safety instructions, **2016 - 2019**, INM-Leibniz Institute for new Materials, Saarbrücken, Germany
6. Annual safety instructions in biological and chemical laboratories, **2016 - 2019**, INM-Leibniz Institute for new Materials, Saarbrücken, Germany

Participation in soft skills seminars

1. Arbeitmarkt und Jobmessen, March **2020**, Agentur für Arbeit Saarland, Saarbrücken, Germany
2. Writing, Presenting, Networking – Tools for a Scientific Career, Symposium for Female Scientists, October **2019**, INM-Leibniz Institute for new Materials, Saarbrücken, Germany
3. Career development in industry, March **2018**, BASF, Ludwigshafen, Germany
4. First aid course - training, September **2018**, Universität des Saarlandes, Saarbrücken, Germany
5. Academic English, Doctoral Training Program of Saarland University (GradUS global), winter semester **2017 – 2018**, Universität des Saarlandes, Saarbrücken, Germany

6. Deutsch als Fremdsprache für Doktoranden (A1-2), Doctoral Training Program of Saarland University (GradUS global), winter semester **2017 – 2018**, Universität des Saarlandes, Saarbrücken, Germany
7. Starting your own company, September **2017**, CNRS/ESPCI, Paris, France
8. Fundamentals about IP protection, September **2017**, CNRS/ESPCI, Paris, France
9. Funding in Academia, September **2017**, CNRS/ESPCI, Paris, France
11. Writing of manuscripts, March **2017**, Leibniz-Institut für Polymerforschung Dresden e.V., IPF Dresden, Germany
12. Scientific Presentation Skills, March **2017**, Leibniz-Institut für Polymerforschung Dresden e.V., IPF Dresden, Germany
13. Patenting and Licensing, March **2017**, Leibniz-Institut für Polymerforschung Dresden e.V., IPF Dresden, Germany
10. Annual Good Scientific Practice seminar, **2016 - 2019**, INM-Leibniz Institute for new Materials, Saarbrücken, Germany

Secondment (8-12.10.2018)

In URG0 company (URGO Dijon, France) where I was exposed to clinical product development and visited the main manufacturing site, attending a number of presentations about IP, Regulatory, Project management, Innovation, and biomedical material research. I rotated in different laboratories, where several scientists demonstrated techniques in charge of formulation - performance of biomaterials and their physico-chemical analysis.



MARIA VILLIOU

Marie Curie PhD candidate withinHorizon 2020



Working and Academic Experience

08.2016 – 08.2020

Marie Skłodowska-Curie Early Stage Researcher (PhD) on Chemistry and Biomaterials

INM-Leibniz Institute for New Materials, Saarbrücken, DE

- Thesis: Photodegradable Hydrogels for tissue gluing
- Scientific member of Early Stage Researcher's comitee

02.2015 - 07.2016

Teaching Assistant

School Of Medicine, University Of Patras, GR



Education

11.2014 - 08.2016

MSc in Biomedical Sciences – Field of Stem Cells & Regenerative Medicine

School of Medicine, University of Patras, GR

- Thesis: Geminin protein in colorectal cancer induction, in cancer stem cells and intestinal organoids
- 2 Publications as co-author
- Graduated with 91.00 (A) GPA, in Top 5% of Class

09.2010 - 06.2014

BSc in Chemistry – Field of Organic Synthesis, Biochemistry, Bioapplication

Department of Chemistry, Aristotle University of Thessaloniki, GR

- Thesis: Kinetic investigation of the isomerization of fatty acids by free radicals and attempt to block this alteration
- Graduated with 71.30 (B) GPA, in Top 10% of Class



Internships

08.2015 - 09.2015

Intern in Bioelectronics

Ecole Nationale Supérieure de Mines de Saint Etienne, FR

- Topic: Development of hybrid conducting polymer-based device to monitor the brain activity and record neural activity.

07.2014 - 10.2014

Student Intern in Bioelectronics

Ecole Nationale Supérieure de Mines de Saint Etienne, FR

- Topic: Development of an *in vitro* toxicology platform using conducting polymer device arrays coupled with cell cultures and tissue murine slices.

07.2013 -09.2013

Internship Student in ISO standard ChemicalAnalysis

General State Laboratory Thessaloniki, Greece



Further Qualifications & Trainings

07.2017	Certificate on Histology, Institute of Molecular Biology gGmbH (IMB) - Mainz, DE
04.2016	Training on Human Pluripotent Stem Cells Culture, University College London, UK
05.2015	Diploma in Nanomedicine, School of Medicine, National and Kapodistrian University of Athens, GR
12.2014	Certificate in Use of Animals in Biomedical Research, Faculty of Medicine, University of Patras, GR



Voluntary & Interests

- Volunteer: University Hospital of Thessaloniki AHEPA & University Hospital of Patras (Rio) section children with cancer
- Hobbies: Swimming, piano, Latin dance, gymnastics

